Democratic and Popular Algerian Republic

Ministry of Higher Education and Scientific Research

University of 20 August 1955 Skikda

Faculty of Science

Department of Chemistry

Order N° :

THESIS

Presented with a view to obtaining the diploma of

DOCTORAT LMD

Field: Chemistry

Speciality: Environmental Chemistry

THEME:

Intensification of advanced oxidation processes (POAs) for the elimination of persistent organic pollutants (POPs) in water.

Presented by:

BOUGOUIZI NESRINE

Defended on : 09/07/2025

Before the Jury composed of:

President	Pr. emeritus Fayçal DJAZI	University of 20 August 1955 Skikda
Rapporteur	Pr. Mahdi CHIHA	University of 20 August 1955 Skikda
Co-Rapporteur	Dr. Fatiha AHMEDCHEKKAT	University of 20 August 1955 Skikda
Examiner	Pr. Hocine AKKARI	University of Batna 2
Examiner	Pr. Abdelhak CHETTAH	University of 20 August 1955 Skikda
Examiner	Dr. Hassen AYADI	University of 20 August 1955 Skikda

Acknowledgments

I thank God for what I am and have, recognising a debt that will remain etched in my memory from a period rich in learning and benefits. I feel immense gratitude towards all my professors who contributed to my training, and my dear parents.

I thank my thesis supervisor, Mr. Mahdi CHIHA, Professor at the University of Skikda and Director of the Laboratory of Anticorrosion, Materials, Environment, and Structures (LAMES), for his guidance throughout my doctoral work. Thank you for trusting me, for the skills and knowledge you shared, and for the autonomy you taught me. I particularly appreciate your availability and rigorous adherence to deadlines for reviewing my documents. A big thank you for everything.

I would also like to express my deep gratitude to my thesis co-supervisor, Mrs. Fatiha AHMEDCHEKKAT, Associate Professor A at the University of Skikda, for her unwavering availability, extreme kindness, and human, pedagogical, and scientific qualities. May she find here the expression of my most sincere gratitude.

My sincere thanks also go to Mr. Fayçal DJAZI, Professor Emeritus at the University of Skikda, who honoured me by chairing the jury for this work. I extend my gratitude and feelings of respect to her.

I warmly thank Mr. Hocine AKKARI, a Professor at the University of Batna 2, Mr. Abdelhak CHETTAH, a professor at the University of Skikda, and Mr. Hassen AYADI, Associate Professor A at the University of Skikda, for accepting to be examiners for this thesis. Their support is valuable and greatly appreciated.

Thanks to the engineers in the laboratories of the Technology Hall at the University of Skikda, especially Houda, for their valuable assistance, encouragement, and above all, their kindness.

I would also like to warmly thank my colleagues in the laboratory, with whom I have shared many enriching moments, both scientifically and personally. Of course, I would like to thank my "teammates" from the LAMES laboratory, particularly Dr. Hayat CHAMEKH and PhD students Amina BOUSIREB, Nour el Houda SOUAMES, Khadidja KAHOUL, and Nour BRAHMI, for their team spirit, their help, and their encouragement throughout these years. To all of you, I say thank you and wish you much courage for the future.

Acknowledgments

Finally, my heartfelt thanks go to my parents, without whom none of this would have been possible. I am infinitely grateful to my husband, daughter Sila Dania, sister Roumaissa, brother Yassine, and grandparents.

"Nothing is lost, nothing is created, everything is transformed."

Antoine Lavoisier

Dedication

I dedicate this work, the result of my studies, to all the people who have contributed to my journey:

To my dear father, who has always supported, encouraged, and believed in me, even during moments of doubt. You have been a divine blessing in my life, and I thank God for having you as my father.

To my tender and warm mother, for her unwavering support and discreet presence, which have allowed me to become who I am today.

To my dear husband, for all the happiness he has brought into my life since he entered it, his moral and financial support, and his encouragement during the most difficult times.

To my precious treasure, my beloved daughter Sila Dania, whose immeasurable love and support are my most outstanding achievement. May God grant me the time necessary to love you and watch you grow into a magnificent woman.

To my dear sister, Maïssa, sweet and sensitive.

To my dear brother, Yacine, generous and supportive.

Dedication

To my dear grandfather, who has always thought of me, may God protect him.

To my dear grandmother, may God heal and protect her.

To those who asked me, "When will you defend your thesis?", here we are!

And finally, to all those who have given me everything without expecting anything in return.

"When everything is going well, you can count on others;

When everything goes wrong, you can only count on your family."

Abstract

This study investigates the application of two advanced oxidation processes: the activation of inorganic oxidising species, specifically persulfate (PS) and Glidarc-type humid air plasma, for the treatment of an aqueous solution containing the azo dye "Orange G." UV-visible analysis was employed to monitor the degradation of the pollutant, while mineralisation was tracked by measuring the chemical oxygen demand (COD).

Initially, an oxidation process based on the radical sulfate ($SO_4^{\bullet -}$), generated by the thermal activation of PS and by the heat/Fe(II)/PS process, was evaluated. Several parameters were studied, including reaction temperature (20–70°C), pH (2–12), potassium persulfate (PPS) and ammonium persulfate (APS) dose (100–1000 mg/L), initial concentration of OG (10–70 mg/L), and concentration of $FeSO_4.7H_2O$ (10–50 mg/L) and $(NH_4)_2Fe(SO_4)_2$ (8–100 mg/L), as well as the impact of organic additives. These parameters were investigated to determine their influence on the efficiency of the process.

The results show that the oxidation of OG follows a pseudo-first-order kinetic model, with a high correlation coefficient ($R^2 = 0.99$). Complete decolourisation of 50 mg/L of OG was achieved in 150 minutes at 70°C and in 240 minutes at 65°C, in the presence of 1 g/L of PPS. The apparent activation energy was estimated to be 157.3 kJ/mol.

Furthermore, the results suggest a direct correlation between the oxidation of OG and high persulfate concentrations, while an inverse relationship was observed with the initial substrate concentrations. It was also found that higher reaction temperatures and a neutral initial pH favoured the degradation of OG.

The results indicate that the sulfate radical ($SO_4^{\bullet -}$) is the primary agent responsible for the oxidation of OG. Additionally, the presence of Cr (VI) ions in solution exhibited an inhibitory effect on the degradation process. The coexistence of ferrous ions and persulfate at high temperature demonstrated a synergistic effect, accelerating the oxidation of OG. In contrast, the heat/persulfate/Fe (II) process achieved a relatively low mineralisation rate of 75.41% after 260 minutes of treatment.

Furthermore, the degradation of Orange G in aqueous solution using the Glidarc humid air plasma process was investigated. Various concentrations of catalysts and oxidants were introduced into the Glydarc reactor to optimise the conditions and improve the system's performance. Under optimal treatment conditions, the degradation rates obtained were 66.46%, 100%, 72.79%, 71.19%, 90.48%, and 90.27%, respectively, using Glidarc alone, Glidarc/H_2O_2, Glidarc/IO^{4-}, Glidarc/Fe^{3+}, Glidarc/Fenton, and Glidarc/PPS, after treatment times of 210 min, 80 min, 210 min, 210 min, 12 min, and 180 min. Furthermore, the energy efficiency of the

Abstract

pollutant degradation was calculated to be 0.022 g/kWh, 0.0054 g/kWh, and 0.004 g/kWh for the Glidarc/Fenton, Glidarc/PPS, and Glidarc alone processes, respectively.

Keywords:

Advanced oxidation process, Orange G, Heat-activated persulfate, Sulfate radicals, Humid air plasma, Hydroxyl radicals

Résumé

Cette étude examine l'application de deux procédés d'oxydation avancée : l'activation des espèces inorganiques oxydantes, en particulier le persulfate, et le plasma d'air humide de type Glydarc, pour traiter une solution aqueuse contenant le colorant azoïque « Orange G ».

L'analyse UV-Visible a été utilisée pour suivre la dégradation du polluant, tandis que la minéralisation a été suivie par la mesure de la demande chimique en oxygène (DCO).

Dans un premier temps, un processus d'oxydation basé sur le sulfate radical ($SO_4^{\bullet-}$), généré par l'activation thermique du persulfate et par le processus chaleur/Fe(II), a été évalué. Plusieurs paramètres ont été étudiés, notamment la température de réaction (20–70°C), le pH (2–12), la dose de persulfate de potassium et d'ammonium (PSP) (100–1000 mg/L), la concentration initiale d'OG (10–70 mg/L), la concentration en $FeSO_4.7H_2O$ (10–50 mg/L) et en $(NH_4)_2Fe(SO_4)_2$ (8–100 mg/L), ainsi que l'impact des ajouts organiques. Ces paramètres ont été investigués afin de déterminer leur influence sur l'efficacité du processus.

Les résultats obtenus montrent que l'oxydation de l'OG suit une cinétique de pseudo-premier ordre, avec un coefficient de corrélation élevé (R^2 = 0,99). La décoloration complète de 50 mg/L d'OG a été réalisée en 150 minutes à 70°C et en 240 minutes à 65°C, en présence de 1 g/L de PS. L'énergie d'activation apparente a été estimée à 157,3 kJ/mol.

En outre, les résultats suggèrent une corrélation directe entre l'oxydation de l'OG et les concentrations élevées de persulfate, tandis qu'une relation inverse a été observée avec les concentrations initiales du substrat. Il a également été constaté que des températures de réaction plus élevées et un pH initial neutre favorisaient la dégradation de l'OG.

Les résultats indiquent que le radical sulfate ($SO_4^{\bullet-}$) est l'agent principal responsable de l'oxydation de l'OG. De plus, la présence d'ions Cr(VI) en solution a montré un effet inhibiteur sur le processus de dégradation. La coexistence des ions ferreux et du persulfate à haute température a induit un effet synergique, accélérant l'oxydation de l'OG. En revanche, le procédé chaleur/persulfate/Fe(II) a permis une dégradation de l'Orange G avec un taux de minéralisation relativement faible de 75,41 % après 260 minutes de traitement.

Abstract

En outre, la dégradation de l'Orange G en solution aqueuse en utilisant le processus de plasma d'air humide de type Glydarc a été étudiée. Différentes concentrations de catalyseurs et d'oxydants ont été introduites dans le réacteur Glydarc pour optimiser les conditions et améliorer la performance du système. Dans des conditions de traitement optimales, les taux de dégradation obtenus étaient respectivement de l'orde de 66,46 %, 100 %, 72,79 %, 71,19 %, 90,48 % et 90,27 %, en utilisant Glydarc seul, Glydarc/H_2O_2, Glydarc/IO^{4-}, Glydarc/Fe^{3+}, Glydarc/Fenton et Glydarc/PPS, après des temps de traitement de 210 min, 80 min, 210 min, 210 min, 12 min et 180 min. De plus, l'efficacité énergétique de la dégradation du polluant a été calculée à 0,022 g/KWh, 0,0054 g/KWh et 0,004 g/KWh pour les processus Glydarc/Fenton, Glydarc/PPS et Glydarc seul respectivement.

Mots-clés :

Procédés d'oxydation avancés, Orange G, Persulfate activé par la chaleur, Radicaux sulfates, Plasma d'air humide, Radicaux hydroxyles

ملخص

تهتم هذه الدراسة بتطبيق عمليتين من عمليات الأكسدة المتقدمة: تنشيط الأنواع المؤكسدة غير العضوية، وتحديدًا بيرسلفات والبلازما الهوائية الرطبة من نوع غليدارك، لمعالجة محلول مائي يحتوي على صبغة "برتقالي جي" تم استخدام التحليل الطيفي للأشعة فوق البنفسجية-المرئية لمراقبة تحلل الملوث، بينما تم تتبع التمعدن من خلال قياس الطلب الكيميائي على الأكسجين.

في البداية، تم تقييم عملية الأكسدة القائمة على الجذير الكبريتي ، الذي يتم توليده عن طريق التنشيط الحراري و التنشيط عند طريق الحديد الثنائي والحرارة في آن واحد للبرسلفات تم دراسة عدة عوامل تؤثر على هذه العملية، بما في ذلك درجة حرارة التفاعل (20–70 درجة مئوية)، الأس الهيدروجيني (2–12)،التركيز الابتدائي لصبغة برتقالي جي (10–70 ملغ/لتر)، وتركيزبرسلفات الأمونيوم وبيرسلفات البوتاسيوم ،(100–1000ملغ/لتر)، تركيز كبريتات الحديد (10–50 ملغ/لتر) و كذلك تر كيز كبريتات الأمونيوم و الحديد الثنائي (8–100 ملغ/لتر)،كما تم دراسة تأثير الإضافات العضوية لتحديد تأثيرها على كفاءة العملية.

أظهرت النتائج أن أكسدة برتقالي جي تتبع نموذجًا حركيًا من شبه الدرجة الأولى، مع معامل ارتباط عالٍ يقارب 0,99 كما أنه قد تم تحقيق إزالة اللون كليا ل50 مع/لتر من البرتقالي جي في وجود 1غرام/لترمن البرسيلفات وذلك خلال 150 دقيقة عند 70 درجة مئوية و خلال 240 دقيقة عند 65 درجة مئوية كما قد تم تقديرتم تقدير طاقة التنشيط الظاهرة لتكون 157,3 كيلوجول/مول علاوة على ذلك، تشير النتائج إلى وجود علاقة ارتباط مباشرة بين أكسدة صبغة البرتقالي جي وتركيزات عالية من البيرسلفات، في حين لوحظت علاقة عكسية مع التركيزات الأولية للركيزة. كما تم العثور على أن درجات حرارة التفاعل المرتفعة والأس الهيدروجيني الابتدائي المحايد تفضل تحلل برتقالي جي.

تشير النتائج إلى أن الجذير الكبريتي هو العامل الرئيسي المسؤول عن أكسدة برتقالي جي. بالإضافة إلى ذلك، أظهر وجود أيونات الكروم السداسي في المحلول تأثيرًا مثبطًا على عملية التحلل. كما ان التواجد التفعيل الثنائي لشوارد السيلفاط بواسط

Abstract

الحرارة والحديد الثنائي أظهر تأثيرا تآزري، مما سرع من عملية أكسدة الملون ولكن معدل التمعدن انخفض نسبيا إلى 75,41بالمئة.

علاوة على ذلك، تم دراسة تحلل برتقالي جي في المحلول المائي باستخدام عملية البلازما الهوائية الرطبة من نوع غليدارك. تم إدخال تركيزات مختلفة من المحفزات والمؤكسدات إلى مفاعل غليدارك لتحسين الظروف وتحسين أداء النظام. في ظل ظروف العلاج المثلى، كانت معدلات التحلل التي تم الحصول عليها 66.46%، 100%، 72.79%، 71.19%، 90.48% و90.27%، باستخدام غليدارك فقط، غليدارك/ماء أكسيجيني، غليدارك/حمض البريوديك، غليدارك/الحديد الثلاثي، غليدارك/ فنتون، غليدارك/برسيلفات، على التوالي، بعد أوقات معالجة بلغت 210 دقيقة، 80 دقيقة، 210 دقيقة، 210 دقيقة، 12 دقيقة، و180 دقيقة. علاوة على ذلك، تم حساب كفاءة الطاقة لتحلل الملوث لتكون 0.022 غرام/ك.و.س، 0.0054 غرام/ك.و.س، و0.004 غرام/ك.وس لعمليات غليدارك/ فنتون، غليدارك/ برسيلفات، وغليدارك فقط.

الكلمات المفتاحية:

عملية الأكسدة المتقدمة، برتقالي جي، بيرسلفات المنشط حراريًا، الجذور الكبريتية، البلازما الهوائية الرطبة، الجدور الهيدروكسلية

Table of contents

Chapter II: Experimental Procedures and Analysis Methods

Chapter III: Elimination of Orange G dye by Heat-activated persulfate process and Heat/Metal Co-Activated persulfate process

Chapter IV: Elimination of Orange G Dye using Non-Thermal Plasma - Gliding-Arc Discharge

List of Tables

Chapter I

Chapter II

Chapter III

Chapter IV

List of Figures

Chapter I

Chapter II

Chapter III

Chapter IV

List of Schemes

Chapter I

Abbreviations

°C	Degrees Celsius
µM	Micromole
λ	Wavelength
hν	The energy of incident photons
ε	Molar extinction coefficient
AOPs	Advanced oxidation processes
COD	Chemical oxygen demand
C	Substrate concentration
C_0	Substrate concentration at time t=0
C_t	Substrate concentration at time t
ENH	Normal hydrogen electrode
GAD	Gliding arc discharge
ISCO	In situ chemical oxidation
K_{app}	Apparent rate constant
mm	Millimetre
mM	Millimole
MPs	Micropollutants
NTP	Non-thermal plasma
OG	Orange G
pH	Hydrogen potential
PDS	Peroxydisulfate
PMS	Peroxymonosulfate
PS	Persulfate
ROS	Reactive oxygen species
RNS	Reactive nitrogen species

SR-AOP	Sulfate radical-based advanced oxidation process
T	Temperature
TAP	Thermal activation of persulfate
UV	Ultraviolet

INTRODUCTION

I. INTRODUCTION

Water resource contamination, primarily caused by the discharge of untreated effluents, poses a significant environmental challenge. These effluents from various industrial activities contain substances harmful to human health and aquatic ecosystems. Although present at low concentrations, these substances can become particularly toxic when accumulated in living organisms, creating chronic risks for exposed populations [1].

Industrialisation, especially in the chemical, pharmaceutical, and agro-industrial sectors, released numerous chemical pollutants into aquatic environments, such as pesticides, antibiotics, steroid hormones, and organic dyes. These substances, often resistant to biodegradation, threaten the natural balance and public health [2]. Dyes, used in various industries (textiles, plastics, leather, etc.), are of particular concern. Approximately 106 tonnes of commercial dyes are produced worldwide each year, with 5 to 10% being lost in industrial effluents, at concentrations ranging from 10 to 10,000 mg/L [3,4]. These dyes degrade water quality, hinder photosynthesis, and slow the growth of aquatic organisms. They may also pose human health risks, such as allergies, irritations, and toxic or even carcinogenic effects [5].

Authorities and industries must, therefore, develop efficient and cost-effective treatment technologies to eliminate these dyes before their release into aquatic environments to meet environmental standards and protect biodiversity. However, conventional water treatment plants cannot effectively remove these micropollutants, as biological processes are not suited to this type of contamination. Moreover, although useful, conventional treatment methods such as coagulation-flocculation, precipitation, adsorption, and ultrafiltration are non-destructive and generate sludges and concentrates that require further treatment [6,7].

In this context, advanced oxidation processes (AOPs) emerge as a promising solution. These processes, which rely on generating highly reactive radicals such as hydroxyl radicals and sulfate radicals, allow the complete mineralisation of organic contaminants into CO_2, H_2O, and mineral salts. AOPs include homogeneous chemical processes (such as Fenton's reagent, ozonation, peroxonation, etc.), photochemical processes (such as H_2O_2 photolysis, heterogeneous photocatalysis, and photo-Fenton, etc.), electrochemical processes (such as anodic oxidation and electro-Fenton), processes based on the activation of persulfates/peroxomonosulfates, and discharge-based processes (e.g., humid air plasma).

Among these processes, the activation of persulfates, which generates sulfate radicals, has garnered increasing interest. Various methods can achieve this activation, including thermal energy or transition metals. These techniques offer notable advantages, particularly their efficiency and environmental friendliness. Furthermore, discharge-based processes, particularly Glidarc plasma, are increasingly used to depollution liquid effluents due to their ability to remove recalcitrant organic pollutants effectively.

This study aims to evaluate the potential of advanced oxidation processes, specifically the activation of persulfates and humid air Glidarc plasma, to remove an azo dye commonly used in the textile industry: Orange G.

This thesis is structured into four chapters: The first chapter provides a literature review on textile dyes and their environmental impact. A summary of wastewater treatment methods is then presented, focusing on advanced oxidation processes (AOPs). The second chapter outlines this study's analytical techniques, products, and experimental protocols. The third chapter first presents an investigation into the operational conditions for the degradation of the substrate via thermal activation of persulfates, followed by the analysis of the results obtained. Next, the results of the co-activation of persulfates using thermal and metallic methods for decolourising Orange G will be presented and discussed. Finally, the last chapter examines the results obtained from the study of the degradation of Orange G by humid air Glidarc plasma. The combination of plasma with ferric ions, as well as the effect of the presence of different oxidising species, is also investigated.

Bibliographical References

1. Chamekh Hayet. Élimination des composés organiques récalcitrants par les procédés d'oxydation avancés (POAs) en milieu aqueux [Thesis]. [Algeria]: University of 20 August1955 Skikda.

2. Donia AM, Atia AA, Al-amrani WA, El-Nahas AM. Effect of structural properties of acid dyes on their adsorption behaviour from aqueous solutions by amine modified silica. J Hazard Mater. 2009 Jan;161(2–3):1544–50.

3. Figueroa S, Vázquez L, Alvarez-Gallegos A. Decolorizing textile wastewater with Fenton's reagent electrogenerated with a solar photovoltaic cell. Water Res. 2009 Feb;43(2):283–94.

4. Sanromán MA, Pazos M, Ricart MT, Cameselle C. Decolourisation of textile indigo dye by DC electric current. Eng Geol. 2005 Mar;77(3–4):253–61.

5. Gan G, Liu J, Zhu Z, Yang Z, Zhang C, Hou X. A novel magnetic nanoscaled Fe3O4/CeO2 composite prepared by oxidation-precipitation process and its application for degradation of orange G in aqueous solution as Fenton-like heterogeneous catalyst. Chemosphere. 2017 Feb;168:254–63.

6. Rodriguez S, Vasquez L, Costa D, Romero A, Santos A. Oxidation of Orange G by persulfate activated by Fe(II), Fe(III) and zero valent iron (ZVI). Chemosphere. 2014 Apr;101:86–92.

7. Arvaniti OS, Ioannidi AA, Politi A, Miserli K, Konstantinou I, Mantzavinos D, et al. Dexamethasone degradation in aqueous medium by a thermally activated persulfate system: Kinetics and transformation products. J Water Process Eng. 2022 Oct;49:103134.

CHAPTER I

Literature Review

I. WATER POLLUTION

Water pollution is defined by the physical, chemical, biological, or bacteriological degradation of its natural qualities due to various inadequately treated wastes from human activities. Among these is the waste generated by the aqueous effluents of the textile industries, specifically azo dyes, which constitute the majority of dyes used in these industries and are responsible for pollution once discharged into the waters.

II. AZO DYES

II.1. Generalities

Azo dyes are characterised by one or more azo groups $(-N \equiv N -)$ linking two radicals that can be aryl or alkyl[1]. The azo group can be associated with benzene rings, naphthalenes, aromatic heterocycles, or enolisable aliphatic groups[2]. Depending on the number of azo groups in a single dye molecule, they are classified as monoazo, diazo, triazo, and polyazo[3]. Thanks to the simplicity of their synthesis procedures, great structural diversity, high molar extinction coefficient, and medium to high stability properties in light and humidity, azo dyes currently represent the largest group of organic dyes produced in the world[4]. **Scheme I.1** presents the general chemical structure of a dye, where the azo bonds, along with the chromophores and auxochromes to which they are linked, define the specific colour of azo dyes[5].

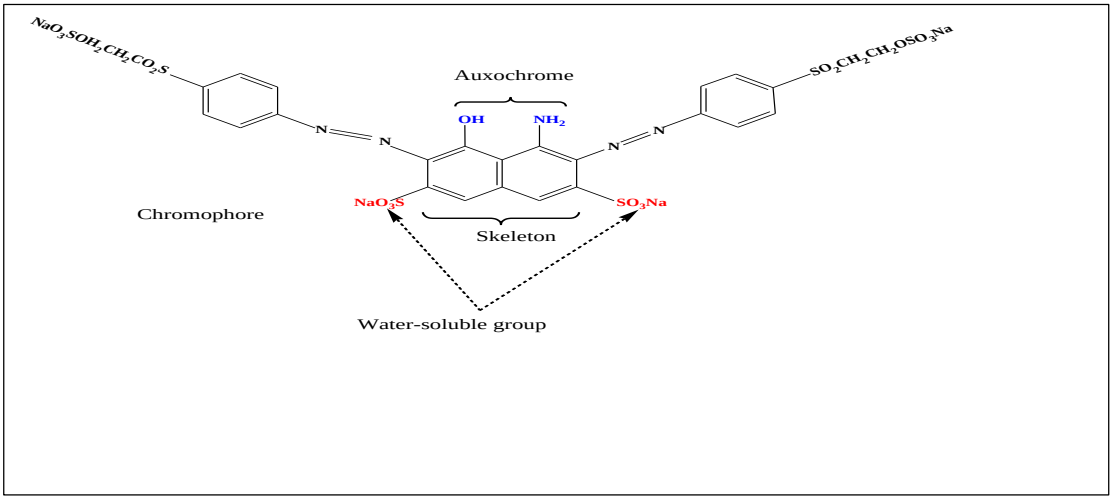

Scheme I.1. Structure of the azo reactive dye.

The different substitutions of aromatic rings lead to variations in the degree of conjugation of the system in azo dyes, which explains the molecule's ability to absorb light in the visible region, hence the colour variations[6,7]. Azo dyes come in various bright colours, such as yellow, orange, red, green, and blue[8]. These dyes have different absorption spectra and are associated with an electronic transition between molecular orbitals[3].

II.2. Synthesis of azo dyes

II.2.1. Chemical synthesis through the diazotisation/coupling reaction

The diazotisation/azo coupling reaction is one of the most critical reactions in the development of industrial organic chemistry**.** The process of this synthesis is based on two steps[9] illustrated in **Scheme I.2** :

The first involves treating a diazo component, a primary amine ($Ar-NH_2$), with nitrite in an acidic medium at 0-5°C. To form a diazonium salt ($ArN_2^+Cl^-$), which is relatively unstable, it is necessary to use it immediately in the coupling reaction.

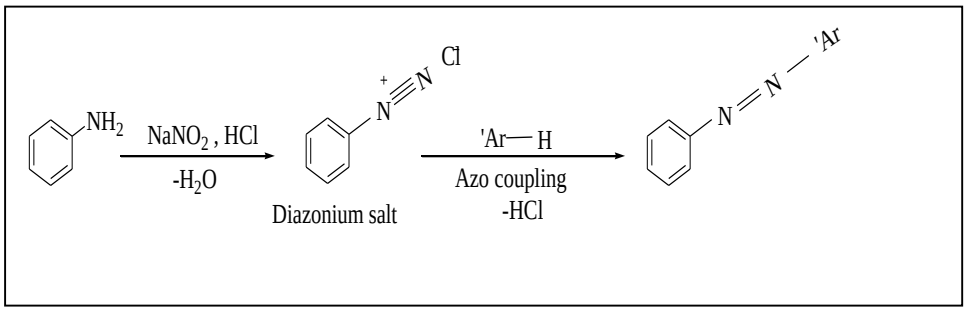

Scheme I.2. Diazotation and azo coupling.

The second step of the azo dye synthesis involves a reaction between the diazonium salt and a coupling component, which can be a phenol, an aniline, or a β-ketoacid derivative. **Scheme I.3** shows how methyl yellow, orange, yellow, and red azo dyes are synthesised.

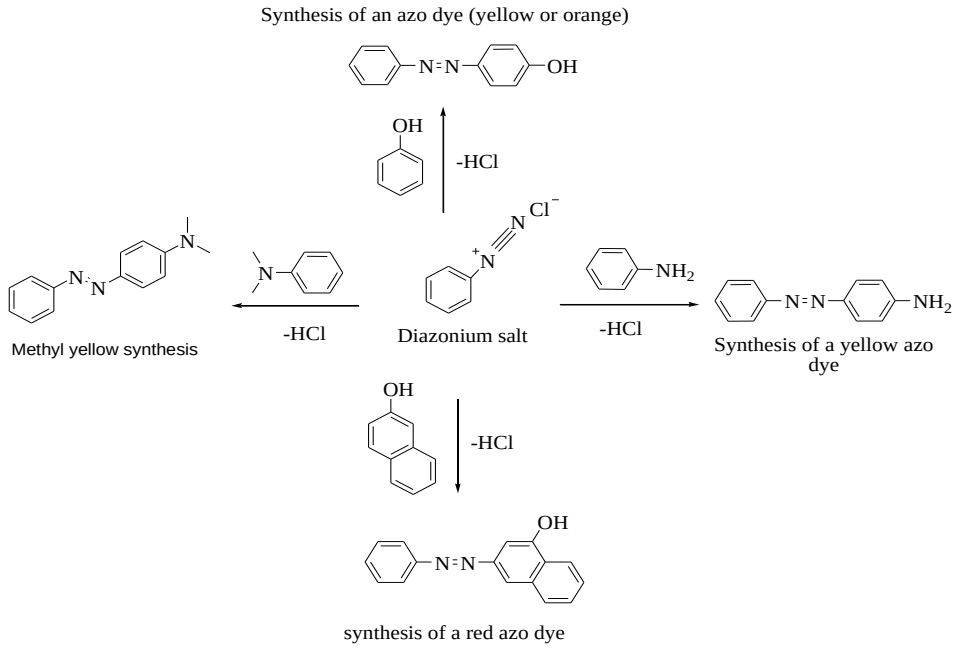

Scheme I.3. Diazo coupling reactions

II.3. Use of azo dyes and their impact on the environment and human health

Azo dyes constitute the largest category of synthetic aromatic dyes, with around 3,000 dyes classified as acid dyes, basic dyes, direct dyes, disperse dyes, mordant dyes, reactive dyes, and solvent dyes; of great commercial interest, they are primarily used by the textile, leather tanning, cosmetics, food, and paper production industries[3,4,10,11].

Due to their synthetic nature and predominantly aromatic structure, most azo dyes are water-soluble and non-biodegradable[3]. Their toxic degradation by-products, mainly benzidines and their derivatives, as well as aniline, nitrosamines, and dimethylamine, easily penetrate aquatic organisms and can increase the dissolved oxygen demand of receiving waters, threatening marine life and overall water quality[12]. Through the food chain, these dyes reach humans, and contact with the skin or inhalation poses a risk of cancer, mutations, or causes allergies, dermatitis, skin irritations, dysfunctions of the kidneys, liver, brain, reproductive system, and central nervous system[13–15]. The toxic effects of certain azo dyes are listed in **Table I.1**

Table I.1. The poisonous effect of some azo dyes[4,16].

Azo dye	Toxic effect	Field of application
Acid Violet 7	Cause lipid peroxidation, chromosomal abnormalities and acetylcholinesterase in mice.	Medicine, food, printing on paper, cosmetics and, in particular, the textile and tanning industries[17].
Acid Orange 7	It causes eye, skin, and respiratory tract irritation and long-term toxicity for aquatic life.	Textile industries[18].
Direct Black 38	Carcinoma of the human urinary bladder.	Textile, food and pharmaceutical industries[19].
Methyl Orange	Mutagenic and harmful to aquatic life.	Indicators in various fields[20].
Reactive brilliant Red	Inhibits human serum albumin function.	Textile dyeing factories[21].
Reactive Black 5	It can cause allergies, breathing difficulties or asthma and reduce urease activity.	Industrial dyeing[22].
Congo Red	It may cause severe allergic reactions, anaphylactic shock, and carcinogenic effects.	The textile, printing, paper, leather and plastics industries[20].

II.4. Environment legislation

Azo dyes are subject to strict regulations due to their potential ecotoxicological effects and to minimise their harmful impact on the environment.

Arylamine-based azo dyes have been banned in the United Kingdom (UK) since 1967 and subsequently in the United States (USA)[23].

The European Union (EU) has banned 22 aromatic amines generated by specific azo dyes in products likely to come into direct or prolonged contact with the human skin or oral cavity

following Directive76/769/EEC, which deals with ‘prohibitions on the use and marketing of certain dangerous substances and preparations[24].

Environmental legislation in Algeria is defined by Law 06-141 of 19 April 2006 on the discharge of industrial liquid effluents. This law sets out the specifications for liquid discharges. **Table I.2** shows the Algerian regulatory limits for liquid effluents from specific industries [25].

Table I.2. Limit values for industrial effluent discharge parameters[25].

Type of industry	Parameters	Unit	Limit values	Tolerance to limit values of old installation
Textiles	Temperature	°C	30	35
	pH	-	6.5-8.5	6-9
	BOD_5	mg/L	150	200
	COD	mg/L	250	
	Decantable matter	mg/L	0.4	300
	Undissolved matter	mg/L	30	0.5
	Oxidability	mg/L	100	40
	Permanganate	mg/L	20	120
				25
Tannery and leather goods	BOD_5	mg/L	350	400
	COD	mg/L	850	1000
	Suspended matter	mg/L	400	500
	Total chromium	mg/L	3	4

III. TREATMENT METHODS FOR AQUEOUS EFFLUENTS

Due to population growth and the intensification of industrial activities, including the increased use of synthetic organic compounds such as dyes, the world is experiencing freshwater shortages. This has led communities to protect the environment by treating aqueous effluents before discharging them into the environment. Several techniques at different technological levels exist to eliminate these pollutants from wastewater. The initial implementations were those known as conventional methods.

III.1. Conventional methods

III.1.1. Physical methods

Physical or mechanical operations are mainly used to transfer pollutants from one aqueous medium to another, such as a solid adsorbent, a membrane, etc. These methods are used to carry out preliminary treatment of raw water. Physical processes include:

III.1.1.1. Adsorption

This technique involves transferring a pollutant from the liquid phase to an adsorbent with specific properties that favour the adsorption of the pollutant. Activated carbon is widely favoured because of its great capacity to adsorb molecules[26]. However, it has limitations in specific categories of dyes (cationic dyes, mordant dyes, disperse and reactive dyes) and in specific pH ranges[27].

III.1.1.2. Membrane technology

It is a technique for selectively separating liquid phases based on the principle of permeation through a permeable membrane under the effect of a transfer force, in this case, a pressure difference on either side of the membrane[28]. The nature of the membrane varies, and its application to water treatment is highly dependent on it. There are porous membranes (microfiltration and ultrafiltration), dense membranes (reverse osmosis), and ion exchange membranes[28]. For example, reverse osmosis can be used to desalinate seawater and produce ultra-pure water, while the other membrane processes are used pre- or post-treatment[29,30].

III.1.1.3. Coagulation and Flocculation

These physicochemical operations involve destabilising and precipitating suspended particles by injecting chemicals (coagulants and flocculants) that promote agglomeration and facilitate sedimentation. Hydrolytic aluminium and iron salts are the most commonly used coagulants[31]. The effectiveness of this method is influenced by various factors such as type and dosage of coagulant/flocculant, pH, temperature, retention time, mixing duration and speed[32]. However, this technique generates large quantities of sludge at the end of the treatment, requiring additional investments to manage it.

III.1.2. Biological methods

Biological treatment processes are based on the microbial biotransformation of pollutants. They use bacteria, algae, fungi, and yeasts to remove contaminants from the environment[33]. Although these methods are suitable for a wide range of organic pollutants, they are not always applicable to industrial effluents, such as those from the textile industry, because of the high concentrations of contaminants, the toxicity that can lead to the death of microorganisms or their non-biodegradability. In addition, these techniques generate large quantities of biological sludge that require further treatment.

III.1.3. Chemical methods

Chemical oxidation techniques are generally applied when biological processes are ineffective or as a pre-treatment for biological processes. Chemical oxidation is also used to treat hazardous organic compounds in low concentrations and effluents resistant to biodegradation methods. Potassium permanganate, chlorine, ozone, hydrogen peroxide, Fenton's reagent and chlorine dioxide are the reagents used in this type of oxidation, with hydrogen peroxide, ozone and chlorine being the most commonly used. This classic oxidation process allows organic products to be oxidised into water and carbon dioxide or other easily biodegradable products such as alcohols, aldehydes, ketones and carboxylic acids; however, in certain cases, this system is not sufficient to completely decompose organic pollutants[34], either because of slow kinetics, because some pollutants are refractory, or because oxidation remains partial and leads to the formation of intermediates that are more toxic than the initial

pollutant. In these cases, we call on emerging advanced oxidation technologies, which are even more effective, based on the in situ formation of radical oxidising species.

III.2. Advanced oxidation process

Advanced oxidation processes were first developed by Glaze et al. in 1987 for treating wastewater at ambient temperature and pressure[35,36]. Since then, AOPs have been extensively researched as environmentally friendly methods for their ability to disinfect and treat contaminants and have become very attractive in recent years (**Figure I.1**).

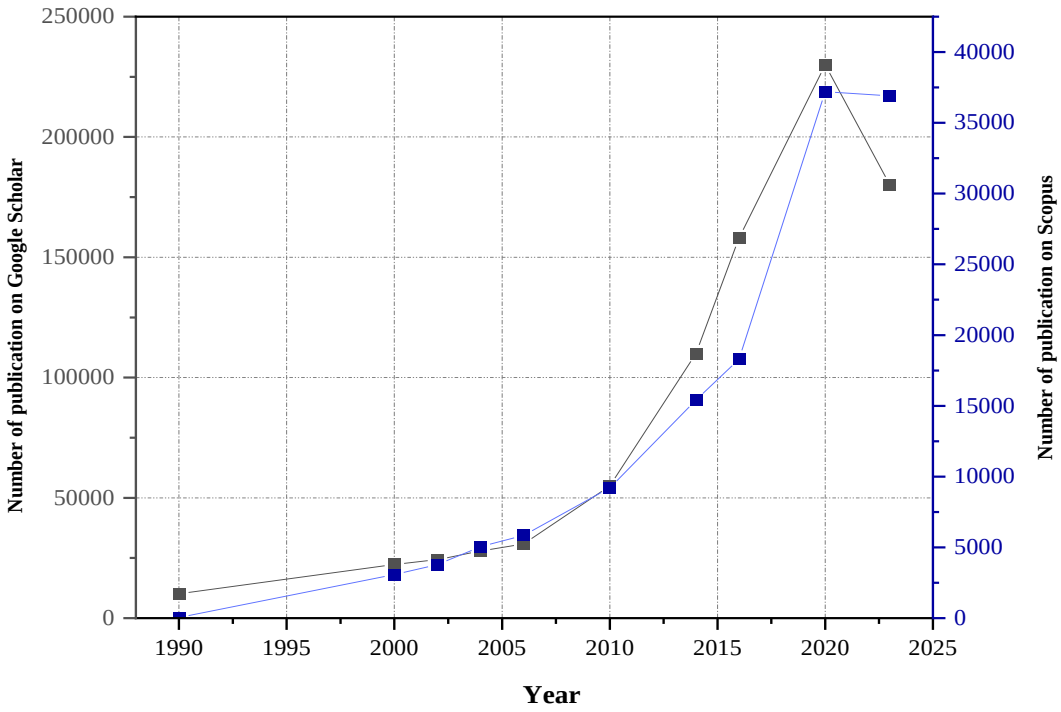

Figure I.1. Trends in annual publications concerning the use of advanced oxidation processes in water treatment on the Google Scholar and Scopus databases. Consulted on 02/10/2024.

The advanced oxidation process (AOP) is an innovative technology based on the in situ formation of reactive oxygen species to degrade organic pollutants, with the main aim of completely mineralising them into CO_2, H_2O and harmless end products. Reactive oxygen species are free radicals that possess at least one unpaired electron, including the hydroxyl radical ($HO^{\bullet}$), the sulfate radical ($SO_4^{\bullet -}$), the carbonate radical (CO_3^{-}), and others and are responsible for the oxidation process[37].

A series of steps define the functioning of the advanced oxidation process[38]:

- The first is a preliminary step involving forming reactive species with a high reduction potential through an oxidation reaction using either a catalyst, an application of energy or a chemical reaction.
- The second step reveals the reaction between the formed radical species and the organic pollutant to form a biodegradable intermediate compound.
- The final step consists of the oxidation of the intermediate compounds and their transformation into stable inorganic compounds (complete mineralisation).

Table I.3 shows the reduction potential of certain oxidants. The reduction potential measures the tendency of a given chemical species to be reduced and to oxidise other species. The higher the potential, the greater the acceptor's affinity for electrons. In fact, the higher an oxidant's potential, the more powerful it is.

Table I.3. Redox potential of various oxidants

Oxidising agent	Oxidation potential E°(V/ENH)
Fluorine (F_2)	3.03
Hydroxyl radical ($HO^{\bullet}$)	2.8
Sulfate radical ($SO_4^{\bullet -}$)	2.6
Atomic oxygen (O)	2.42
Ozone (O_3)	2.07
Persulfate ion ($S_2O_2^{2-}$)	2.01
Hydrogen peroxide (H_2O_2)	1.77

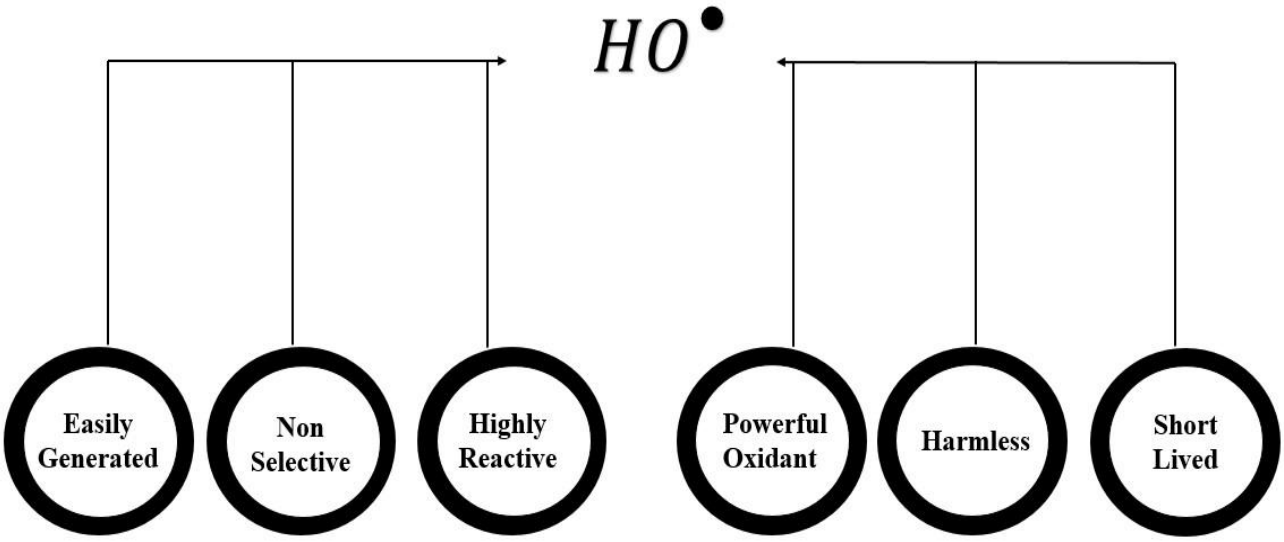

Scheme I.4. Description and characteristics of HO•.

III.2.1. Hydroxyl radicals

Hydroxyl radicals are reactive oxidising agents made when a covalent bond breaks homolytically. They have a high oxidation potential of 2.8 V/ENH, positioning it as the second most reactive oxidant known when compared to other reactive oxygen species (**Table I.3**). In addition to its high reduction potential, the hydroxyl radical (HO•) has several advantages (as illustrated in **Scheme I.4**). Some of its essential characteristics include:

- The ability to rapidly attack, with a rate constant generally between 10^6 and 10^9 $M^{-1}s^{-1}$, and non-selectively recalcitrant pollutant species in water by processes such as hydrogen abstraction, radical addition, and electron transfer[39,40].
- It is an eco-friendly and harmless oxidant that can be easily produced using various methods[37].
- Additionally, HO• has a short lifetime of a few nanoseconds in water, leading to its self-elimination from the treatment system[41].

III.2.1.1. Hydroxyl radical oxidation mechanism

The nature of the polluting substrate can vary, including its aliphatic or aromatic structure, its saturation or unsaturation, and the presence of activating and/or deactivating groups, which is why hydroxyl radicals ($HO^{\bullet}$)react with them using three main mechanisms [36,42]:

- **Hydrogen abstraction:**

The reaction where a hydroxyl radical ($HO^{\bullet}$) removes a hydrogen atom by the homolytic cleavage of a C-H band from a saturated aliphatic compound (R-H), resulting in the formation of a new organic radical ($R^{\bullet}$)

$$HO^{\bullet} + RH \rightarrow R^{\bullet} + H_2O \qquad \text{(I.1)}$$

- **Electrophile addition:**

The hydroxyl radical ($HO^{\bullet}$) acts as an electrophile, reacting with the π-bond of an unsaturated organic molecule or aromatic to give hydroxyalkyl or cyclohexadienyl radicals.

$$HO^{\bullet} + ArX \rightarrow HOArX^{\bullet} \qquad \text{(I.2)}$$

- **Electron transfer:**

Reactions can occur when the compound contains halogen substituents or steric hindrance that prevents electrophilic addition or hydrogen atom abstraction reactions. In that case, the hydroxyl radical (HO•) acts as an oxidant and is reduced to hydroxide (OH^-).

$$HO^{\bullet} + RX \rightarrow RX^{\bullet +} + OH^- \qquad \text{(I.3)}$$

III.2.2. Classification of the AOP process

As reported in the literature, Advanced Oxidation Processes (AOPs) are classified based on the production method of hydroxyl radicals, depending on the type of energy applied (e.g., light, ultrasound, electricity) and the chemical agents used (e.g., H_2O_2, O_3, persulfate ion, iron salts). The classification of AOPs can be broadly categorised into chemical oxidation, photochemical, electrochemical, sonochemical, sulfate radical-based AOPs, plasma-based AOPs, and some other types of AOPs such as catalytic wet air oxidation, supercritical water oxidation, carbonate radical-based AOPs, and combined AOPs[37,43]. **Scheme I.5** illustrates the classification of non-conventional oxidation processes.

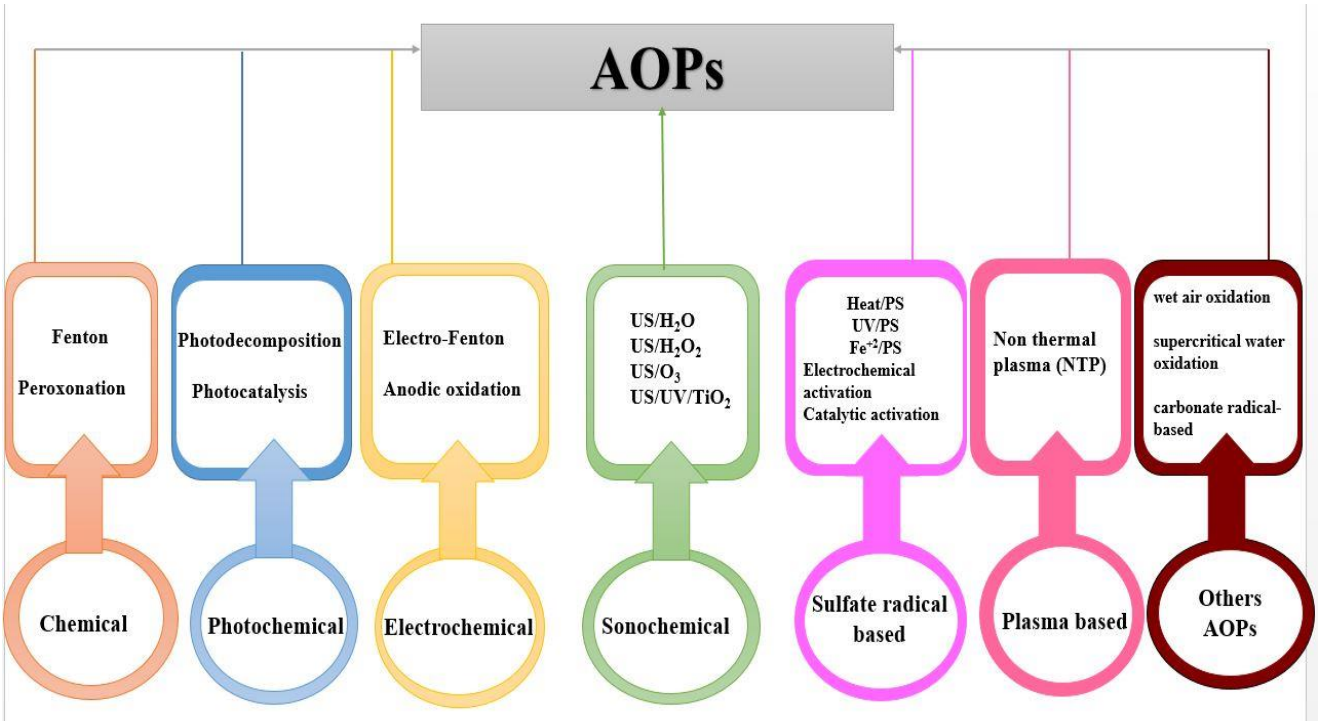

Scheme I.5. Classification of the AOP process.

III.2.2.1.Chemical oxidation

Chemical oxidation is the process of using powerful reagents like hydrogen peroxide (H_2O_2), ozone (O_3), and chlorine dioxide(ClO_2) to reduce residual COD, non-biodegradable compounds, and trace organic compounds[44].

III.2.2.1.1. Fenton's process

It is among the oldest Advanced Oxidation Processes (AOPs). First developed in 1894 by **H.J.H. Fenton**, it was reported that ferrous salts could activate hydrogen peroxide to oxidise tartaric acid. In 1930[45], **Haber and Weiss** demonstrated that the decomposition proceeded through a complex chain reaction[35].

The Fenton process generally involves the reaction of hydrogen peroxide (H_2O_2) with iron ions (Fe^{2+}) according to **Equation I.4** in an acidic medium to produce a potent oxidising agent, namely the hydroxyl radical($HO^{\bullet}$), which subsequently degrades the pollutants[46,47].

$$Fe^{2+} + H_2O_2 \longrightarrow Fe^{3+} + OH^- + HO^{\bullet} \qquad k=40\text{-}80\ M^{-1}\ s^{-1} \qquad (I.4)$$

In a cyclic mechanism, the generated ferric ions (Fe^{3+}) can be reduced by reacting with an excess of hydrogen peroxide to regenerate ferrous (Fe^{2+}) ions (**Equation I.5**).

$$Fe^{3+} + H_2O_2 \longrightarrow HOO^{\bullet} + Fe^{2+} + H^{+} \qquad k=9.1\times10^{-7}\ M^{-1}\ s^{-1} \qquad (I.5)$$

This reaction is referred to as a Fenton-type reaction. It is kinetically slower than the Fenton reaction. The reaction indicates that this process also generates hydroperoxyl radicals ($HOO^{\bullet}$), which exhibit lower reactivity than hydroxyl radicals.

The Fenton process's efficiency heavily depends on various factors such as temperature, medium pH, catalyst concentration, and H_2O_2. It also depends on the optimal molar ratio between the iron ions and hydrogen peroxide, which must be determined experimentally to avoid scavenging[46].

III.2.2.1.2. Peroxone process

The Peroxone process is an Advanced Oxidation Process (AOP) that generates hydroxyl radicals ($HO^{\bullet}$) through the interaction of two strong oxidising agents, ozone and hydrogen peroxide, for pollutant remediation. This process was initially identified by Hoigné and Staehelin in their significant pioneering research[48]. The researchers determined that the reaction progresses as hydrogen peroxide in aqueous solution dissociates into protons and hydroperoxide ions (**Equation I.6**). Subsequently, the hydroperoxide ions react with ozone, leading to its decomposition. The overall reaction can be summarised as follows[48,49]:

$$H_2O_2 \leftrightarrow HO_2^{-} + H^{+} \qquad (I.6)$$

$$H_2O_2 + O_3 \longrightarrow HO^{\bullet} + O_2^{-} + O_2 \qquad (I.7)$$

The Peroxone technique treats wastewater discharged from various industries. A hybrid method, such as incorporating a catalyst or an energy source (e.g., UV light, electricity), could improve the treatment's efficiency.

III.2.2.2. Photochemical oxidation

Photochemistry is a branch of chemistry that studies the chemical reactions resulting from the absorption of ultraviolet, visible, or infrared light, focusing on the absorption of light energy[50]. This can be grouped as follows:

III.2.2.2.1. Photodecomposition

Photolysis, also known as photodecomposition, is a chemical process in which photons, alone or in combination with strong oxidants like H_2O_2 and O_3, break down an inorganic or organic chemical[51].

III.2.2.2.1.1. Direct photolysis

UV/Photolysis is a method that uses UV irradiation, devoid of oxidants and catalysts, to decompose pollutants into smaller molecules. The water molecule is dissociated under UV irradiation, yielding hydrogen and hydroxyl radicals[52]. The following equations can schematise the pollutant's photolysis reaction.

$$Pollutant \xrightarrow{h\upsilon} Pollutant^* \qquad \text{(I.8)}$$

$$Pollutant^* \xrightarrow{h\upsilon} Photoproduct \qquad \text{(I.9)}$$

This process is less effective than others involving combining radiation with hydrogen peroxide or ozone or using homogeneous or heterogeneous photocatalysis[53].

III.2.2.2.1.2. Photolysis of hydrogen peroxide (UV/H_2O_2)

The UV/H_2O_2 process initiates with the decomposition of hydrogen peroxide under UV radiation, absorbed at the 185–400 nm wavelength range, especially in the shorter range of 200–300 nm, which activates and cleaves the O—O bond of H_2O_2[54], forming hydroxyl radicals according to **Equation I.10**.

$$H_2O_2 \xrightarrow{h\upsilon} 2\,HO^{\bullet} \qquad \text{(I.10)}$$

These free radicals then continue to promote the decomposition of H_2O_2 through a series of chain reactions. Next, a series of radical reactions take place [55]:

- Propagation reactions:

$$HO^{\bullet} + H_2O_2 \longrightarrow H_2O + HOO^{\bullet} \qquad \text{(I.11)}$$

$$HOO^{\bullet} + H_2O_2 \longrightarrow HO^{\bullet} + H_2O + O_2 \qquad \text{(I.12)}$$

$$HO^{\bullet} + HO_2^- \longrightarrow HOO^{\bullet} + OH^- \qquad \text{(I.13)}$$

- Termination reactions :

$$2HOO^{\bullet} \longrightarrow H_2O_2 + O_2 \qquad \text{(I.14)}$$

$$HO^{\bullet} + HOO^{\bullet} \longrightarrow H_2O + O_2 \qquad \text{(I.15)}$$

$$2\ HO^{\bullet} \longrightarrow H_2O_2 \qquad \text{(I.16)}$$

The UV/H_2O_2 process is frequently used for groundwater purification and degrading contaminants containing photosensitive compounds[49]. The reaction rate is influenced by various elements, including pH, temperature, pollutant type, the type of UV lamp, the transmittance of the quartz sleeve, the length of the optical path through the reactor medium, the optical properties of the effluent, and the concentration of peroxide to avoid scavenging radicals[49,55]. However, the main constraint of this process is the low absorption coefficient of H_2O_2 (ε = 18.6 L mol^{-1} cm^{-1} at 253.7 nm)[56]

III.2.2.2.1.3. Photolysis of ozone (UV/O_3)

In an aqueous solution, ozone (O_3) has a maximum molar absorption coefficient (ε_{max} = 3600 $L\,mol^{-1}cm^{-1}$) at λ =253.7 nm, while hydrogen peroxide only has a (ε_{max} = 19,7 $L\,mol^{-1}cm^{-1}$) at the same wavelength. This enables ozone to absorb UV light at 253.7 nm more efficiently, leading to a higher generation of hydroxyl radicals ($HO^{\bullet}$) [38,40]. These radicals effectively oxidise and destroy toxic organic compounds in wastewater, as illustrated in the following equations:

- Photolytic dissociation:

$$O_3 + H_2O \xrightarrow{h\upsilon} 2\ HO^{\bullet} + O_2 \qquad \text{(I.17)}$$

- Conversion to peroxyl radical:

$$O_3 + \ HO^{\bullet} \longrightarrow HOO^{\bullet} + O_2 \qquad \text{(I.18)}$$

$$O_3 + HOO^{\bullet} \longrightarrow \ HO^{\bullet} + 2O_2 \qquad \text{(I.19)}$$

- Conversion to harmless products:

$$HO^{\bullet} + HOO^{\bullet} \longrightarrow H_2O + O_2 \qquad \text{(I.20)}$$

Numerous variables, including pH, temperature, traps in the influent, turbidity, UV intensity, the lamp's spectral characteristics, and the type(s) of pollutant in the system, can affect this system's effectiveness. This system has demonstrated its efficiency in eliminating chlorophenols[57,58].

III.2.2.2.2. Photocatalysis

Photocatalysis is a process where light activates a photocatalyst, enhancing the rate of a chemical reaction without being involved in the transformation. It involves semiconductor material absorbing sufficient light energy to facilitate the transfer of electrons from the valence band to the conduction band, forming electron-hole pairs. These pairs generate free radicals that oxidise organic materials and degrade pollutants. Photocatalysis is classified into homogeneous and heterogeneous types, depending on the catalyst phase[59].

III.2.2.2.2.1. Homogeneous photocatalysis

Homogeneous photocatalysis is a process in which a photocatalyst is present in the same phase as the reactants (liquid solution). Transition metal complexes commonly serve as homogeneous photocatalysts due to their stability and appropriate electronic band gap[60]. Processes frequently used by homogeneous photocatalysts include the photo-Fenton process.

III.2.2.2.2.1.1. Photo-Fenton Process (UV/Fe^{+2}/H_2O_2)

The photo-Fenton (Fe^{2+}/H_2O_2/UV-Vis) process improves the traditional Fenton reaction by using light in the ‘near UV to visible’ range, with wavelengths up to 600 nm[61]. This modification solves the problem of the accumulation of Fe^{3+} ions during the Fenton process, which leads to sludge formation. Therefore, this process accelerates the photolytic reduction of ferric ion (Fe^{3+}) to ferrous ion (Fe^{2+})**Equation (I.22)**, which ultimately regenerates the catalyst required for the process, resulting in lower amounts of iron needed for photo-Fenton than Fenton[62,63], The reduction of ferric ion also creates another hydroxyl radical resulting in the hydrogen peroxide being fully converted into two radicals[64]. A simplified mechanism for the process can be described as follows:

$$Fe^{3+} + H_2O \longrightarrow Fe(OH)^{2+} + H^{+} \qquad \text{(I.21)}$$

$$Fe(OH)^{2+} \xrightarrow{h\upsilon} Fe^{2+} + HO^{\bullet} \quad \text{(I.22)}$$

$$Fe^{2+} + H_2O_2 \longrightarrow Fe(OH)^{2+} + HO^{\bullet} \quad \text{(I.4)}$$

$$H_2O_2 \xrightarrow{h\upsilon} 2\ HO^{\bullet} \quad \text{(I.10)}$$

The rate of photo-reduction of Fe^{3+}, as well as the rate of production of the $HO^{\bullet}$radical, depends on the irradiation wavelength and the pH, as each ferric iron species does not exhibit the same photo-reactivity. **Table I.4** presents the quantum yield values for the different species of ferric iron[65,66].

Table I.4. Quantum yield of hydroxyl radical production by UV/visible irradiation of Fe^{3+} solution

λ_{nm}	Species	ε_{max}(L $mol^{-1}cm^{-1}$)	Quantum yield of $HO^{\bullet}$production.
254	Fe^{3+}	1500	0.065
313	$Fe(OH)^{2+}$	2000	0.140
360	$Fe(OH)^{2+}$	400	0.017

The $Fe(OH)^{2+}$ complex has the highest quantum yield (0.14) at 313 nm and dominates under slightly acidic conditions. The photolysis of Fe^{+3} and the Fenton reaction enhances the efficiency of the radical hydroxyl $HO^{\bullet}$ production process. In contrast, the photolysis of H_2O_2 **Equation (I.10)** contributes minimally due to its low absorption of UV and visible light[67], so $Fe(OH)^{2+}$ represents the most reactive species for hydroxyl radical production[68].

The photo-Fenton process has already been used to remove several contaminants and works particularly well on organic recalcitrant substances such as dyes[69], pesticides[70], pharmaceuticals and phenols[71,72].

The precipitation of Fe(III) in water at pH levels above 5 is the main challenge of the photo-Fenton process, necessitating acidic conditions to prevent excessive iron sludge

formation[73]. Organic ligands like EDTA, oxalate, and EDDS have been introduced to improve the process's performance and increase the production of hydroxyl radicals (HO•) [37].

III.2.2.2.2.1. Heterogeneous photocatalysis

Heterogeneous photocatalysis is mainly based on irradiating semiconductor materials with light energy (UV, near-UV, or visible light) to initiate chemical reactions on their surfaces.

The fundamental mechanism of photocatalysis involves the creation of electron-hole pairs, which, upon separation, initiate redox reactions of species adsorbed on the active surface[74]

III.2.2.2.2.1.1. TiO_2 photocatalysis (UV/TiO_2)

Researchers have reported that titanium oxide TiO_2, due to its high stability, wide band gap, and strong ultraviolet absorption, is one the most effective semiconducting photocatalysts and performs best when exposed to UV light. It facilitates the photocatalytic decomposition of organic compounds on its surface in water and air[75,76]. Based on its crystal structure, TiO_2 can exist in three different forms: anatase, rutile, and brookite. While Anatase and rutile have been extensively studied, reports on brookite remain limited[77–80].

Regarding its mechanism, when TiO_2 is exposed to UV light with energy equal to or larger than its band gap energy DE_{bg} (3.0 eV for rutile and 3.2 eV for anatase), an electron is excited from the valance band to the conduction band **Figure I.2.** This excitation creates a positive hole (h_{VB}^+) in the valance band and an electron (e_{CB}^-) in the conduction band. The positive hole (h_{VB}^+) can either oxidise pollutants directly or react with water to produce HO•radicals, while the electron in the conduction band (e_{CB}^-) reduces oxygen adsorbed on a photocatalyst's surface**. Equations (I.23)-(I.28)** represent the abovementioned mechanism[76,80].

$$TiO2 \xrightarrow{h\nu} h_{VB}^+ + e_{CB}^- \quad \text{(I.23)}$$

$$e_{CB}^- + O_2 \longrightarrow O_2^{\bullet -} \quad \text{(I.24)}$$

$$h_{VB}^+ + Organic\ pollutant \longrightarrow Oxidation\ products \quad \text{(I.25)}$$

$$h_{VB}^+ + H_2O \longrightarrow HO^\bullet + H^+ \quad \text{(I.26)}$$

$$HO^\bullet + Organic\ pollutant \longrightarrow Degradation\ products \quad \text{(I.27)}$$

$$e_{CB}^{-} + Organic\ pollutant \longrightarrow Reduction\ products \qquad (I.28)$$

When the reduction process of oxygen and the oxidation of contaminants do not proceed simultaneously during the photocatalytic degradation of pollutants, an electron accumulation occurs in the conduction band, leading to the rapid recombination of electrons and positive holes. Therefore, improving the separation efficiency of photogenerated electrons and holes in a semiconductor catalyst is essential to improve its photocatalytic performance[81].

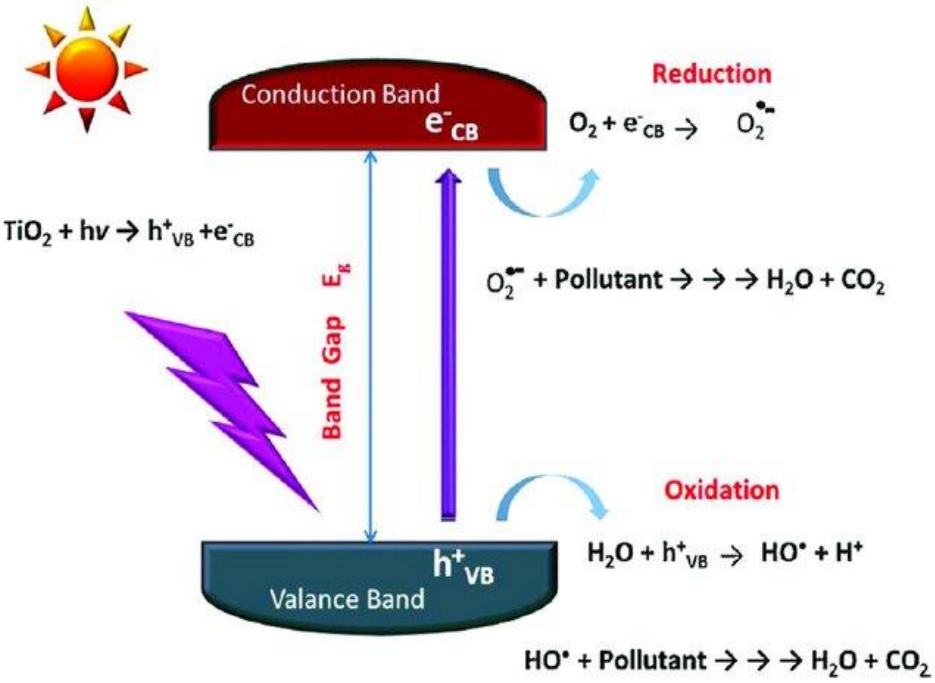

Figure I.2. Schematic illustration of the photocatalytic oxidation of organic compounds in textile wastewater, initiated by photoexcitation of pure TiO_2 under UV light[82].

III.2.2.3. Electrochemical oxidation

Electrochemical oxidation involves applying an electric current or voltage between two electrodes (anode and cathode) that generate hydroxyl radicals or other oxidising agents, depending on the type of anode material and supporting electrolyte used without sludge production [83]. This process can be direct or indirect. In direct electrooxidation, pollutants are degraded directly at the anode by charge transfer reactions. In indirect electro-oxidation, the pollutants are eliminated by reactive species formed during oxidation of the water or electrolytes in the solution [84].

III.2.2.3.1. Electro-Fenton process

The electro-Fenton (EF) process uses electrochemistry as an advanced method to generate and control the Fenton reagent by producing hydrogen peroxide (H_2O_2) directly in solution through a reduction of two-electron oxygen (O_2) in an acidic medium **Equation (I.29)**[85]. In this process, H_2O_2 reacts with iron (Fe^{2+}) to produce hydroxyl radicals($HO^{\bullet}$) that degrade organic pollutants. The regeneration of Fe^{2+} at the cathode ensures a steady supply of $HO^{\bullet}$ **Equation (I.30),** preventing the accumulation of Fenton's reagent and minimising side reactions [86,87].

$$O_2 + 2H^+ + 2é \longrightarrow H_2O_2 \qquad (I.29)$$

$$Fe^{3+} + é \longrightarrow Fe^{2+} \qquad (I.30)$$

The EF process offers several advantages over traditional chemical Fenton systems[88]:

- On-site production of H_2O_2 reduces transport and storage risks.
- Controlled reaction kinetics for precise oxidation and degradation.
- Improved pollutant removal thanks to continuous regeneration of Fe^{2+}.
- Reduced use of chemical reagents and sludge production.
- Cost-effective mineralisation occurs under optimised operating conditions.

The process involves selecting effective cathodic and anodic materials for efficient and sustainable hydroxyl radical generation. It focuses on the practical design of open and undivided electrochemical reactors[88].

III.2.2.3.2. Anodic oxidation process

The anodic oxidation (AO) process is a treatment method for pollutants in which substances near the anode undergo oxidation during electrolysis. Organic pollutants can be oxidised directly on the electrode surface or indirectly through hydroxyl radicals ($HO^{\bullet}$) generated by water oxidation on the anode surface. This process operates via two main mechanisms: direct electron transfer (direct oxidation) and oxidation by reactive species (indirect oxidation)[89].

Several factors influence the AO mechanism, including the type of contaminant, electrode material, electrolyte type, and applied current or voltage. These variables affect the formation and stability of reactive species and the likelihood of secondary oxidant production[90]. A variety of anode materials have been used in the anodic oxidation process, including a metal (Pt)[91,92], metal oxides (RuO_2[93], IrO_2[94], PbO_2 [95] and SnO_2[96]), and carbonaceous materials (BDD[97]).

AO is widely used in wastewater treatment, effectively removing synthetic dyes, phenols, organic pesticides, pharmaceuticals, and resistant pollutants[98].

III.2.2.4. Sonochemical oxidation

Sonochemistry involves chemical reactions induced by powerful ultrasound radiation (20 kHz–10 MHz) via acoustic cavitation phenomena[99,100].

Ultrasound (US) passes through a liquid and forms bubbles from gas nuclei. These bubbles oscillate and can collapse violently, creating localised temperatures of up to 5000 K and pressures in the hundreds of atmospheres[101] **Scheme I.6.**

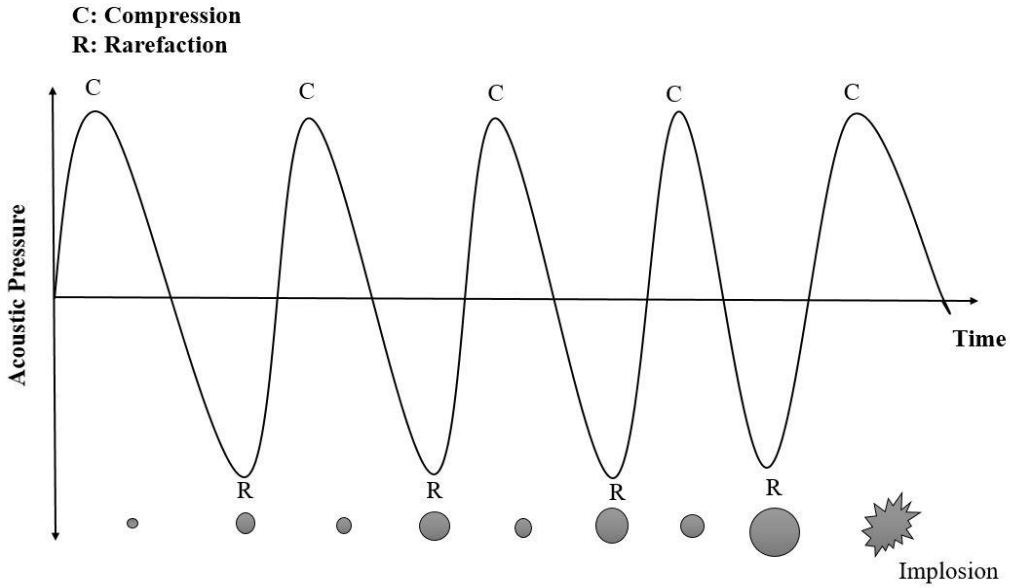

Scheme I.6. Diagram of acoustic cavitation, bubble growth, and cavity implosion.

On the other hand, this extreme environment leads to the thermal dissociation of water vapour, producing reactive hydroxyl radicals ($HO^{\bullet}$) and hydrogen atoms ($H^{\bullet}$) **Equation (I.31)**,

which can form additional radicals in the presence of O_2 and H_2O. In pure water, these radicals typically recombine to form hydrogen peroxide (H_2O_2), while with organic solutes, various reactions occur depending on the solute's characteristics[102,103]. The chemical effects caused by cavitation depend on the specific characteristics of the dissolved gas and solute in the solution.

$$H_2O + US \longrightarrow HO^{\bullet} + H^{\bullet} \qquad \text{(I.31)}$$

According to the "hot spot" theory, sonochemical reactions occur in three zones[104]:

- Within the cavitation bubble, where volatile and hydrophobic molecules undergo pyrolysis.
- At the bubble–liquid interface, where hydroxyl radical reactions dominate.
- In the bulk solution, free radicals migrate from the bubble–liquid interface into the liquid, driving secondary sonochemical reactions.

III.2.2.5. Process based on the sulfate radical

The sulfate radical-based advanced oxidation process (SR-AOP) is an emerging water treatment technology that has attracted attention for its exceptional effectiveness in removing and mineralising pollutants, particularly those resistant to traditional treatment methods[105].

SR-AOP used radical oxidising species (ROS), precisely sulfate radicals ($SO_4^{\bullet -}$), typically generated through the activation of peroxydisulfate (PDS) or peroxymonosulfate (PMS), to degrade organic pollutants effectively. As a result, SR-AOP is considered one of the most promising advanced oxidation processes for water and wastewater treatment[106,107]. **Table I.5** summarises the advantages and disadvantages of sulfate radical-based AOPs.

Table I.5. Advantages and disadvantages of SR-AOP.

Advantages	limitations
The high oxidation power of $SO_4^{\bullet -}$ and $HO^{\bullet}$ The extended half-life of $SO_4^{\bullet -}$ Suitability across a broad pH range Safe storage of oxidant agents on a large scale	High selectivity for oxidation due to $SO_4^{\bullet -}$ Expensive compared to H_2O_2 Risk of generating toxic by-products in the presence of Cl^- and Br^-

III.2.2.5.1. Properties of peroxydisulfate and peroxymonosulfate

Peroxydisulfate (PDS, $S_2O_8^{2-}$), commonly called persulfate (PS), and peroxymonosulfate (PMS, HSO_5^-) are both oxidising agents used in situ Chemical Oxidation (ISCO), which are characterised by an oxygen-oxygen (O–O) bond similar to hydrogen peroxide [108]. **Figure I.3.**

Figure I.3. Chemical structures of $S_2O_8^{2-}$ and HSO_5^-.

PMS is generally a compound salt comprised of potassium hydrogen sulfate, potassium sulfate and potassium peroxymonosulfate in a 1:1:2 ratio[108]. In contrast, PDS contains sulfate ions and cations, exhibiting a longer O-O bond length of 1.497 Å and lower bond energy of 33.5 kcal mol^{-1} compared to PMS, which has an O-O bond length of 1.453 Å[109,110]. The asymmetric structure of PMS results from the substitution of hydrogen atoms in H_2O_2 by SO_3. However, PDS is chemically more stable and has a higher redox potential (E_0=2.01 V compared with E_0=1.77 V for PMS)[107].

Both compounds have gained increasing attention due to their value for water solubility, affordability, ease of storage, and environmental friendliness. **Table I.6** outlines the various properties of peroxymonosulfate (PMS) and peroxydisulfate (PDS). **Figure I.4** shows the evolution of the number of publications on applying persulfate activation in situ chemical oxidation in recent years, based on the results of the Scopus and Google Scholar databases.

Table I.6. Various properties of PMS and PDS.[106,108]

Properties	PDS	PMS
Quantum yield of radical generation	1.8	0.52
Relative absorbance	0.044	0.024
Solubility in water at 25°C ($g.L^{-1}$)	92	377
Estimated lifetime in groundwater	> 5 months	Hours to days
Molecule formula	$K_2S_2O_8$- $Na_2S_2O_8$- $(NH_4)_2S_2O_8$	$KHSO_5$- $KHSO_4$- K_2SO_4

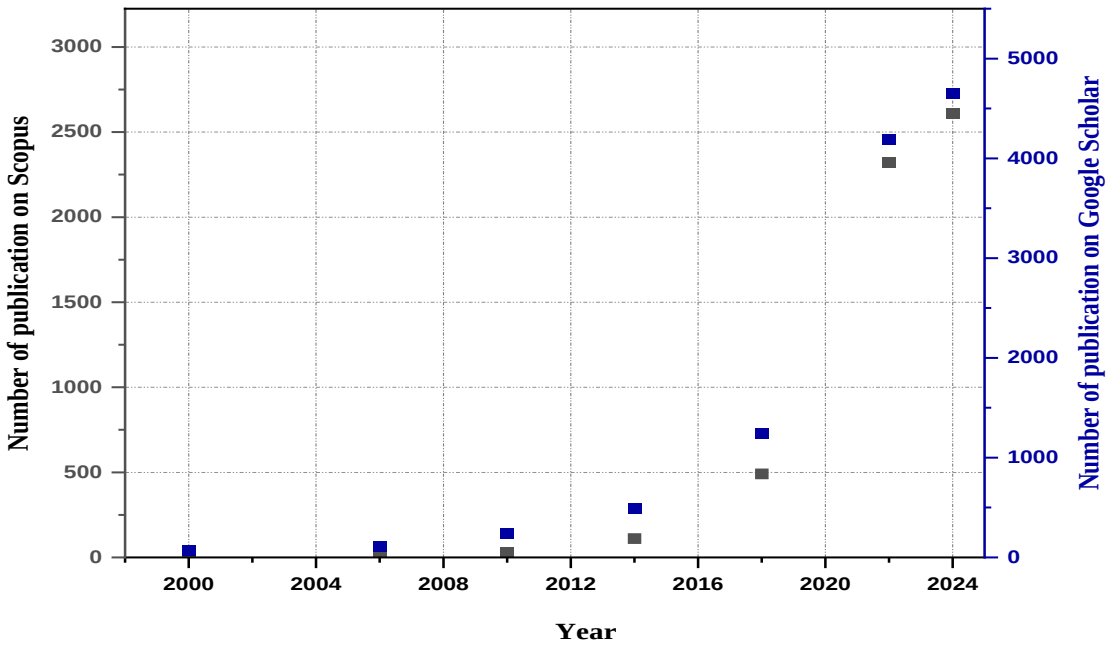

Figure I.4. The yearly evolution in the number of publications searched using the terms 'sulfate radical' and 'persulfate activation in situ chemical oxidation' in the Scopus and Google Scholar databases. Consulted on 17/11/2024.

III.2.2.5.2. Sulfate radicals based AOPs

III.2.2.5.2.1. Definition and general principles

The physicochemical activation of persulfate (PS) can generate sulfate radicals ($SO_4^{\bullet-}$)by dissociating peroxide bonds through energy transfer or one-electron reduction[111]. Sulfate radicals ($SO_4^{\bullet-}$) have attracted significant attention as an oxidising agent for pollutant degradation due to their high acid-base adaptability and selectivity toward organic chemical bonds, and they also have a relatively longer half-life (30–40 μs) compared to traditional hydroxyl radicals ($HO^{\bullet}$), offering additional advantages for advanced oxidation processes (**Scheme I.7**) [109].

With a high oxidation potential (E° ($SO_4^{\bullet-}/SO_4^{2-}$) = 2.6–3.1 V/ENH)[112], $SO_4^{\bullet-}$radicals can attack organic pollutants through at least three primary mechanisms[113]:

- Hydrogen abstraction from saturated carbon atoms

- Addition reactions on double bonds
- Electron transfer

The oxidation capability of $SO_4^{\bullet -}$ radicals is particularly effective in environments containing carbonate and phosphate buffer solutions, ammoniacal nitrogen in wastewater, and various micropollutants. Reaction rates range from 10^6 to 10^9 M^{-1} s^{-1}[114], which exceed those of $HO^{\bullet}$-based advanced oxidation processes (AOPs). Research has shown that $SO_4^{\bullet -}$ is less affected by competing constituents, such as alkalinity and natural organic matter in real water matrices. This resistance to interference suggests that $SO_4^{\bullet -}$ is more effective for degrading highly reactive organic contaminants[112,115,116].

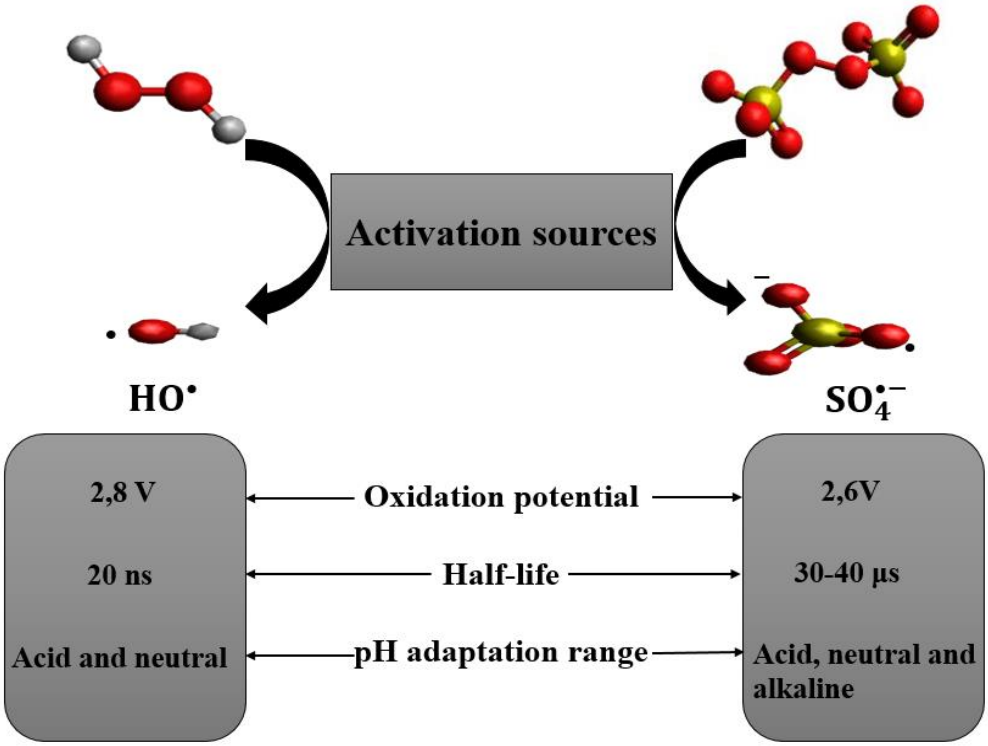

Scheme I.7. Comparison of $HO^{\bullet}$ and $SO_4^{\bullet -}$ characteristics.

III.2.2.5.2.2. Reactivity of sulfate radicals

The decomposition of the persulfate ion in aqueous solution is crucial for generating sulfate radicals. These radicals, valued for their high reactivity and stability, are instrumental in the efficiency of advanced oxidation processes (AOPs) to remove organic contaminants from the environment. Nonetheless, the decomposition mechanism of persulfate in the absence of solutes has been minimally studied and is still not fully understood. The reduction in sulfate radical concentration is attributed to the following reactions[117]:

- Biomolecular reaction:

$$SO_4^{\bullet -} + SO_4^{\bullet -} \longrightarrow S_2O_8^{2-} \qquad k=8.1\times 10^8\ M^{-1}s^{-1} \qquad \text{(I.32)}$$

- Reaction with persulfate ion:

$$SO_4^{\bullet -} + S_2O_8^{2-} \longrightarrow S_2O_8^{\bullet -} + SO_4^{2-} \quad k=6.62\times 10^5 M^{-1}s^{-1} \qquad \text{(I.33)}$$

- Reaction with water :

$$SO_4^{\bullet -} + H_2O \longrightarrow SO_4^{2-} + HO^{\bullet} + H^+ \quad k=9.4\times 10^3 M^{-1}s^{-1} \qquad \text{(I.34)}$$

III.2.2.5.3. PS activation mode

The activation of PS and PMS is essential for generating the $SO_4^{\bullet -}$ radical in an aqueous medium by breaking the peroxide bond (O-O) to achieve the removal of organic contaminants in water and soil by a series of radical reactions[113,118,119] **Equations (I.35)** and **(I.36)**, in addition to $SO_4^{\bullet -}$there is also indirect generations of $HO^{\bullet}$ radical, superoxide radical ($O_2^{\bullet}$) or other reactive species, however $SO_4^{\bullet -}$remains the primary species responsible for the effectiveness of removal of pollutants[120].

$$S_2O_8^{2-} \xrightarrow{Energy(heat,hv)} 2SO_4^{\bullet -} \qquad \text{(I.35)}$$

$$HSO_5^- \xrightarrow{Energy(heat,hv)} SO_4^{\bullet -} + HO^{\bullet} \qquad \text{(I.36)}$$

When sulfate radicals ($SO_4^{\bullet -}$) interact with organic compounds, they can trigger a sequence of radical chain reactions **Equations (I.37)** and **(I.38)**. These reactions often result in the oxidation or complete mineralisation of the organic compound.

$$SO_4^{\bullet-} + RH \longrightarrow SO_4^{2-} + H^+ + R^\bullet \quad \text{(I.37)}$$

$$HO^\bullet + RH \longrightarrow H_2O + R^\bullet \quad \text{(I.38)}$$

Moreover, due to the ease of activation, PS is the most commonly used reagent for $SO_4^{\bullet-}$ radical productions [113]**Equation (I.39)**.

$$S_2O_8^{2-} + activator \longrightarrow SO_4^{\bullet-} + (SO_4^{\bullet-} or\ SO_4^{2-}) \quad \text{(I.39)}$$

PS can be activated through various methods, including[107,121,122]:

- Photochemical activation: Primarily includes UV activation.
- Chemical activation: Involves techniques such as alkali activation, transition metal ions and metal oxide activation, and activation using carbon-based material.
- Physical Activation: includes thermal (heat) activation, plasma activation, and ultrasound (US) activation.
- Coupled activation methods: combines multiple activation techniques, such as heat/transition metal ions/PS or US/heating/PS.

Figure I.5 provides an overview of the various activation methods for persulfate, while **Table I.7** summarises them.

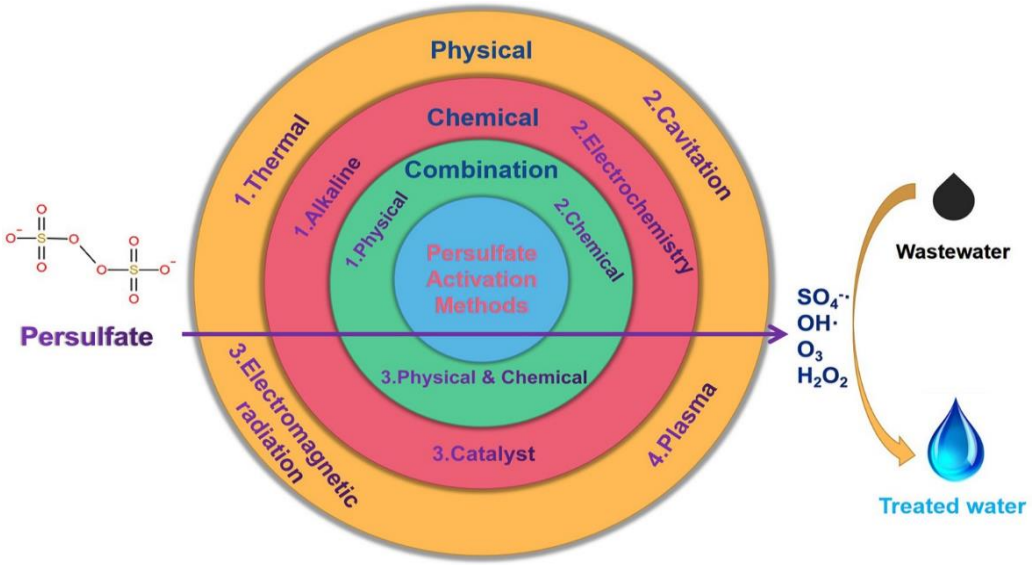

Figure I.5. Various persulfate activation modes [122]**.**

Table I.7. PS activation methods.

Method	Mechanism	Predominant Radical species
Heat	Homolysis of peroxide bond	$SO_4^{\bullet -}$/ $HO^{\bullet}$
UV Radiation	Homolysis of peroxide bond	$SO_4^{\bullet -}$
Transition Metals	One electron transfer	$SO_4^{\bullet -}$
Alkaline pH	Base-catalysed hydrolysis of PS leads to hydroperoxide formation, subsequently triggering radical generation.	$SO_4^{\bullet -}$/ $HO^{\bullet}$

III.2.2.5.3.1. UV Activation

UV irradiation has been employed to activate persulfate (PS) and degrade various organic pollutants. During this process, active radicals generated from the activation of PS break the chemical bonds of pollutants under UV irradiation. Specifically, the radical species $SO_4^{\bullet -}$ are formed from the fission of the peroxide bond (–O–O–).

The wavelength of UV light plays a crucial role in the activation process within UV/PS systems. Research indicates that visible light with wavelengths longer than $\lambda > 420$ nm has little effect on PS activation. When the wavelength exceeds $\lambda > 300$ nm, the absorption rate of PS remains low. The highest absorption rate occurs at 254 nm, with an absorption coefficient of $\varepsilon = 27.5 \pm 1.1$ M cm^{-1}[123,124].

Most studies employ UV at 254 nm, which provides sufficient energy to break the –O–O– bond in PS[125]. Upon UV irradiation, PS activation forms two $SO_4^{\bullet -}$ radicals, as shown in **Equation (I.35)**. In solution, some $SO_4^{\bullet -}$ can spontaneously convert to $HO^{\bullet}$, particularly in alkaline pH[106], as in **Equations (I.34)** and **(I.40)**.

$$S_2O_8^{2-} \xrightarrow{h\nu} 2SO_4^{\bullet -} \qquad \text{(I.35)}$$

$$SO_4^{\bullet -} + H_2O \longrightarrow SO_4^{2-} + HO^{\bullet} + H^+ \qquad \text{(I.34)}$$

$$SO_4^{\bullet -} + OH^- \longrightarrow SO_4^{2-} + HO^{\bullet} \qquad \text{(I.40)}$$

The UV/PS system has recently been used to degrade various resistant organic pollutants; many studies have demonstrated its high oxidation capacity due to its higher quantum yield[126]. However, as UV light constitutes only a tiny fraction of sunlight (3-5%), efforts have been made to extend the photoactivation range of PS from UV to visible and sunlight wavelengths[107,127].

III.2.2.5.3.2. Alkali activation

The alkaline activation of PS is highly dependent on pH; typically, increasing the pH to levels above 11, often achieved by adding sodium or potassium hydroxide (NaOH, KOH), is crucial for the activation process[128,129]. During this process, the hydrolysis of a persulfate molecule produces a hydrogen peroxide anion (HO_2^-), which subsequently generates superoxide radicals ($O_2^{\bullet -}$). These reactions are pivotal in the activation mechanism **Equations (I.41)** and **(I.42**).

$$S_2O_8^{2-} + H_2O \longrightarrow 2SO_4^{2-} + HO_2^- + H^+ \qquad \text{(I.41)}$$

$$S_2O_8^{2-} + HO_2^- \longrightarrow SO_4^{2-} + SO_4^{\bullet -} + O_2^{\bullet -} + H^+ \qquad \text{(I.42)}$$

Also, sulfate radicals ($SO_4^{\bullet -}$) can transform under alkaline conditions into hydroxyl radicals $HO^{\bullet}$ **Equation (I.40)**[130].

$$SO_4^{\bullet -} + OH^- \longrightarrow SO_4^{2-} + HO^{\bullet} \qquad \text{(I.40)}$$

However, compared to activation methods such as heating, UV irradiation, or metal-based approaches, alkali-activated persulfate systems are less effective and require longer degradation times.

III.2.2.5.3.3. Transition metal activation

Persulfate (PS) can be activated at room temperature and neutral pH through electron transfer from metals with relatively low valence states, such as cobalt (Co^{2+}), silver (Ag^{+}), manganese (Mn^{2+}), and iron (Fe^{2+}). This process generates $SO_4^{\bullet -}$radicals, with the primary activation mechanism described as follows, where M represents typical metal ions:

$$S_2O_8^{2-} + M^n \longrightarrow M^{(n+1)} + SO_4^{\bullet -} + SO_4^{2-} \qquad \text{(I.43)}$$

Among these metals, Fe^{2+} is frequently used in persulfate-based in situ chemical oxidation (ISCO) due to its environmental compatibility, non-toxicity, and cost-effectiveness[131]. The activation of persulfate by Fe^{2+} occurs through a one-electron transfer, where Fe^{2+} provides an electron to the persulfate anion ($S_2O_8^{2-}$) with an activation energy of 50,23 kJ mol^{-1}[132], as shown in **Equation (I.44)**.

$$S_2O_8^{2-} + Fe^{2+} \longrightarrow Fe^{3+} + SO_4^{\bullet-} + SO_4^{2-} \qquad \text{(I.44)}$$

The Fe^{2+}/PS system has been proven effective in degrading various refractory pollutants at optimal Fe^{2+} concentrations. However, an excess of Fe^{2+} ions can lead to competitive side reactions that decrease the generation of sulfate radicals[133], as demonstrated in **Equation (I.45)**.

$$Fe^{2+} + SO_4^{\bullet-} \longrightarrow Fe^{3+} + SO_4^{2-} \qquad \text{(I.45)}$$

III.2.2.5.3.4. Ultrasonic activation

The activation of persulfate by ultrasonic methods is based on generating cavitation bubbles in wastewater through ultrasound. The collapse of these bubbles produces localised high temperatures (up to 5000 K), which induce homolysis of the O-O bonds in persulfate. This reaction generates reactive species, such as $SO_4^{\bullet-}$, through a mechanism comparable to heat- and UV-induced radical generation[134,135].

$$S_2O_8^{2-} \xrightarrow{ultrasound} 2\,SO_4^{\bullet-} \qquad \text{(I.46)}$$

Ultrasonic activation is notable for its chemical efficacy and stability[136]. However, challenges such as high energy consumption and limited processing capacity hinder its broader adoption and application.

III.2.2.5.3.5. Plasma activation

Activated persulfate using plasma technologies has emerged as an effective method for degrading organic pollutants in wastewater treatment. Physical and chemical reactions are triggered when high-energy ions and electrons from the plasma collide with molecules in the liquid. During this process, the ions and molecules in the liquid interact with the high-energy electrons and ions in the plasma, leading to the excitation or ionisation of the chemicals in the

solution. This interaction can activate PS, producing sulfate radicals ($SO_4^{\bullet -}$), which exhibit strong oxidising properties, significantly improving the degradation efficiency of persistent organic contaminants[137].

III.2.2.5.3.6. Thermal activation

Thermal activation of persulfate (TAP) occurs when sufficient energy equivalent to dissociation energy of the peroxide bond (ranging from 140 to 213,3 kJ mol^{-1}) is supplied to the persulfate anion($S_2O_8^{2-}$) [130,138]. This process generates two sulfate radicals ($SO_4^{\bullet -}$) with a rate constant ranging from 1×10^{-7} s^{-1} at 25°C to 5.7×10^{-5} s^{-1}at 70°C[129], as shown in **Equation (I.35),** which can react with water (H_2O) to produce hydroxyl radicals ($HO^{\bullet}$) lowering the pH of the solution, and is also an effective species for treating persistent pollutants[139]. However, this reaction **Equation (I.34)** is relatively slow under most conditions, with a rate constant of less than k= 2×10^{-3} s^{-1}. Nevertheless, it becomes much faster at higher temperatures, highlighting temperature's critical role in accelerating reaction rates[140].

$$S_2O_8^{2-} \xrightarrow{heat} 2SO_4^{\bullet -} \qquad \text{(I.35)}$$

$$SO_4^{\bullet -} + H_2O \leftrightarrow SO_4^{2-} + HO^{\bullet} + H^+ \qquad \text{(I.34)}$$

TAP system is typically conducted at temperatures above 30°C and offers several significant advantages:

- Sustainability: Heat is a sustainable and environmentally friendly energy source for pollutant removal, minimising or eliminating the use of harmful chemical activators.
- High Efficiency: Thermal energy is an effective activator, significantly reducing reaction times and improving overall efficiency.
- Simplicity: The Ease of Use of the TAP system has made it a valuable method for studying the mechanisms and kinetics of pollutant degradation.
- Versatility: The combination of TAP with renewable energy sources makes it a promising approach for the remediation of organic pollutants.

III.2.2.5.3.6.1. Effect of process operating conditions

- **The impact of temperature:**

The effect of temperature on heat-activated persulfate (TAP) systems, especially regarding the decomposition rate and efficiency in degrading micropollutants (MPs), is a crucial factor to consider. As temperature increases, the decomposition rate of MPs also rises. This is because the concentration of reactive species, such as $SO_4^{\bullet-}$ radicals, increases, making them more readily available to degrade the MPs.

For instance, **Wang et al**. highlighted the significance of temperature in enhancing the decomposition rate of micropollutants (MPs) when using TAP systems for spiramycin removal. They found that at 40°C and 50°C, spiramycin removal reached 53.5% and 97%, respectively, within 60 minutes. However, when the temperature was raised to 60°C and 70°C, the removal increased to 88% and 100% within 20 minutes[141]. In a similar study, **Chen et al.** reported that as the temperature increased from 50°C to 70°C, diclofenac removal improved from 60% after 600 to 90% after 120 minutes[142].

Table I.8 presents the removal efficiencies of various categories of pollutants using the TAP process, further emphasising the critical role of thermal conditions in optimising persulfate activation for effective pollutant removal.

On the other hand, while higher temperatures generally enhance the TAP process by increasing radical generation, they can also make energy costs prohibitive. Additionally, the rapid formation of $SO_4^{\bullet-}$ radicals at elevated temperatures can lead to their rapid self-scavenging **Equation (I.32)**, resulting in excessive persulfate consumption[143]. Furthermore, increasing the temperature can initiate side reactions due to the unproductive decomposition of persulfate anion [144], as shown in **Equation (I.47)**.

$$SO_4^{\bullet-} + SO_4^{\bullet-} \longrightarrow S_2O_8^{2-} \qquad \text{(I.32)}$$

$$S_2O_8^{2-} + H_2O \rightarrow 2H^+ + 2SO_4^{2-} + \frac{1}{2}O_2 \qquad \text{(I.47)}$$

Therefore, from a technical standpoint, selecting the optimal temperature requires careful consideration of energy and chemical costs to achieve the desired efficiency within a reasonable industrial processing time[145].

Table I.8. Effect of temperature on several organic compounds eliminated by thermally activated persulfate (TAP).

Contaminant Class	pollutants	Experimental condition	Temperature °C	Removal (%)	Time (min)	Ref.
Active Pharmaceutical Compounds	Amoxicillin	C_0=100 µM, [PS]=10 mM, pH=7	40 50 55 60	32 91 100 100	330 330 330 90	[146]
	Diclofenac	C_0=47 µM, [PS]=0,47 mM, pH=7	50 60 65 70	60 90 90 90	600 600 240 120	[142]
	Ketoprofen	C_0=10 µM, [PS]=2 mM, pH=7	40 50 60 70	10 55 90 100	30 30 30 30	[147]
	Sulfamethazine	C_0=30 µM, [PS]=2 Mm, pH=7	40 50 60	≈ 33 67/100 100	90 90/360 90	[148]
	Sulfamethoxazole	C_0=100 mg/L, [PS]=10 mM, pH=7	40 50 60 70 80	≈ 20 ≈ 34 ≈ 70 100 100	140 140 60 80 20	[149]
	Valsartan	C_0=1 µM, [PS]=0,42 mM, pH=6	40 50 60	≈ 50 100 100	30 30 10	[145]
Pesticides	Atrazine	C_0=50 µM, [PS]=1 mM, pH=7	20 40 50 60	0 ≈ 22 ≈ 68 100	120 120 120 120	[150]
	Thiamethoxam	C_0=2 mg/L, [PS]=100 mg/L,	40 50 60	25 58 100	30 30 30	[151]

Industrial contaminants		pH=7	70	100	30	
	Bisphenol A	C_0=220 mg/L, [PS]=625 mg/L, pH=7	40 50 60 70	40 100 100 100	30 30 7,5 2,5	[152]
	Bisphenol S	C_0=25 µM, [PS]=0,5 mM, pH=7	55 60 65 70	48,4 70 100 ≈ 100	180 180 180 120	[153]
	p-nitrophenol	C_0=720 µM, [PS]=30 mM, pH=7	25 50 60 70 90	3 26,4 73,6 100 100	180 180 180 180 20	[154]
	Congo red	C_0=20 mg/L, [PS]=1 mM, pH=7	30-40 80	<2 98	180 180	[155]
	Methylene bleu	C_0=15,6 µM, [PS]=1 mM, pH=7	50 70	64 100	120 60	[156]
	Sudan black B	C_0=220 mg/L, [PS]=625 mg/L, pH=7	40 60	37/43,5 97	80/120 80	[157]

- **Effect of pH :**

The pH of the aquatic solution also plays a critical role in determining the degradation rate of MPs in the TAP process. Depending on the pH level, the elimination of MPs can be enhanced, hindered, or remain unaffected. Research by **Liang and Su** and **Feng et al.** has shown that the pH of the solution influences the distribution and production of reactive species, which in turn affects MP degradation[147,158].

Both reactive species ($SO_4^{\bullet-}$ and $HO^{\bullet}$) contribute to the degradation process at neutral pH. Under acidic conditions, persulfate undergoes acid-catalysed decomposition to generate $SO_4^{\bullet-}$, as described in **Equation (I.48)**. In contrast, under basic conditions, $SO_4^{\bullet-}$ reacts to

produce $HO^{\bullet}$, as outlined in **Equation (I.40)** and **Equation (I.34)**[158,159]. Although basic conditions promote $HO^{\bullet}$ formation, the lower redox potential of $HO^{\bullet}$(≈2.0 V) reduces its oxidative capacity[160].

$$S_2O_8^{2-} + H^+ \rightarrow HS_2O_8^- \rightarrow SO_4^{\bullet-} + SO_4^{2-} + H^+ \quad \text{(I.48)}$$

$$SO_4^{\bullet-} + OH^- \longrightarrow SO_4^{2-} + HO^{\bullet} \quad \text{(I.40)}$$

$$SO_4^{\bullet-} + H_2O \leftrightarrow SO_4^{2-} + HO^{\bullet} + H^+ \quad \text{(I.34)}$$

The reactivity of these species differs considerably: $HO^{\bullet}$ interacts mainly with carbon double bonds and removes hydrogen from N–H, C–H, or O–H bonds[161]. Meanwhile, $SO_4^{\bullet-}$exhibits excellent selectivity, reacting with target compounds through electron transfer, hydrogen abstraction, and addition-elimination mechanisms[112,161,162]. Ultimately, the predominant reactive species dictate the degradation pathway of MPs.

- **Effect of persulfate concentration :**

The initial concentration of persulfate is critical in the heat-activated PS oxidation of MPs. Studies on compounds such as propranolol, sulfamethazine, and atenolol have demonstrated that increasing the persulfate concentration enhances the degradation rate of MPs[148,163,164]. Researchers, including **Arvaniti et al.** and **Miao et al.**, have reported a linear relationship between the apparent rate constant (K_{app}) and the initial PS concentration[145,164]. This indicates that higher persulfate concentrations promote the formation of $SO_4^{\bullet-}$ radicals, leading to a consistent radical yield per persulfate dose. Consequently, the degradation rate becomes proportional to the persulfate concentration at a given temperature[145,163,165].

However, excessive persulfate concentrations may result in an oversupply of $SO_4^{\bullet-}$ radicals, potentially causing undesirable reactions between the radicals or with persulfate itself, as described in **Equations (I.32)** and **(I.33)**[146,166,167]. While higher persulfate levels generally improve degradation efficiency, they also increase operational costs and contribute to sulfate ion (SO_4^{2-}) pollution. Elevated SO_4^{2-} levels are a concern, as the World Health Organization (WHO) recommends limiting sulfate concentrations in drinking water to 250–500 mg/L [168].

$$SO_4^{\bullet-} + SO_4^{\bullet-} \longrightarrow S_2O_8^{2-} \quad \text{(I.32)}$$

$$SO_4^{\bullet-} + S_2O_8^{2-} \longrightarrow S_2O_8^{\bullet-} + SO_4^{2-} \qquad \text{(I.33)}$$

Therefore, optimising the persulfate dosage is essential to balance degradation efficiency and environmental safety.

- **Effect of the initial concentration of the target micropollutant:**

Environmental pollutants exist in varying concentrations in natural and wastewater systems. Understanding how treatment performance changes with initial pollutant concentrations is crucial for optimising processes. Research indicates that higher initial concentrations of micropollutants (MPs) can significantly hinder degradation performance during treatment.

For instance, studies on bisphenol A (BPA) and spiramycin (SPM) under specific temperatures and persulfate concentrations reveal that higher concentrations of MP lead to a marked decrease in removal efficiency[141,152]. This is primarily due to a reduced reactive species/pollutants ratio. Although experimental setups often use excess oxidants, the constant generation rate of reactive species limits removal efficiency as pollutant concentrations rise[142,145].

In contrast, real-world systems show that the initial concentration of MPs has a minor impact on degradation compared to the influence of other scavengers of reactive species present in the matrix[169].

- **Effect of organic matter:**

Natural organic matter (NOM) is widely present in wastewater and natural water systems, significantly influencing treatment efficiency. NOM comprises both condensed components, such as humic acid (HA), fulvic acid (FA), humin substances, and lignin, and amorphous components, like fatty acids, peptides, and phenolic compounds[170]. It contains diverse hydrophilic and hydrophobic functional groups, including alkyl chains, aromatic rings, hydroxyl groups, and carbonyl groups, which govern its interactions with other substances[170–172].

Humic acid (HA) and fulvic acid (FA) are commonly used as representative compounds of NOM. Research has demonstrated that NOM can inhibit contaminant degradation during

AOP and TAP. For example, a study by **Gao et al.** showed that the presence of FA significantly reduced triclosan (TCS) removal efficiency during TAP treatment. Specifically, The degradation efficiency decreased by 30% and 40% with the addition of 10 mg/L and 20 mg/L of FA, respectively[173]. The researchers attributed this decline to competition between fulvic acid and TCS to sulfate radicals.

Similarly, a study by **Liu et al.** reported that adding 1 and 5 mg/L of HA decreased the removal efficiency of sulfachloropyridazine by 25% and 96%, respectively[174]. This decline is attributed to consuming reactive oxygen species (ROS), such as sulfate radicals and hydroxyl radicals, by electron-rich sites within humic substances[174,175]. Consequently, HA acts as scavengers of $SO_4^{\bullet-}$ and $HO^{\bullet}$ **Equations (I.49)** and **(I.50)**.

$$\text{NOM} + SO_4^{\bullet-} \rightarrow NOM^{\bullet-} + SO_4^{2-} \qquad k=2.35\times 10^{7}\ M^{-1}s^{-1} \qquad \text{(I.49)}$$

$$\text{NOM} + HO^{\bullet} \rightarrow NOM^{\bullet-} + OH^{-} \qquad k=3\times 10^{8}\ M^{-1}s^{-1} \qquad \text{(I.50)}$$

In conclusion, the co-presence of NOM in wastewater reduces the oxidative capacity of TAP by consuming ROS. Notably, higher NOM concentrations (>5 mg/L) exacerbate the suppression of treatment efficiency[176].

- **Effect of inorganic anions:**

Inorganic anions are widely present in natural water and can influence TAP performance in wastewater treatment[175]. Among the common inorganic species, carbonates CO_3^{2-}, bicarbonates HCO_3^{-}, nitrates NO_3^{-}, sulfates SO_4^{2-}, chlorides Cl^{-} and phosphate ions ($H_2PO_4^{-}$, HPO_4^{2-} and PO_4^{3-}) have received particular attention in AOP research. These coexisting anions can interact with $SO_4^{\bullet-}$ and $HO^{\bullet}$ radicals in TAP systems, forming reactive species with lower oxidation potential, as described in **Equations (I.51)-(I.66)**. This interaction can either promote or inhibit the degradation of recalcitrant organic contaminants.

$$SO_4^{\bullet-} + Cl^{-} \rightarrow SO_4^{2-} + Cl^{\bullet} \qquad k=3\times 10^{8}\ M^{-1}s^{-1} \qquad E^{\circ} = 2.6\ V \qquad \text{(I.51)}$$

$$HO^{\bullet} + Cl^{-} \rightarrow OH^{-} + Cl^{\bullet} \qquad \text{(I.52)}$$

$$Cl^{\bullet} + Cl^{-} \rightarrow Cl_2^{\bullet-} \qquad E^{\circ} = 2.41\ V \qquad \text{(I.53)}$$

$Cl_2^{\bullet-} + Cl_2^{\bullet-} \rightarrow Cl_2 + 2Cl^-$ $E^\circ = 1.36\ V$ (I.54)

$Cl_2 + H_2O \rightarrow HOCl + H^+ + Cl^-$ $E^\circ = 1.48\ V$ (I.55)

$Cl^- + HO^\bullet \rightarrow HClO^{\bullet-}$ k=4.3× $10^9\ M^{-1}s^{-1}$ (I.56)

$HCO_3^- \leftrightarrow H^+ + CO_3^{2-}$ (I.57)

$HCO_3^- + SO_4^{\bullet-} \rightarrow SO_4^{2-} + HCO_3^\bullet$ k=1.6× $10^6\ M^{-1}s^{-1}$ (I.58)

$HCO_3^- + HO^\bullet \rightarrow CO_3^{\bullet-} + H_2O$ k=8.5× $10^6\ M^{-1}s^{-1}$ (I.59)

$HCO_3^\bullet \leftrightarrow H^+ + CO_3^{\bullet-}$ (I.60)

$CO_3^{2-} + SO_4^{\bullet-} \rightarrow SO_4^{2-} + CO_3^{\bullet-}$ k=6.5× $10^6\ M^{-1}s^{-1}$ (I.61)

$CO_3^{2-} + HO^\bullet \rightarrow OH^- + CO_3^{\bullet-}$ k=3.9× $10^8\ M^{-1}s^{-1}$ (I.62)

$NO_3^- + SO_4^{\bullet-} \rightarrow SO_4^{2-} + NO_3^\bullet$ k=2.1× $10^6\ M^{-1}s^{-1}$ $E^\circ = 2.5\ V$ (I.63)

$H_2PO_4^- + SO_4^{\bullet-} \rightarrow SO_4^{2-} + H_2PO_4^\bullet$ k<7.2× $10^4\ M^{-1}s^{-1}$ (I.64)

$HPO_4^{-2} + SO_4^{\bullet-} \rightarrow SO_4^{2-} + HPO_4^{\bullet-}$ k=1.2× $10^6\ M^{-1}s^{-1}$ (I.65)

$HPO_4^{-2} + HO^\bullet \rightarrow OH^- + HPO_4^{\bullet-}$ k=1.5× $10^5\ M^{-1}s^{-1}$ (I.66)

The effect of chloride ions (Cl^-)on the degradation of micropollutants (MPs) during heat-activated sulfate radical processes varies depending on the system's conditions. Cl^-, a common anion in aqueous matrices, can positively or negatively affect the degradation efficiency. For instance, **Bruton and Sedlak** reported no significant effect of salinity on the persulfate oxidation of perfluoroalkyl acids[177]. At the same time, studies by **Chen et al.** and **Ji et al.** have shown that high Cl^-concentrations can decrease the removal of the degradation of methyl paraben and ethyl paraben, by 22.8% and 26%, respectively, can also inhibit atrazine degradation, with minimal effect at 20 mM[150,178]. This trend was also consistent for other pollutants such as pharmaceuticals, endocrine disruptors, and pesticides[151,153,167].

Conversely, **Zhao et al.** demonstrated that a high concentration of chloride ions (Cl^-) enhances the degradation efficiency of amoxicillin, yielding a slightly higher apparent rate constant (K_{app}) than that observed in deionised water. Specifically, the amoxicillin removal rate increased from 0.071 min^{-1} without Cl^- to 0.082 min^{-1} with Cl^-addition[146]. Comparable findings were reported in studies investigating removing antihypertensive drugs, such as valsartan and losartan, under TAP processes, where the inclusion of chloride ions modestly improved the reaction rates[145,179].

The dual behaviour of Cl^- in the degradation of MPs has also been highlighted in several studies. For example, **Gao et al.** observed that the degradation of triclosan is affected by low concentrations of Cl^- (<10 mM), while degradation is facilitated by higher concentrations (20-50 mM)[173]. Similarly, at Cl^- concentrations above 10 mM, **Qian et al.** reported increased oxidation of cefalexin[175]. Contrarily, **Chen et al.** found that diclofenac degradation was significantly enhanced at Cl^- levels of 1-10 mM, but it was inhibited as concentrations increased to 10–500 mM[142]. This effect is attributed to the formation of reactive chlorine species, such as chloride radicals ($Cl^{\bullet}$,$Cl_2^{\bullet-}$), free chlorine (Cl_2), and hypochlorous acid radicals ($HOCl^{\bullet}$), whose distribution and reactivity depend on operational parameters like temperature, pH, and ion concentrations, influencing their selectivity for degrading MPs and their by-products.

Bicarbonate ions (HCO_3^-), among water's most abundant inorganic ions, significantly influence contaminant degradation in heat-activated PS systems. Typically, increasing HCO_3^- concentrations inhibit degradation rates due to its quenching effects on reactive radicals ($HO^{\bullet}$ and $SO_4^{\bullet-}$), yielding less reactive carbonate radicals ($HCO_3^{\bullet}$ /$CO_3^{\bullet-}$). However, studies by **Fan et al.**, **Ji et al.**, and **Ghauch et al.** revealed exceptions where HCO_3^- enhanced the degradation of specific micropollutants like sulfamethazine, sulfamethoxazole, and naproxen[148,180,181]. This enhancement is attributed to the higher reactivity of carbonate radicals toward certain MP and the pH changes induced by it, which further affect removal efficiency.

The impact of nitrate (NO_3^-) on the degradation of emerging contaminants varied. While its presence showed negligible effects on compounds such as spiramycin, bisphenol S, and atenolol[141,153,164], it significantly enhanced naproxen and theophylline degradation at

specific concentrations. For example, NO_3^- at 20 µM increased the rate of theophylline degradation, but higher concentrations caused a slight decrease[165,181]. This behaviour may result from the formation of $NO_3^{\bullet}$ **Equation (I.63)**, a potent oxidant, which promotes degradation at optimal concentrations but undergoes self-quenching at higher levels, reducing efficiency.

Sulfates (SO_4^{2-}), carbonates (CO_3^{2-}), and phosphates ($H_2PO_4^-$, HPO_4^{2-}) exhibit minimal impact on organic pollutant removal, such as ketoprofen, and naproxen[147,181]. Their low reactivity with $SO_4^{\bullet-}$ limits their influence on the efficiency of the TAP process.

Studies have shown that inorganic cations such as calcium (Ca^{2+}) and magnesium (Mg^{2+}) have negligible effects on heat-activated PS systems since their presence (1mM) does not influence the degradation of pollutants such as amoxicillin or ketoprofen. This suggests these cations cannot quench the radicals generated in the concentration range examined[146,147].

Conversely, trace metals such as iron (Fe^{2+}) and manganese (Mn^{2+}) in natural waters can activate persulfates. For example, 2 mg/L Fe^{2+} combined with 20 mg/L PS completely removed 500 µg/L piroxicam under ambient conditions in less than 20 minutes [182]. However, most studies focus on the design of catalytic materials rather than actual environmental concentrations, often using levels of metals much higher than those naturally present.

III.2.2.6. Process based on non-thermal plasma

III.2.2.6.1. Generalities about plasmas

The term ‘plasma’ was coined by Irving Langmuir in 1928 to describe a state of matter consisting of a mixture of balanced charges, including electrons and ions[183,184]. Plasma is considered the fourth state of matter, after solids, liquids, and gases, and can exist in both ground and excited states while maintaining overall charge (**Figure I.6)**. It is a highly energetic, partially or totally ionised gas containing charged ions, free electrons, and neutral atoms and molecules. Various electrical discharges can generate plasma, which can emit different types of electromagnetic radiation, including ultraviolet (UV), visible and infrared light[185].

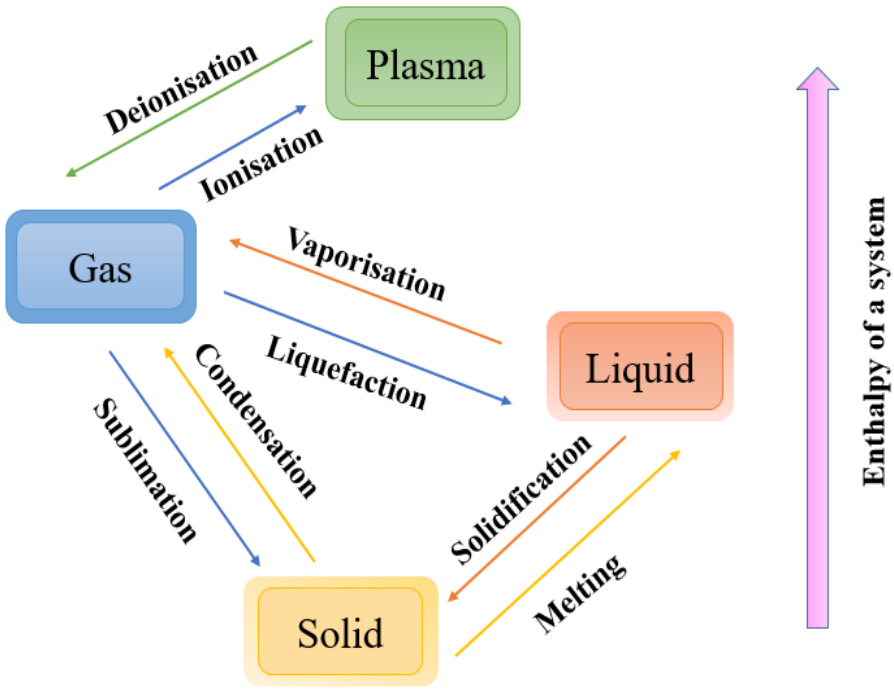

Figure I.6. Diagram of the four states of matter.

Plasma systems are generally classified into two main categories based on their electron density or temperature: thermal and non-thermal plasmas[186]. Thermal plasmas, such as those generated by arc discharges, torches, or radiofrequency discharges, require significant energy to bring the plasma components to thermal equilibrium. Conversely, non-thermal plasmas are produced using lower energy sources, such as corona discharge, dielectric barrier discharge, gliding arc discharge, glow discharge and spark discharge. These are characterised by an electron temperature much higher than the bulk gas molecules. In non-thermal plasma, high-energy electrons interact with background molecules (e.g. N_2, O_2, H_2O)[187], producing secondary electrons, photons, ions and radicals. Plasma is the most prevalent form of visible matter in the universe. In conclusion, the unique properties of plasmas can be systematically categorised based on various criteria, as illustrated in **Figure 1.7** below.

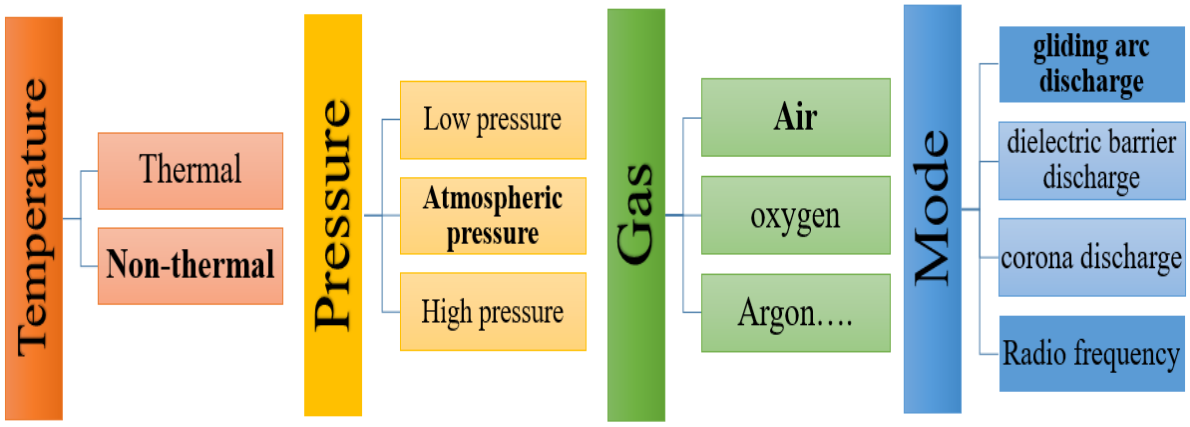

Figure 1.7. Key properties for plasma qualification and classification

III.2.2.6.2. Thermal classification of plasmas

In a plasma, each particle possesses energy that is characterised by a temperature, which in turn defines the thermodynamic state of the plasma. At low pressures, when electrons (with a temperature denoted as Te) and heavy species, such as ions or radical species (with a temperature denoted as Tg), exhibit different energy levels (Te >Tg)[188], the plasma is said to be out of thermodynamic equilibrium, it is referred to as "non-thermal". Conversely, when the temperatures of the electrons and heavy species are similar (Te ≈ Tg)[186], the plasma is considered to be in thermodynamic or thermal equilibrium. These plasmas are typically generated at pressures above atmospheric pressure (**Figure I.8**).

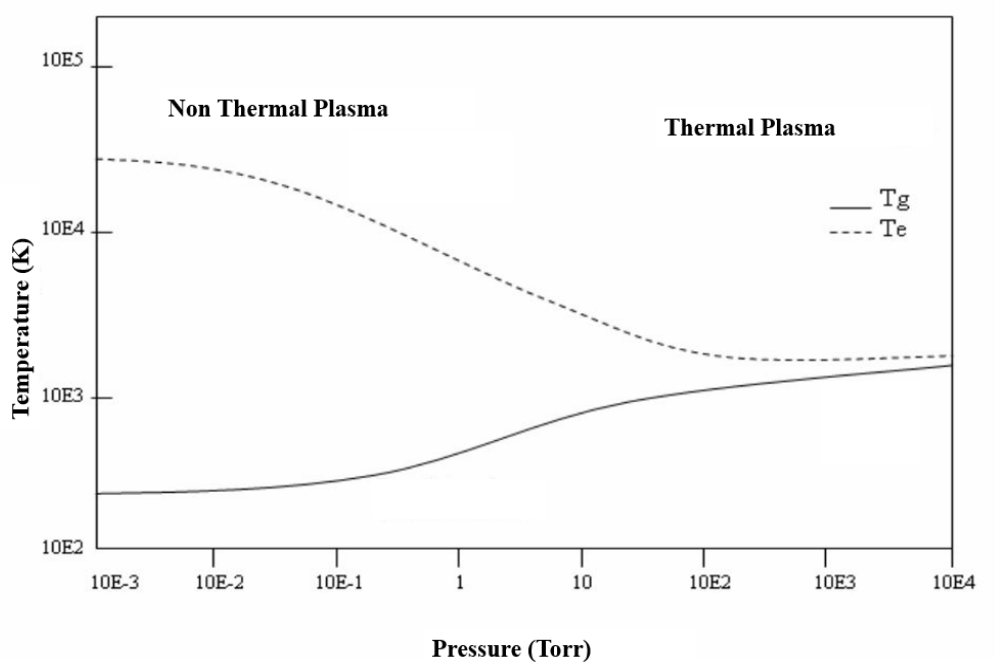

Figure I.8. Gas and electron temperatures in plasma[189].

Table I.9 summarises the key characteristics of both thermal and non-thermal plasmas.

Table I.9. Characteristics of thermal and non-thermal plasmas[190].

Plasma classification	Thermal plasma	Non-thermal plasma
Plasma state	Te ≈ Tg	Te >> Tg
Electronic energy	1-3 eV	1-10 eV
Electron density	$< 10^{21} - 10^{24}$	$< 10^{19}$
Temperatures	Te ≈ Tg ≈ 10 000 K	Te ≈ 10 000- 100 000 K Tg ≈ 300- 1000 K

III.2.2.6.2.1. Thermal plasma

Thermal plasmas are plasmas with a high degree of ionisation; they are created at high densities and temperatures. They are characterised by a similar energy distribution among all the elements present (ions, electrons, molecules), indicating a thermodynamic equilibrium. They are somewhat more exotic than cold plasmas. In fact, they are found in particular regions of our universe, such as stars, supernova remnants, thermonuclear fusion processes, thermal arc torches and plasma jets emitted by black holes[189].

III.2.2.6.2.1. Non-thermal plasma

Non-thermal, or cold plasma (NTP), is a type of plasma in which electrons have significantly higher temperatures than heavier species due to their mass difference. When energy is applied, the gas breaks down into various reactive species, leading to ionisation, excitation, or de-excitation reactions[191].

Cold plasma discharges were initially generated using alternating current (AC), pulsed, or direct current (DC) electrical fields. Different power supply methods, such as capacitively coupled plasma (CCP), inductively coupled plasma (ICP), and pulsed DC plasma, were employed for this purpose[192]. However, modern techniques, including atmospheric pressure plasma jets, corona discharge, radio frequency, microwave-induced plasma, gliding arc discharge, and dielectric barrier discharge, have become more prevalent for generating cold plasma discharges[193].

These discharges offer several advantages, making them commercially viable. One key benefit is their energy efficiency and high selectivity in chemical reactions, as cold plasma does not establish a localised thermodynamic equilibrium. Due to these properties, the application of cold plasma technology is expanding rapidly, particularly in wastewater treatment, attracting significant interest from technologists[194].

Figure I.9. Lists some advantages of different types of non-thermal plasma discharge[185].

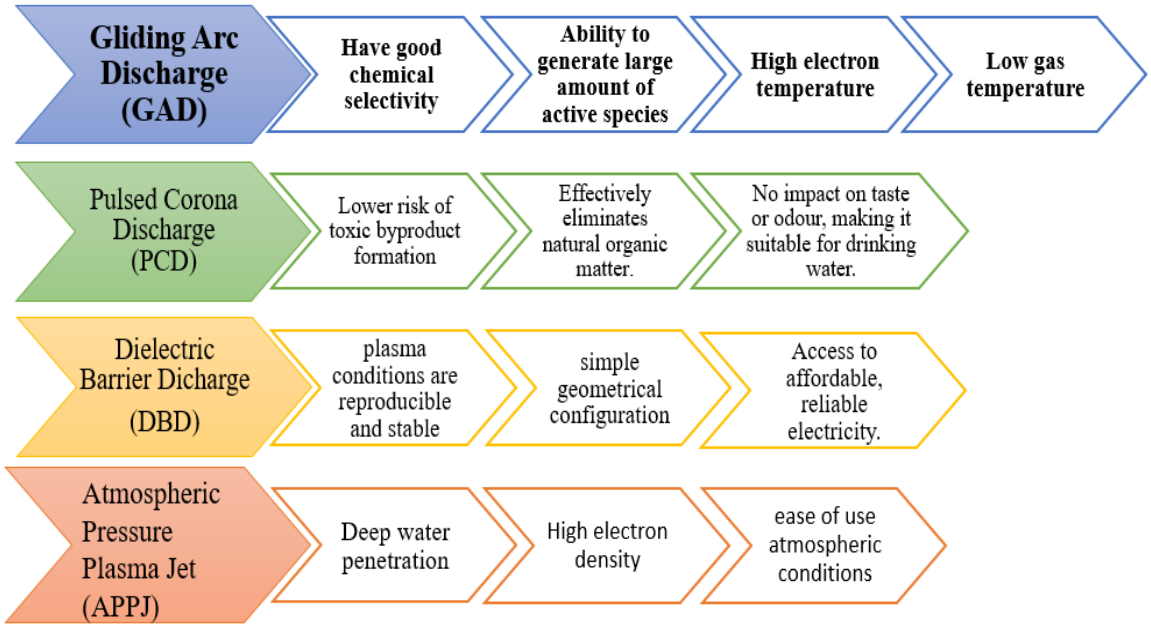

Figure I.9. Advantages of using cold plasma discharge methods in wastewater treatment.

III.2.2.6.2.1.1. Gliding arc discharge (GAD)

The gliding arc discharge (GAD) of non-thermal plasma was initially developed by Czernichowski[195] and later refined by Lesueur et al.[196] , has been extensively utilised for wastewater treatment applications. GAD offers significant advantages compared to other plasma discharge types, including high operating pressure, enhanced power output, and increased plasma density[197]. Notably, GAD exhibits characteristics of both thermal and non-thermal plasmas.

Structurally, the system comprises an impedance, a nozzle, divergent "knife-edge" electrodes through which a high voltage is applied, an insulating cover, and a high-power supply (**Figure I.10)**. Arc discharge occurs when the applied electric field reaches approximately 3 kV/mm. Due to the high gas velocity, the arc length extends, resulting in an initial increase in temperature, characteristic of thermal plasma. However, as the ionised gas expands, its temperature decreases, transitioning to a non-thermal plasma state[198].

Operating at atmospheric pressure, GAD technology has been widely recognised for its efficacy in degrading various organic contaminants present in wastewater[199,200].

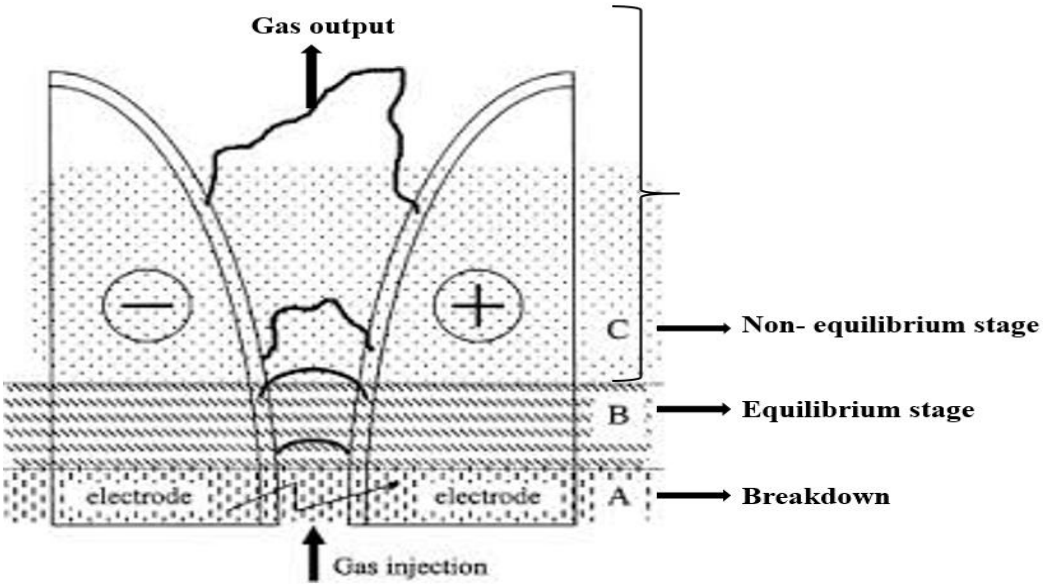

Figure I.10. Schematic view of gliding arc discharge**.**

III.2.2.6.2.1.1.1. Electrical characteristics of Gliding arc plasma

Understanding the different operating regimes of plasma discharges generated by the Glidarc system can be achieved by assuming that the utilised electrical circuit is equivalent to an electrical system comprising resistance and the electric arc, as depicted in **Figure I.11**.

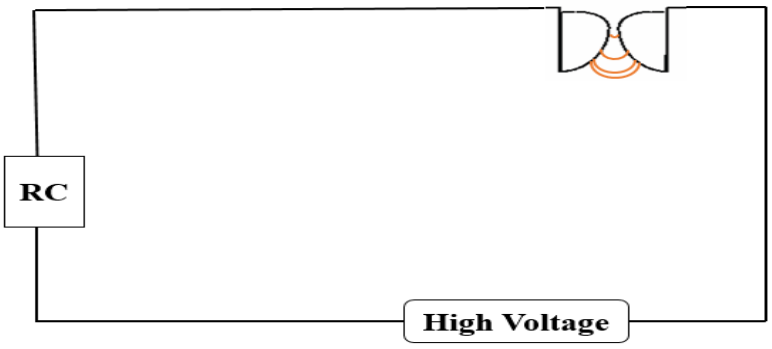

Figure I.11. Experimental plasma creation device.

The resistance RC represents the generator's internal resistance. The electric arc is established between the electrodes at the minimum gap, allowing the passage of electrical

current and consequently leading to a relatively low resistance of the formed gas plasma. High-voltage generators compensate for transferring electrical energy into thermal energy supplied to gas molecules. As the electric arc extends along the electrodes, its resistance increases, as does the voltage across them. The arc's behaviour is analogous to a resistance that increases with its length. In addition, these discharges are obtained at relatively low supply voltages, ranging from 5 to 10 kV, compared to dielectric barrier and corona discharges, which require significantly higher voltage values (> 10 kV)[201].

III.2.2.6.2.1.1.2. Chemical characteristics of gliding arc plasma

Gliding arc plasma (NTP) generates a variety of reactive oxygen species (ROS) and reactive nitrogen species (RNS) through high-energy electron collisions with neutral molecules. ROS such as hydroxyl radicals ($HO^{\bullet}$), superoxide anions ($O_2^{\bullet-}$), hydrogen peroxide (H_2O_2), atomic oxygen (O), ozone (O_3), and singlet oxygen ($^1O_2$) are produced alongside RNS, including nitric oxide (NO), nitrogen dioxide (NO_2), dinitrogen pentoxide (N_2O_5), and atomic nitrogen (N). These species have short lifetimes, typically in the microsecond range, and are highly reactive. The formation of primary reactive species, including electrons, ionised and excited gases, and atomic species, occurs through electron-induced collisions, leading to secondary species like H_2O_2, NO_2, NO_3, and O_3. When these species dissolve in the liquid phase, they form tertiary species such as H_2O_2, NO^{2-}, and NO^{3-}. These longer-lived species, such as O_3, H_2O_2, NO^{3-}, and NO^{2-}, can persist from milliseconds to days and are soluble in water, lowering the pH of the solution by up to 2 units. The formation and dissolution of reactive species vary depending on whether the target is dry or aqueous. NTP's generation of ROS and RNS plays a crucial role in environmental applications, such as water purification, where these species interact to degrade pollutants and alter pH levels, enhancing the overall efficiency of the treatment process[202,203].

- **Formation pathway for important reactive chemicals in NTP:**

Due to the absence of local thermodynamic equilibrium, non-thermal plasmas provide highly effective energy for chemical reactions [204]. In fact, short-lived reactive species, such as the hydroxyl radical ($HO^{\bullet}$) and nitrogen oxide (NO) radical, have been shown to play a crucial role in NTP (Non-Thermal Plasma) wastewater treatment. The lifetimes of these species range from nanoseconds to microseconds.

- **Reactive oxygen species ($HO^{\bullet}$, O_3 , H_2O_2):**

The presence of water molecules in electric discharges leads to the formation of hydroxyl ($HO^{\bullet}$) and hydrogen ($H^{\bullet}$) radicals through various mechanisms[194,205]. These include the photolysis of hydrogen peroxide **Equation (I.10)** and the photolysis or electron bombardment of water molecules. Excited water molecules can also generate additional reactive species while relaxing to the ground state. When dioxygen is exposed to an electric discharge, oxygen atoms ($E°O^{\bullet}/H_2O$ = 2.42V/ESH) can form through dissociation, further enhancing hydroxyl radical production. Hydroxyl radicals' short lifespan (10-100 ns in the gas phase) makes their diffusion from the plasma to the aqueous solution nearly impossible[206,207]. Due to their even shorter lifetime in solution (1 ns), these radicals must immediately react with surrounding molecules or recombine to generate hydrogen peroxide ($E°H_2O_2/H_2O$ = 1.77V/ESH)[208]. Hydrogen peroxide is formed in both phases through recombination **Equation (I.16)**, radical deactivation (**Equations (I.77) and (I.78)**), and photochemical activation **Equation (I.79)** as well as acid-base equilibrium **Equation (I.80)**. Additionally, oxygen atoms may react with contaminants or combine with dioxygen to form ozone (O_3) ($E°O_3/O_2$ = 2.1V/ESH)[209]. Ozone can act as an electron acceptor for metal ion oxidation, an electrophile for organic compound oxidation, or by addition to carbon-carbon double bonds. However, ozone decomposes in neutral or basic environments through a chain mechanism, producing hydroxyl radicals[210]. Thus, the hydrogen peroxide formed in an electric discharge indirectly enhances the overall oxidizing capacity of the plasma and plays a crucial role in plasma chemistry.

$$H_2O + h\nu \rightarrow 2HO^{\bullet} \quad \text{(I.10)}$$

$$2\ HO^{\bullet} \longrightarrow H_2O_2 \quad \text{(I.16)}$$

$$H_2O + \text{é} + h\nu \rightarrow HO^{\bullet} + H^{\bullet} \quad \text{(I.67)}$$

$$O_3 + HO_2^{\bullet} + h\nu \rightarrow O_2^{\bullet} + HO^{\bullet} + O_2 \quad \text{(I.68)}$$

$$H_2O + \text{é} \rightarrow H_2O^{+} + 2\text{é} \quad \text{(I.69)}$$

$$H_2O + H_2O^{+} \rightarrow H_3O^{+} + HO^{\bullet} \quad \text{(I.70)}$$

$$H_2O_2 + \text{é} + H^{+} \rightarrow HO^{\bullet} + H_2O \quad \text{(I.71)}$$

$$H_2O + \text{é} \rightarrow H_2O^{*} + \text{é} \quad \text{(I.72)}$$

$$H_2O^* + H_2O \rightarrow H_2O + HO^\bullet + H^\bullet \quad \text{(I.73)}$$

$$H_2O^* + H_2O \rightarrow H_2O + O^\bullet + H_2 \quad \text{(I.74)}$$

$$H_2O^* + H_2O \rightarrow H_2O + O^\bullet + 2H^\bullet \quad \text{(I.75)}$$

$$O^\bullet + H_2O \rightarrow 2HO^\bullet \quad \text{(I.76)}$$

$$HO_2^\bullet + HO_2^\bullet \rightarrow H_2O_2 + O_2 \quad \text{(I.77)}$$

$$O^\bullet + H_2O \rightarrow H_2O_2 \quad \text{(I.78)}$$

$$O_3 + H_2O + h\nu \rightarrow H_2O_2 + O_2 \quad \text{(I.79)}$$

$$H^+ + HO_2^- \rightarrow H_2O_2 \quad \text{(I.80)}$$

- **Reactive nitrogen species :**

In the discharge zone, several reactions occur when nitrogen or air is introduced. The nitrogen molecule is dissociated, like oxygen and water. This phase initiates a series of reactions, the primary ones leading to forming more or less reactive nitrogen species **Equations (I.81)-(I.90)**. Among these nitrogen species generated in the plasma phase, nitrites are particularly unstable and react with hydrogen peroxide **Equation (I.91)** or are rapidly converted into nitrates **Equations (I.92)** and **(I.93)**[211]. Peroxynitrous acid (pKa = 6.8) and its conjugate base are oxidative species capable of oxidising certain organic pollutants. For instance, the acidic form has a redox standard potential of 2.0 V/ESH. However, it is important to note the instability of this species, which can be converted into nitrous acid via isomerisation **Equation (I.93)** or decomposed into NO_2 and $HO^\bullet$ **Equation (I.94)** . In addition to the contribution of oxidative species in pollutant removal, the presence of reductive species enables potential reductive degradation of contaminants in aqueous solutions. The $H^\bullet$radicals ($E°H_2O/H^\bullet$= -2.30 V/ESH) formed by electron collisions with water molecules and/or by the reaction of hydrated electrons with acids can interact with organic compounds in two ways[212]:

- Addition to unsaturated bonds.
- Hydrogen abstraction from saturated compounds.

$$N_2 + é^* \longrightarrow 2N^\bullet + é \quad \text{(I.81)}$$

$$O_2 + é^* \rightarrow 2O^\bullet + é \quad \text{(I.82)}$$

$$N^\bullet + O^\bullet \longrightarrow NO^\bullet \quad \text{(I.83)}$$

$$NO^\bullet + O^\bullet \longrightarrow NO_2^\bullet \quad \text{(I.84)}$$

$$N^\bullet + HO^\bullet \longrightarrow NO^\bullet + H^\bullet \quad \text{(I.85)}$$

$$NO^\bullet + HO^\bullet \longrightarrow HNO_2 \quad \text{(I.86)}$$

$$HNO_2 + HO^\bullet \longrightarrow NO_2^\bullet + H_2O \quad \text{(I.87)}$$

$$NO_2^\bullet + HO^\bullet \longrightarrow NO_3^- + H^+ \quad \text{(I.88)}$$

$$NO_2^- + H_2O \longrightarrow NO_3^- + H_2O \quad \text{(I.89)}$$

$$HNO_2 + O^\bullet \longrightarrow NO_3^- + H^+ \quad \text{(I.90)}$$

$$NO_2^- + H_2O_2 + H_3O^+ \longrightarrow ONOOH + 2H_2O \quad \text{(I.91)}$$

$$ONOOH + H_2O \longrightarrow ONO_2^- + H_3O^+ \quad \text{(I.92)}$$

$$ONOOH \longrightarrow HNO_3 \quad \text{(I.93)}$$

$$ONOOH \longrightarrow NO_2 + HO^\bullet \quad \text{(I.94)}$$

- **Plasmagenic gas :**

The formation of reactive species in plasma discharges inherently depends on the carrier gas composition. The selection of an appropriate gas mixture is crucial to optimise the generation of targeted reactive species, which play a fundamental role in various plasma-based applications[201,213,214].

When oxygen (O_2) is used as the carrier gas, the discharge mainly produces oxygen-derived species such as atomic oxygen (O°) and ozone (O_3). In contrast, when dry air (a mixture of nitrogen and oxygen) is used as the plasmagenic gas, interactions between N_2 and O_2 lead to forming a broader range of reactive species, including O°, O_3, NOx, N°, and NO°.

The presence of water vapour in humid air introduces additional reaction pathways, allowing further interactions among O_2, N_2, and H_2O. This promotes the formation of highly reactive hydroxyl radicals (OH°) and hydrated hydroxyl radicals (°OH_2), significantly influencing the plasma chemistry. In particular, humidity suppresses ozone production by promoting the production of OH° radicals and hydrogen peroxide (H_2O_2) in the discharge.

Furthermore, the presence of water increases plasma acidity by facilitating the formation of nitrous acid (HNO_2) in the plasmagenic phase. Once generated, these reactive species undergo gas-to-liquid phase transfer, enabling subsequent oxidation reactions, which are particularly relevant in environmental applications, such as pollutant degradation and advanced oxidation processes.

- **UV light:**

Ultraviolet (UV) light emitted by plasmas containing water molecules arises from the relaxation of excited species. This emitted light can directly induce the photodegradation of organic molecules (M), as described by the following process[209,215]**:**

$$M + h\nu \rightarrow M^* \rightarrow \text{Products} \qquad \text{(I.95)}$$

$$M^* + O_2 \longrightarrow M^{\bullet +} + O_2^{\bullet -} \qquad \text{(I.96)}$$

Additionally, the excited molecule can undergo photodissociation through homolytic cleavage of a C-H bond, potentially leading to a reaction with oxygen, producing an organic superoxide anion:

$$MH + h\nu \rightarrow M^{\bullet} + H^{\bullet} \qquad \text{(I.97)}$$

$$M^{\bullet} + O_2 \rightarrow + MO_2^{\bullet} \qquad \text{(I.98)}$$

The UV light generated within electrical discharges over an aqueous phase spans various wavelengths. However, only radiation with wavelengths longer than 200 nm penetrates the solution and interacts with organic molecules[216]**.** Radiation between 75 and 200 nm is rapidly absorbed by surrounding water molecules:

$$H_2O + h\nu \longrightarrow H_2O^* \longrightarrow HO^{\bullet} + H^{\bullet} \qquad \text{(I.99)}$$

III.2.2.6.2.1.2. Gliding arc applications in dye wastewater degradation

Strict regulations require the textile industry to remove dyes from wastewater. Plasma Glidarc, which generates reactive species such as hydroxyl radicals and ozone, effectively degrades dyes into harmless compounds.

In this context, **Liu et al.** studied the degradation of methyl violet using a gas-liquid two-phase gliding arc plasma system, with the wastewater entering the plasma via an atomisation nozzle. They found that the degradation rate exceeded 99% after 20 minutes of treatment in air and O_2 atmospheres [217]. In another study, **Yan et al.** explored the synergistic effect of zero-valent iron and gliding arc in the decolourisation of Acid Orange II, noting that zero-valent iron enhanced the Fenton reaction by producing H_2O_2 and $HO^{\bullet}$, resulting in a 5% increase in the degradation rate, which reached over 90% under optimal conditions [218].

In another research**,** they examined the degradation of Acid Orange 7 (AO7) in a TiO2 photocatalyst-assisted gliding arc plasma system, where the degradation rate reached 43.6% after 40 minutes of treatment. The immobilised γ–Al2O3–TiO2 catalyst significantly improved the removal efficiency [219]. **Ghezzar et al.** developed a new method by introducing a film-like liquid into the flowing stream to degrade anthraquinone green 25 (AG25) in gliding arc plasma, achieving decolourisation and degradation rates of 95% and 90%, respectively, after 180 minutes of treatment in the air [220]. Subsequent experiments demonstrated that TiO2 coating, deposited via magnetron sputtering, reduced treatment time to 60 minutes while maintaining the same degradation rate, confirming the scalability of the TiO2-enhanced plasma technology [221].

Ni et al. studied AO7 degradation in printing and dyeing wastewater using a gas-liquid gliding arc, achieving a 99.3% degradation rate and a 37.9% COD removal with an initial concentration of 100 mg/l. The addition of zero-valent iron further increased the degradation rate to 97.8% at an initial concentration of 200 mg/L [222]. Several studies have identified the possible degradation mechanisms of dyes, with plasma generating O_3 and H_2O_2, which effectively break down organic matter. At the same time, $HO^{\bullet}$, produced from H_2O, plays a crucial role in the degradation process [223].

IV. TARGET CONTAMINANT:

IV.1. Orange G

IV.1.1. Background

Orange G (OG) is an emerging contaminant and synthetic dye classified as an azo dye - more precisely, a monoazo and anionic compound. It is highly soluble in water and remains chemically stable over a wide pH range[224]. In aqueous solutions, OG exists mainly as a sodium salt in two tautomeric forms, while organic solvents tend to stabilise the azo form[225].

Historically, OG was widely used in the United States as a cosmetic dye in pharmaceutical products, but these applications were later discontinued. Today, OG is commonly used in the textile and printing industries for dyeing materials such as silk and wool and in paper and leather production[226,227]. It also plays a crucial role in histology, serving as a key component in many staining techniques used by pathologists[228].

The chemical structure of OG consists of 7-hydroxy-8-[(E)-phenyldiazenyl] naphthalene-1,3-disulfonic acid, as shown in **Figure I.12**. Its orange colour is attributed to the azo group, while auxochromes such as $-SO_3$ and $-OH$ enhance its binding properties [229].

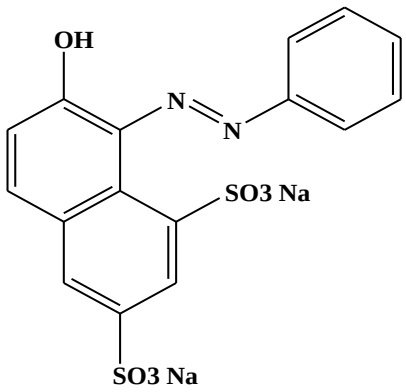

Figure I.12. Chemical structure of OG.

IV.1.2. Toxicological effect

The dye (OG) has been identified as a significant environmental risk, particularly to aquatic organisms and the wider aquatic ecosystem. As a highly toxic anionic dye, OG has been shown to induce chromosomal damage and clastogenic activity[230,231]. The azo group in its molecular structure is primarily responsible for its pronounced toxic, carcinogenic and teratogenic properties[232,233]. In addition, the intermediates generated during the degradation of OG are just as dangerous, amplifying the ecological threat it represents. Furthermore, due to its impact on aquatic life, OG harms terrestrial plants, flora and fauna[234]. In humans, exposure to OG has been associated with irritation of the gastrointestinal and respiratory systems [227]. Its genotoxicity has also been demonstrated in experimental models, notably in Swiss albino mice and the anaerobic biomass of aqueous systems[228,235].

IV.1.3. Previous studies on the degradation of OG

Due to the many adverse effects of OG on humans, aquatic organisms and plants, researchers have sought to develop effective wastewater treatment methods to reduce the presence of this harmful pollutant in environmental water systems. Various technologies have been studied and documented for wastewater treatment, including adsorption[236], photocatalytic degradation[237], ultrasonic degradation[238], electrochemical oxidation[239], activated persulfate oxidation[240] and non-thermal plasma degradation[241].

- **Comparative analysis of OG degradation using SR-AOP with different activation methods:**

There is growing interest in using persulfate (PS) activation due to its favourable properties, including its ability to promote efficient reactions, economic and practical advantages, safety benefits, chemical stability, and effectiveness in removing micropollutants (MPs) and treating wastewater. The following table summarises studies on the removal of Orange G using various persulfate activation methods.

Table I.10. Degradation of OG using SR-AOP.

Process	Operating conditions	Removal efficiency	time	Ref
PS/Fe^{2+}	➢ [OG]=0.1mM / pH=3.5 / [PS]=4mM / [Fe^{2+}]=4Mm. ➢ The variation in persulfate and iron concentrations significantly influenced the elimination rate. ➢ Increasing the temperature positively affected the process. Under identical operating conditions, raising the ambient temperature to 293 K and 313 K improved the elimination rate to 76% and 100% within 5 min of treatment.	99%	30 min	[242]
Co_3O_4/PS	➢ [OG]=0.1mM / pH=7 / [PS]=2 mM / T=25°C / [Co_3O_4]nano=0,5g/L. ➢ [OG]=0.1mM / pH=7 / [PS]=2 mM / T=25°C / [Co_3O_4]not nano=0.5g/L. ➢ The process is influenced by pH; the degradation rate increases with rising pH but decreases when the pH reaches 10.	90.7% 38.7%	3h 3h	[243]
$FeMoO_4$/PS	➢ 100ml of [OG]=0.2 mM /pH=2.8/ [PS]= 4Mm /T=25∓0.5°C /[$FeMoO_4$]=0.3g/L. ➢ The variation in the concentration of [$FeMoO_4$]₀ influenced the degradation rate. ➢ [$FeMoO_4$]=0.1- 0.2- 0.3- 0.4- 0.5 g/L	95% 90%	40 min 60-40-30-25-20 min	[244]
Pyrite/PS	➢ [OG]= 100 µM/ [PS] = 5mM / T=30∓0.5°C / [Pyrite]=1g/L/ pH=3-6-9. ➢ The partial size of the pyrite had a significant impact on the rate of OG degradation.	97.9%-47.9%-17.6%	20 min	[245]
Mn-SDBC/PS	➢ 50ml of [OG]=1500 mg/L / [PS]=3 mM / [biochar]=1g/L / pH=6/ SDBC without metal.	34%	720 min	[246]

	➢ 50ml of [OG]=1500 mg/L / [PS]=3 mM / [biochar]=1g/L / pH=6 / Mn-SDBC: [Mn]= 40mM. ➢ A high concentration of Mn above 40 mM did not effectively promote the degradation of the dye. ➢ The pH showed no significant influence on the process. ➢ Increasing the biochar concentration from 0.5 g/L to 2 g/L enhanced the removal of OG by 5.66%. ➢ Increasing the PS concentration from 1 mM to 7 mM improved the removal rate from 55.8% to 97.21%.	90.28%		
Fe/SGAC	➢ [OG]=0.2 mM / [PS]= 2Mm / pH= ambiant / T=25°C / [catalyste]=1g/L: 0.5%Fe/SGAC. ➢ [OG]=0.2 mM / [PS] = 2Mm / pH =ambiant / T=25°C / [catalyste]=1g/L: 0.5%Fe/GAC. ➢ The increase in iron concentration inhibited the elimination of OG. ➢ Acidic conditions were more conducive to eliminating the OG dye in this process.	99% 96%	3h	[247]

- **Mechanism of OG Oxidation using SR-AOP process**

➢ **Via iron-activated PS**

The reaction intermediates resulting from the oxidation of OG via Fe(II) / PS process were analysed by GC/MS and HPLC, with the proposed degradation mechanism illustrated in **Scheme I.8**. The degradation pathway suggests that the process begins with cleavage of the azo bond, which then leads to decomposition of the aromatic structures and eventual formation of organic acids. The main intermediates identified are phenolic compounds, aniline, naphthalene and quinone derivatives. Key intermediates such as hydroquinone (HQ), benzoquinone (BQ), phthalic acid and short-chain organic acids (including oxalic, fumaric and maleic acids) were detected. Despite these transformations, only 15% of the nitrogen in the system was converted to molecular nitrogen (N_2) [240]

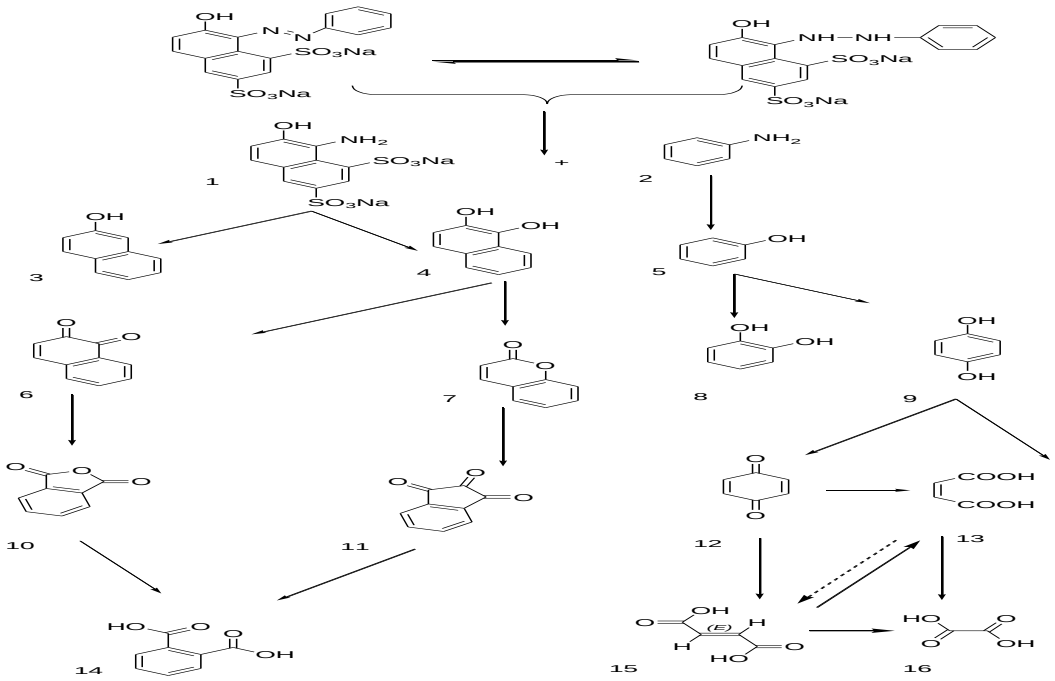

Scheme I.8. Mechanism of OG degradation via iron-activated PS [240].

➢ **Via Co_3O_4 nanoparticles-activated PS :**

GC/MS analysis identified the OG degradation products in the nano-Co_3O_4/PS process, with mechanistic pathways illustrated in **Scheme I.9**. Most of the by-products had lower molecular weights than their parent compounds. The proposed degradation mechanism suggests that $SO_4^{\bullet -}$ and $HO^{\bullet}$ radicals first attack the aromatic ring, leading to the cleavage of characteristic functional groups such as (SO_3H), (phenyl), (OH), and (phenyl-N=N). Subsequent radical-induced transformations generate hydroxylated intermediates and quinone derivatives; thus, the loss of (phenyl) and (phenyl-N=N) groups directly facilitates the decolourisation of OG in the activated PS process[243].

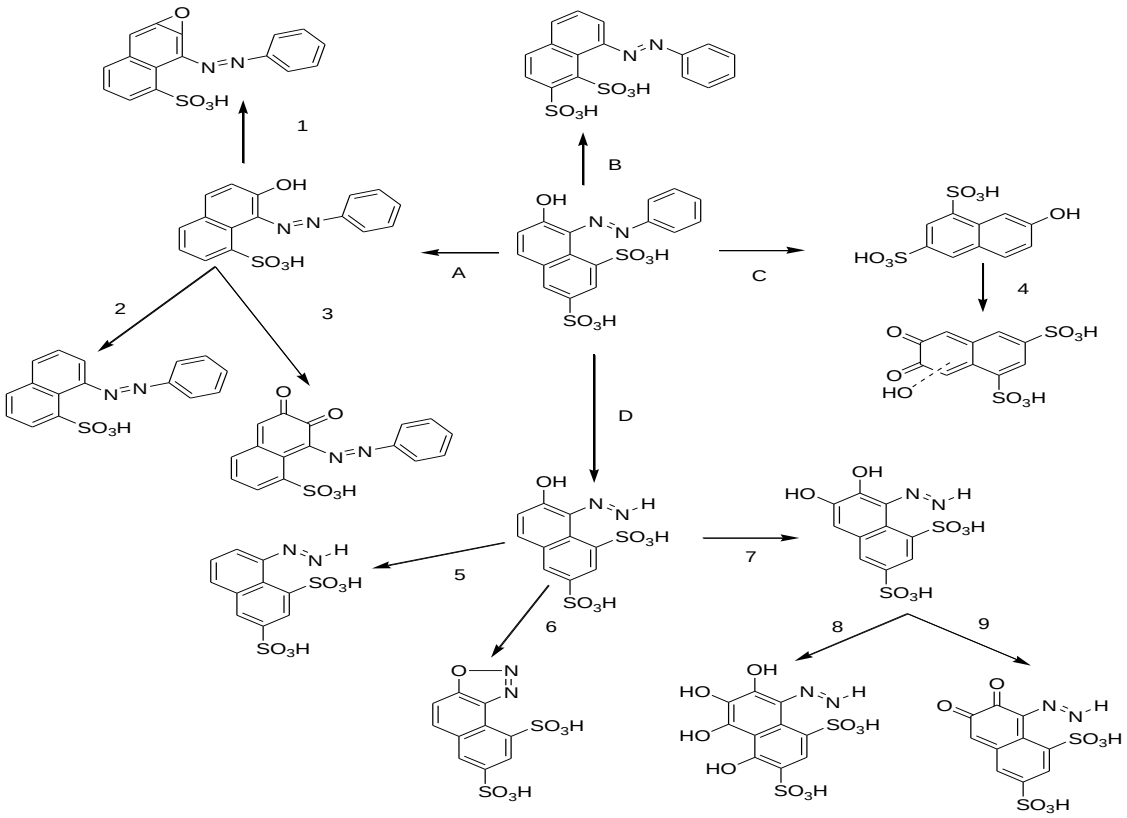

Scheme I.9. Mechanism of OG degradation by Co_3O_4 nanoparticles-activated PS[243].

- **Comparative analysis of OG degradation using Gliding arc plasma :**

Gliding arc plasma has shown considerable potential for energy conversion and chemical reactions. Due to its unique properties, arc discharge possesses superior thermal characteristics compared to non-thermal plasma, making it effective for the removal of organic pollutants. The table below summarises the studies on gliding arc discharge plasma for the degradation of Orange G.

Table I.11. Degradation of OG using Gliding arc discharge.

Process	Operating parameters	Removal efficiency	Time	Ref
GAD/Laterite soil	Gliding arc plasma reactor 500 ml of OG solution; pH adjusted to 3–10 3g/L Ltérite soil	17% with GAD alone Nearly 100% with GAD/ laterite soil	60min	[248]
GAD/ TiO_2	Gliding arc plasma reactor 500 ml of OG solution; 0.16 g/L P_{25} TiO_2	17% with GAD alone Nearly 56% with GAD/ catalyst	60min	[248]
GAD/TiO2/Fe_2O_3	Gliding arc plasma reactor 500 ml of OG solution; 3g/L TiO_2/Fe_2O_3	17% with GAD alone Nearly 75 with GAD/TiO_2/Fe_2O_3	60min	[248]

BIBLIOGRAPHICAL REFERENCES

1. King-Thom Chung. Azo dyes and human health: A review. Disponible sur: https://doi.org/10.1080/10590501.2016.1236602

2. Towns AD. Developments in azo disperse dyes derived from heterocyclic diazo components. Dyes Pigments. avr 1999;42(1):3-28.

3. M.Sudha, A.Saranya, G. Selvakumar, N. Sivakumar. Microbial degradation of Azo Dyes: A review. Disponible sur: http://www.ijcmas.com/

4. Amit Bafana, Sivanesan Saravana Dev, Tapan Chakrabarti. Azo dyes: past, present and the future. Disponible sur: doi:10.1139/A11-018

5. Gürses A, Açıkyıldız M, Güneş K, Gürses MS. Classification of Dye and Pigments. In: Dyes and Pigments [Internet]. Cham: Springer International Publishing; 2016 [cité 13 août 2024]. p. 31-45. (SpringerBriefs in Molecular Science). Disponible sur: http://link.springer.com/10.1007/978-3-319-33892-7_3

6. Eltaboni F, Bader N, ElKailany R, Elsharif N, Ahmida A. Chemistry and Applications of Azo Dyes: A Comprehensive Review. J Chem Rev [Internet]. août 2022 [cité 14 août 2024];(Online First). Disponible sur: https://doi.org/10.22034/jcr.2022.349827.1177

7. Tölgyesi Á, Sharma VK. Quantification of aromatic amines derived from azo colorants in textile by ion-pairing liquid chromatography tandem mass spectrometry. J Chromatogr B. janv 2020;1137:121957.

8. Crespi S, Simeth NA, König B. Heteroaryl azo dyes as molecular photoswitches. Nat Rev Chem. 8 févr 2019;3(3):133-46.

9. Shankarling GS, Deshmukh PP, Joglekar AR. Process intensification in azo dyes. J Environ Chem Eng. août 2017;5(4):3302-8.

10. Chung KT. Azo dyes and human health: A review. J Environ Sci Health Part C. oct 2016;34(4):233-61.

11. Mezgebe K, Mulugeta E. Synthesis and pharmacological activities of azo dye derivatives incorporating heterocyclic scaffolds: a review. RSC Adv. 2022;12(40):25932-46.

12. Gürses A, Açıkyıldız M, Güneş K, Gürses MS. Colorants in Health and Environmental Aspects. In: Dyes and Pigments [Internet]. Cham: Springer

International Publishing; 2016 [cité 18 août 2024]. p. 69-83. (SpringerBriefs in Molecular Science). Disponible sur: http://link.springer.com/10.1007/978-3-319-33892-7_5

13. Akram Hijazi, Ali Mcheik, Hassan Rammal, Wassim Rammal, Houssein Annan, Joumana Toufaily, et al. BIOSORPTION OF METHYLENE BLUE FROM WASTE WATER USING LEBANESE CYMBOPOGON CITRATUS (CITRONNELLE). Disponible sur: https://eujournal.org/index.php/esj/article/view/6002

14. He F, Hu W, Li Y. Biodegradation mechanisms and kinetics of azo dye 4BS by a microbial consortium. Chemosphere. oct 2004;57(4):293-301.

15. Asad S, Amoozegar MA, Pourbabaee AA, Sarbolouki MN, Dastgheib SMM. Decolorization of textile azo dyes by newly isolated halophilic and halotolerant bacteria. Bioresour Technol. août 2007;98(11):2082-8.

16. Verma P, Samanta SK. Microwave-enhanced advanced oxidation processes for the degradation of dyes in water. Environ Chem Lett. sept 2018;16(3):969-1007.

17. Roy N, Alex SA, Chandrasekaran N, Kannabiran K, Mukherjee A. Studies on the removal of acid violet 7 dye from aqueous solutions by green ZnO@Fe3O4 chitosan–alginate nanocomposite synthesized using Camellia sinensis extract. J Environ Manage. févr 2022;303:114128.

18. Xia Y, Wang G, Guo L, Dai Q, Ma X. Electrochemical oxidation of Acid Orange 7 azo dye using a PbO2 electrode: Parameter optimization, reaction mechanism and toxicity evaluation. Chemosphere. févr 2020;241:125010.

19. Seyyedi K, Jahromi MAF. Decolorization of Azo Dye C.I. Direct Black 38 by Photocatalytic Method Using TiO2 and Optimizing of Process. APCBEE Procedia. 2014;10:115-9.

20. Nandhini NT, Rajeshkumar S, Mythili S. The possible mechanism of eco-friendly synthesized nanoparticles on hazardous dyes degradation. Biocatal Agric Biotechnol. mai 2019;19:101138.

21. Wang X, Yao Z, Wang J, Guo W, Li G. Degradation of reactive brilliant red in aqueous solution by ultrasonic cavitation. Ultrason Sonochem. janv 2008;15(1):43-8.

22. Ngo ACR, Tischler D. Microbial Degradation of Azo Dyes: Approaches and Prospects for a Hazard-Free Conversion by Microorganisms. Int J Environ Res Public Health. 14 avr 2022;19(8):4740.

23. Vineis P, Pirastu R. Aromatic amines and cancer. Cancer Causes Control. 1997;8(3):346-55.

24. Imtiazuddin SM, Tiki A. Textile Azo Dyes; Significance, Ecological, Health, and Safety issues. Pak J Chem. 7 juin 2021;10((1-4)):35.

25. Official Journal of the People's Democratic Republic of Algeria, 2006. Decree no. 06-141 of 20 Rabie Elaouel 1427, corresponding to 19 April 2006, defining the limit values for industrial waste.

26. Adeyemo AA, Adeoye IO, Bello OS. Adsorption of dyes using different types of clay: a review. Appl Water Sci. mai 2017;7(2):543-68.

27. Khenifi A, Bouberka Z, Sekrane F, Kameche M, Derriche Z. Adsorption study of an industrial dye by an organic clay. Adsorption. 27 sept 2007;13(2):149-58.

28. Romain Prulho. Analyse multi-échelle de la dégradation de membranes polymères d'ultrafiltration au contact de l'hypochlorite de sodium. Autre. Université Blaise Pascal - Clermont-Ferrand II, 2013. Français. ffNNT : 2013CLF22346ff. fftel-00866935f.

29. Hilal N, Kim GJ, Somerfield C. Boron removal from saline water: A comprehensive review. Desalination. juin 2011;273(1):23-35.

30. Obotey Ezugbe E, Rathilal S. Membrane Technologies in Wastewater Treatment: A Review. Membranes. 30 avr 2020;10(5):89.

31. Zinicovscaia I. Conventional Methods of Wastewater Treatment. In: Zinicovscaia I, Cepoi L, éditeurs. Cyanobacteria for Bioremediation of Wastewaters [Internet]. Cham: Springer International Publishing; 2016 [cité 29 sept 2024]. p. 17-25. Disponible sur: http://link.springer.com/10.1007/978-3-319-26751-7_3

32. Khouni I, Marrot B, Moulin P, Ben Amar R. Decolourization of the reconstituted textile effluent by different process treatments: Enzymatic catalysis, coagulation/flocculation and nanofiltration processes. Desalination. mars 2011;268(1-3):27-37.

33. Bala S, Garg D, Thirumalesh BV, Sharma M, Sridhar K, Inbaraj BS, et al. Recent Strategies for Bioremediation of Emerging Pollutants: A Review for a Green and Sustainable Environment. Toxics. 19 août 2022;10(8):484.

34. Gupta VK, Ali I, Saleh TA, Nayak A, Agarwal S. Chemical treatment technologies for waste-water recycling—an overview. RSC Adv. 2012;2(16):6380.

35. Khan JA, Sayed M, Khan S, Shah NS, Dionysiou DD, Boczkaj G. Advanced oxidation processes for the treatment of contaminants of emerging concern. In: Contaminants of Emerging Concern in Water and Wastewater [Internet]. Elsevier; 2020 [cité 2 oct 2024]. p. 299-365. Disponible sur: https://linkinghub.elsevier.com/retrieve/pii/B9780128135617000092

36. O'Shea KE, Dionysiou DD. Advanced Oxidation Processes for Water Treatment. J Phys Chem Lett. 2 août 2012;3(15):2112-3.

37. Kumari P, Kumar A. ADVANCED OXIDATION PROCESS: A remediation technique for organic and non-biodegradable pollutant. Results Surf Interfaces. mai 2023;11:100122.

38. Saravanan A, Deivayanai VC, Kumar PS, Rangasamy G, Hemavathy RV, Harshana T, et al. A detailed review on advanced oxidation process in treatment of wastewater: Mechanism, challenges and future outlook. Chemosphere. déc 2022;308:136524.

39. Gautam P, Kumar S, Lokhandwala S. Advanced oxidation processes for treatment of leachate from hazardous waste landfill: A critical review. J Clean Prod. nov 2019;237:117639.

40. Khan AH, Khan NA, Ahmed S, Dhingra A, Singh CP, Khan SU, et al. Application of advanced oxidation processes followed by different treatment technologies for hospital wastewater treatment. J Clean Prod. oct 2020;269:122411.

41. Zhang Y, Zhang J, Xiao Y, Chang VWC, Lim TT. Kinetic and mechanistic investigation of azathioprine degradation in water by UV, UV/H 2 O 2 and UV/persulfate. Chem Eng J. oct 2016;302:526-34.

42. Legrini O, Oliveros E, Braun AM. Photochemical processes for water treatment. Chem Rev. 1 mars 1993;93(2):671-98.

43. Ribeiro AR, Nunes OC, Pereira MFR, Silva AMT. An overview on the advanced oxidation processes applied for the treatment of water pollutants defined in the recently launched Directive 2013/39/EU. Environ Int. févr 2015;75:33-51.

44. Jafarinejad S. Treatment of Oily Wastewater. In: Petroleum Waste Treatment and Pollution Control [Internet]. Elsevier; 2017 [cité 7 oct 2024]. p. 185-267. Disponible sur: https://linkinghub.elsevier.com/retrieve/pii/B9780128092439000067

45. Fenton HJH. LXXIII.—Oxidation of tartaric acid in presence of iron. J Chem Soc Trans. 1894;65(0):899-910.

46. Babuponnusami A, Muthukumar K. A review on Fenton and improvements to the Fenton process for wastewater treatment. J Environ Chem Eng. mars 2014;2(1):557-72.

47. Ziembowicz S, Kida M. Limitations and future directions of application of the Fenton-like process in micropollutants degradation in water and wastewater treatment: A critical review. Chemosphere. juin 2022;296:134041.

48. Merényi G, Lind J, Naumov S, Sonntag CV. Reaction of Ozone with Hydrogen Peroxide (Peroxone Process): A Revision of Current Mechanistic Concepts Based on Thermokinetic and Quantum-Chemical Considerations. Environ Sci Technol. 1 mai 2010;44(9):3505-7.

49. Cuerda-Correa EM, Alexandre-Franco MF, Fernández-González C. Advanced Oxidation Processes for the Removal of Antibiotics from Water. An Overview. Water. 27 déc 2019;12(1):102.

50. Photochemistry of organic compounds: from concepts to practice. Chichester, U.K: Wiley; 2010.

51. Speight JG. Redox Transformations. In: Reaction Mechanisms in Environmental Engineering [Internet]. Elsevier; 2018 [cité 7 oct 2024]. p. 231-67. Disponible sur: https://linkinghub.elsevier.com/retrieve/pii/B9780128044223000079

52. Anisuzzaman SM, Joseph CG, Pang CK, Affandi NA, Maruja SN, Vijayan V. Current Trends in the Utilization of Photolysis and Photocatalysis Treatment Processes for the Remediation of Dye Wastewater: A Short Review. ChemEngineering. 1 août 2022;6(4):58.

53. Asghar A, Abdul Raman AA, Wan Daud WMA. Advanced oxidation processes for in-situ production of hydrogen peroxide/hydroxyl radical for textile wastewater treatment: a review. J Clean Prod. janv 2015;87:826-38.

54. Zang Y, Farnood R. Effects of hydrogen peroxide concentration and ultraviolet light intensity on methyl tert-butyl ether degradation kinetics. Chem Eng Sci. mars 2005;60(6):1641-8.

55. Mierzwa JC, Rodrigues R, Teixeira ACSC. UV-Hydrogen Peroxide Processes. In: Advanced Oxidation Processes for Waste Water Treatment [Internet]. Elsevier; 2018 [cité 7 oct 2024]. p. 13-48. Disponible sur: https://linkinghub.elsevier.com/retrieve/pii/B9780128104996000024

56. Rodríguez M, Abderrazik NB, Contreras S, Chamarro E, Gimenez J, Esplugas S. Iron(III) photoxidation of organic compounds in aqueous solutions. Appl Catal B Environ. avr 2002;37(2):131-7.

57. Wood PC, Wydeven T, Tsuji O. Critical Process Variables for UV-Ozone Etching of Photoresist. MRS Online Proc Libr. déc 1993;315(1):237-42.

58. Kuo WS. Synergistic effects of combination of photolysis and ozonation on destruction of chlorophenols in water. Chemosphere. nov 1999;39(11):1853-60.

59. Panda D, Venkatesh N, Sakthivel P. MXene-based materials for remediation of environmental pollutants. In: Mxenes and their Composites [Internet]. Elsevier; 2022 [cité 11 oct 2024]. p. 553-94. Disponible sur: https://linkinghub.elsevier.com/retrieve/pii/B9780128233610000149

60. Mrowetz M, Balcerski W, Colussi AJ, Hoffmann MR. Oxidative Power of Nitrogen-Doped TiO_2 Photocatalysts under Visible Illumination. J Phys Chem B. 1 nov 2004;108(45):17269-73.

61. Chong MN, Jin B, Chow CWK, Saint C. Recent developments in photocatalytic water treatment technology: A review. Water Res. mai 2010;44(10):2997-3027.

62. Kavitha V, Palanivelu K. The role of ferrous ion in Fenton and photo-Fenton processes for the degradation of phenol. Chemosphere. juin 2004;55(9):1235-43.

63. Ameta R, K. Chohadia A, Jain A, Punjabi PB. Fenton and Photo-Fenton Processes. In: Advanced Oxidation Processes for Waste Water Treatment

[Internet]. Elsevier; 2018 [cité 11 oct 2024]. p. 49-87. Disponible sur: https://linkinghub.elsevier.com/retrieve/pii/B9780128104996000036

64. Liou MJ, Lu MC, Chen JN. Oxidation of explosives by Fenton and photo-Fenton processes. Water Res. juill 2003;37(13):3172-9.

65. Knight RJ, Sylva RN. Spectrophotometric investigation of iron(III) hydrolysis in light and heavy water at 25°C. J Inorg Nucl Chem. mars 1975;37(3):779-83.

66. Faust BC, Hoigné J. Photolysis of Fe (III)-hydroxy complexes as sources of OH radicals in clouds, fog and rain. Atmospheric Environ Part Gen Top. janv 1990;24(1):79-89.

67. Zhao XK, Yang GP, Wang YJ, Gao XC. Photochemical degradation of dimethyl phthalate by Fenton reagent. J Photochem Photobiol Chem. janv 2004;161(2-3):215-20.

68. Mazellier P, Jirkovsky J, Bolte M. Degradation of Diuron Photoinduced by Iron(III) in Aqueous Solution. Pestic Sci. mars 1997;49(3):259-67.

69. Monteagudo JM, Durán A, López-Almodóvar C. Homogeneus ferrioxalate-assisted solar photo-Fenton degradation of Orange II aqueous solutions. Appl Catal B Environ. sept 2008;83(1-2):46-55.

70. Pignatello JJ, Sun Y. Complete oxidation of metolachlor and methyl parathion in water by the photoassisted Fenton reaction. Water Res. août 1995;29(8):1837-44.

71. Alalm MG, Tawfik A, Ookawara S. Degradation of four pharmaceuticals by solar photo-Fenton process: Kinetics and costs estimation. J Environ Chem Eng. mars 2015;3(1):46-51.

72. Kiwi J, Pulgarin C, Peringer P. Effect of Fenton and photo-Fenton reactions on the degradation and biodegradability of 2 and 4-nitrophenols in water treatment. Appl Catal B Environ. mai 1994;3(4):335-50.

73. Hübner U, Spahr S, Lutze H, Wieland A, Rüting S, Gernjak W, et al. Advanced oxidation processes for water and wastewater treatment – Guidance for systematic future research. Heliyon. mai 2024;10(9):e30402.

74. Loddo V, Bellardita M, Camera-Roda G, Parrino F, Palmisano L. Heterogeneous Photocatalysis. In: Current Trends and Future Developments on (Bio-) Membranes [Internet]. Elsevier; 2018 [cité 22 oct

2024]. p. 1-43. Disponible sur: https://linkinghub.elsevier.com/retrieve/pii/B9780128135495000013

75. Hu Q, Liu B, Zhang Z, Song M, Zhao X. Temperature effect on the photocatalytic degradation of methyl orange under UV-vis light irradiation. J Wuhan Univ Technol-Mater Sci Ed. avr 2010;25(2):210-3.

76. Al-Mamun MR, Kader S, Islam MS, Khan MZH. Photocatalytic activity improvement and application of UV-TiO2 photocatalysis in textile wastewater treatment: A review. J Environ Chem Eng. oct 2019;7(5):103248.

77. Palmisano L, Schiavello M, Sclafani A, Martra G, Borello E, Coluccia S. Photocatalytic oxidation of phenol on TiO2 powders. A Fourier transform infrared study. Appl Catal B Environ. févr 1994;3(2-3):117-32.

78. Rivera AP, Tanaka K, Hisanaga T. Photocatalytic degradation of pollutant over TiO2 in different crystal structures. Appl Catal B Environ. déc 1993;3(1):37-44.

79. Sun B, Smirniotis PG. Interaction of anatase and rutile TiO2 particles in aqueous photooxidation. Catal Today. déc 2003;88(1-2):49-59.

80. Thiruvenkatachari R, Vigneswaran S, Moon IS. A review on UV/TiO2 photocatalytic oxidation process (Journal Review). Korean J Chem Eng. janv 2008;25(1):64-72.

81. Deng H, Qin C, Pei K, Wu G, Wang M, Ni H, et al. TiO2/reduced hydroxylated graphene nanocomposite photocatalysts: Improved electron–hole separation and migration. Mater Chem Phys. sept 2021;270:124796.

82. Banerjee S, Dionysiou DD, Pillai SC. Self-cleaning applications of TiO2 by photo-induced hydrophilicity and photocatalysis. Appl Catal B Environ. oct 2015;176-177:396-428.

83. Krishnan S, Karim AV, Sethulekshmi S, Shriwastav A. Removal of pharmaceutically active compounds from wastewater by hybrid advanced oxidation processes. In: Concept of Zero Liquid Discharge [Internet]. Elsevier; 2023 [cité 26 oct 2024]. p. 187-223. Disponible sur: https://linkinghub.elsevier.com/retrieve/pii/B9780323917452000073

84. Martín-Pozo L, Gómez-Regalado MDC, García-Córcoles MT, Zafra-Gómez A. Removal of quinolone antibiotics from wastewaters and sewage sludge. In: Emerging Contaminants in the Environment [Internet].

Elsevier; 2022 [cité 26 oct 2024]. p. 381-406. Disponible sur: https://linkinghub.elsevier.com/retrieve/pii/B9780323851602000159

85. Brillas E, Bastida RM, Llosa E, Casado J. Electrochemical Destruction of Aniline and 4-Chloroaniline for Wastewater Treatment Using a Carbon-PTFE O 2 - Fed Cathode. J Electrochem Soc. 1 juin 1995;142(6):1733-41.

86. Oturan MA, Pinson J. Hydroxylation by Electrochemically Generated OH.bul. Radicals. Mono- and Polyhydroxylation of Benzoic Acid: Products and Isomer Distribution. J Phys Chem. sept 1995;99(38):13948-54.

87. Brillas E. Mineralization of 2,4-D by advanced electrochemical oxidation processes. Water Res. juin 2000;34(8):2253-62.

88. Oturan N, Oturan MA. Electro-Fenton Process: Background, New Developments, and Applications. In: Electrochemical Water and Wastewater Treatment [Internet]. Elsevier; 2018 [cité 27 oct 2024]. p. 193-221. Disponible sur: https://linkinghub.elsevier.com/retrieve/pii/B9780128131602000080

89. Fu R, Zhang PS, Jiang YX, Sun L, Sun XH. Wastewater treatment by anodic oxidation in electrochemical advanced oxidation process: Advance in mechanism, direct and indirect oxidation detection methods. Chemosphere. janv 2023;311:136993.

90. Ganiyu SO, Martínez-Huitle CA, Oturan MA. Electrochemical advanced oxidation processes for wastewater treatment: Advances in formation and detection of reactive species and mechanisms. Curr Opin Electrochem. juin 2021;27:100678.

91. Brillas E, Garcia-Segura S, Skoumal M, Arias C. Electrochemical incineration of diclofenac in neutral aqueous medium by anodic oxidation using Pt and boron-doped diamond anodes. Chemosphere. avr 2010;79(6):605-12.

92. Li X yan, Cui Y hong, Feng Y jie, Xie Z ming, Gu JD. Reaction pathways and mechanisms of the electrochemical degradation of phenol on different electrodes. Water Res. mai 2005;39(10):1972-81.

93. Goyal A, Srivastava VC. Treatment of highly acidic wastewater containing high energetic compounds using dimensionally stable anode. Chem Eng J. oct 2017;325:289-99.

94. Chatzisymeon E, Dimou A, Mantzavinos D, Katsaounis A. Electrochemical oxidation of model compounds and olive mill wastewater over DSA electrodes: 1. The case of Ti/IrO2 anode. J Hazard Mater. 15 août 2009;167(1-3):268-74.

95. Tan X, Zhao Y, Sun W, Jin C, Chen L, Wei H, et al. Three-dimensional hierarchically porous PbO2 electrode for electrochemical degradation of m-cresol. J Electroanal Chem. janv 2020;856:113726.

96. Mu Y, Huang C, Li H, Chen L, Zhang D, Yang Z. Electrochemical degradation of ciprofloxacin with a Sb-doped SnO_2 electrode: performance, influencing factors and degradation pathways. RSC Adv. 2019;9(51):29796-804.

97. Cai J, Zhou M, Pan Y, Lu X. Degradation of 2,4-dichlorophenoxyacetic acid by anodic oxidation and electro-Fenton using BDD anode: Influencing factors and mechanism. Sep Purif Technol. janv 2020;230:115867.

98. Jiang Y, Zhao H, Liang J, Yue L, Li T, Luo Y, et al. Anodic oxidation for the degradation of organic pollutants: Anode materials, operating conditions and mechanisms. A mini review. Electrochem Commun. févr 2021;123:106912.

99. Chatterjee T, Rahaman SK, Alam SM. Sonochemical synthesis of metal–organic frameworks. In: Synthesis of Metal-Organic Frameworks Via Water-based Routes [Internet]. Elsevier; 2024 [cité 28 oct 2024]. p. 121-42. Disponible sur: https://linkinghub.elsevier.com/retrieve/pii/B9780323959391000150

100. Qiao SZ, Liu J, Max Lu GQ. Synthetic Chemistry of Nanomaterials. In: Modern Inorganic Synthetic Chemistry [Internet]. Elsevier; 2017 [cité 28 oct 2024]. p. 613-40. Disponible sur: https://linkinghub.elsevier.com/retrieve/pii/B9780444635914000215

101. Ahmedchekkat F, Medjram MS, Chiha M, Mahmoud Ali Al-bsoul A. Sonophotocatalytic degradation of Rhodamine B using a novel reactor geometry: Effect of operating conditions. Chem Eng J. déc 2011;178:244-51.

102. Chiha M, Hamdaoui O, Baup S, Gondrexon N. Sonolytic degradation of endocrine disrupting chemical 4-cumylphenol in water. Ultrason Sonochem. sept 2011;18(5):943-50.

103. Yang L, Sostaric JZ, Rathman JF, Kuppusamy P, Weavers LK. Effects of Pulsed Ultrasound on the Adsorption of *n* -Alkyl Anionic Surfactants at the Gas/Solution Interface of Cavitation Bubbles. J Phys Chem B. 1 févr 2007;111(6):1361-7.

104. Adewuyi YG. Sonochemistry: Environmental Science and Engineering Applications. Ind Eng Chem Res. 1 oct 2001;40(22):4681-715.

105. Wang F, Wang W, Yuan S, Wang W, Hu ZH. Comparison of UV/H2O2 and UV/PS processes for the degradation of thiamphenicol in aqueous solution. J Photochem Photobiol Chem. nov 2017;348:79-88.

106. Yang Q, Ma Y, Chen F, Yao F, Sun J, Wang S, et al. Recent advances in photo-activated sulfate radical-advanced oxidation process (SR-AOP) for refractory organic pollutants removal in water. Chem Eng J. déc 2019;378:122149.

107. Xia X, Zhu F, Li J, Yang H, Wei L, Li Q, et al. A Review Study on Sulfate-Radical-Based Advanced Oxidation Processes for Domestic/Industrial Wastewater Treatment: Degradation, Efficiency, and Mechanism. Front Chem. 27 nov 2020;8:592056.

108. Wacławek S, Lutze HV, Grübel K, Padil VVT, Černík M, Dionysiou DionysiosD. Chemistry of persulfates in water and wastewater treatment: A review. Chem Eng J. déc 2017;330:44-62.

109. Chao L, Mengfei L, Xueqing X, Shilong H, Yunzhi Q. Activation mechanism and strengthening strategies of perovskites activated peroxymonosulfate for organic pollutants degradation: Recent advances and perspective. J Alloys Compd. févr 2024;973:172898.

110. Xiao R, Luo Z, Wei Z, Luo S, Spinney R, Yang W, et al. Activation of peroxymonosulfate/persulfate by nanomaterials for sulfate radical-based advanced oxidation technologies. Curr Opin Chem Eng. mars 2018;19:51-8.

111. Choi J, Kim H il, Lee J, Lee H. Role of nitrite ligands in enhancing sulfate radical production via catalytic peroxymonosulfate activation by cobalt complexes. Sep Purif Technol. déc 2021;279:119698.

112. Neta P, Huie RE, Ross AB. Rate Constants for Reactions of Inorganic Radicals in Aqueous Solution. J Phys Chem Ref Data. 1 juill 1988;17(3):1027-284.

113. Nidheesh PV, Divyapriya G, Ezzahra Titchou F, Hamdani M. Treatment of textile wastewater by sulfate radical based advanced oxidation processes. Sep Purif Technol. juill 2022;293:121115.

114. Ushani U, Lu X, Wang J, Zhang Z, Dai J, Tan Y, et al. Sulfate radicals-based advanced oxidation technology in various environmental remediation: A state-of-the–art review. Chem Eng J. déc 2020;402:126232.

115. Lutze HV, Bircher S, Rapp I, Kerlin N, Bakkour R, Geisler M, et al. Degradation of Chlorotriazine Pesticides by Sulfate Radicals and the Influence of Organic Matter. Environ Sci Technol. 3 févr 2015;49(3):1673-80.

116. Gara PMD, Bosio GN, Gonzalez MC, Mártire DO. Kinetics of the sulfate radical-mediated photo-oxidation of humic substances. Int J Chem Kinet. janv 2008;40(1):19-24.

117. Liliane Ismail. Étude de la dégradation de la sulfaclozine par les radicaux OH• et SO4•– et évaluation de l'influence des principaux constituants des eaux sur ces dégradations [THESE de DOCTORAT]. [FRANCE]: UNIVERSITE DE LYON; 2016.

118. Zhou Y, Xiang Y, He Y, Yang Y, Zhang J, Luo L, et al. Applications and factors influencing of the persulfate-based advanced oxidation processes for the remediation of groundwater and soil contaminated with organic compounds. J Hazard Mater. oct 2018;359:396-407.

119. House DA. Kinetics and Mechanism of Oxidations by Peroxydisulfate. Chem Rev. 1 juin 1962;62(3):185-203.

120. Li S, Zhang T, Zheng H, Dong X, Leong YK, Chang JS. Advances and challenges in the removal of organic pollutants via sulfate radical-based advanced oxidation processes by Fe-based metal-organic frameworks: A review. Sci Total Environ. mai 2024;926:171885.

121. Mora VC, Rosso JA. Treatment of PAH-contaminated soil by persulfate: a review. Curr Opin Chem Eng. sept 2022;37:100842.

122. Wang B, Wang Y. A comprehensive review on persulfate activation treatment of wastewater. Sci Total Environ. juill 2022;831:154906.

123. Yang Y, Ji Y, Yang P, Wang L, Lu J, Ferronato C, et al. UV-activated persulfate oxidation of the insensitive munitions compound 2,4-

dinitroanisole in water: Kinetics, products, and influence of natural photoinducers. J Photochem Photobiol Chem. juin 2018;360:188-95.

124. Herrmann H. On the photolysis of simple anions and neutral molecules as sources of O^- /OH, SO_x^- and Cl in aqueous solution. Phys Chem Chem Phys. 2007;9(30):3935-64.

125. Ghanbari F, Moradi M. Application of peroxymonosulfate and its activation methods for degradation of environmental organic pollutants: Review. Chem Eng J. févr 2017;310:41-62.

126. Carlson JC, Stefan MI, Parnis JM, Metcalfe CD. Direct UV photolysis of selected pharmaceuticals, personal care products and endocrine disruptors in aqueous solution. Water Res. nov 2015;84:350-61.

127. Yang J, Zhu M, Dionysiou DD. What is the role of light in persulfate-based advanced oxidation for water treatment? Water Res. févr 2021;189:116627.

128. Petri BG, Watts RJ, Tsitonaki A, Crimi M, Thomson NR, Teel AL. Fundamentals of ISCO Using Persulfate. In: Siegrist RL, Crimi M, Simpkin TJ, éditeurs. In Situ Chemical Oxidation for Groundwater Remediation [Internet]. New York, NY: Springer New York; 2011 [cité 21 nov 2024]. p. 147-91. (SERDP/ESTCP Environmental Remediation Technology; vol. 3). Disponible sur: http://link.springer.com/10.1007/978-1-4419-7826-4_4

129. Matzek LW, Carter KE. Activated persulfate for organic chemical degradation: A review. Chemosphere. mai 2016;151:178-88.

130. Wang J, Wang S. Activation of persulfate (PS) and peroxymonosulfate (PMS) and application for the degradation of emerging contaminants. Chem Eng J. févr 2018;334:1502-17.

131. Wei L, Xia X, Zhu F, Li Q, Xue M, Li J, et al. Dewatering efficiency of sewage sludge during Fe2+-activated persulfate oxidation: Effect of hydrophobic/hydrophilic properties of sludge EPS. Water Res. août 2020;181:115903.

132. Fordham JWL, Williams HL. The Persulfate-Iron(II) Initiator System for Free Radical Polymerizations[1]. J Am Chem Soc. oct 1951;73(10):4855-9.

133. Rastogi A, Al-Abed SR, Dionysiou DD. Sulfate radical-based ferrous–peroxymonosulfate oxidative system for PCBs degradation in aqueous and sediment systems. Appl Catal B Environ. janv 2009;85(3-4):171-9.

134. Yang L, Xue J, He L, Wu L, Ma Y, Chen H, et al. Review on ultrasound assisted persulfate degradation of organic contaminants in wastewater: Influences, mechanisms and prospective. Chem Eng J. déc 2019;378:122146.

135. Chakma S, Praneeth S, Moholkar VS. Mechanistic investigations in sono-hybrid (ultrasound/Fe2+/UVC) techniques of persulfate activation for degradation of Azorubine. Ultrason Sonochem. sept 2017;38:652-63.

136. Su R, Li Z, Cheng F, Dai X, Wang H, Luo Y, et al. Advances in the Degradation of Emerging Contaminants by Persulfate Oxidation Technology. Water Air Soil Pollut. déc 2023;234(12):754.

137. Guo H, Pan S, Hu Z, Wang Y, Jiang W, Yang Y, et al. Persulfate activated by non-thermal plasma for organic pollutants degradation: A review. Chem Eng J. août 2023;470:144094.

138. Sonawane S, Rayaroth MP, Landge VK, Fedorov K, Boczkaj G. Thermally activated persulfate-based Advanced Oxidation Processes — recent progress and challenges in mineralization of persistent organic chemicals: a review. Curr Opin Chem Eng. sept 2022;37:100839.

139. Hassani A, Scaria J, Ghanbari F, Nidheesh PV. Sulfate radicals-based advanced oxidation processes for the degradation of pharmaceuticals and personal care products: A review on relevant activation mechanisms, performance, and perspectives. Environ Res. janv 2023;217:114789.

140. Yang L, He L, Xue J, Ma Y, Xie Z, Wu L, et al. Persulfate-based degradation of perfluorooctanoic acid (PFOA) and perfluorooctane sulfonate (PFOS) in aqueous solution: Review on influences, mechanisms and prospective. J Hazard Mater. juill 2020;393:122405.

141. Wang G, Wang P, Liu H, Wang J, Dai X, Xin Y. Degradation of spiramycin by thermally activated peroxydisulfate: Kinetics study, oxidation products and acute toxicity. Chem Eng J. mars 2021;408:127255.

142. Chen J, Qian Y, Liu H, Huang T. Oxidative degradation of diclofenac by thermally activated persulfate: implication for ISCO. Environ Sci Pollut Res. févr 2016;23(4):3824-33.

143. Peyton GR. The free-radical chemistry of persulfate-based total organic carbon analyzers. Mar Chem. janv 1993;41(1-3):91-103.

144. Dominguez CM, Romero A, Lorenzo D, Santos A. Thermally activated persulfate for the chemical oxidation of chlorinated organic compounds in groundwater. J Environ Manage. mai 2020;261:110240.

145. Arvaniti OS, Bairamis F, Konstantinou I, Mantzavinos D, Frontistis Z. Degradation of antihypertensive drug valsartan in water matrices by heat and heat/ultrasound activated persulfate: Kinetics, synergy effect and transformation products. Chem Eng J Adv. déc 2020;4:100062.

146. Zhao J, Sun Y, Wu F, Shi M, Liu X. Oxidative Degradation of Amoxicillin in Aqueous Solution by Thermally Activated Persulfate. J Chem. 12 mars 2019;2019:1-10.

147. Feng Y, Song Q, Lv W, Liu G. Degradation of ketoprofen by sulfate radical-based advanced oxidation processes: Kinetics, mechanisms, and effects of natural water matrices. Chemosphere. déc 2017;189:643-51.

148. Fan Y, Ji Y, Kong D, Lu J, Zhou Q. Kinetic and mechanistic investigations of the degradation of sulfamethazine in heat-activated persulfate oxidation process. J Hazard Mater. déc 2015;300:39-47.

149. Milh H, Schoenaers B, Stesmans A, Cabooter D, Dewil R. Degradation of sulfamethoxazole by heat-activated persulfate oxidation: Elucidation of the degradation mechanism and influence of process parameters. Chem Eng J. janv 2020;379:122234.

150. Ji Y, Dong C, Kong D, Lu J, Zhou Q. Heat-activated persulfate oxidation of atrazine: Implications for remediation of groundwater contaminated by herbicides. Chem Eng J. mars 2015;263:45-54.

151. Lebik-Elhadi H, Frontistis Z, Ait-Amar H, Madjene F, Mantzavinos D. Degradation of pesticide thiamethoxam by heat – activated and ultrasound – activated persulfate: Effect of key operating parameters and the water matrix. Process Saf Environ Prot. févr 2020;134:197-207.

152. Potakis N, Frontistis Z, Antonopoulou M, Konstantinou I, Mantzavinos D. Oxidation of bisphenol A in water by heat-activated persulfate. J Environ Manage. juin 2017;195:125-32.

153. Wang Q, Lu X, Cao Y, Ma J, Jiang J, Bai X, et al. Degradation of Bisphenol S by heat activated persulfate: Kinetics study, transformation

pathways and influences of co-existing chemicals. Chem Eng J. nov 2017;328:236-45.

154. Zhang M, Chen X, Zhou H, Murugananthan M, Zhang Y. Degradation of p-nitrophenol by heat and metal ions co-activated persulfate. Chem Eng J. mars 2015;264:39-47.

155. Luo C, Wu D, Gan L, Cheng X, Ma Q, Tan F, et al. Oxidation of Congo red by thermally activated persulfate process: Kinetics and transformation pathway. Sep Purif Technol. août 2020;244:116839.

156. Ghauch A, Tuqan AM, Kibbi N, Geryes S. Methylene blue discoloration by heated persulfate in aqueous solution. Chem Eng J. déc 2012;213:259-71.

157. Shuchi SB, Suhan MdBK, Humayun SB, Haque ME, Islam MdS. Heat-activated potassium persulfate treatment of Sudan Black B dye: Degradation kinetic and thermodynamic studies. J Water Process Eng. févr 2021;39:101690.

158. Liang C, Su HW. Identification of Sulfate and Hydroxyl Radicals in Thermally Activated Persulfate. Ind Eng Chem Res. 3 juin 2009;48(11):5558-62.

159. Hayon E, Treinin A, Wilf J. Electronic spectra, photochemistry, and autoxidation mechanism of the sulfite-bisulfite-pyrosulfite systems. SO2-, SO3-, SO4-, and SO5- radicals. J Am Chem Soc. janv 1972;94(1):47-57.

160. Gao Y qiong, Gao N yun, Deng Y, Yang Y qiong, Ma Y. Ultraviolet (UV) light-activated persulfate oxidation of sulfamethazine in water. Chem Eng J. juill 2012;195-196:248-53.

161. Pignatello JJ, Oliveros E, MacKay A. Advanced Oxidation Processes for Organic Contaminant Destruction Based on the Fenton Reaction and Related Chemistry. Crit Rev Environ Sci Technol. janv 2006;36(1):1-84.

162. Merga G, Aravindakumar CT, Rao BSM, Mohan H, Mittal JP. Pulse radiolysis study of the reactions of $SO^{\cdot}_{-4}$ with some substituted benzenes in aqueous solution. J Chem Soc Faraday Trans. 1994;90(4):597-604.

163. Gao Y qiong, Fang J nan, Gao N yun, Yi X nong, Mao W, Zhang J. Kinetic and mechanistic investigations of the degradation of propranolol in heat activated persulfate process. RSC Adv. 2018;8(72):41163-71.

164. Miao D, Peng J, Zhou X, Qian L, Wang M, Zhai L, et al. Oxidative degradation of atenolol by heat-activated persulfate: Kinetics, degradation pathways and distribution of transformation intermediates. Chemosphere. sept 2018;207:174-82.

165. Al Hakim S, Baalbaki A, Tantawi O, Ghauch A. Chemically and thermally activated persulfate for theophylline degradation and application to pharmaceutical factory effluent. RSC Adv. 2019;9(57):33472-85.

166. Zhou R, Li T, Su Y, Ma T, Zhang L, Ren H. Oxidative removal of metronidazole from aqueous solution by thermally activated persulfate process: kinetics and mechanisms. Environ Sci Pollut Res. janv 2018;25(3):2466-75.

167. Norzaee S, Taghavi M, Djahed B, Kord Mostafapour F. Degradation of Penicillin G by heat activated persulfate in aqueous solution. J Environ Manage. juin 2018;215:316-23.

168. Ioannidi A, Frontistis Z, Mantzavinos D. Destruction of propyl paraben by persulfate activated with UV-A light emitting diodes. J Environ Chem Eng. avr 2018;6(2):2992-7.

169. Arvaniti OS, Ioannidi AA, Mantzavinos D, Frontistis Z. Heat-activated persulfate for the degradation of micropollutants in water: A comprehensive review and future perspectives. J Environ Manage. sept 2022;318:115568.

170. Luo D, Lin H, Li X, Wang Y, Ye L, Mai Y, et al. The Dual Role of Natural Organic Matter in the Degradation of Organic Pollutants by Persulfate-Based Advanced Oxidation Processes: A Mini-Review. Toxics. 23 oct 2024;12(11):770.

171. Sillanpää M, Ncibi MC, Matilainen A. Advanced oxidation processes for the removal of natural organic matter from drinking water sources: A comprehensive review. J Environ Manage. févr 2018;208:56-76.

172. Jia J, Liu D, Tian J, Wang W, Ni J, Wang X. Visible-light-excited humic acid for peroxymonosulfate activation to degrade bisphenol A. Chem Eng J. nov 2020;400:125853.

173. Gao H, Chen J, Zhang Y, Zhou X. Sulfate radicals induced degradation of Triclosan in thermally activated persulfate system. Chem Eng J. déc 2016;306:522-30.

174. Liu L, Lin S, Zhang W, Farooq U, Shen G, Hu S. Kinetic and mechanistic investigations of the degradation of sulfachloropyridazine in heat-activated persulfate oxidation process. Chem Eng J. août 2018;346:515-24.

175. Qian Y, Xue G, Chen J, Luo J, Zhou X, Gao P, et al. Oxidation of cefalexin by thermally activated persulfate: Kinetics, products, and antibacterial activity change. J Hazard Mater. juill 2018;354:153-60.

176. Li N, Wu S, Dai H, Cheng Z, Peng W, Yan B, et al. Thermal activation of persulfates for organic wastewater purification: Heating modes, mechanism and influencing factors. Chem Eng J. déc 2022;450:137976.

177. Bruton TA, Sedlak DL. Treatment of perfluoroalkyl acids by heat-activated persulfate under conditions representative of in situ chemical oxidation. Chemosphere. sept 2018;206:457-64.

178. Chen Y, Deng P, Xie P, Shang R, Wang Z, Wang S. Heat-activated persulfate oxidation of methyl- and ethyl-parabens: Effect, kinetics, and mechanism. Chemosphere. févr 2017;168:1628-36.

179. Ioannidi A, Arvaniti OS, Nika MC, Aalizadeh R, Thomaidis NS, Mantzavinos D, et al. Removal of drug losartan in environmental aquatic matrices by heat-activated persulfate: Kinetics, transformation products and synergistic effects. Chemosphere. janv 2022;287:131952.

180. Ji Y, Fan Y, Liu K, Kong D, Lu J. Thermo activated persulfate oxidation of antibiotic sulfamethoxazole and structurally related compounds. Water Res. déc 2015;87:1-9.

181. Ghauch A, Tuqan AM, Kibbi N. Naproxen abatement by thermally activated persulfate in aqueous systems. Chem Eng J. nov 2015;279:861-73.

182. Frontistis Z. Degradation of the Nonsteroidal Anti-Inflammatory Drug Piroxicam by Iron Activated Persulfate: The Role of Water Matrix and Ultrasound Synergy. Int J Environ Res Public Health. 21 nov 2018;15(11):2600.

183. Langmuir I. Oscillations in Ionized Gases. Proc Natl Acad Sci. août 1928;14(8):627-37.

184. Li S, Dang X, Yu X, Abbas G, Zhang Q, Cao L. The application of dielectric barrier discharge non-thermal plasma in VOCs abatement: A review. Chem Eng J. mai 2020;388:124275.

185. Gururani P, Bhatnagar P, Bisht B, Kumar V, Joshi NC, Tomar MS, et al. Cold plasma technology: advanced and sustainable approach for wastewater treatment. Environ Sci Pollut Res. déc 2021;28(46):65062-82.

186. Bogaerts A, Neyts E, Gijbels R, Van Der Mullen J. Gas discharge plasmas and their applications. Spectrochim Acta Part B At Spectrosc. avr 2002;57(4):609-58.

187. Vandenbroucke AM, Morent R, De Geyter N, Leys C. Non-thermal plasmas for non-catalytic and catalytic VOC abatement. J Hazard Mater. nov 2011;195:30-54.

188. Becker KH, Kogelschatz U, Schoenbach KH, Barker RJ, éditeurs. Non-Equilibrium Air Plasmas at Atmospheric Pressure [Internet]. 0 éd. CRC Press; 2004 [cité 5 févr 2025]. Disponible sur: https://www.taylorfrancis.com/books/9781482269123

189. M.I Boulos, P.Fauchais, Emil Pfender. Thermal Plasmas: Fundamentals and Applications.

190. Antoissi Mohamed Ali. Etude d'un procédé d'oxydation avancée couplé plasma non thermique/carbone activé fonctionnalisé pour le traitement d'herbicides dans l'eau. Autre. Université d'Orléans, 2024. Français. ffNNT : 2024ORLE1004ff. fftel-04555900f.

191. Chizoba Ekezie FG, Sun DW, Cheng JH. A review on recent advances in cold plasma technology for the food industry: Current applications and future trends. Trends Food Sci Technol. nov 2017;69:46-58.

192. Firdaus Zainal MN, Redzuan N, Misnal MFI. BRIEF REVIEW: COLD PLASMA. J Teknol [Internet]. 21 juin 2015 [cité 2 mars 2025];74(10). Disponible sur: https://journals.utm.my/index.php/jurnalteknologi/article/view/4834

193. Guo J, Huang K, Wang J. Bactericidal effect of various non-thermal plasma agents and the influence of experimental conditions in microbial inactivation: A review. Food Control. avr 2015;50:482-90.

194. Jiang B, Zheng J, Qiu S, Wu M, Zhang Q, Yan Z, et al. Review on electrical discharge plasma technology for wastewater remediation. Chem Eng J. janv 2014;236:348-68.

195. Czernichowski A. Gliding arc: Applications to engineering and environment control. Pure Appl Chem. 1 janv 1994;66(6):1301-10.

196. Fridman AA. Plasma chemistry. First paperback edition. Cambridge: Cambridge University Press; 2012. 978 p.

197. Krishna S, Maslani A, Izdebski T, Horakova M, Klementova S, Spatenka P. Degradation of Verapamil hydrochloride in water by gliding arc discharge. Chemosphere. juin 2016;152:47-54.

198. Kim HS, Lee DH, Fridman A, Cho YI. Residual effects and energy cost of gliding arc discharge treatment on the inactivation of Escherichia coli in water. Int J Heat Mass Transf. oct 2014;77:1075-83.

199. Tiya-Djowe A, Acayanka E, Lontio-Nkouongfo G, Laminsi S, Gaigneaux EM. Enhanced discolouration of methyl violet 10B in a gliding arc plasma reactor by the maghemite nanoparticles used as heterogeneous catalyst. J Environ Chem Eng. juin 2015;3(2):953-60.

200. Slamani S, Abdelmalek F, Ghezzar MR, Addou A. Initiation of Fenton process by plasma gliding arc discharge for the degradation of paracetamol in water. J Photochem Photobiol Chem. mai 2018;359:1-10.

201. Iya-Sou Djakaou. Elimination de solutés organiques polluants d'effluents liquides par plasma non thermique : comparaison des processus mis en jeu à l'interface liquide-plasma dans les procédés Glidarc et DBD. Génie des procédés. Université Pierre et Marie Curie - Paris VI, 2012. Français. ffNNT : 2012PAO66213ff. fftel-00831334f.

202. Mumtaz S, Khan R, Rana JN, Javed R, Iqbal M, Choi EH, et al. Review on the Biomedical and Environmental Applications of Nonthermal Plasma. Catalysts. 31 mars 2023;13(4):685.

203. Bradu C, Kutasi K, Magureanu M, Puač N, Živković S. Reactive nitrogen species in plasma-activated water: generation, chemistry and application in agriculture. J Phys Appl Phys. 27 mai 2020;53(22):223001.

204. Gomez E, Rani DA, Cheeseman CR, Deegan D, Wise M, Boccaccini AR. Thermal plasma technology for the treatment of wastes: A critical review. J Hazard Mater. janv 2009;161(2-3):614-26.

205. Joshi AA, Locke BR, Arce P, Finney WC. Formation of hydroxyl radicals, hydrogen peroxide and aqueous electrons by pulsed streamer corona discharge in aqueous solution. J Hazard Mater. avr 1995;41(1):3-30.

206. Roots R, Okada S. Estimation of Life Times and Diffusion Distances of Radicals Involved in X-Ray-Induced DNA Strand Breaks or Killing of Mammalian Cells. Radiat Res. nov 1975;64(2):306.

207. Locke BR, Shih KY. Review of the methods to form hydrogen peroxide in electrical discharge plasma with liquid water. Plasma Sources Sci Technol. 1 juin 2011;20(3):034006.

208. Vanraes P, Willems G, Daels N, Van Hulle SWH, De Clerck K, Surmont P, et al. Decomposition of atrazine traces in water by combination of non-thermal electrical discharge and adsorption on nanofiber membrane. Water Res. avr 2015;72:361-71.

209. Joshi RP, Thagard SM. Streamer-Like Electrical Discharges in Water: Part II. Environmental Applications. Plasma Chem Plasma Process. févr 2013;33(1):17-49.

210. Glaze WH. Drinking-water treatment with ozone. Environ Sci Technol. mars 1987;21(3):224-30.

211. Cadorin BM, Tralli VD, Ceriani E, Benetoli LODB, Marotta E, Ceretta C, et al. Treatment of methyl orange by nitrogen non-thermal plasma in a corona reactor: The role of reactive nitrogen species. J Hazard Mater. déc 2015;300:754-64.

212. Neta P. Reactions of hydrogen atoms in aqueous solutions. Chem Rev. 1 oct 1972;72(5):533-43.

213. Sandra Schröter. Reactive oxygen and hydrogen species generation in radio-frequency atmospheric pressure plasmas. 2017.

214. Brisset JL, Benstaali B, Moussa D, Fanmoe J, Njoyim-Tamungang E. Acidity control of plasma-chemical oxidation: applications to dye removal, urban waste abatement and microbial inactivation. Plasma Sources Sci Technol. 1 juin 2011;20(3):034021.

215. Willberg DM, Lang PS, Höchemer RH, Kratel A, Hoffmann MR. Degradation of 4-Chlorophenol, 3,4-Dichloroaniline, and 2,4,6-Trinitrotoluene in an Electrohydraulic Discharge Reactor. Environ Sci Technol. 1 juill 1996;30(8):2526-34.

216. Anpilov AM, Barkhudarov EM, Bark YB, Zadiraka YV, Christofi M, Kozlov YN, et al. Electric discharge in water as a source of UV radiation,

ozone and hydrogen peroxide. J Phys Appl Phys. 21 mars 2001;34(6):993-9.

217. Liu Y na, Zhu S fa, Tian H, Zhou M, Miao J. Effect of Inorganic Ions on the Oxidation of Methyl Violet with Gliding Arc Plasma Discharge. Plasma Chem Plasma Process. août 2013;33(4):737-49.

218. Yan JH, Liu YN, Bo Zh, Li XD, Cen KF. Degradation of gas–liquid gliding arc discharge on Acid Orange II. J Hazard Mater. sept 2008;157(2-3):441-7.

219. Liu H, Du CM, Wang J, Li HX, Zhang L, Zhang LL. Comparison of Acid Orange 7 Degradation in Solution by Gliding Arc Discharge with Different Forms of TiO_2. Plasma Process Polym. mars 2012;9(3):285-97.

220. Ghezzar MR, Saïm N, Belhachemi S, Abdelmalek F, Addou A. New prototype for the treatment of falling film liquid effluents by gliding arc discharge part I: Application to the discoloration and degradation of anthraquinonic Acid Green 25. Chem Eng Process Process Intensif. oct 2013;72:42-50.

221. Saïm N, Ghezzar MR, Guyon C, Abdelmalek F, Tatoulian M, Addou A. New prototype for the treatment of falling film liquid effluents by gliding arc discharge part II: Plasmacatalytic activity of TiO2 thin film deposited by magnetron sputterin. Chem Eng Process Process Intensif. déc 2015;98:32-40.

222. Ni M, Yang H, Chen T, Zhang H, Wu A, Du C, et al. Degradation of Acid Orange 7 in an Atmospheric-Pressure Plasma-Solution System (Gliding Discharge). Plasma Sci Technol. mars 2015;17(3):209-15.

223. He B, Gong X, Wang X, Li J, Xiong Q, Chen Q, et al. What Are the Effective Reactants in the Plasma-Induced Wastewater Treatment? J Electrochem Soc. 2018;165(10):E454-9.

224. Gan G, Liu J, Zhu Z, Yang Z, Zhang C, Hou X. A novel magnetic nanoscaled Fe3O4/CeO2 composite prepared by oxidation-precipitation process and its application for degradation of orange G in aqueous solution as Fenton-like heterogeneous catalyst. Chemosphere. févr 2017;168:254-63.

225. Kyriakopoulos J, Kordouli E, Bourikas K, Kordulis C, Lycourghiotis A. Decolorization of Orange-G Aqueous Solutions over C60/MCM-41 Photocatalysts. Appl Sci. 13 mai 2019;9(9):1958.

226. Benselka-Hadj Abdelkader N, Bentouami A, Derriche Z, Bettahar N, De Ménorval LC. Synthesis and characterization of Mg–Fe layer double hydroxides and its application on adsorption of Orange G from aqueous solution. Chem Eng J. mai 2011;169(1-3):231-8.

227. Dulman V, Cucu-Man SM, Bunia I, Dumitras M. Batch and fixed bed column studies on removal of Orange G acid dye by a weak base functionalized polymer. Desalination Water Treat. juill 2016;57(31):14708-27.

228. Dulman V, Cucu-Man SM, Olariu RI, Buhaceanu R, Dumitraş M, Bunia I. A new heterogeneous catalytic system for decolorization and mineralization of Orange G acid dye based on hydrogen peroxide and a macroporous chelating polymer. Dyes Pigments. oct 2012;95(1):79-88.

229. Wang Y, Priambodo R, Zhang H, Huang YH. Degradation of the azo dye Orange G in a fluidized bed reactor using iron oxide as a heterogeneous photo-Fenton catalyst. RSC Adv. 2015;5(56):45276-83.

230. Li Y, Yang Z, Zhang H, Tong X, Feng J. Fabrication of sewage sludge-derived magnetic nanocomposites as heterogeneous catalyst for persulfate activation of Orange G degradation. Colloids Surf Physicochem Eng Asp. sept 2017;529:856-63.

231. Tarkwa JB, Oturan N, Acayanka E, Laminsi S, Oturan MA. Photo-Fenton oxidation of Orange G azo dye: process optimization and mineralization mechanism. Environ Chem Lett. mars 2019;17(1):473-9.

232. Kaveh A, Behdad GA, Amirhossein Haji AK. Equilibrium and Kinetic Adsorption Study of the Removal of Orange-G Dye Using Carbon Mesoporous Material: Equilibrium and Kinetic Adsorption Study of the Removal of Orange-G Dye Using Carbon Mesoporous Material. J Inorg Mater. 16 août 2012;27(6):660-6.

233. Nassar MY, Mohamed TY, Ahmed IS, Mohamed NM, Khatab M. Hydrothermally Synthesized Co3O4, α-Fe2O3, and CoFe2O4 Nanostructures: Efficient Nano-adsorbents for the Removal of Orange G Textile Dye from Aqueous Media. J Inorg Organomet Polym Mater. sept 2017;27(5):1526-37.

234. Banerjee S, Chattopadhyaya MC, Chandra Sharma Y. Removal of an azo dye (Orange G) from aqueous solution using modified sawdust. J Water Sanit Hyg Dev. 1 juin 2015;5(2):235-43.

235. Muthukumar M, Karuppiah MT, Raju GB. Electrochemical removal of CI Acid orange 10 from aqueous solutions. Sep Purif Technol. 15 juin 2007;55(2):198-205.

236. Arulkumar M, Sathishkumar P, Palvannan T. Optimization of Orange G dye adsorption by activated carbon of Thespesia populnea pods using response surface methodology. J Hazard Mater. févr 2011;186(1):827-34.

237. Hayet Chamekh, Mahdi Chiha, Fatiha Ahmedchekkat, Nour El Houda Souames. Degradation of Orange G by UV/TiO2/IO4 ¯process: Effect of operational parameters and estimation of electrical energy consumption. Indian J Chem Technol [Internet]. 2023 [cité 12 janv 2025]; Disponible sur: http://op.niscpr.res.in/index.php/IJCT/article/view/62814

238. Saharan VK, Rizwani MA, Malani AA, Pandit AB. Effect of geometry of hydrodynamically cavitating device on degradation of orange-G. Ultrason Sonochem. janv 2013;20(1):345-53.

239. Yuksel A, Sasaki M, Goto M. Complete degradation of Orange G by electrolysis in sub-critical water. J Hazard Mater. juin 2011;190(1-3):1058-62.

240. Rodriguez S, Vasquez L, Costa D, Romero A, Santos A. Oxidation of Orange G by persulfate activated by Fe(II), Fe(III) and zero valent iron (ZVI). Chemosphere. avr 2014;101:86-92.

241. Sang W, Lu W, Mei L, Jia D, Cao C, Li Q, et al. Research on different oxidants synergy with dielectric barrier discharge plasma in degradation of Orange G: Efficiency and mechanism. Sep Purif Technol. déc 2021;277:119473.

242. Xu XR, Li XZ. Degradation of azo dye Orange G in aqueous solutions by persulfate with ferrous ion. Sep Purif Technol. 30 mars 2010;72(1):105-11.

243. Zhang J, Chen M, Zhu L. Activation of persulfate by Co_3 O_4 nanoparticles for orange G degradation. RSC Adv. 2016;6(1):758-68.

244. Lin X, Ma Y, Wan J, Wang Y, Li Y. Efficient degradation of Orange G with persulfate activated by recyclable FeMoO4. Chemosphere. janv 2019;214:642-50.

245. Zhang X, Qin Y, Zhang W, Zhang Y, Yuan GE. Oxidative degradation of Orange G in aqueous solution by persulfate activated with pyrite. Water Sci Technol. 29 juill 2020;wst2020352.

246. Fan Z, Zhang Q, Li M, Sang W, Qiu Y, Xie C. Activation of persulfate by manganese oxide-modified sludge-derived biochar to degrade Orange G in aqueous solution. Environ Pollut Bioavailab. 1 janv 2019;31(1):70-9.

247. Pu M, Ma Y, Wan J, Wang Y, Huang M, Chen Y. Fe/S doped granular activated carbon as a highly active heterogeneous persulfate catalyst toward the degradation of Orange G and diethyl phthalate. J Colloid Interface Sci. mars 2014;418:330-7.

248. Tarkwa JB, Acayanka E, Jiang B, Oturan N, Kamgang GY, Laminsi S, et al. Highly efficient degradation of azo dye Orange G using laterite soil as catalyst under irradiation of non-thermal plasma. Appl Catal B Environ. juin 2019;246:211-20.

CHAPTER II

Experimental Procedures and Analysis Methods

I. Introduction

This chapter presents the equipment, techniques, protocols, and processes used or developed in the context of this thesis. It provides a comprehensive description of the experimental setup, including the reactors used for wastewater treatment.

In the first part, we introduce the model molecule under study, the reactants and the chemicals involved. This is followed by a description of the experimental setup of the thermal activation process of persulfates. Subsequently, the glidarc plasma device, developed at the LAMES laboratory of the University of Skikda, is presented, along with its combined application in the study of the co-degradation of the target pollutant. Finally, the analytical techniques and methods employed are detailed.

II. Materials used

II.1. The target compound

The Orange G, abbreviated to OG, whose molecular structure and physico-chemical properties are listed in **Table II.1,** was purchased from RAL Diagnostics and used without purification.

Table II.1. Physico-chemical properties of orange G.

Orange G	
Molecular structure	

Molecular formula	$C_{16}H_{10}N_2Na_2O_7S_2$
Molecular weight (g/mol)	452.37
IUPAC name	7-hydroxy-8-phenyldiazenylnaphthalene-1,3-Disulfonate
Case number	1936-15-8
λ_{max} (nm)	478
Pka	11.5
Solubility in water (g/L)	80 at 25°C

I.2. Chemical reagent and solvent

The chemicals used during this work are listed in **Table II.2** below. These are mainly solvents and reagents used without prior purification to adjust or control pH or as additives. These chemicals are of analytical quality, stored at room temperature and protected from light.

Table II.2. Characteristics of the chemicals used.

Product	Molecular formula	Quality	Manufacturer
Potassium persulfate	$K_2S_2O_8$	98%	Pamracic
Ammonium persulfate	$(NH_4)_2S_2O_8$	98%	Prolabo
Sulfuric acid	H_2SO_4	96%	Cheminova

Sodium hydroxide	NaOH	97%	Bichem
Iron (II) sulfate heptahydrate	$FeSO_4.7H_20$	97%	Acros
Potassium dichromate	$K_2Cr_2O_7$	99,5%	Fluka
Ammonium iron (II) sulfate hexahydrate	$(NH_4)_2(FeSO_4)_2.6(H_2O)$	99%	Sigma-Aldrich
Ferric oxide	Fe_2O_3	98%	Fluka
Hydrogen peroxide	H_2O_2	30%	Biochem
Potassium Iodide	KI	≥ 99%	Sigma-Aldrich
Periodic acid	H_5IO_6	99,5%	Biochem
Ethanol	C_2H_5OH	96%	Riedel de Haen
EDTA	$C_{10}H_{16}N_2O_8$	99%	Sigma-Aldrich
Ter-butanol	C_4H_9OH	≥ 99%	Sigma-Aldrich

II.3. Water matrix used

The solutions were prepared using distilled water with a 1.5 to 2.5 $\mu s.cm^{-1}$ Conductivity. Different types of water were tested to study the effect of the aqueous matrix. **Table II.3** lists the characteristics of each matrix.

Table II.3. Characteristics of the water matrices used.

type of matrix	Distilled water	Mediterranean seawater (Algeria)	Raw spring water	Zemem water
pH	6.5	6.8	6.5	7
HCO_3^-	/	140	/	285
SO_4^{2-}	/	2650	/	610.53
Cl^-	/	20000	/	147.5
Br-	/	65	/	/

III. Experimental procedures

III.1. Heat-activated persulfate process device

Advanced oxidation processes based on sulfate radicals were employed to remove Orange G from an aqueous solution, specifically (heat/persulfate) and (heat/persulfate/iron). The process was conducted in a glass (quartz) reactor with a capacity of 500 mL and a relatively dense thickness (13 mm). The reactor was well covered to minimise potential losses due to evaporation and was placed in a thermostated bath equipped with a thermostat and a thermocouple containing two temperature sensors. The system was maintained under mechanical stirring at a fixed speed.

Once the target temperature was reached, the appropriate amount of inorganic oxidant (PS) was introduced into 400 mL of OG-loaded aqueous solution. Samples were taken regularly using a sampling system, immediately cooled, and analysed with a UV-visible

spectrophotometer to determine the OG concentration. The experimental setup used is illustrated in **FigureII.1.**

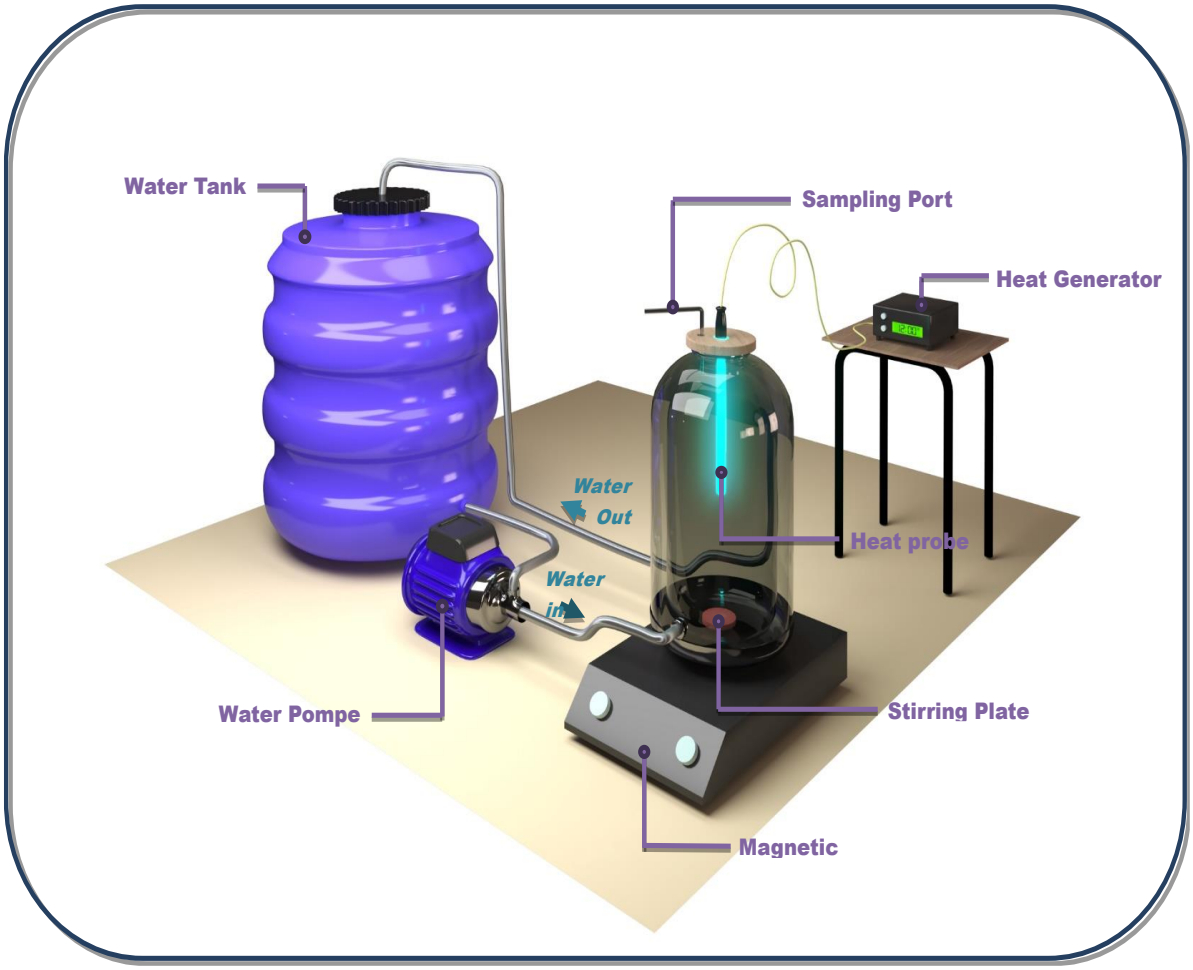

Figure II.1. Experimental setup for heat-activated persulfate process**.**

III.2. Gliding Arc Discharge (GAD) Plasma Device

The first-generation Glidarc device was utilised in this work to treat the pollutant molecule Orange G.

Figure II.2 and **II.3** illustrate the experimental setup developed in the laboratory and used in this study. The system consists of two divergent stainless-steel electrodes, which have a melting temperature exceeding 1420°C, symmetrically positioned around a gas supply nozzle with a diameter of $\phi = 1.3$ mm. The entire setup is placed in a double-walled Pyrex reactor, which is equipped with a cooling system and a mechanical stirring mechanism operating at a fixed speed. The two electrodes are connected to a high-voltage generator (Siet: 10 kV, 50 Hz).

The plasma gas used in this experiment is air-sourced directly from a compressor. Before entering the system, the air passes through a water-filled bubbler for humidification, followed by a ball flowmeter arranged in series.

The gliding discharge is initially initiated at a minimum electrode gap of 3 mm, forming a thermal plasma in thermodynamic equilibrium. Under the influence of the humid air flow, the discharge propagates along the electrodes, eventually breaking into a plume that interacts with the surface of the solution to be treated (**Figure II.3)**. This propagation disrupts the thermodynamic equilibrium, causing a sudden drop in plasma temperature and leading to the formation of cold plasma.

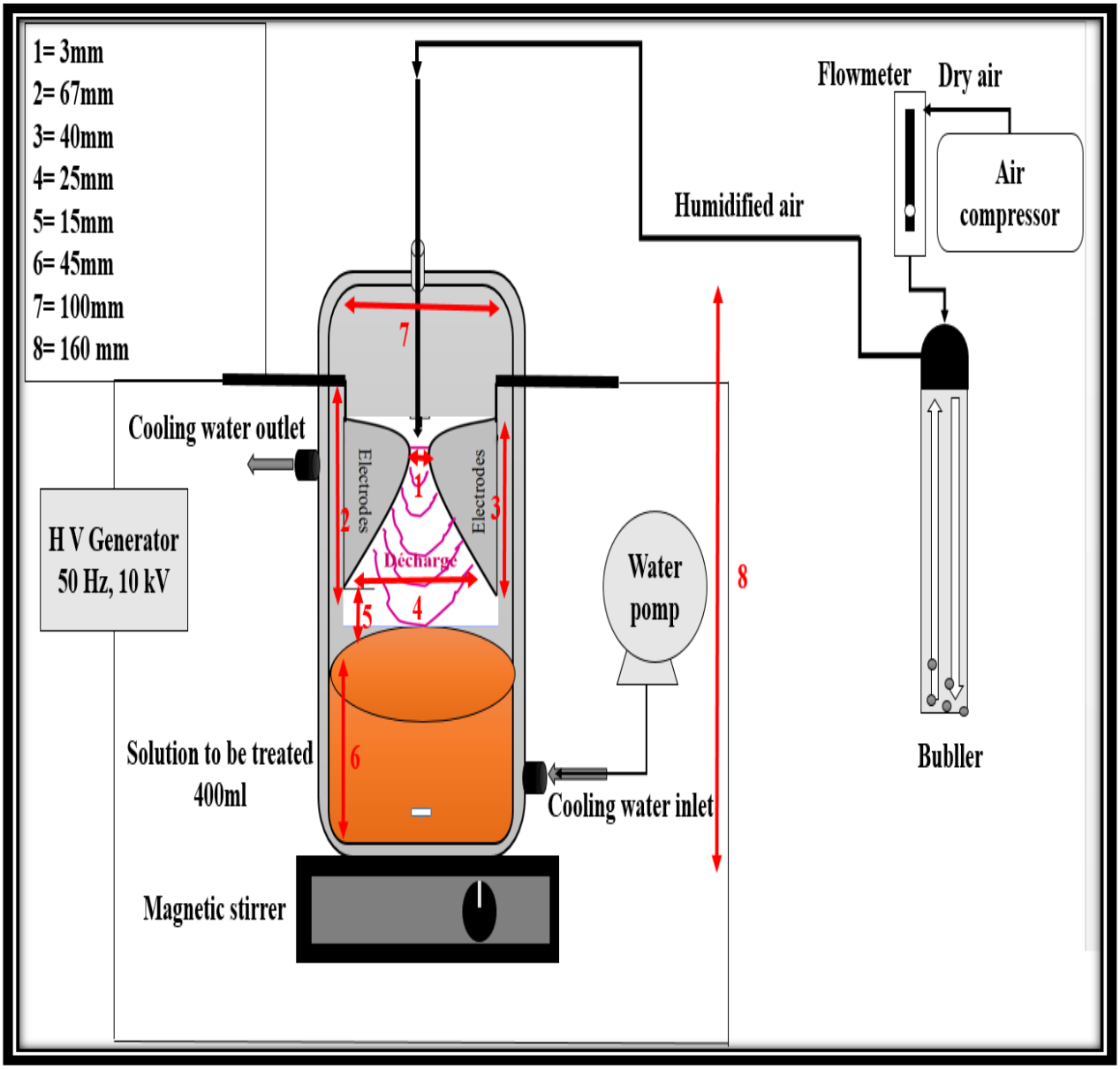

Figure II.2. Experimental Setup of the gliding Arc Plasma 'Glidarc'.

The electrode-solution distance, set at approximately 15 mm, is optimised to ensure that the electrodes are sufficiently close to the target to be treated while avoiding splashing onto the reactor walls. This spacing enhances gas-liquid interaction time, facilitates the effective capture of short-lived reactive species, and promotes the penetration of UV radiation into the solution. The volume of liquid introduced into the reactor is 400 ml. The entire system is placed on a magnetic stirrer to ensure continuous homogenisation of the solution, thereby facilitating the diffusion of target molecules towards the plasma-solution interface, which serves as the principal site for reactions between plasma-generated species and the target molecules.

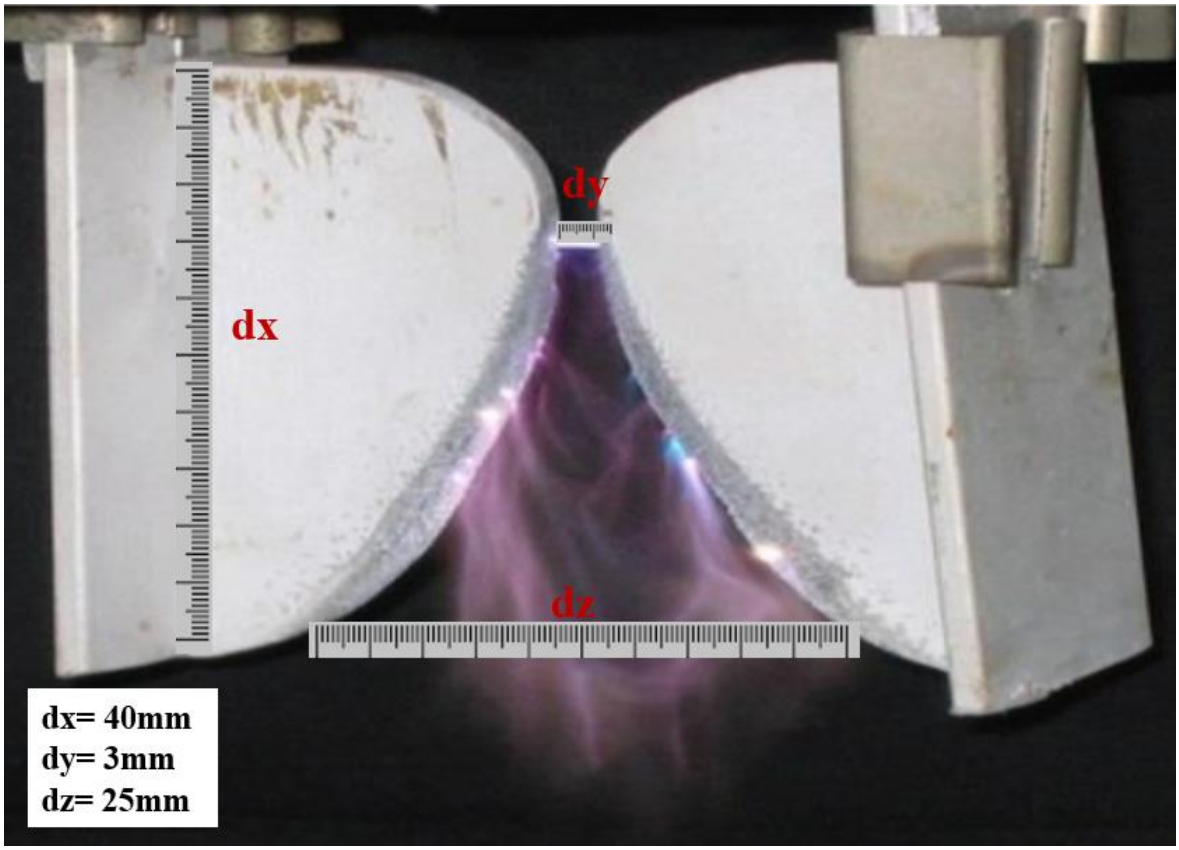

Figure II.3. Visualisation of the evolution of a gliding arc plasma[1].

IV. Analytical procedure

IV.1. UV-Visible Spectrophotometry

Ultraviolet-visible (UV–visible) spectrophotometry is a predominantly quantitative analytical method that focuses on the absorption of near-UV (180–390 nm) or visible (390–780 nm) light by chemical substances in solution. Different colours of visible light and their complementary colours in solutions absorb at specific wavelengths. Due to the overlap of vibrational and rotational transitions, the UV–visible spectrum of analytes in solution exhibits minimal fine structure. Consequently, this technique is rarely employed for identification purposes (although every molecule will have a wavelength corresponding to its maximum absorption). Still, it remains one of the most commonly utilised methods for quantitative analysis. Under carefully controlled experimental conditions, the amount of absorbed radiation can be directly correlated with the analyte concentration in the solution, as described by Beer's law. It is applicable for quantifying organic (mainly in the near-UV range) and inorganic (primarily in the visible range) substances[2].

IV.1.1. Principle

UV-visible spectroscopy is a spectroscopic technique based on the interaction between matter and electromagnetic waves. Following this interaction, radiation will be absorbed or emitted. The latter is subsequently analysed to determine the material's properties to be studied, according to the Beer-Lambert law [136].

- **Beer-Lambert law:**

The Beer-Lambert Law, also known as Beer's Law, is a fundamental principle in spectroscopy that describes the attenuation of light as it passes through a substance. It establishes a direct, linear relationship between the absorbance of light by a solution and the concentration of the solute, the molar absorption coefficient, and the optical path length of the solution. The Beer-Lambert law is expressed as:

$$A = log\frac{I_0}{I} = \varepsilon LC \qquad \text{(II.1)}$$

Where:

A: is the absorbance or optical density at a given wavelength (dimensionless).

I0: is the incident light intensity.

I: is the transmitted light intensity.

ε: is the Molar extinction coefficient (in units of $Lmol^{-1}cm^{-1}$).

L: is the Optical path length, corresponds to the width of the cuvette used (cm).

C: is the concentration of the absorbing substance ($molL^{-1}$).

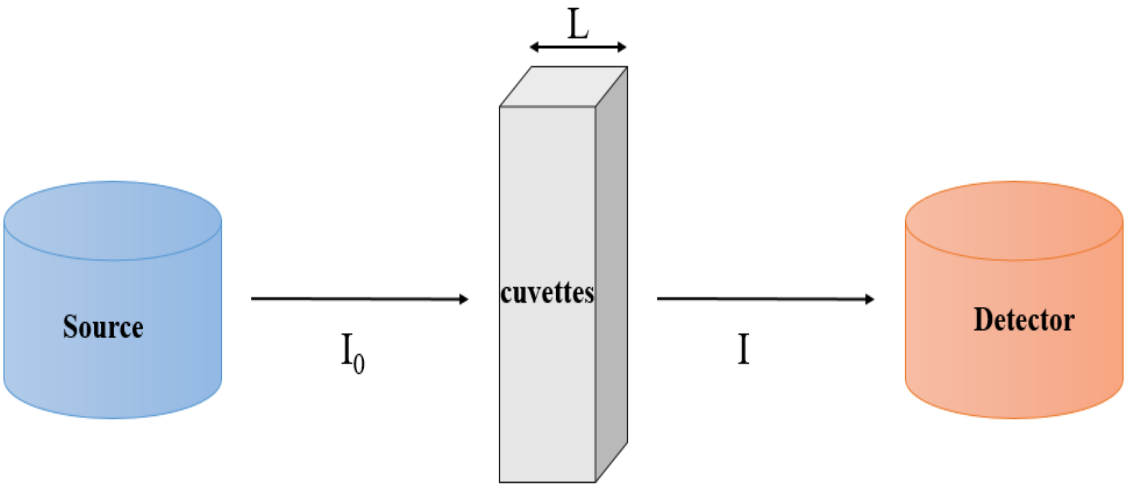

Figure II.4. Schematic representation of the UV-Visible spectroscopy principle.

In this study, the spectrophotometric measurements were performed using an "Agilent Cary 60" device controlled by a computer with "Cary WinUV" software. This setup enables a scan range from 200 nm (UV) to 800 nm (visible). The cuvettes used for the sample analysis or the blank (reference) are made of quartz and have an optical path length of 1 cm.

Figure II.5. "Agilent Cary 60" spectrophotometer.

The experimental UV-visible spectrum of the Orange G solution at free pH (6.5) shows a major band in the visible region with maximum absorption at 478 nm (λmax) and a band Localised at 330 nm (**Figure II.6**).

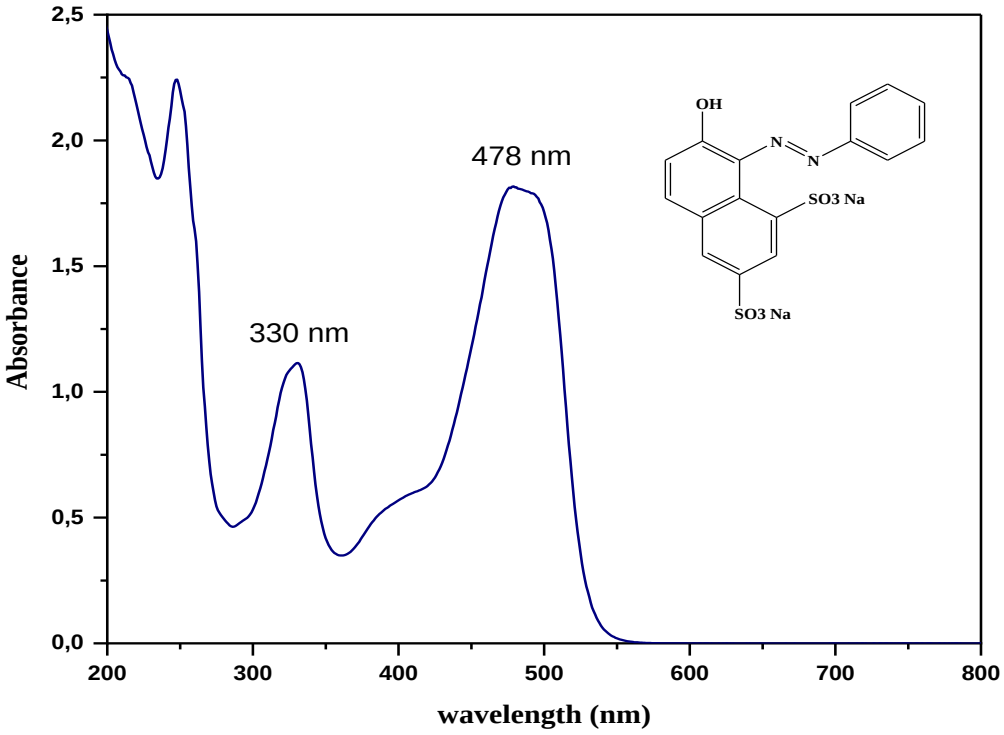

Figure II.6. Absorption spectrum of OG at free pH.

A scan between 200 and 800 nm was also performed for the $K_2S_2O_8$ reagent, and its absorption spectrum is presented below.

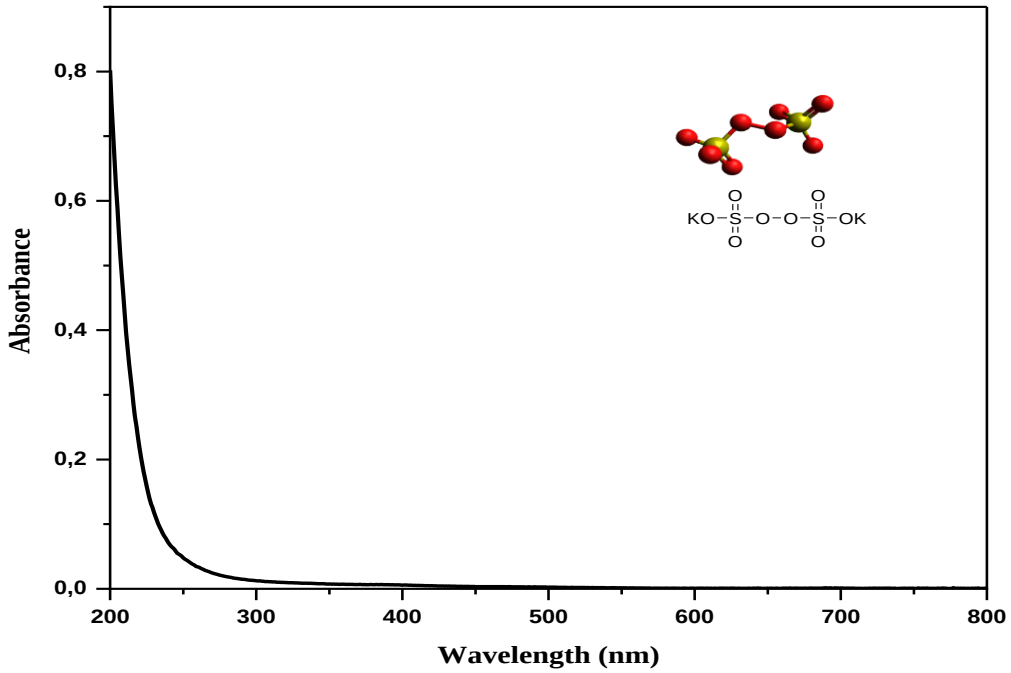

Figure II.7. Absorption spectrum of $K_2S_2O_8$.

IV.2. Chemical oxygen demand (COD)

The Chemical Oxygen Demand (COD) is a key indicator of the quantity of oxygen that reactions within a specified solution can consume. It is typically expressed as the mass of oxygen consumed per volume of solution, with the standard unit being milligrams per litre (mg.L^{-1}) in the SI system. A COD test is widely employed to quantify the concentration of organic matter in water. Its primary application lies in measuring the levels of oxidisable pollutants in surface water or wastewater. In water quality, COD serves as a valuable metric for assessing the potential impact of an effluent on the receiving water body[3].

In this study, Chemical Oxygen Demand (COD) was determined using a method outlined by Thomas and Mazas[4], where potassium dichromate ($K_2Cr_2O_7$)served as the oxidising agent in a strongly acidic environment. Silver sulfate acted as the catalyst (Ag_2SO_4), and mercury sulfate ($HgSO_4$) helped to complex chloride ions (Cl^-). The process involved adding specific quantities (3ml) of an acidic solution, mercury sulfate (0,1g), the sample (or distilled water for the blank) (1ml), and potassium dichromate (1ml) into a tube, which was sealed and

homogenised. The tube was then heated at 148°C for 2 hours. The dichromate oxidised the organic material during this time, forming chromate ions **(Equation II.2)**.

$$2OM + 2Cr_2O_7^{2-} + 16H^+ \longrightarrow 2OM^{6+} + 6O^{2-} + 4Cr^{3+} + 8H_2O \qquad \text{(II.2)}$$

The COD was calculated based on the amount of dichromate consumed. The final concentration of residual oxidant was determined by measuring the absorbance of the reaction mixture at 440 nm after cooling.

Figure II.8. WTW thermoreactor for COD measurement.

IV.3. pH measurement

During all advanced oxidation process experiments, pH measurements were conducted using a 197 WTW pH meter equipped with a SenTix 41 (WTW) electrode (**Figure II.9)**. The pH was adjusted to different values using sulfuric acid or sodium hydroxide for acidic or basic

conditions. pH meter calibration was performed before each experiment using buffer solutions (pH = 4, 7, and 10).

Figure II.9. 197 WTW pH meter.

IV.4. Conductivity measurement

Conductivity refers to the capacity of an aqueous solution to conduct an electric current. This current is transported by ions, so conductivity is directly influenced by the ion concentration, their mobility, and the temperature of the water. In this study Conductivity measurement were conducted using a WTW inoLab Cond 7310 conductivity Meter (**Figure II.10**).

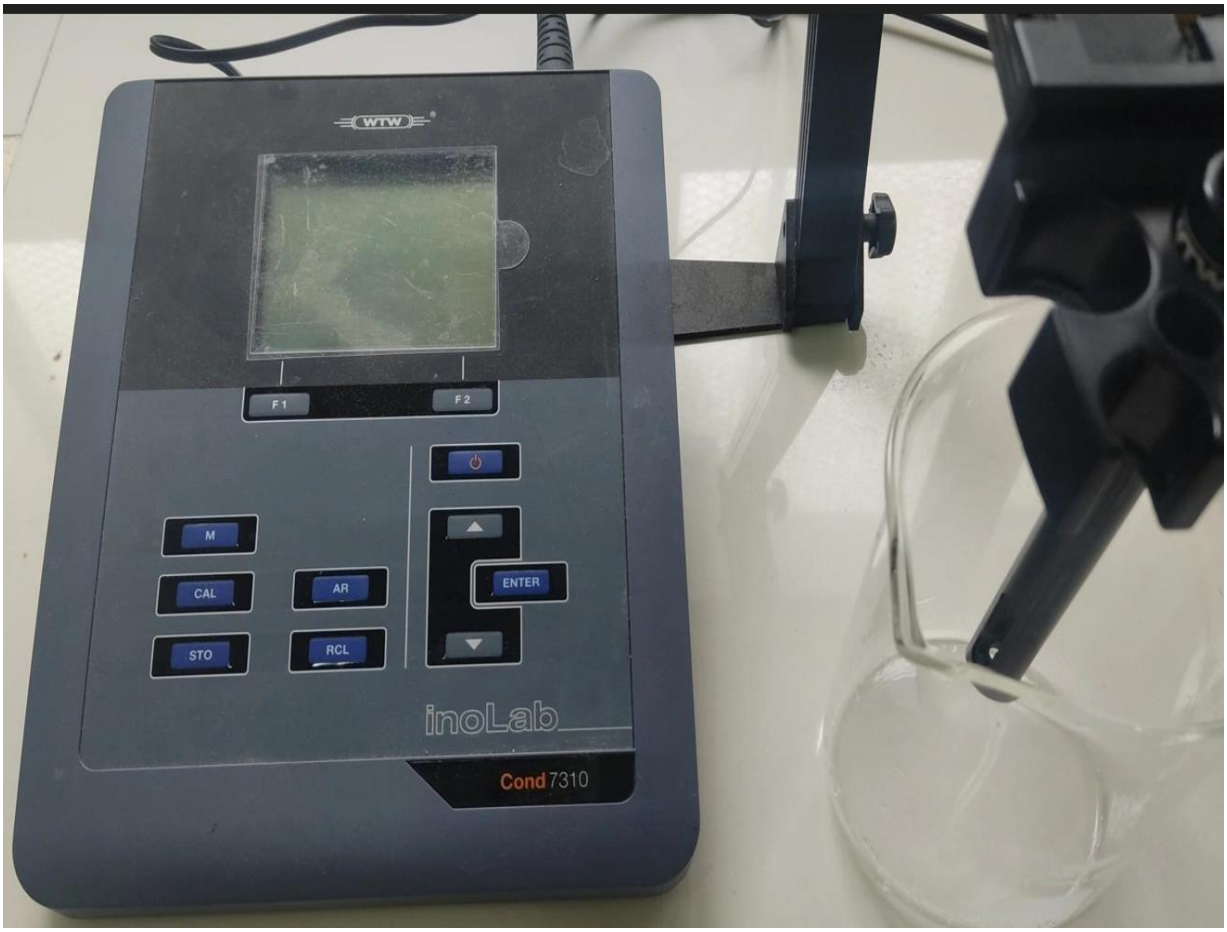

Figure II.10. WTW inoLab Cond 7310 conductivity Meter.

V. Preparation of solution

To ensure the precise and efficient execution of this work, the solutions were prepared strictly according to the established conventional protocols. These protocols were meticulously followed to account for the specific physical properties of each solution, thereby ensuring the reliability and consistency of the preparation process.

V.1. Aqueous solutions of Orange G

The stock solutions of Orange G were prepared by dissolving a defined amount of the dye in distilled water, considering its solubility. The standard solutions used for analytical studies were then obtained by successive dilutions to achieve the desired concentrations. Calibration curves were constructed to quantify the residual concentrations using different experimental methodologies.

To examine the influence of the water type on the degradation process of Orange G via the thermal activation of persulfates (TAP), solutions were prepared by directly dissolving the dye powder in various water matrices designated for this study.

V.2. Sulfuric acid solution

A 1M sulfuric acid solution was prepared by diluting a commercial solution from the Cheminova brand, which has a density of 1.84 and a purity of 96%. This solution was mainly used to adjust the pH of solutions containing the target molecule, thereby allowing the monitoring of its degradation process under different pH conditions.

V.3. Sodium hydroxide solution

A 1M Sodium hydroxide solution was prepared by dissolving a known amount of NaOH crystals in a measured volume of distilled water. This solution was used to adjust the pH, facilitating the observation of the degradation of target molecules as a function of pH values, moving towards an alkaline pH.

V.4. Potassium iodide solution

A 1M potassium iodide solution was prepared by dissolving the appropriate amount of KI (Sigma-Aldrich) in distilled water. This solution was then used to demonstrate the oxidising properties of humid air plasma.

VI. Representation of Experimental Results

The experimental results detailed in the following sections are presented using formulations that facilitate a comprehensive analysis and a clearer interpretation of the influence of different parameters on the progression of target pollutant oxidation experiments.

VI.1. Pollutant degradation rate

The degradation rate of the pollutant indicates the proportion of the pollutant that undergoes conversion during the oxidation reaction. The following equation defines this parameter:

$$\% \text{ Degradation} = \frac{(C_0 - C_t)}{C_0} \times 100 \qquad \text{(II.3)}$$

Where C_0 and C_t represent, respectively, the initial and remaining concentrations of the pollutant at a treatment time t.

VI.2. Mineralisation Rate

The mineralisation rate quantifies the extent to which a pollutant is fully oxidised into its final degradation products: CO_2, H_2O, and inorganic ions.

This parameter is crucial in assessing the efficiency of advanced oxidation processes (AOPs) and other wastewater treatment methods.

The mineralisation rate is typically expressed as a percentage using the following formula:

$$\% \text{ Mineralisation} = \frac{COD_0 - COD_t}{COD_\circ} \times 100 \qquad \text{(II.4)}$$

COD_0 represents the initial chemical oxygen demand (COD), and COD_t denotes the remaining COD at a given time t.

The COD measurement reflects the amount of oxygen required to chemically oxidise organic and some inorganic substances in water, making it a key parameter for evaluating pollutant degradation.

VI.3. Thermodynamic aspect

VI.3.1. Gibbs free energy (ΔG)

Gibbs free energy (ΔG) is a thermodynamic quantity that represents the energy available to perform work and determines the spontaneity of a reaction. A negative ΔG indicates that the reaction occurs spontaneously at all temperatures, whereas a positive ΔG suggests that the reaction is not spontaneous and requires external energy[5].

Mathematically, the equation used to calculate Gibbs free energy is as follows:

$$\Delta G = \Delta H - T\Delta S \qquad \text{(II.5)}$$

Under standard conditions, the Gibbs free energy is given by the expression below:

$$\Delta G^0 = \Delta H^0 - T\Delta S^0 \quad \text{(II.6)}$$

Where, the standard entropy (ΔS˚) measures the disorder of the system, and the standard enthalpy of reaction (ΔH˚) represents the total energy contents of the system[6].

VII. Conclusion

This chapter provided an in-depth exploration of the organic pollutant investigated in this study, highlighting its physicochemical characteristics. It also details the chemicals employed in the experimental procedures.

A comprehensive discussion is presented on the experimental protocols through which this pollutant undergoes degradation, with particular emphasis on their operational modes.

The chapter further describes the analytical techniques used to assess and monitor the degradation of this refractory compound, ensuring the accuracy and reliability of the data throughout this research.

BIBLIOGRAPHICAL REFERENCES

1. Thierry-Jocker Koyaouili. Thierry-Jocker Koyaouili. Etude des procédés plasmas dans l'élimination des polluants organiques persistants dans les effluents aqueux. Chimie-Physique [physics.chem-ph]. Université Pierre et Marie Curie - Paris VI; Université de Yaoundé I, 2016. Français. ffNNT : 2016PA066727ff. fftel-01622082 [Internet]. [FRANCE]: Université Pierre et Marie Curie - Paris VI; Université de Yaoundé I,; 2016 [cited 2025 Mar 8]. Available from: https://theses.hal.science/tel-01622082v1

2. Worsfold PJ. SPECTROPHOTOMETRY | Overview. In: Encyclopedia of Analytical Science [Internet]. Elsevier; 2005 [cited 2025 Mar 9]. p. 318–21. Available from: https://linkinghub.elsevier.com/retrieve/pii/B0123693977007147

3. Li D, Liu S. Detection of River Water Quality. In: Water Quality Monitoring and Management [Internet]. Elsevier; 2019 [cited 2025 Mar 9]. p. 211–20. Available from: https://linkinghub.elsevier.com/retrieve/pii/B9780128113301000077

4. O. Thomas, N. Mazas. O. Thomas, N. Mazas, La mesure de la demande chimique en oxygène dans les milieux faiblement pollués, Analusis, 14 (1986) 300-302.

5. Kamran M. Fuel cell. In: Renewable Energy Conversion Systems [Internet]. Elsevier; 2021 [cited 2025 Apr 4]. p. 221–42. Available from: https://linkinghub.elsevier.com/retrieve/pii/B9780128235386000051

6. Kazmi M, Irfan M, Zhou L, Yuan S, Fatima H, Tian LY, et al. Electron donors and mediators in the thermodynamics and kinetics of CO2 bioreduction. Renew Sustain Energy Rev. 2022 Mar;156:111997.

CHAPTER III

Elimination of Orange G Dye by Heat-Activated Persulfate Process And Heat/Metal Co-Activated Persulfate Process

I. INTRODUCTION

Peroxydisulfate (also known as persulfate, $S_2O_8^{2-}$) has gained significant attention in recent years for its role in advanced oxidation processes used for wastewater and industrial waste treatment, as well as for in situ chemical oxidation (ISCO) in the remediation of contaminated soils and groundwater [1]. In these applications, persulfate is activated into highly reactive sulfate ($SO_4^{\bullet-}$) and hydroxyl ($HO^{\bullet}$) radicals, potent oxidants that can degrade various organic pollutants.

Persulfate activation can be achieved through various methods, including heat, transition metals, alkaline conditions, UV irradiation, ultrasound, and other mechanisms [2–6] . Among these, heat activation is particularly prevalent due to its unique advantages, drawing considerable attention in recent research. This method produces two moles of $SO_4^{\bullet-}$ for each mole of persulfate activated, in contrast to the typical one mole generated through activation with transition metal ions. Additionally, heat activation is considered an environmentally friendly in situ chemical oxidation approach [7,8]. Numerous studies have highlighted the effectiveness of thermally activated persulfate for degrading a range of contaminants, including antibiotics [9,10], herbicides [11,12], and industrial chemicals [4,13].

This study focuses on the degradation of Orange G, an azo dye, from an aqueous solution using heat-activated persulfate and heat/ metal co-activated persulfate. In the first section, we explore the impact of activation temperature on the removal of Orange G, considering the effects of potassium persulfate (PPS) concentration, initial dye concentration, and pH during the oxidation process. The study also examines the influence of radical scavengers and the water matrix on the dye removal efficiency. In addition, the degradation kinetics and thermodynamic parameters, including Gibbs free energy, activation energy, reaction entropies, and energy estimates, are analysed and presented. The evaluation of the process is based on the decolourisation of the Orange G dye-loaded solution. In the second section, emphasis was placed on studying the co-activation (heat/metal) of potassium persulfate for the Orange G degradation process. The effect of the initial concentrations of the metals and the initial pH of the solutions was examined. In addition, the study addressed the issue of dye mineralisation. Finally, particular attention was paid to the synergy between the two processes studied, which was evaluated. The evaluation of the process is based on the decolourisation of the Orange G dye-loaded solution.

Orange G was chosen as the model compound because of its widespread presence as an azo dye and the increasing amount of research focusing on the removal of these micropollutants. As conventional wastewater treatment plants often have difficulty removing these contaminants, biological treatment processes are generally ineffective in treating effluents containing these substances [9,14], and conventional treatment techniques are not destructive and produce sludge and concentrates that require further treatment[15].

II. ELIMINATION OF OG BY HEAT-ACTIVATED PERSULFATE: EFFECT OF OPERATIONAL PARAMETERS, THERMODYNAMIC ANALYSIS, AND ENERGY CONSUMPTION REQUIREMENTS.

II.1. The role of temperature on the degradation of orange G by heat/PS process.

Temperature plays a significant role in removing persistent organic pollutants using activated oxidising inorganic species such as persulfate. To assess the effect of elevated temperatures on the degradation of 400 ml solution of organic compounds (OG), a series of experiments were conducted at various temperatures (20, 40, 50, 55, 60, 65, and 70°C) while maintaining a constant initial dye concentration and fixed concentrations of PS (Ammonium persulfate (APS) $(NH_4)_2S_2O_8$ and Potassium persulfate (PPS) $K_2S_2O_8$ at the initial pH of the water treatment.Samples were taken at regular intervals over a period of 260 minutes and then analysed by UV-Visible spectrophotometry to measure absorbance at 478 nm.The results are shown in the figures below.

- **Effect of temperature on degradation of OG by heat/APS process**

The degradation of the OG at 50 mg/L was monitored as a function of temperature, varying within a range of 20°C to 70°C, in the presence of 1 g/L of Ammonium persulfate ($(NH_4)_2S_2O_8$) and at free pH of 6 **(Figure III.1)**.

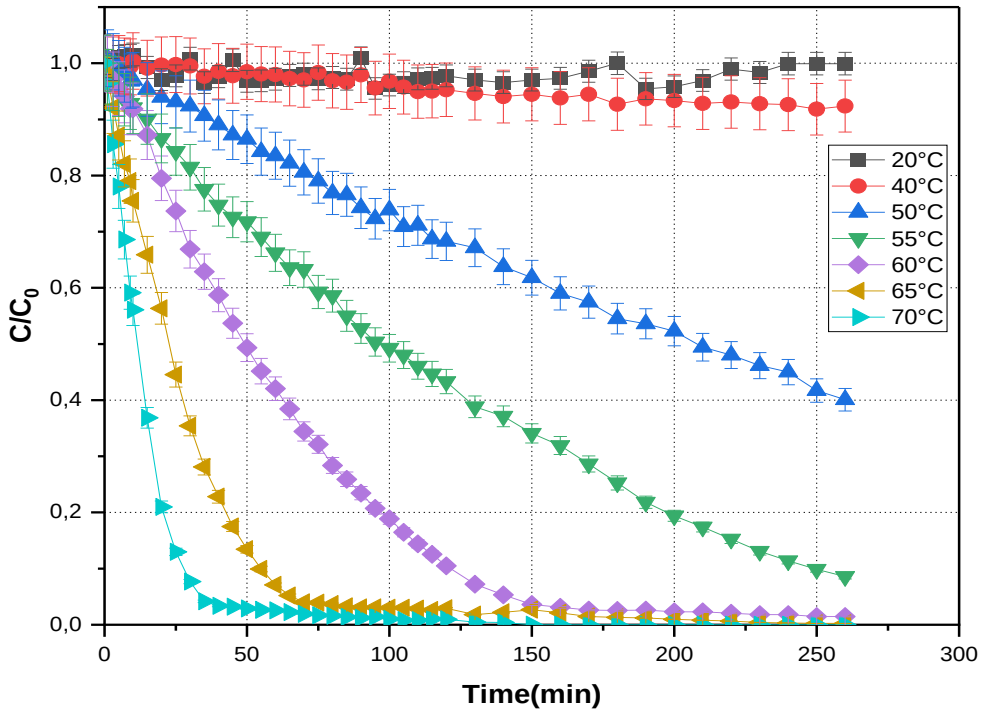

Figure III.1. Effect of reaction temperature on the OG degradation by heat/ APS process. Experimental conditions: $[OG]_0$ =50 mg/L ,$[APS]_0$ =1g/L, pH=6.

➢ **Effect of temperature on the degradation of OG by heat/PPS process**

This time, another series of experiments was conducted with 1 g/L of potassium persulfate ($K_2S_2O_8$) **(Figure III.2)** at temperatures varying from 20°C to 70°C.

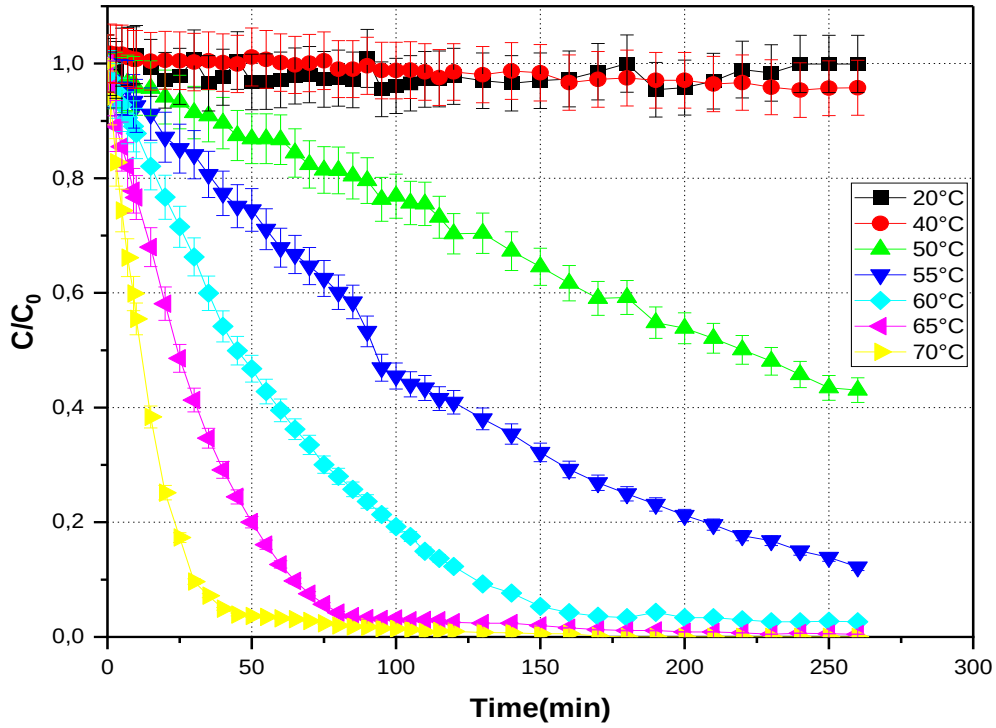

Figure III.2. Effect of reaction temperature on the OG degradation by heat/PPS process. Experimental conditions: $[OG]_0$ =50 mg/L ,$[PPS]_0$ =1g/L, pH=6.

The data presented in Figures III.1 and III.2 indicate that the heat/PS activation process was ineffective at 20°C. At this temperature, the rate of degradation of the organic compound (OG) was markedly low, reflecting slow reaction kinetics. However, when the temperature was increased from 20°C to 70°C, the degradation efficiency improved significantly. Complete decolourisation was achieved at 65°C and 70°C after 240 and 150 minutes of treatment, respectively, with activated APS, and at 70°C after 180 minutes with PPS.

For the other temperatures tested, the efficiency of OG degradation using heat-activated APS ranged from 11.15% to 96.88% (20, 40, 50, 55, 60°C), while the performance of heat-activated PPS ranged from 4.22% to 99.51% (20, 40, 50, 55, 60, 65°C). These results suggest that elevating the temperature accelerates the conversion of persulfate (PS) to sulfate radicals $SO_4^{\bullet-}$ ($E° = 2.6\,V$, selective), as described in **Equation (III.1)**.

$$S_2O_8^{2-} \xrightarrow{Heat} 2SO_4^{\bullet-} \qquad \text{(III.1)}$$

This activation initiates a series of secondary reactions (**Equations (III.2)-(III.5)**, generating additional radicals and strong oxidants such as hydroxyl radicals $OH^{\bullet}(E° = 2.8\,V, \text{non} - \text{selective})$, which then engage in the degradation of the target recalcitrant organic pollutant [16,17].

$$SO_4^{\bullet -} + H_2O \rightarrow HO^{\bullet} + H^+ + SO_4^{2-} \quad \text{(III.2)}$$

$$SO_4^{\bullet -} + OH^- \rightarrow SO_4^{2-} + OH^{\bullet} \quad \text{(III.3)}$$

$$SO_4^{\bullet -} + OG \rightarrow SO_4^{2-} + Product \quad \text{(III.4)}$$

$$HO^{\bullet} + OG \rightarrow HO^- + Product \quad \text{(III.5)}$$

To better visualise and confirm the effect of increasing temperature on the removal of OG by the heat/PS process, a series of experiments were carried out as a function of time over a temperature range from 40°C to 70°C for different concentrations of PPS.

II.1.1. Kinetic studies of OG degradation via heat-activated PS process

The kinetics of heat-activated PPS and APS processes for the removal of Orange G have been studied.

The degradation reactions of Orange G by heat-activated persulfate follow a pseudo-first-order kinetic model.

The apparent rate constants (K_{app}) for the Heat/persulfate process were determined by plotting the curve $\ln(C_0/C)$ as a function of time, according to **Equation (III.6)**, which produces a straight line whose slope is equal to K_{app} (**Figure III.3**).

$$-ln\frac{[OG]}{[OG]_0} = K_{app} \times t \quad \text{(III.6)}$$

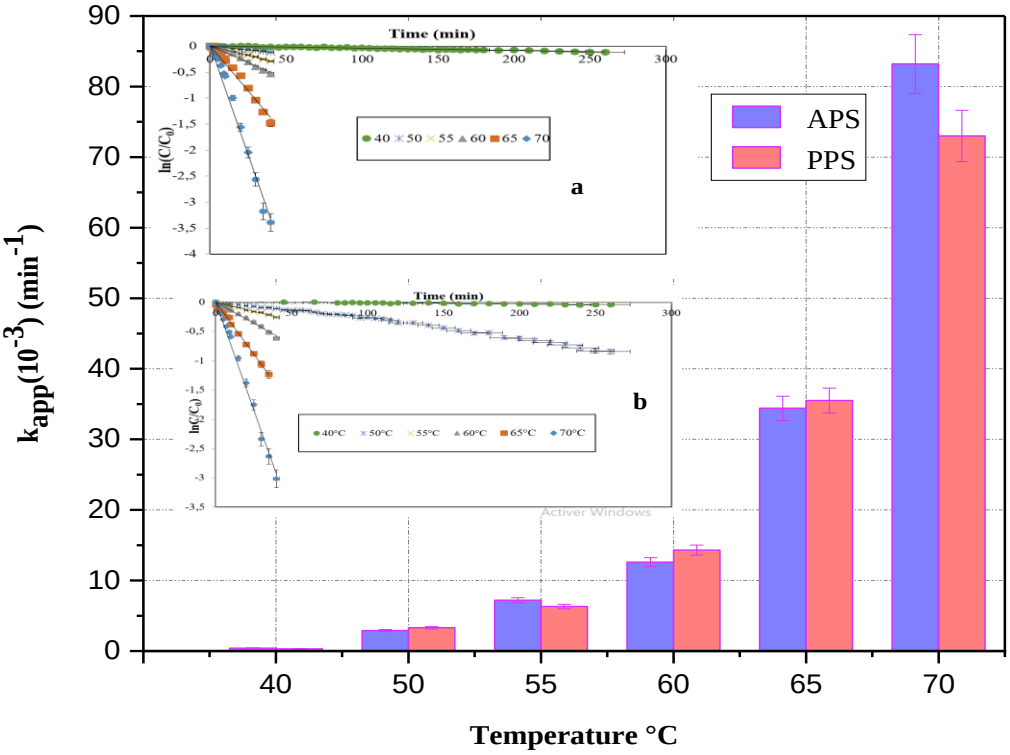

Figure III.3. Representation of the apparent rate constant for the OG degradation by the heat/PS process according to the pseudo-first-order kinetic model: Experimental conditions: $[OG]_0$ =50 mg/L, $[APS]_0$ =1g/L, $[PPS]_0$ =1g/L, pH=6.

Table III.1 presents the results of the rate constants k_{app}. The study demonstrates that increasing the temperature of PS activation leads to increases in the apparent rate constant (k_{app}) with a high regression coefficient (R^2).

Table III.1. The kinetic constants and regression coefficients predicted by the pseudo-first-order kinetic model

Temperature °C	APS		PPS	
	$k_{app}(min^{-1})\times 10^{-3}$	R^2 %	$k_{app}(min^{-1})\times 10^{-3}$	R^2 %
40	0.4	97	0.3	96
50	2.9	98	3.3	99
55	7.2	99	6.3	97
60	12.6	98	14.3	99
65	34.4	98	35.5	99
70	83.2	98	73	99

II.2. Choice of oxidant

Figure III.4 compares the degradation kinetics of OG in the presence of oxidising additives (APS and PPS) activated at different temperatures under constant operating conditions to optimise the operational parameters for enhanced oxidation of the studied micropollutant while minimising the electrical energy consumed relative to the quantity of oxidant (EE/O).

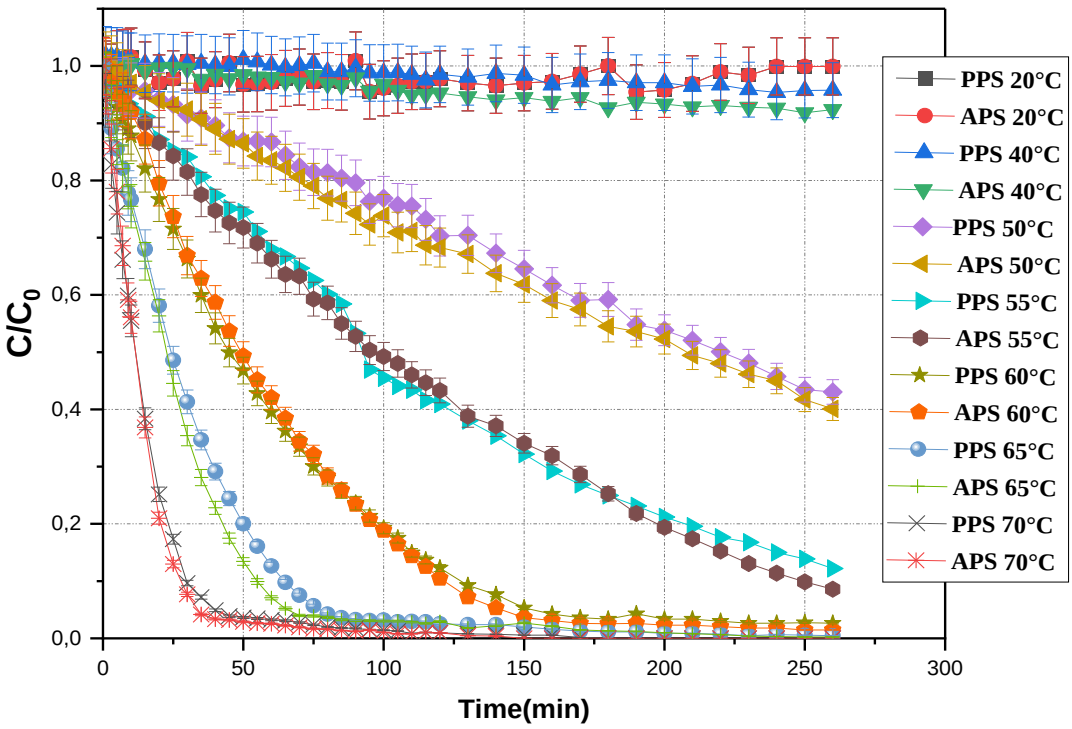

Figure III.4. Effect of temperature on the OG degradation by heat/PS process. Experimental conditions: $[OG]_0$ =50 mg/L, $[APS]_0$ =1g/L, $[PPS]_0$ =1g/L, pH=6 ,

The results illustrate that the degradation kinetics of the OG substrate are nearly identical for both types of inorganic oxidants used. The minor difference observed in the degradation kinetics of OG dye in the presence of the two persulfate additives (APS, PPS) allowed for the free selection of either additive.

II.3. Degradation of orange G using the heat-activated potassium persulfate (PPS) process

II.3.1. Effect of initial PPS concentrations

To demonstrate the vital importance and effect of the PS dosage on the degradation of persistent pollutants via thermal activation of PS, a series of experiments were carried out using various PPS concentrations (ranging from 1g/L to 100 mg/L). These tests were performed with a concentration of 50 mg/L of OG while keeping the neutral pH constant. The results are presented in **Figure III.5.**

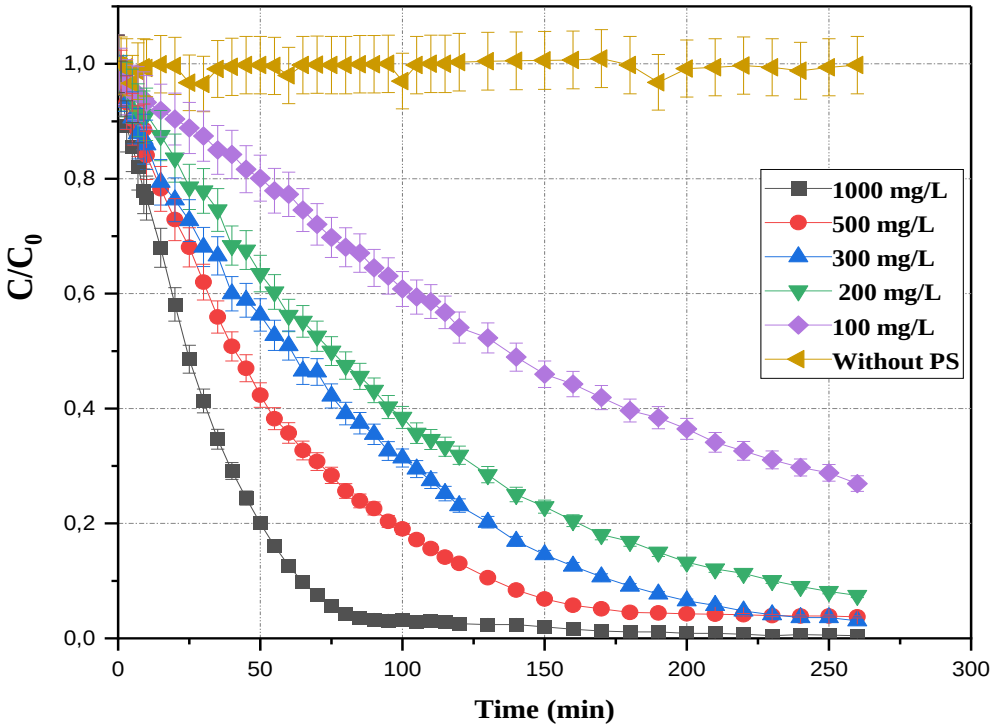

Figure III.5. Effect of PPS concentrations on the OG degradation by heat/PS process at fixed temperature and OG concentration. Experimental condition: $[OG]_0$ =50 mg/ L, T= 65°C, pH=6.

The results presented in **Figure III.5** show that increasing the dosage of PPS from 100 mg/L to 1g/L improved the rate of OG degradation, rising from 74.79% to 99.51% over a reaction period of 260 minutes. A similar trend was observed for various other environmental pollutants, including diuron [11], the azole fungicide fluconazole [18], Sudan black B [19], and bisphenol A [20].

This pattern is attributed to the interaction between OG and radicals (including $SO_4^{\bullet -}$ and $HO^{\bullet}$) generated by the amount of activated PS present in the solution, with this effect becoming more pronounced as PPS dosages increase. However, the literature highlights that an excessively high initial PS concentration might result in the heightened production of $SO_4^{\bullet -}$, which could inhibit the oxidation of contaminants with self-scavenging reactions **(Equations (III.7) and (III.8))** [9,21,22]**.**

$$SO_4^{\bullet -} + S_2O_8^{2-} \xrightarrow{K=6{,}1.10^5\ M^{-1}\ s^{-1}} SO_4^{2-} + S_2O_8^{\bullet -} \qquad \text{(III.7)}$$

$$SO_4^{\bullet -} + SO_4^{\bullet -} \xrightarrow{K=4.10^8\ M^{-1}\ s^{-1}} S_2O_8^{2-} \qquad \text{(III.8)}$$

On the other hand, the OG elimination reaction became 8.75 times faster in the presence of 1g.L^{-1} PPS dose than in the presence of a dose of 100 mg.L^{-1} PPS, where the apparent rate constants k_{app} increased from $0.4.\ 10^{-2}$ min^{-1} to $3.5.\ 10^{-2}$ min^{-1}(**Figure III.6)**, this is probably due to the increase in the amount of radical oxidising species in solution and their reaction with the OG according to equation **(Equations (III.4)**, **(III.5)**, **(III.7)** and **(III.8))**, as well as the reaction of the PS, which can undergo direct reaction with the organic compound according to the **Equation (III.9)**, leading to the formation of sulfate radicals. This process then triggers the progressive degradation of the OG [13].

$$SO_4^{\bullet -} + OG \rightarrow SO_4^{2-} + Product \qquad \text{(III.4)}$$

$$HO^{\bullet} + OG \rightarrow HO^{-} + Product \qquad \text{(III.5)}$$

$$S_2O_8^{2-} + OG \rightarrow 2SO_4^{\bullet -} + OG^{\bullet} \qquad \text{(III.9)}$$

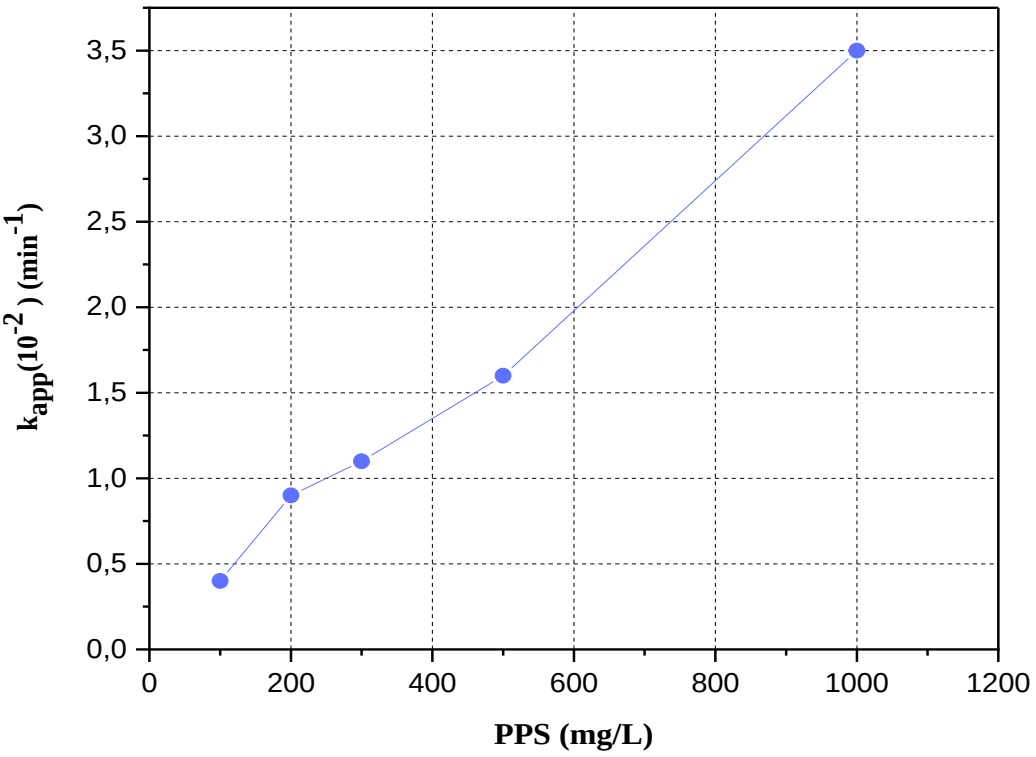

Figure III.6. Plot of rate constant k_{app} versus PPS dose. Experimental condition: $[OG]_0$ =50 mg/L, T= 65°C, pH=6.

Reinforcing our previous interpretations, **Figure III.7** confirms the correlation between the degradation kinetics of OG, the initial concentrations of PS, and the activation temperature.

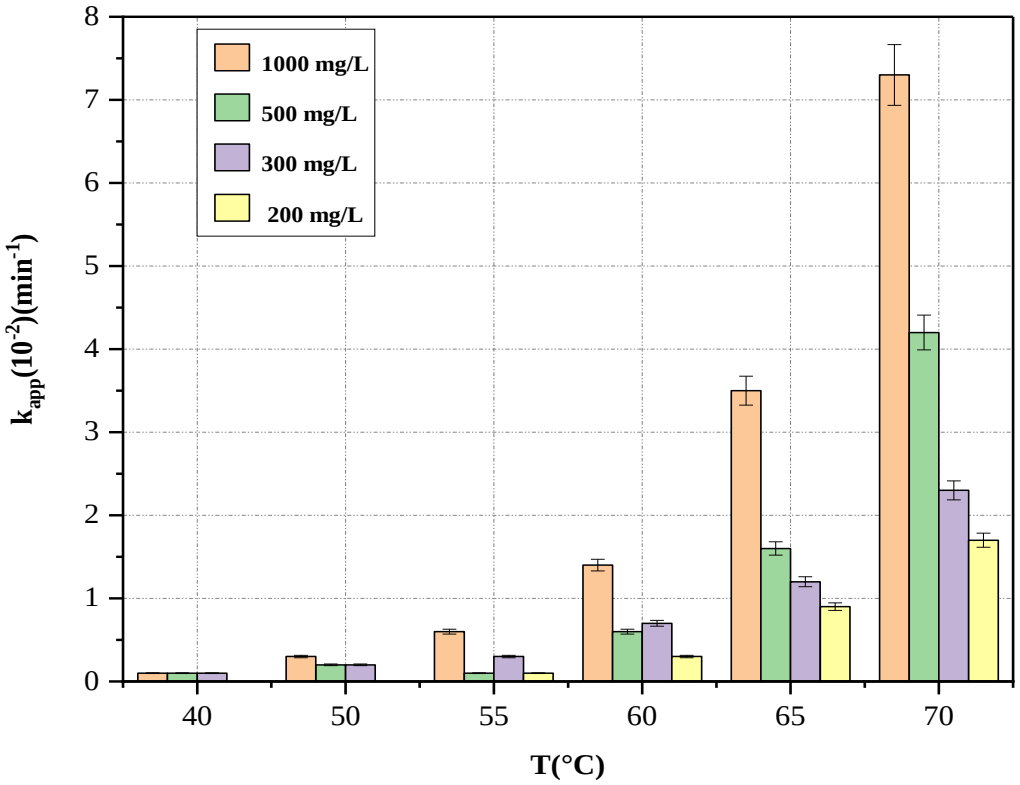

Figure III.7. Plot of k_{app} rate constants as a function of different temperatures for different doses of PS. Experimental condition: $[OG]_0$ =50 mg/L, T= 40-70°C, pH=6.

The results indicate that at low temperatures (< 60°C), the degradation kinetics of OG are weakly influenced by the amount of PS added to the solution. However, beyond 60°C, the degradation of OG becomes strongly correlated with the initial amount of PS.

Finally, as expected, the results confirmed the central role of temperature and the amount of oxidising inorganic species in the process of generating oxidising radical entities that oxidise the OG dye via the heat/PS process.

II.3.2. Effect of initial OG concentrations

The research examined the impact of different initial concentrations of OG, ranging from 10 mg/L to 70 mg/L, on their degradation via a heat-activated persulfate process. The study involved using varying concentrations of PS, while keeping the temperature constant at 65°C and the reaction time at 260 minutes. Furthermore, the experiment was carried out under natural pH conditions.

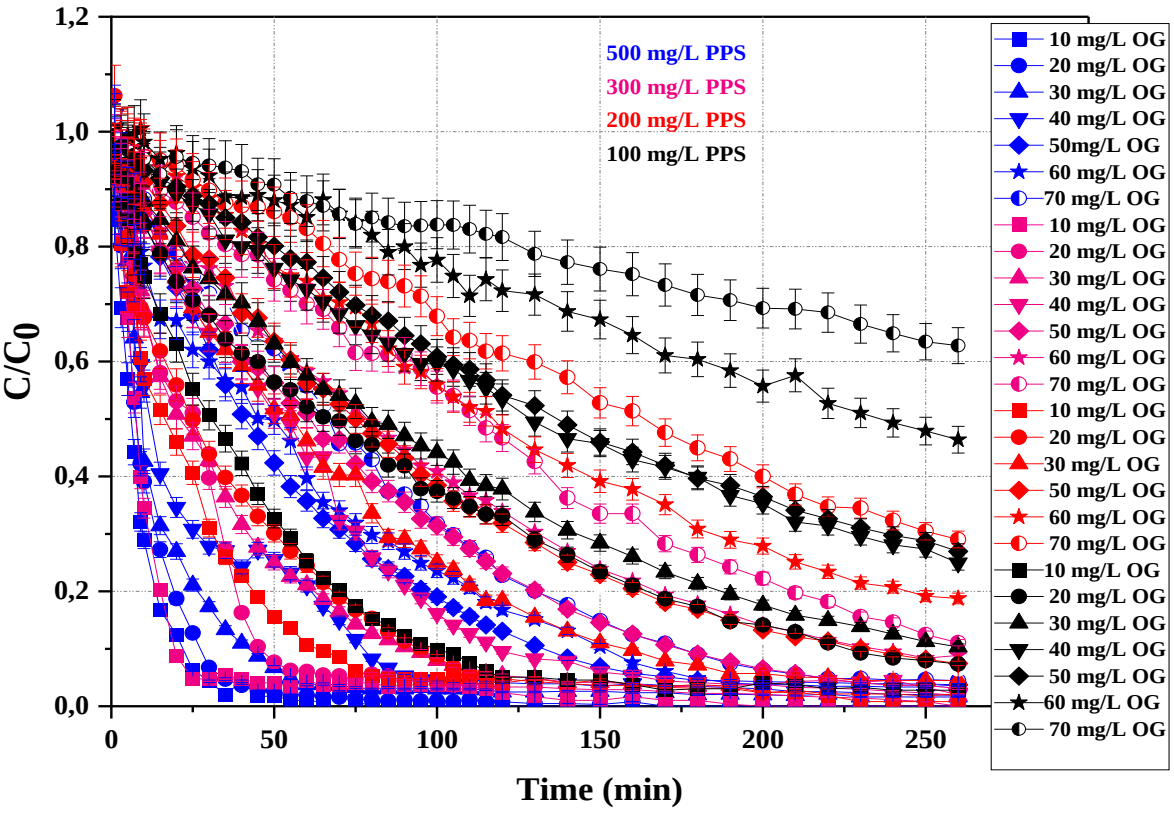

Figure III.8. Effect of OG concentration on its degradation by heat/PPS process. Experimental conditions: $[OG]_0$ =10-70 mg/L ,$[PPS]_0$ =100-500 mg/L, pH=6.

Figure III.8 shows that the elimination of OG decreased with increasing dye concentration from 10 mg/L to 70 mg/L for all the PS doses tested. The elimination rates presented in **Figure III.9** exhibited variations, ranging from complete degradation to 95.6% using 500 mg/L of PS, from 100% down to 88.9% with 300 mg/L of PS, from 99.2% to 71% with 200 mg/L of PS, and finally, from 97.2% to 37.2% with 100 mg/L of PS.

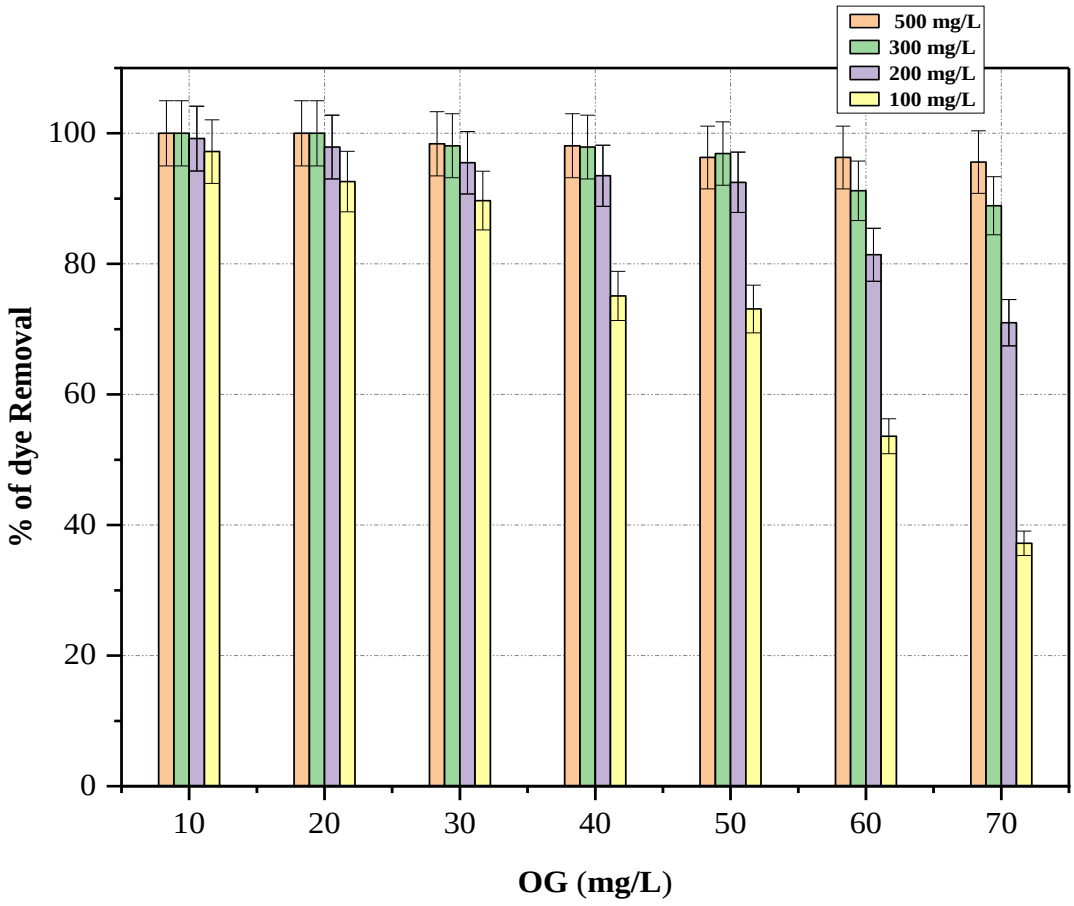

Figure III.9. Effect of OG concentration on its elimination by the heat/PPS process. Experimental condition: $[OG]_0$ =10-70 mg/L ,$[PPS]_0$ =100-500 mg/L, T= 65°C, pH=6.

On the other hand, pseudo-first-order kinetic behaviour was observed in all the reactions, with a high regression coefficient (**see appendix**). **Figure III.10** illustrates the effect of OG concentration on the rate constants of its degradation via heat-activated persulfate.

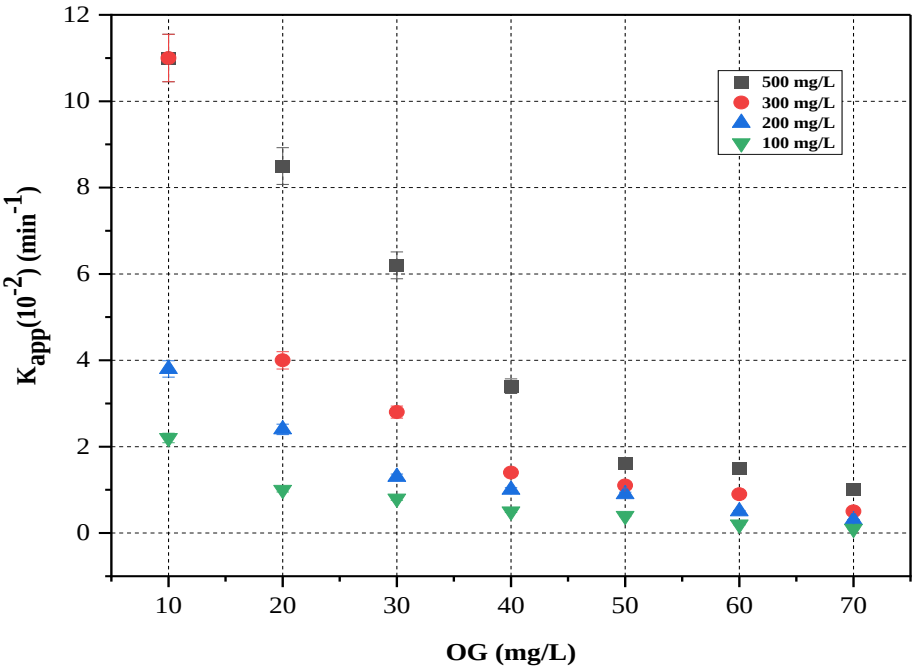

Figure III.10. Effect of OG concentration on the rate constants of its degradation by heat/PS process. Experimental condition: $[OG]_0$ =10-70 mg/L, $[PPS]_0$ =100-500 mg/L, T= 65°C, pH=6.

For instance, as shown in **Figure III.10**, when the temperature was maintained at 65°C and initial OG concentrations ranging from 10 to 70 mg/L were considered (with values of 10-20-30-40-50-60-70 mg/L the rate constant k_{aap}, showed a gradual decrease. Specifically, at a PPS concentration of 500 mg/L, the rate constant decreased from 11.10^{-2} min^{-1} to 1.10^{-2} min^{-1}. With 300 mg/L PPS, the rate constant reduced from 11.10^{-2} min^{-1} to $0.5.10^{-2}$ min^{-1}. At 200 mg/L PPS, the rate constant decreased from $3.8.10^{-2}$ min^{-1} to $0.3.10^{-2}$ min^{-1}. Finally, with 100 mg/L PPS, the rate constant decreased from $2.2.10^{-2}$ to $0.1.10^{-2}$ min^{-1}.

The decline in OG degradation efficiency as the initial OG concentration increased might stem from the interaction between the free oxidising radical species in the solution and the intermediate products of OG degradation. These intermediates might engage in a competitive parallel reaction with the oxidising species at higher dye concentrations. Consequently, the ratio between the reactive species and the pollutant decreased as the OG concentration increased. This decreasing ratio led to a decrease in the dye removal [19,23].

II.3.3. Effect of initial pH

pH is widely recognised as a critical parameter affecting chemical reactions. In particular, the initial pH of the solution plays an essential role in the heat-activated persulfate for OG degradation. This influence arises from its ability to alter the distribution of oxidising species, affect the overall rate of PS decomposition, and modify the speciation of the target pollutant [24,25].

To investigate this effect, a series of experiments were carried out using unbuffered solutions with pH values ranging from 2 to 12, adjusted using 0.1 mol/L NaOH or H_2SO_4. The initial concentrations of PS and OG were kept constant, and the temperature was maintained at 65°C throughout the study.

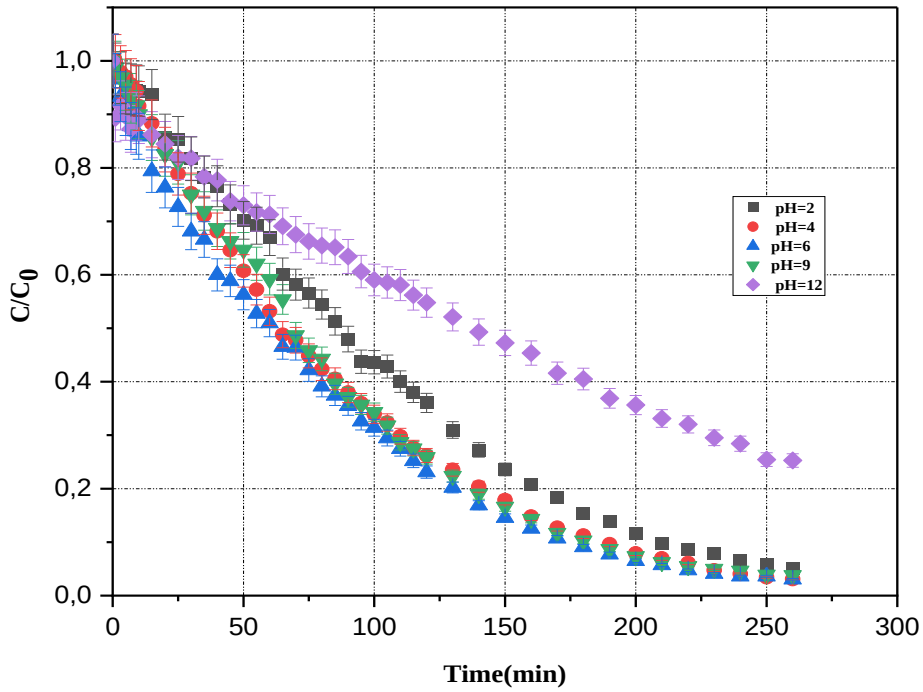

Figure III.11. Effect of initial solution pH on the OG degradation by heat/PPS process. Experimental conditions: $[OG]_0$ =50 mg/L, $[PPS]_0$=300 mg/L, T=65°C.

As shown in **Figures III.11.and III.12,** the OG degradation process is virtually the same for pH 4, 6 and 9, with elimination rates equal to 96.9%, 96.94% and 96.2%, respectively, and rate constants varying between 1.10^{-2} min^{-1} and $1.1.10^{-2}$ min^{-1}, so that, in this specific pH range,

no significant impact was observed on the degradation of the OG, comparable results were obtained when the degradation of paracetamol was studied using heat activated peroxydisulphate [26]**.** However, when the pH was adjusted to 2, the degradation of OG was only slightly influenced, with a decrease in the elimination rate to 94.9% and a decrease in the apparent constant to k_{app}= $0.8.10^{-2}$ min^{-1}; in contrast, at a strongly basic pH (pH=12), the degradation process of OG was strongly influenced, so that the elimination rate of the dye decreased to 74.7% and its rate constant to k_{app}=$0.5.10^{-2}$ min^{-1}.

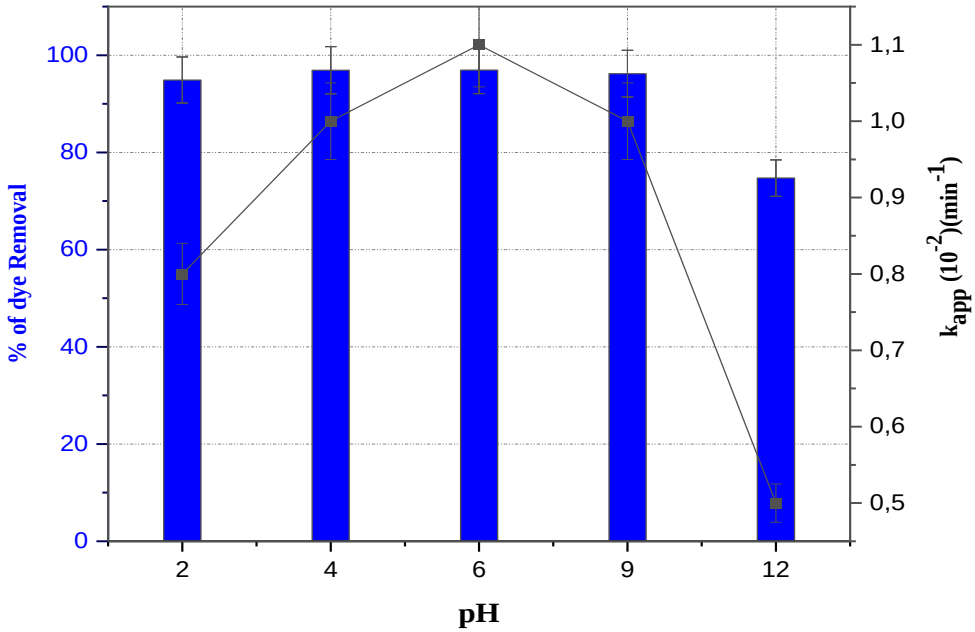

Figure III.12. Effect of initial solution pH on the process of OG dye removal rate and the variations in pseudo-first-order rate constants. Experimental conditions: $[OG]_0$ =50 mg/L, $[PPS]_0$=300 mg/L, T=65°C.

These results could be justified by the distribution of the sulfate radical $SO_4^{\bullet -}$ and the hydroxyl radical $HO^{\bullet}$ which, at a pH close to natural, both radical species existed simultaneously in the solution; moreover, at a pH below 7, the sulfate radical $SO_4^{\bullet -}$ predominated due to its formation during the reaction of H^+ with the persulfate anion $S_2O_8^{-2}$ according to **(Equations (III.10)** and **(III.11)**, whereas at very basic pH conditions, noted pH=12, the formation of the $HO^{\bullet}$ radical was favoured **(Equation (III.3))**, which had a lower redox potential and a shorter lifetime than $SO_4^{\bullet -}$ [9,23,27].

$$SO_4^{\bullet -} + OH^- \rightarrow SO_4^{2-} + OH^{\bullet} \qquad \text{(III.3)}$$

$$S_2O_8^{2-} + H^+ \longrightarrow HS_2O_8^- \quad \text{(III.10)}$$

$$HS_2O_8^- \longrightarrow SO_4^{2-} + SO_4^{\bullet -} + H^+ \quad \text{(III.11)}$$

II.3.4. Effect of water matrix

To better simulate real-life conditions, Orange G degradation experiments were carried out using different aqueous matrices: raw spring water, Zemzem water, and Mediterranean Sea water. To achieve an initial substrate concentration of 50 mg/L, synthetic solutions were prepared by directly dissolving the OG dye powder in an aqueous medium. The main characteristics of the waters used are detailed in **Chapter II**.

The results, illustrated in **Figures III.13** and **III.14**, show that the nature of the aqueous matrix used negatively influenced the degradation process by thermal activation of the PPS.

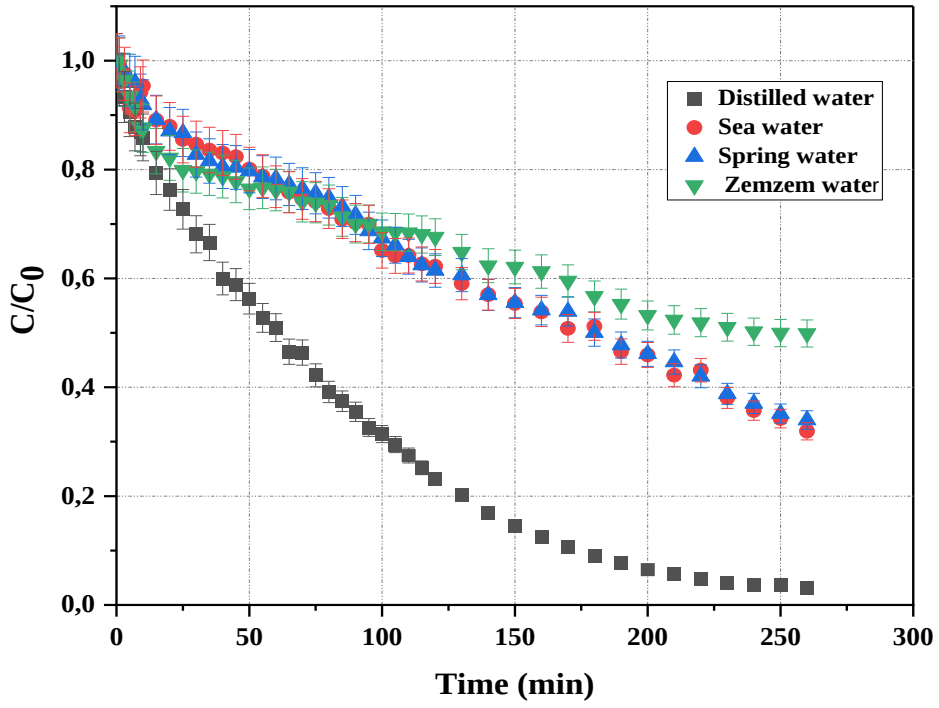

Figure III.13. Effect of the type of water used on the OG degradation by heat/PPS process. Experimental conditions: $[OG]_0$ =50 mg/L, V=400 mL, $[PPS]_0$=300 mg/L, T=65°C,pH=6.

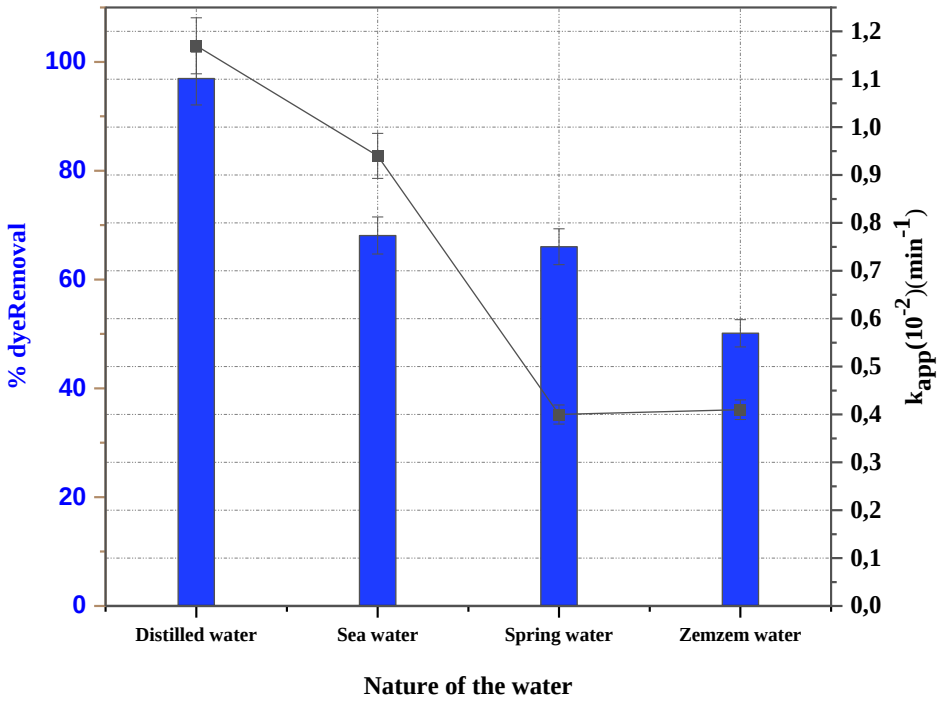

Figure III.14. Effect of the type of water used in the heat/PPS process on the OG dye removal rate and the variations in pseudo-first-order rate constants. Experimental conditions: $[OG]_0$ =50 mg/L, V=400 mL, $[PPS]_0$=300 mg/L, T=65°C,pH=6.

It has been observed that the rate of elimination of Orange G (OG) varies according to the aqueous matrix used. Since each type of water has a specific chemical composition, it remains challenging to identify the constituents responsible for inhibiting the degradation process. However, these results suggest that, in a large-scale application, the heat-activated PS degradation process could be influenced favourably or unfavourably by the presence of coexisting substances in natural aquatic environments, such as chloride ions, as confirmed by several studies in the literature[20,28].

II.3.5. Effect of Hexavalent chromium (VI)

Hexavalent chromium (Cr (VI)) refers to chromium in one of its most common oxidation states. In aqueous solutions, it can exist in various forms, including CrO_4^{2-}, $HCrO_4^-$, H_2CrO_4, $H_2CrO_7^-$, $Cr_2O_7^{2-}$, depending on the pH of the medium. At low pH, the predominant species is generally hydrogen chromate ($HCrO_4^-$) [29–31].

Figures III.15 and **III.16** illustrate the effect of varying concentrations of $Cr_2O_7^{2-}$on the removal efficiencies and degradation rate constants of 50 mg/L OG via the heat-activated PPS process.

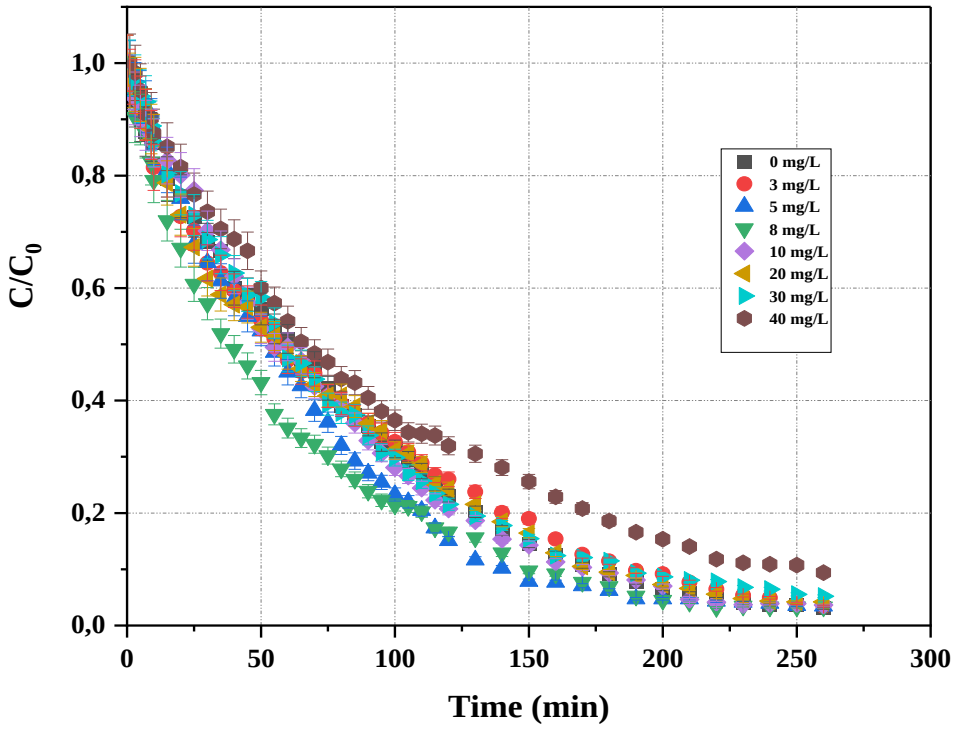

Figure III.15. Effect of different concentrations of $K_2Cr_2O_7$ on the OG degradation by heat/PS process. Experimental conditions: $[OG]_0$=50 mg/L, $[PPS]_0$=300 mg/L, $[Cr_2O_7^{2-}]$=0-40mg/L, T=65°C.

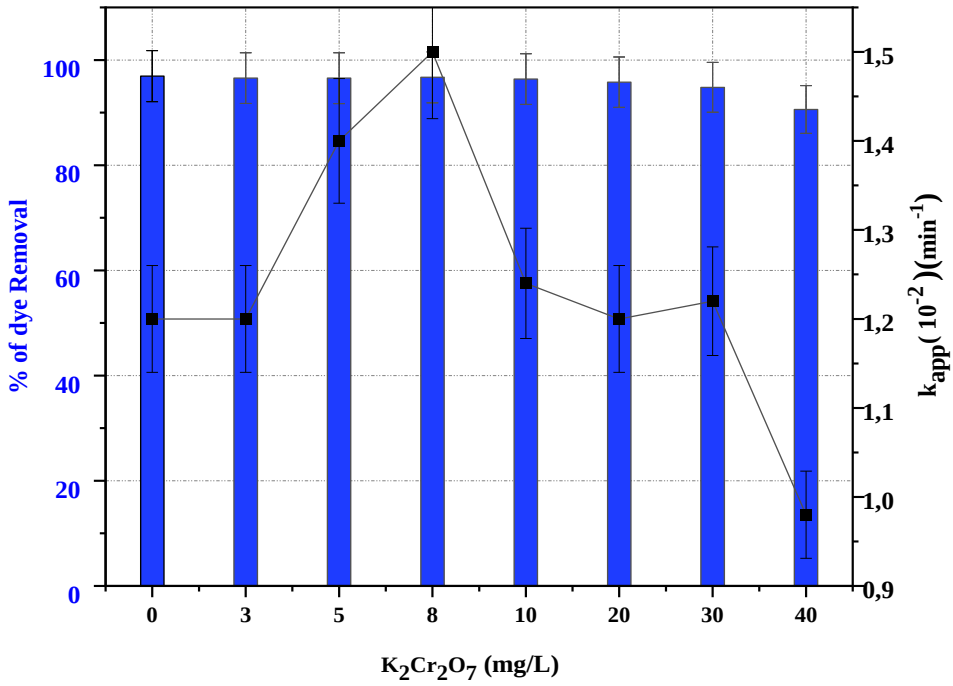

Figure III.16. Effect of different concentrations of $K_2Cr_2O_7$ in the heat/PPS process for the OG dye removal rate and the variations in pseudo-first-order rate constants. Experimental conditions: $[OG]_0$ =50 mg/L, ,$[Cr_2O_7^{2-}]$=0-40 mg/L, $[PPS]_0$=300 mg/L, T=65°C,pH=6.

The results presented in the figures above show that the degradation of Orange G was significantly inhibited for all tested concentrations of dichromate ($Cr_2O_7^{2-}$), namely (3, 5, 8, 10, 20, 30, and 40 mg/L). Indeed, the removal rates of the micropollutant decreased significantly: from 96.96% in the absence of Cr (VI) to only 90.59% at the maximum concentration of 40 mg/L of $Cr_2O_7^{2-}$ (see **Table III.2**).

This inhibition can be attributed to the competitive consumption of sulfate radicals ($SO_4^{\bullet-}$) generated by the thermal activation of persulfate (PPS). These radicals are partly diverted towards reducing the Cr (VI) ion to Cr (III), a much less toxic form. This phenomenon is consistent with the proposed reduction reaction **(Equation (III.33)**, suggesting that the oxidising species produced are no longer fully available for the oxidation of OG in the presence of Cr (VI) [31,32].

$$Cr^{6+} + SO_4^{\bullet-} + 2H_2O \longrightarrow Cr^{3+} + SO_4^{2-} + 4H^+ + O_2 \quad \text{(III.12)}$$

Table III.2. The rate of OG elimination by PS in the presence of Cr (VI) after 260 min of treatment

$[Cr_2O_7^{2-}]$ (mg/L)	% Removal
Without Cr (VI)	**96.94**
3	96.57
5	96.55
8	96.71
10	96.36
20	95.8
30	94.8
40	90.59

II.4. Indirect identification of radical species

In the context of the heat-activated PS process, which involves the degradation of organic compounds, it is essential to note that both sulfate ($SO_4^{\bullet-}$) and hydroxyl ($HO^{\bullet}$) radicals play significant roles as reactive oxidative species [33].

To assess the contribution of these radicals to the degradation of OG by heat-activated PS at neutral pH (pH =6), conventional quenching tests were carried out by adding a constant volume = 0.025% (V/V) of various radical-scavengers: EtOH, TerOH, EDTA to the treated

solution containing a fixed concentration of OG and PS and at a stable temperature of 65°C. The quenching results were described in **Figure III.17**, while the kinetic study was presented in **Figure III.18**.

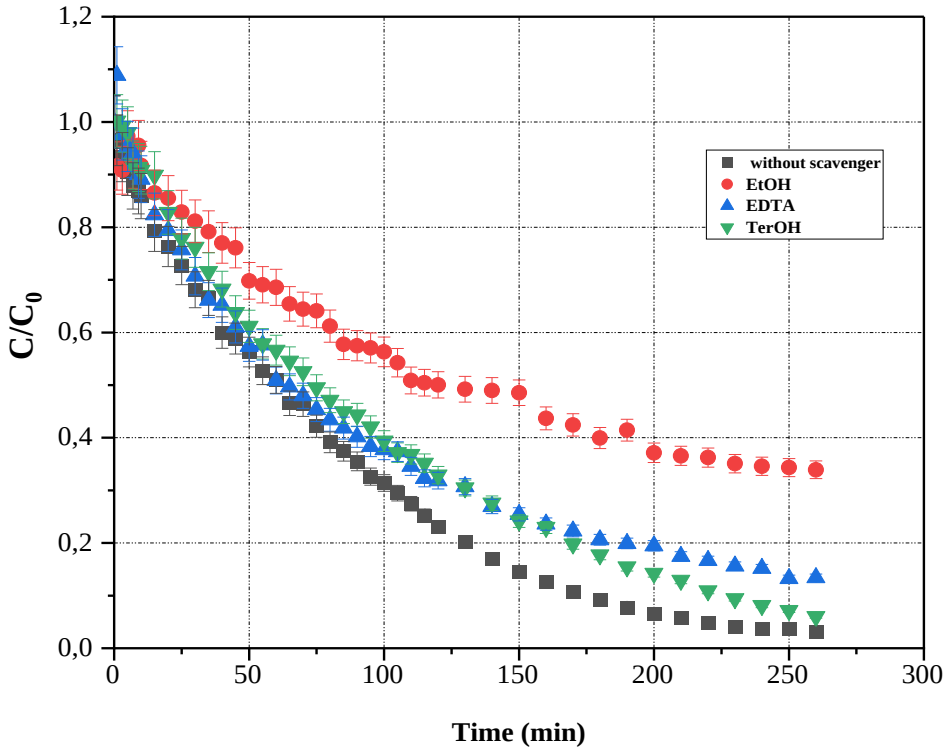

Figure III.17. Effect of a radical scavenger on the OG degradation by heat/PS process. Experimental conditions: $[Scavenger]_0$ =0.025% V/V,$[OG]_0$ =50 mg/L, $[PPS]_0$=300 mg/L, T=65°C.

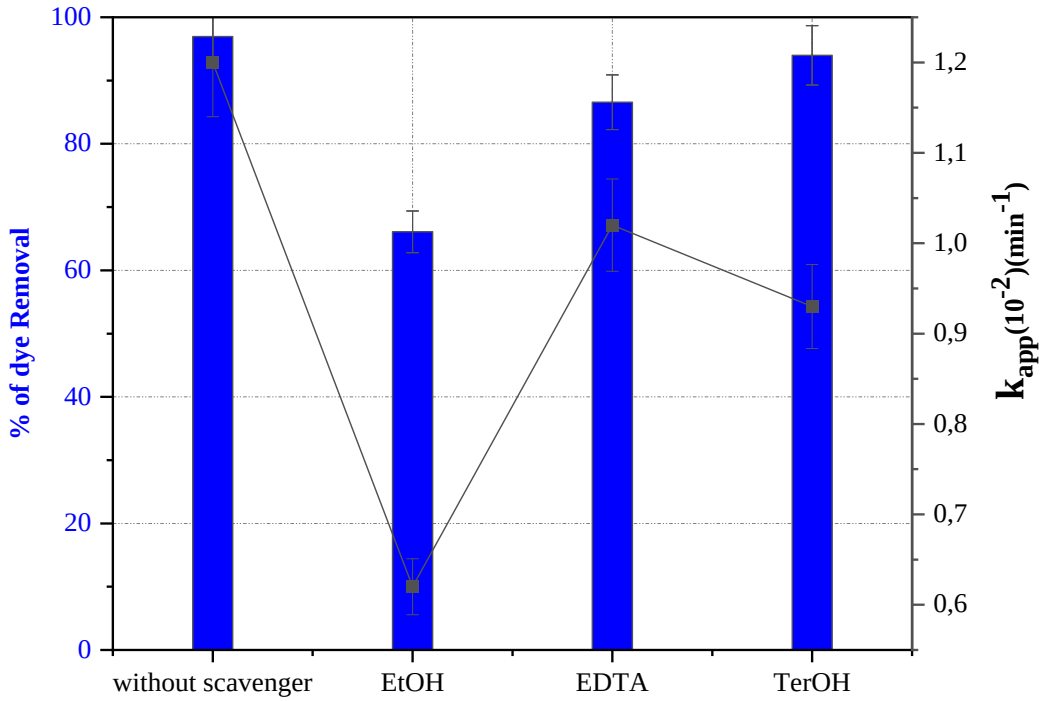

Figure III.18. Effect of a radical scavenger on the elimination of OG and the variations in pseudo-first-order rate constants. Experimental conditions:[Scavenger]$_0$ =0.025% V/V,[OG]$_0$ =50 mg/L, [PPS]$_0$= 300mg/L, T=65°C .

As can be seen from the data above, the efficiency of OG removal decreased from an initial value of 96.94% (without scavenger) to 66.09%, 86.58%, and 93.98% using ETOH, EDTA, and TerOH, respectively, at 260 minutes of treatment.

Tert-butanol (TerOH) is known for its great ability to scavenge $HO^{\bullet}$ radicals ($K_{HO^{\bullet}}$/TerOH = 3.8×10^8 -7.6×10^8 $M^{-1}s^{-1}$) compared to $SO_4^{\bullet-}$ radicals ($K_{SO_4^{\bullet-}}$ /TerOH = 4×10^5 - 9×1.10^5 $M^{-1}s^{-1}$) on the other hand ethanol (EtOH) act as effective scavengers, reacting with hydroxyl radicals ($HO^{\bullet}$) and sulfate radicals ($SO_4^{\bullet-}$) at a similar rate constant [2,34,35]; Moreover, EDTA represents an organic compound capable of undergoing reactions with $HO^{\bullet}$ and $SO_4^{\bullet-}$ Hence, it is essential to steer clear of introducing an excessive quantity of EDTA. This precaution is necessary to avoid any potential competition between EDTA and the contaminant for the available reactive radical species [13].

Based on these data, in this study, the degradation of OG by heat-activated persulfate was initiated by 30.95% of sulfate radicals and 6.02% of hydroxyl radicals, implying that $SO_4^{\bullet-}$ plays a crucial role as the primary reactive radical responsible for governing the degradation of organic compounds (OG).

II.5. Thermodynamic evaluation of OG degradation via heat-activated PPS process

In the context of the oxidation of orange G by thermally activated persulfate, the thermodynamic study plays a crucial role in understanding the energy dynamics of the PS activation reaction process. In this case, the apparent rate constants (K_{app}) (calculated in section **II.1.1**) were used to determine the activation energy (E_a) by fitting the data to the Arrhenius equation, as mathematically expressed in **Equations (III.13)** and **(III.14)**:

$$K_{app} = Aexp\left(\frac{-E_a}{RT}\right) \quad \text{(III.13)}$$

$$\ln K_{app} = \ln A - \frac{E_a}{R}\frac{1}{T} \quad \text{(III.14)}$$

Where:

- k_{app} = Rate constant.
- A =Pre-exponential factor.
- E_a = The activation energy.
- R =Gas constant (8.314 $Jmol^{-1}K^{-1}$).
- T = Absolute temperature in Kelvin.

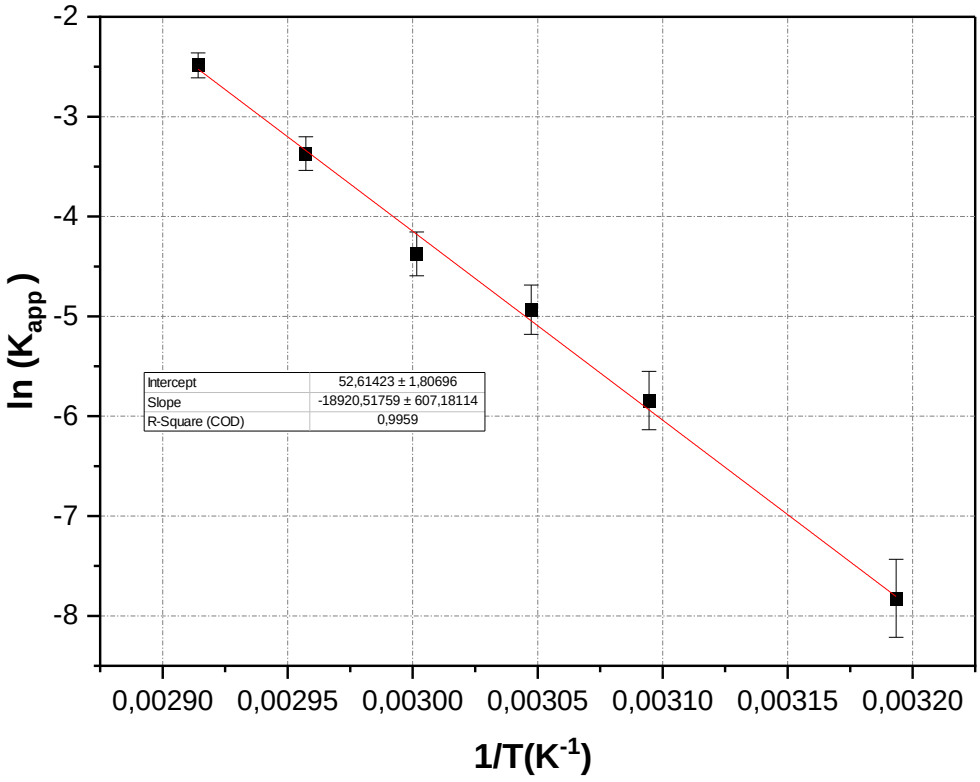

Figure III.19. Plot of ln k_{app} as a function of the inverse of temperature ($1/T$). Experimental conditions: $[OG]_0$ =50 mg/L ,$[PPS]_0$=1g/L , pH=6 , T=40-70°C.

As illustrated in **Figure III.19**, a strong linear correlation was observed between $ln\, k_{app}$ and the inverse of temperature (1/T), with a high regression coefficient R^2 equal to 99.7%. This strong linearity confirms the applicability of the Arrhenius model (**Equation (III.13)**). From the slope of the regression line ($-E_a$=slope× R), the activation energy was calculated to be 157.3 $KJ.mol^{-1}$ within the temperature range of 40–70 °C. This value is comparable to the activation energies reported for the thermal degradation of other compounds via persulfate-based advanced oxidation processes, such as chloroxylenol (130 kJ·mol⁻¹), arsenite (As III) ($119.91 \mp 17.5\ KJ.mol^{-1}$), paracetamol (180 KJ mol⁻¹), Reactive Black 5 (141 kJ·mol⁻¹), bisphenol A (133.5 kJ·mol⁻¹), and dexamethasone (86.9 kJ·mol⁻¹) [2,9,20,26,36,37]; This difference implies that the composition of the impurities and the specific conditions of the experiment can significantly influence the PS oxidation mechanism and could lead to alterations in the rate of contaminant oxidation [9,18].

In order to provide a more in-depth analysis of the energy changes and a reinterpretation offering a better understanding of the phenomenon under study, the thermodynamic parameters of the system, namely the standard Gibbs free energy (ΔG˚), the standard entropy (ΔS˚) and the standard enthalpy of reaction (ΔH˚), were calculated using the Eyring-Polanyi equation **Equation (III.15)**, and more precisely by the specific formulation provided in **Equation (III.17)**.

$$K_{app} = \frac{k_B T}{h} e^{\frac{-\Delta G^0}{RT}} \quad \text{(III.15)}$$

$$\Delta G^0 = \Delta H^0 - T\Delta S^0 \quad \text{(III.16)}$$

$$ln\frac{K_{app}}{T} = -\frac{\Delta H^0}{R}\left(\frac{1}{T}\right) + ln\frac{K_B}{h} + \frac{\Delta S^0}{R} \quad \text{(III.17)}$$

In the provided equations, the constants are defined as follows:

- "k_B" is Boltzmann's constant (1.381×10^{-23} JK^{-1})
- "h" is Planck's constant (6.626×10^{-34} Js)
- "R" is the universal gas constant (8.314 J mol^{-1} K^{-1})
- "T" is the absolute temperature in Kelvin

In addition, "ΔH^0 " represents the enthalpy of activation, "ΔS^0" corresponds to the entropy of activation, and "ΔG^0" is the free energy.

The plot of $\ln\frac{K_{app}}{T}$ as a function of $\frac{1}{T}$ is presented in **Figure III.20**; from which the slope and y-intercept were used to calculate the values of ΔHº and ΔSº. These values were determined to be 153.377 KJ mol^{-1} and 0.18 KJ $mol^{-1}K^{-1}$, respectively.

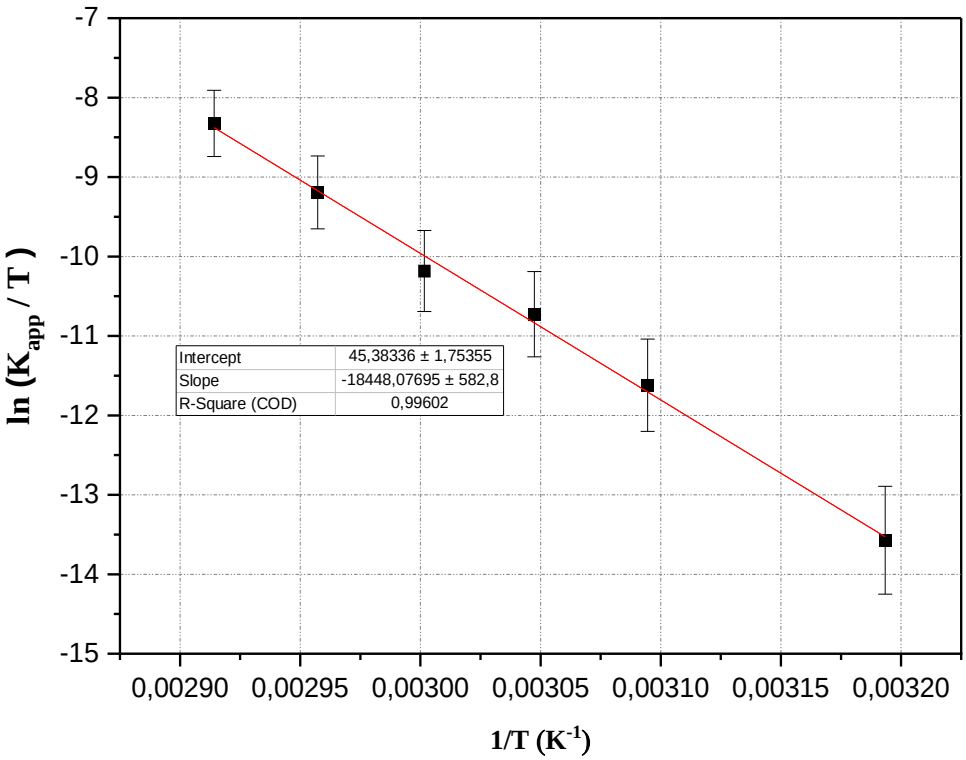

Figure III.20. Plot of $\ln(K_{app}/T)$ as a function of the inverse of temperature $(1/T)$.

Experimental conditions: $[OG]_0$ =50 mg/L, $[PPS]_0$=1g/L, pH=6 , T=40-70°C.

Finally, these results suggest that the process requires energy input to occur, indicating that it is not spontaneous for the tested range of temperature (20-70°C) under standard conditions .

As expected, the results confirm the crucial role of temperature in activating the persulfate and generating free radicals in solution, which are responsible for oxidising the dye Orange G.

II.6. Preliminary assessments of energy demands

The economy is a crucial factor in the wastewater treatment process, with energy consumption playing a significant role in energy-intensive operations, such as the thermal activation of persulfate.

To assess the energy requirements for industrial applications, an initial estimate of the electrical energy needed to degrade 1 mg of organic contaminant (OG) using the heat/PS

process was calculated under specific operating conditions of the heat/PS process: [OG] = 50 mg/L, [PS^{-}] = 300 mg/L; T_f = 65°C, T_i =20°C, and a treated solution volume of 400 mL. This estimate was made using the specific heating equation **(Equation (III.18))**.

$$SE_{H\left[kWh/mg_{OG}\right]} = \frac{Q_{H_{KJ}}}{3600 \times V_L \times [OG]_{mg/L}} \qquad (III.18)$$

Where QH represents the heating energy, calculated using the following equation (**Equation (III.19))**.

$$Q_{H_{KJ}} = \rho_{Kg/L} \times V_L \times C_{P_{KJ/Kg\times K}} \times (T_f - T_i)_K \qquad (III.19)$$

In the given context, ρ denotes the solution density, V represents the solution volume, Cp is the specific heat (4.18 kJ/kg×K), and T_f and T_i correspond to the final and initial temperatures, respectively. In this context, the SE_H was calculated at $1.05.10^{-3}$ kWh/mg_{OG}.

III. ELIMINATION OF OG BY HEAT AND FERROUS IONS CO-ACTIVATED PERSULFATE: SYNERGY EFFECT AND MINERALISATION

Co-activated persulfate with heat and metal is a novel advanced oxidation process (AOP) used to degrade various organic contaminants in water and soil. Activation of PS ($S_2O_8^{2-}$) by heat and metal ions, particularly transition metals such as iron (Fe^{2+}/Fe^{3+}), enhances its oxidative potential, allowing the generation of highly reactive sulfate radicals ($SO_4^{\bullet-}$) and hydroxyl radicals ($OH^{\bullet}$) that can effectively degrade a wide range of recalcitrant organic pollutants, including dyes.

III.1. Effect of the $FeSO_{4.7}H_2O$ dosage on OG degradation

Iron (Fe), a cost-effective and environmentally friendly transition metal [38], plays a crucial role in PS oxidation.

The ferrous ion can catalyse persulfate through a Fenton-type oxidation reaction, resulting in the generation of $SO_4^{\bullet-}$**Equation (III.20)** [39], which are the main radicals involved in the degradation of OG. Therefore, the effect of varying Fe^{2+} concentrations on OG degradation was investigated.

$$Fe^{2+} + S_2O_8^{2-} \longrightarrow Fe^{3+} + SO_4^{\bullet-} + SO_4^{2-} \qquad (III.20)$$

As illustrated in **Figures III.21** and **III.22**, a significant increase in the rate of OG degradation by thermally activated PPS was observed for all $FeSO_4$ concentrations tested. The rate constants increased from $1.2.10^{-2}$ min^{-1} to $4.6.10^{-2}$ min^{-1} when the dose of Fe^{2+} was varied from 0 to 50 mg/L. Furthermore, after 50 minutes of treatment, the OG elimination rate showed a progressive increase of 44.68% (see **Table III.3**). However, after this time, the efficiency of the thermal activation process of PPS in the presence of iron decreased at higher concentrations of Fe^{2+}, leading to a reduction in removal rates (**Table III.3**).

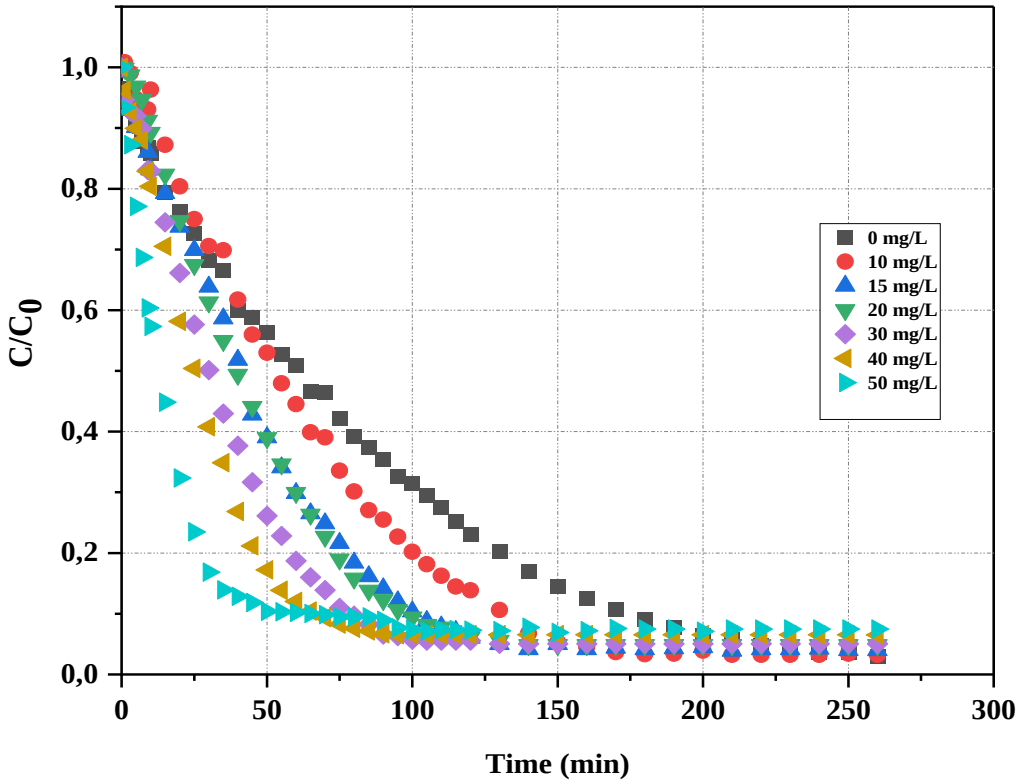

Figure III.21. Effect of the ferrous ions on the OG degradation by heat/PPS process**.** Experimental conditions: $[FeSO_4]_0$ =0-50 mg/L, $[OG]_0$ =50 mg/L, $[PPS]_0$=300 mg/L, T=65°C.

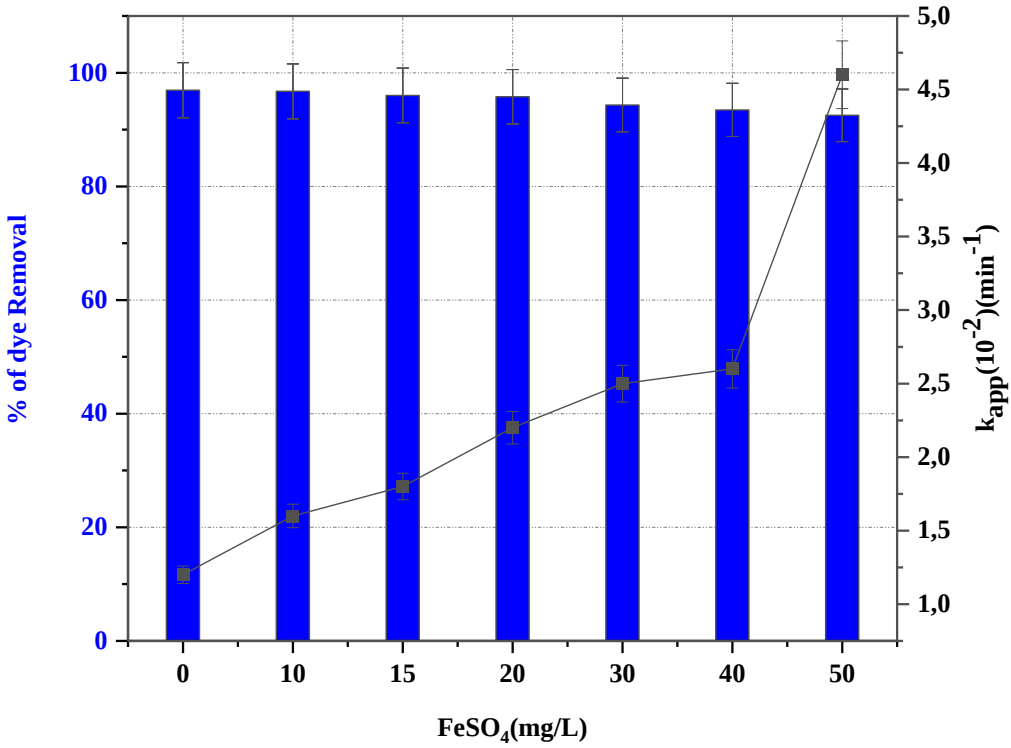

Figure III.22. Effect of the ferrous ions on the dye removal and the variations in pseudo-first-order rate constants. Experimental conditions:$[FeSO_4]_0$ =0-50 mg/L, $[OG]_0$ =50 mg/L, $[PPS]_0$=300 mg/L, T=65°C.

These results suggest that the rapidity of degradation kinetics after the first 50 min of treatment in the presence of high Fe^{2+} concentrations is probably due to the amount of sulfate radical generated in solution following a rapid activation of the PS anion by the Fe^{2+}catalyst (**Equation (III.20))**, as has been reported in the literature for other organic pollutants (Aniline,p-Nitrophenol)[36,39,40]. On the other hand, after 50 min of treatment, the rate of OG elimination decreased as the concentration of iron added to the solution increased and, consequently, the concentration of sulfate radicals $SO_4^{\bullet-}$ resulting from thermal co-activation and using the catalyst Fe^{2+} increased; these results could be attributed to the consumption of the sulfate radicals by its direct reactions with the ferrous ion following **Equation (III.21)** at concentrations of Fe^{2+} in excess.

$$SO_4^{\bullet-} + Fe^{2+} \longrightarrow Fe^{3+} + SO_4^{2-} \qquad \text{(III.21)}$$

Table III.3. Rate of OG elimination by PPS co-activated with heat and Fe^{2+} after 50 and 260 minutes of treatment.

$[Fe^{2+}]$ mg/L	% Removal (50 min)	%Removal (260 min)
Without Fe^{2+}	43.72	96.94
10	47	96.75
15	60.95	96.02
20	61.04	95.79
30	73.88	94.95
40	82.79	93.47
50	88.4	92.53

III.1.1. Effect of pH on heat/ Fe^{2+} co-activated PS for OG degradation

Radicals are important oxidant species in the activated persulfate (PS) oxidation process, and the pH value significantly affects the formation of these radicals. For this reason, the effect of pH on the co-activation of PPS with heat and iron (II) (**Fe^{2+}**) has been investigated.

Based on the data presented in **Figure III.23**, it can be observed that increasing the solution's initial pH from 1.2 to neutral (pH = 6) enhanced the degradation of OG, with the elimination rate rising from 88.6% to 92.53% under optimum conditions of 50mg/L of OG, 50mg/L of Fe_2SO_4, 300 $mg.L^{-1}$ of PPS and temperature of 65°C. These results are attributable to the fact that at pH values below 7, the sulfate radical ($SO_4^{\bullet-}$) is the primary species involved in the PS activation process [41]. In this pH range, the degradation of OG is favoured due to the enhanced oxidation of Fe^{2+} to Fe^{3+} in the presence of PS anions $S_2O_8^{2-}$.

However, the OG degradation process is inhibited at pH values above 7 in alkaline media, and the elimination rate decreases to 35.36%. This is likely due to the loss of soluble iron ions [42].

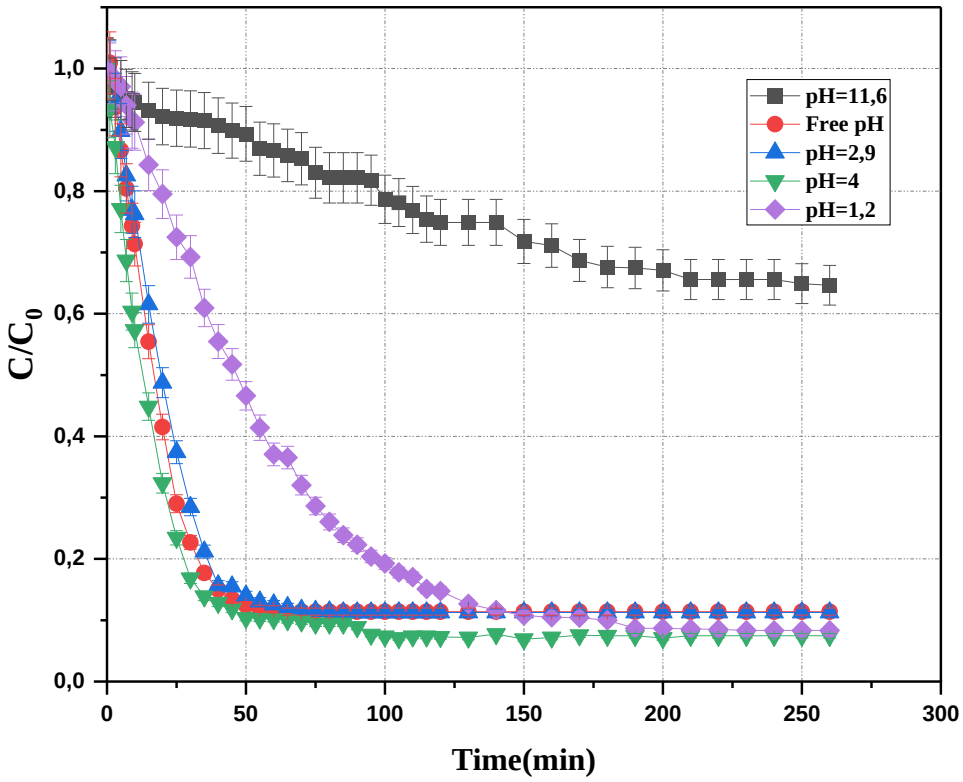

Figure III.23. Effect of initial solution pH on the OG degradation by heat/Fe^{2+} /PPS process. Experimental conditions: $[OG]_0$ =50 mg/L, $[PPS]_0$=300 mg/L, $[FeSO_4]_0$ =50 mg/L, T=65°C.

III.2. Effect of Mohr's salt dosage on OG degradation

Another process involving the co-activation of potassium persulfate by heat and ferrous iron II in the degradation of OG was demonstrated, this time using varying concentrations of Mohr's salt as the source of ferrous ions, as illustrated in **Figures III.24** and **III.25**.

For all concentrations tested, a synergistic improvement in the rate of OG degradation was observed, as shown in **Figure III.25.** The results indicated that the OG dye removal

reaction in the presence of 100 mg/L Fe^{2+} was 12.4 times faster compared to heat-induced PS activation without metal ions. Notably, a moderate increase in degradation was observed with the presence of Fe^{2+} ions, as indicated in **Table III.4**, after a treatment time of 25 minutes. Subsequently, the degradation process was significantly enhanced up to a reaction time of 50 minutes for Fe^{2+} concentrations of 100 and 70 mg/L was added to the solution, 75 minutes for ferrous ion concentrations of 50, 40, 30, and 20 mg/L , 100 minutes for Fe^{2+} concentrations of 10 mg/L , and 125 minutes for Fe^{2+} concentrations of 8 mg/L added in solution, after which the PS/Heat/ Fe^{+2} process began to be ineffective, at which point removal rates stagnated throughout the reaction time (260 min) **(Figures III.24)**

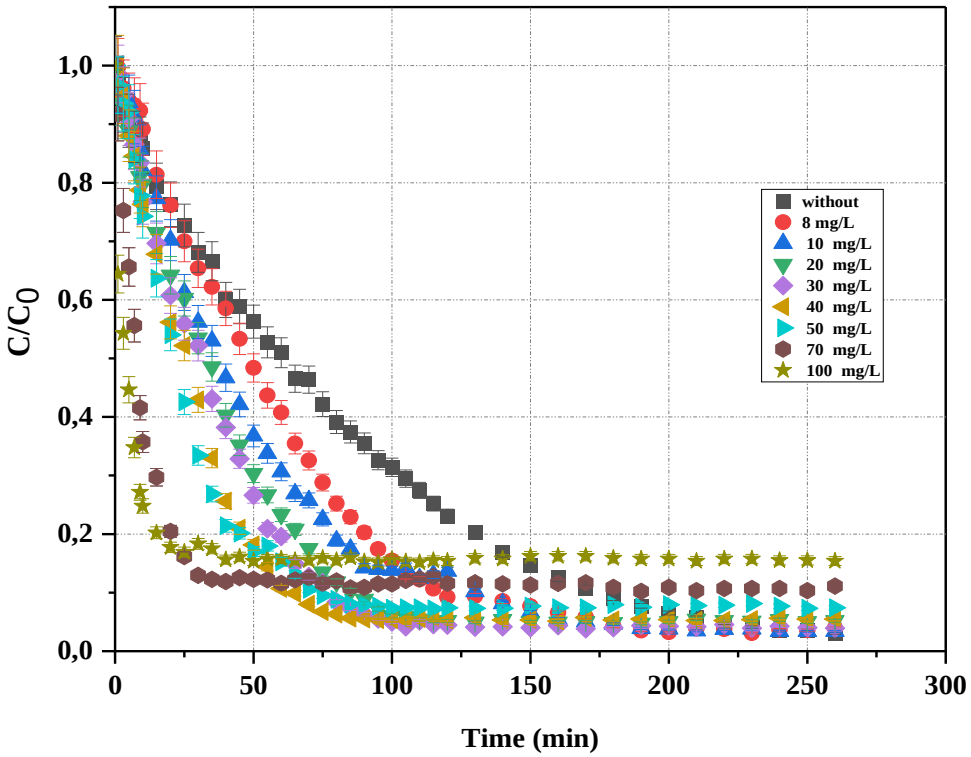

Figure.III.24. Effect of the Mohr salt on the OG degradation by heat/PPS process. Experimental conditions: $[(NH_4)_2Fe(SO_4)_2]_0$ =0-100 mg/L, $[OG]_0$ =50 mg/L, $[PPS]_0$=300 mg/L, T=65°C.

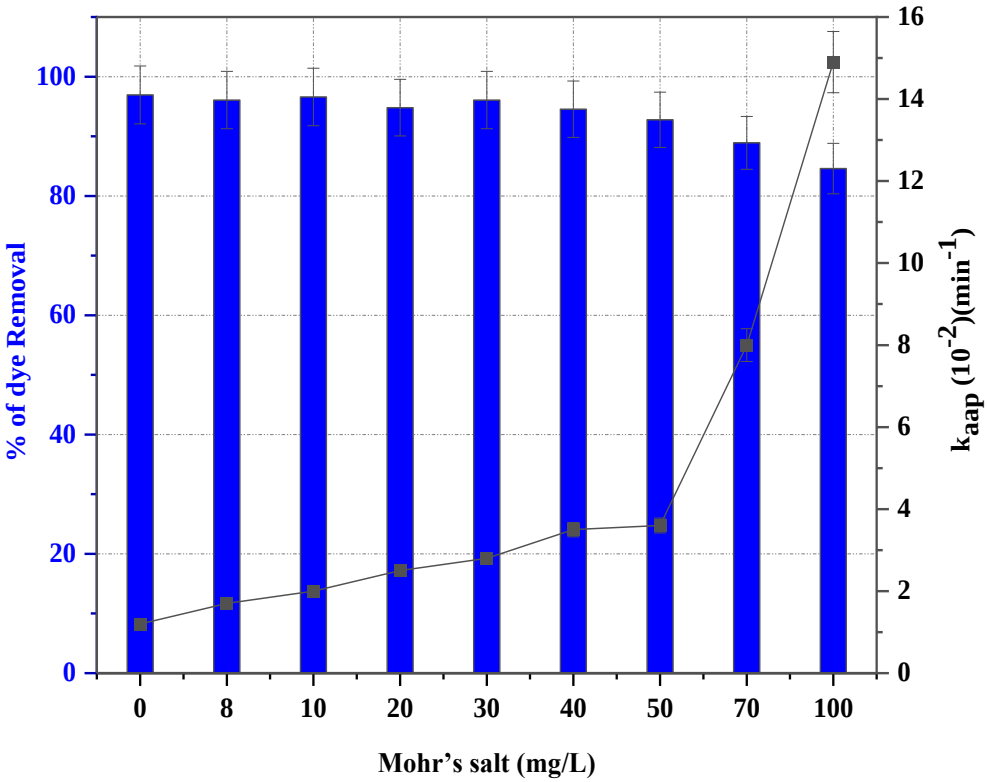

Figure III.25. Effect of the Mohr salt on the process of dye removal and the variations in pseudo-first-order rate constants. Experimental conditions: $[(NH_4)_2Fe(SO_4)_2]_0$ =0-100 mg/L, $[OG]_0$ =50 mg/L ,$[PPS]_0$=300 mg/L, T=65°C;

These compelling results lead to the conclusion that the heat/PS process is more effective at treating an aqueous solution loaded with OG than the heat /PS/ Fe^{+2} process in terms of pollutant removal rate, which is in agreement with the results obtained by ***M. Zhang et al.*** in their work on the degradation of p-Nitrophenol [41].

Table III.4. The rate of OG elimination by PS co-activated with heat and Fe^{2+} after 20 min and 50 min of treatment.

$[Fe^{2+}]$ mg/L	% Removal (25 min)	% Removal (50 min)
Without	27.29	43.72
8	30	51.62
10	38.74	63.25
20	39.77	69.67
30	44.08	73.37
40	47.8	81.87
50	57.45	83.01
70	83.84	87.73
100	83.08	84.6

III.3. Synergistic effect of simultaneous activation of PPS by heat and ferrous ions

The synergistic effect of simultaneous activation of PPS by heat and ferrous ions represents an innovative approach to improving the efficiency of OG degradation.

According to the results presented in **Figures III.26 and III.27,** including ferrous ions in the OG dye degradation process through heat-activated PPS has significantly enhanced the kinetic efficiency of the system under investigation.

Under optimal conditions, including an initial concentration of 50 $mg.L^{-1}$ of OG, 300 mg/L of PS, 50 mg/L of $FeSO_4$, 100 mg/L of Mohr salt, a natural pH, and a reaction time of 260 minutes at room temperature, the removal efficiency of OG were 29.18% and 46.37% in iron[1]/PS and iron[2]/PS processes, respectively. The systems exhibited a kinetic rate constant of $0.25.10^{-2}min^{-1}$ and $0.47.10^{-2}min^{-1}$, as illustrated in **Figure III.27**.

However, by maintaining the same operating conditions with a stabilised temperature of 65 °C, the heat/PS/Fe^{2+} system showed a notable increase in the rate constant, reaching $4.6.10^{-2}$ and $14.9.10^{-2}\ min^{-1}$ in the presence of iron[1] and iron[2] respectively. This improvement indicates that the co-activation of persulfate by heat and ferrous ions accelerates the OG removal process by a factor of 3.8 and 12.4 compared to the heat/PS system and 18.4 and 31.7 compared to the Fe^{2+}/PS system in the presence of $FeSO_4$ and Mohr salt respectively. These results suggest that the heat/PS/Fe^{2+} process has significant synergistic effects.

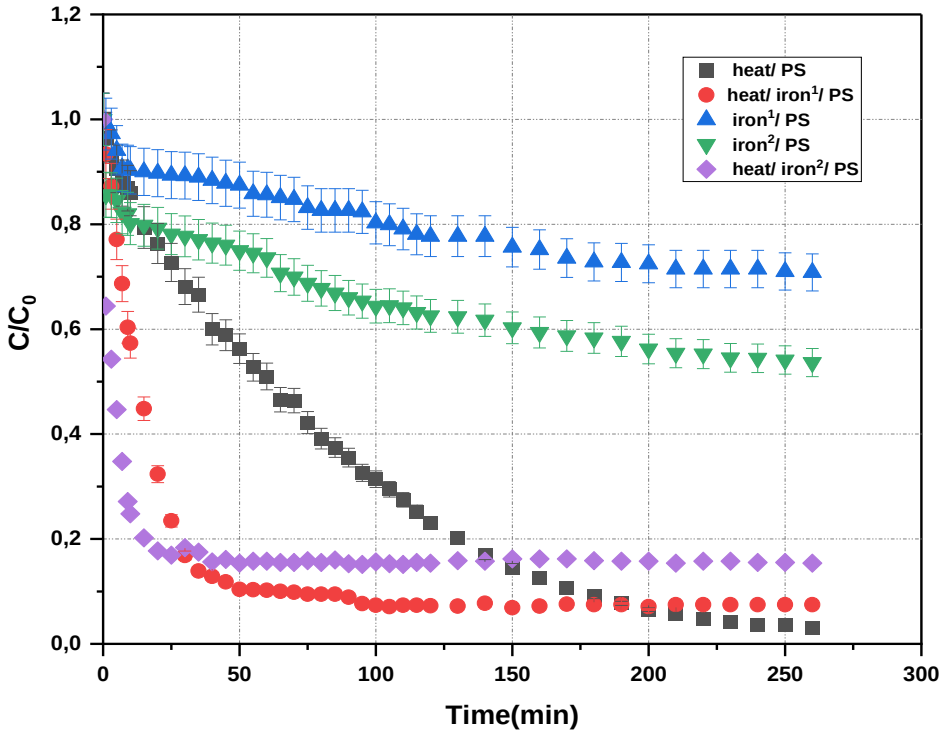

Figure III.26. Removal efficiency of OG degradation in single and co-activated PS system. Experimental conditions: $[OG]_0$ =50 mg/L, $[PSP]_0$=300 mg/L, iron[1]$[FeSO_4]_0$ =50 mg/L, iron[2] [Mohr salt]=100 mg/L ,T=65°C.

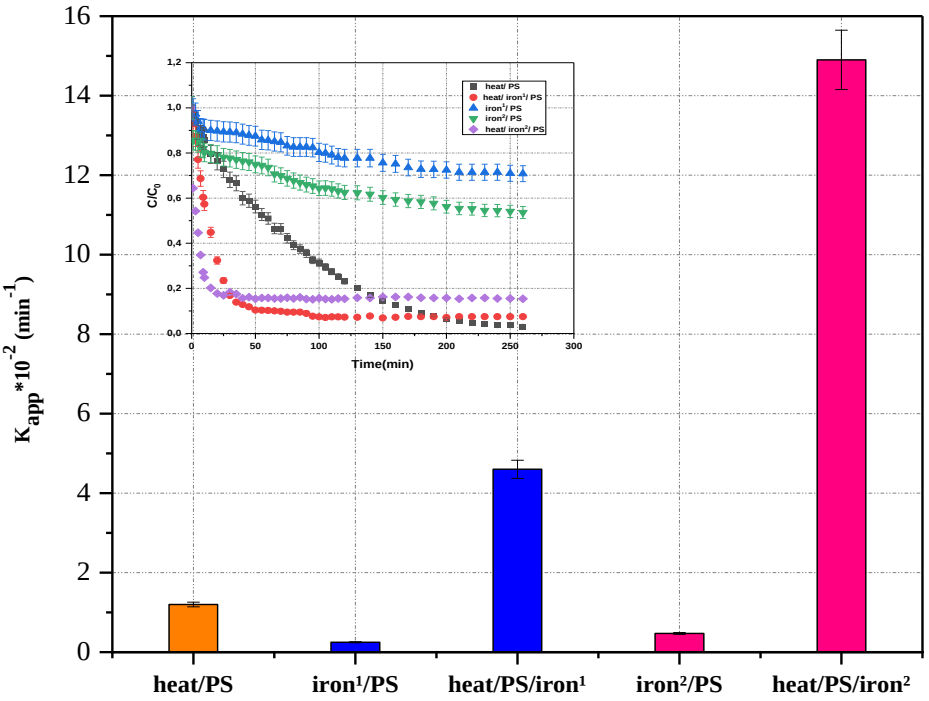

Figure III.27. Pseudo-first-order rate constants of the OG degradation in single and co-activated PPS system $[OG]_0$ =50 mg/L, $[PSP]_0$=300 mg/L, iron^1[$FeSO_4$]$_0$ =50 mg/L, iron^2 [Mohr salt]=100 mg/L, T=65°C,

The percentage of synergy can be calculated according to **Equation (III.22)** [42]:

$$S = \left[1 - \frac{K_{heat/PS} + K_{Fe^{2+}/PS}}{K_{heat/PS/Fe^{2+}}}\right] \times 100 \qquad \text{(III.22)}$$

Where K represents the degradation rate constant of the OG dye in the different activation systems (heat/PS, Fe^{2+}/PS, and heat/PS/Fe^{2+}).

Applying this equation, the synergy percentages in the heat/PS/$FeSO_4$ and heat/PS/Mohr salt processes were calculated as 68.48% and 88.97%, respectively, thus confirming the process's synergistic efficiency.

Previous studies on the TAP/ZnO-GAC oxidation system for AB113 degradation reported a limited synergistic effect between heat and ZnO-GAC, of only 18.36% [42]. Conversely, the

MnO_2/heat/PS oxidation system demonstrated a significantly higher synergistic effect of 88.6% during sulfamethoxazole treatment [43].

III.3. Mineralisation of OG

Chemical Oxygen Demand (COD) is commonly used to quantify the amount of organic compounds that can be chemically oxidised in an aqueous medium and to assess the mineralisation of the compound. The evolution of the initial concentration of the substrate and the COD of a 50 mg/L solution of OG was monitored at time intervals of 0, 20 min, 40 min, 60 min, 120 min, 180 min, and 260 min.

Figure III.28 illustrates the evolution of COD/COD_0 during the heat/iron co-activated persulfate process for the degradation of an OG solution with an initial concentration of 50 mg/L at 65°C and 50 mg/L of Fe^{2+} under neutral pH conditions.

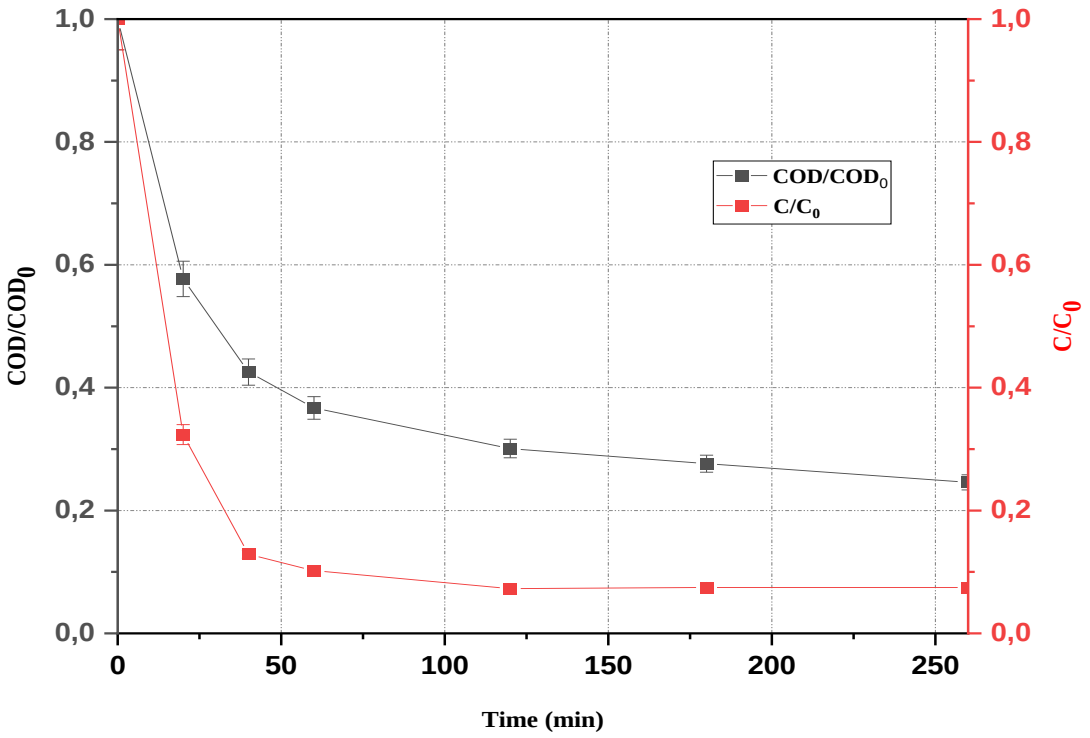

Figure III.28. COD abatement during the OG Degradation with the heat/PS/$FeSO_4$Process. Experimental conditions:$[OG]_0$ =50 mg/L, $[PSP]_0$=300 mg/L,$[FeSO_4]_0$ =50 mg/L, T=65°C.

The results indicate that OG degradation led to a significant decrease in the COD value, indicating the progression of mineralisation. However, the mineralisation of OG occurred at a slower rate than its degradation. After 260 minutes, the COD reduction reached approximately 75.41%, while the degradation rate was 92.53%. These results are consistent with previous studies, which suggest that total mineralisation is rapid at temperatures of ≥90°[44–46] . At this stage, the relatively low mineralisation yield can be considered acceptable, depending on the specific objectives of the treatment process.

IV. CONCLUSION

After this study, the following key points can be drawn:

- The increase in reaction temperature and initial persulfate concentration improved the efficiency of Orange G degradation.
- Under all experimental conditions, the degradation of Orange G follows a pseudo-first-order kinetic model.
- The highest degradation rate was observed under natural pH conditions.
- The optimal parameters included natural pH, a potassium persulfate concentration of 300 mg/L, a reaction time of 260 minutes, a temperature of 65°C, and an Orange G concentration of 50 mg/L, which resulted in a removal efficiency of 96.94%.
- The presence of organic and inorganic substances significantly impacted the removal of Orange G.
- The nature of the water used notably affected the degradation process of Orange G.
- The presence of chromium ions (Cr^{6+}) competes with Orange G and inhibits its degradation.
- Trapping tests (scavenging test) were conducted to identify the predominant reactive species in the neutral solution.
- The specific energy consumption (SEH) was estimated at 1.05×10^{-3} kWh/mg of Orange G.
- The oxidation kinetics of Orange G were faster in the heat/Fe^{2+}/PS process than in the heat/PS process alone, with a calculated synergy effect between the two processes of 68.48% for the heat/PS/$FeSO_4$ process and 88.79% for the heat/PS/Mohr's salt process.
- The removal rate of Orange G was higher in the heat/PS process.
- The reduction in COD in the heat/iron/PPS process was 75.41% after 260 minutes of treatment.

The results obtained confirm that the Heat/PS and Heat/PS/Iron processes can be considered as promising techniques for the treatment of effluents contaminated with azo dyes in terms of efficiency and cost.

BIBLIOGRAPHICAL REFERENCES

1. Lutze HV, Kerlin N, Schmidt TC. Sulfate radical-based water treatment in presence of chloride: Formation of chlorate, inter-conversion of sulfate radicals into hydroxyl radicals and influence of bicarbonate. Water Res. 2015 Apr;72:349–60.

2. Sun Y, Zhao J, Zhang BT, Li J, Shi Y, Zhang Y. Oxidative degradation of chloroxylenol in aqueous solution by thermally activated persulfate: Kinetics, mechanisms and toxicities. Chem Eng J. 2019 Jul;368:553–63.

3. Shu HY, Huang SW, Tsai MK. Comparative study of acid blue 113 wastewater degradation and mineralization by UV/persulfate and UV/Oxone processes. Desalination Water Treat. 2016 Dec;57(60):29517–30.

4. Lalas K, Arvaniti OS, Panagopoulou EI, Thomaidis NS, Mantzavinos D, Frontistis Z. Acesulfame degradation by thermally activated persulfate: Kinetics, transformation products and estimated toxicity. Chemosphere. 2024 Mar;352:141260.

5. Zhuang Q, Li X, Lian X, Hu H, Wang N, Wu J, et al. Catalysis Enhancement of Co_3 O_4 through the Epitaxial Growth of Inert ZnO in Peroxymonosulfate Activation: The Catalytic Mechanism of Surface Hydroxyls in Singlet Oxygen Generation. Cryst Growth Des. 2025 Jan 15;25(2):319–29.

6. Wang B, Wang Y. A comprehensive review on persulfate activation treatment of wastewater. Sci Total Environ. 2022 Jul;831:154906.

7. Wang Z, Shao Y, Gao N, Lu X, An N. Degradation kinetic of phthalate esters and the formation of brominated byproducts in heat-activated persulfate system. Chem Eng J. 2019 Mar;359:1086–96.

8. Mora VC, Rosso JA, Carrillo Le Roux G, Mártire DO, Gonzalez MC. Thermally activated peroxydisulfate in the presence of additives: A clean method for the degradation of pollutants. Chemosphere. 2009 Jun;75(10):1405–9.

9. Arvaniti OS, Ioannidi AA, Politi A, Miserli K, Konstantinou I, Mantzavinos D, et al. Dexamethasone degradation in aqueous medium by a thermally activated persulfate system: Kinetics and transformation products. J Water Process Eng. 2022 Oct;49:103134.

10. Lalas K, Arvaniti OS, Zkeri E, Nika MC, Thomaidis NS, Mantzavinos D, et al. Thermally activated persulfate oxidation of ampicillin: Kinetics, transformation products and ecotoxicity. Sci Total Environ. 2022 Nov;846:157378.

11. Tan C, Gao N, Deng Y, An N, Deng J. Heat-activated persulfate oxidation of diuron in water. Chem Eng J. 2012 Sep;203:294–300.

12. Ji Y, Dong C, Kong D, Lu J, Zhou Q. Heat-activated persulfate oxidation of atrazine: Implications for remediation of groundwater contaminated by herbicides. Chem Eng J. 2015 Mar;263:45–54.

13. Ahmadi S, Igwegbe CA, Rahdar S. The application of thermally activated persulfate for degradation of Acid Blue 92 in aqueous solution. Int J Ind Chem. 2019 Sep;10(3):249–60.

14. Rodriguez S, Vasquez L, Costa D, Romero A, Santos A. Oxidation of Orange G by persulfate activated by Fe(II), Fe(III) and zero valent iron (ZVI). Chemosphere. 2014 Apr;101:86–92.

15. Hayet Chamekh, Mahdi Chiha, Fatiha Ahmedchekkat,, Nour El Houda Souames. Degradation of Orange G by UV/TiO2/IO4 ¯process: Effect of operational parameters and estimation of electrical energy consumption. . Indian J Chem Technol [Internet] 2023 [cited 2024 Feb 12]; Available from: 〈http://op.niscpr res.in/index.php/IJCT/article/view/62814〉.

16. Waldemer RH, Tratnyek PG, Johnson RL, Nurmi JT. Oxidation of Chlorinated Ethenes by Heat-Activated Persulfate: Kinetics and Products. Environ Sci Technol. 2007 Feb 1;41(3):1010–5.

17. Chen Y, Deng P, Xie P, Shang R, Wang Z, Wang S. Heat-activated persulfate oxidation of methyl- and ethyl-parabens: Effect, kinetics, and mechanism. Chemosphere. 2017 Feb;168:1628–36.

18. Yang JF, Yang LM, Zhang SB, Ou LH, Liu CB, Zheng LY, et al. Degradation of azole fungicide fluconazole in aqueous solution by thermally activated persulfate. Chem Eng J. 2017 Aug;321:113–22.

19. Shuchi SB, Suhan MdBK, Humayun SB, Haque ME, Islam MdS. Heat-activated potassium persulfate treatment of Sudan Black B dye: Degradation kinetic and thermodynamic studies. J Water Process Eng. 2021 Feb;39:101690.

20. Potakis N, Frontistis Z, Antonopoulou M, Konstantinou I, Mantzavinos D. Oxidation of bisphenol A in water by heat-activated persulfate. J Environ Manage. 2017 Jun;195:125–32.

21. Olmez-Hanci T, Arslan-Alaton I, Genc B. Bisphenol A treatment by the hot persulfate process: Oxidation products and acute toxicity. J Hazard Mater. 2013 Dec;263:283–90.

22. Liang C, Wang ZS, Bruell CJ. Influence of pH on persulfate oxidation of TCE at ambient temperatures. Chemosphere. 2007 Jan;66(1):106–13.

23. Arvaniti OS, Ioannidi AA, Mantzavinos D, Frontistis Z. Heat-activated persulfate for the degradation of micropollutants in water: A comprehensive review and future perspectives. J Environ Manage. 2022 Sep;318:115568.

24. Fan Y, Ji Y, Kong D, Lu J, Zhou Q. Kinetic and mechanistic investigations of the degradation of sulfamethazine in heat-activated persulfate oxidation process. J Hazard Mater. 2015 Dec;300:39–47.

25. Feng Y, Song Q, Lv W, Liu G. Degradation of ketoprofen by sulfate radical-based advanced oxidation processes: Kinetics, mechanisms, and effects of natural water matrices. Chemosphere. 2017 Dec;189:643–51.

26. Dibene K, Yahiaoui I, Aitali S, Khenniche L, Amrane A, Aissani-Benissad F. Central composite design applied to paracetamol degradation by heat-activated peroxydisulfate oxidation process and its relevance as a pretreatment prior to a biological treatment. Environ Technol. 2021 Mar 8;42(6):905–13.

27. Liang C, Su HW. Identification of Sulfate and Hydroxyl Radicals in Thermally Activated Persulfate. Ind Eng Chem Res. 2009 Jun 3;48(11):5558–62.

28. Bennedsen LR, Muff J, Søgaard EG. Influence of chloride and carbonates on the reactivity of activated persulfate. Chemosphere. 2012 Mar;86(11):1092–7.

29. He P, Zhu J, Chen Y, Chen F, Zhu J, Liu M, et al. Pyrite-activated persulfate for simultaneous 2,4-DCP oxidation and Cr(VI) reduction. Chem Eng J. 2021 Feb;406:126758.

30. Graham AM, Bouwer EJ. Oxidative dissolution of pyrite surfaces by hexavalent chromium: Surface site saturation and surface renewal. Geochim Cosmochim Acta. 2012 Apr;83:379–96.

31. Diao ZH, Xu XR, Chen H, Jiang D, Yang YX, Kong LJ, et al. Simultaneous removal of Cr(VI) and phenol by persulfate activated with bentonite-supported nanoscale zero-valent iron: Reactivity and mechanism. J Hazard Mater. 2016 Oct;316:186–93.

32. Peng H, Guo J, Liu Z, Tao C. Direct advanced oxidation process for chromium(III) with sulfate free radicals. SN Appl Sci. 2019 Jan;1(1):14.

33. Anipsitakis GP, Dionysiou DD. Radical Generation by the Interaction of Transition Metals with Common Oxidants. Environ Sci Technol. 2004 Jul 1;38(13):3705–12.

34. Chen Y, Tong Y, Liu Z, Huang LZ, Yuan J, Xue Y, et al. Enhanced degradation of Orange II using a novel UV/persulfate/sulfite system. Environ Chem Lett. 2019 Sep;17(3):1435–9.

35. Lin CC, Wu MS. UV/S2O82− process for degrading polyvinyl alcohol in aqueous solutions. Chem Eng Process Process Intensif. 2014 Nov;85:209–15.

36. Xu Q, Zhou F, Yu Q, Xiao Y, Jiang X, Zhang W, et al. Aniline degradation and As (III) oxidation and immobilization by thermally activated persulfate. Chemosphere. 2023 Oct;338:139573.

37. Andrew OA, Pirgalıoğlu S, Doğan Ş. Heat activated persulfate oxidation of Reactive Black 5. Desalination Water Treat. 2020 Feb;177:393–9.

38. Deng J, Wang H, Gao R, Ma X, Chen M, Xu D, et al. Enhanced sludge solid-liquid separation based on Fe2+/periodate conditioning coupled with polyoxometalates: Cell destruction and protein adsorption. J Environ Manage. 2025 Jan;373:123552.

39. Rodrigues CSD, Madeira LM. p-Nitrophenol degradation by activated persulfate. Environ Technol Innov. 2021 Feb;21:101265.

40. Ike IA, Linden KG, Orbell JD, Duke M. Critical review of the science and sustainability of persulphate advanced oxidation processes. Chem Eng J. 2018 Apr;338:651–69.

41. Crimi ML, Taylor J. Experimental Evaluation of Catalyzed Hydrogen Peroxide and Sodium Persulfate for Destruction of BTEX Contaminants. Soil Sediment Contam Int J. 2007 Jan;16(1):29–45.

42. Li X, Yuan L, Zhao L. A Comparative Study on Oxidation of Acidic Red 18 by Persulfate with Ferrous and Ferric Ions. Catalysts. 2020 Jun 21;10(6):698.

43. Zhang M, Chen X, Zhou H, Murugananthan M, Zhang Y. Degradation of p-nitrophenol by heat and metal ions co-activated persulfate. Chem Eng J. 2015 Mar;264:39–47.

44. Reza Samarghandi M, Tari K, Shabanloo A, Salari M, Zolghadr Nasab H. Synergistic degradation of acid blue 113 dye in a thermally activated persulfate (TAP)/ZnO-GAC oxidation system: Degradation pathway and application for real textile wastewater. Sep Purif Technol. 2020 Sep;247:116931.

45. Zhou T, Du J, Wang Z, Xiao G, Luo L, Faheem M, et al. Degradation of sulfamethoxazole by MnO2/heat-activated persulfate: Kinetics, synergistic effect and reaction mechanism. Chem Eng J Adv. 2022 Mar;9:100200.

46. Ike IA, Orbell JD, Duke M. Feasibility, mechanisms, and optimisation of organic pollutant degradation by thermally activated persulphate. Chem Eng Res Des. 2018 Aug;136:304–14.

47. Goulden PD, Anthony DHJ. Kinetics of uncatalyzed peroxydisulfate oxidation of organic material in fresh water. Anal Chem. 1978 Jun 1;50(7):953–8.

48. Lee YC, Lo SL, Chiueh PT, Chang DG. Efficient decomposition of perfluorocarboxylic acids in aqueous solution using microwave-induced persulfate. Water Res. 2009 Jun;43(11):2811–6.

CHAPTER IV

Elimination of Orange G Dye using Non-Thermal Plasma: Gliding-Arc Discharge

I. INTRODUCTION

This section is dedicated to studying the oxidation of the azo dye Orange G through an advanced oxidation process, more specifically, an electrical process known as the "Glidarc plasma" process. Humid air is used as the plasmagenic gas.

The study focuses on a first-generation semi-open batch-type Glidarc plasma reactor. As previously described, this process combines several types of advanced oxidation processes simultaneously. Due to its oxidising properties, it can effectively degrade a wide range of organic pollutants.

In the first part, we optimised the Glidarc plasma reactor to determine the optimum treatment conditions. The device used, previously described in Chapter II, was optimised according to the following criteria:

- The flow rate of the plasmagenic gas is 650 L/h
- The diameter of the gas injection nozzle is 1 mm.
- The inter-electrode distance is 3 mm,
- The distance between the electrode and the solution is 15 mm.
- The volume of the solution to be treated is 400 ml.
- The initial concentration of the solution to be treated is 50 mg.L-1

In the second phase, we investigated and highlighted specific properties of non-thermal plasma. We then analysed the degradation of the target molecule using the Glidarc plasma process and examined the impact of various additives on the treatment process. Finally, we explored the combination of the Glidarc process with the Fenton process, examining the effect of the operating parameters. Subsequently, the coupling of the two processes, the activation of persulfates and non-thermal plasma, was carried out. Additionally, we evaluated the energy efficiency associated with pollutant treatment in the plasma reactor.

II. NON-THERMAL GLIDARC PLASMA

A plasma constitutes a complex medium whose composition significantly depends on the type of plasmagenic gas used and the voltage applied between the electrodes. For Glidarc-type plasmas, **Czernichowski et al** [1] proposed a relatively simple technique, yet offering

numerous advantages. This method uses a sliding arc, which moves within a gas flow between two divergent electrodes. The device, operating at atmospheric pressure, thus allows for the generation of cold plasmas. The electrical discharge begins where the distance between the electrodes is smallest and then propagates under the influence of the gas flow towards the electrode ends. The interaction between the arc and the species present in the plasmagenic gas leads to the plasma formation. This type of discharge has been employed in our study for the degradation of the model pollutant molecule, Orange G.

III. HUMID AIR PLASMA

III.1. The chemical composition of a humid air plasma

In a humid air plasma, the reactive species that may be present arise from the molecules constituting the humid air, derived explicitly from N_2, O_2, and H_2O. These parent species form other reactive species, primarily ozone, nitrogen oxides (NO_x), and radicals such as $NO^\bullet$,$HO^\bullet$, and $HO_2^\bullet$. The reactions below represent the main chemical reactions expected in the humid air plasma [2–7].

- **The formation of ozone:**

$$O_{2(g)} + e \longrightarrow 2O^\bullet + e \qquad \text{(IV.1)}$$

$$O_{2(g)} + O^\bullet \longrightarrow O_{3(g)} \qquad \text{(IV.2)}$$

$$O_{3(g)} \longrightarrow O_{3(aq)} \qquad \text{(IV.3)}$$

- **The formation of nitric acid and nitrogen oxides (NOx):**

$$H_2O \longrightarrow HO^\bullet + H^\bullet \qquad \text{(IV.4)}$$

$$N_2 + e \longrightarrow 2N + e \qquad \text{(IV.5)}$$

$$N + HO^\bullet \longrightarrow NO + H \qquad \text{(IV.6)}$$

$$NO + HO^\bullet \longrightarrow HNO_2 \qquad \text{(IV.7)}$$

$$HNO_2 + HO^\bullet \longrightarrow NO_2 + H_2O \qquad \text{(IV.8)}$$

$$NO_2 + HO^{\bullet} \longrightarrow HNO_3 \qquad \text{(IV.9)}$$

- **The formation of radicals :**

$$H_2O + e \longrightarrow HO^{\bullet} + H^{\bullet} \qquad \text{(IV.10)}$$

$$H^{\bullet} + O_2 \longrightarrow HO_2^{\bullet} \qquad \text{(IV.11)}$$

$$HO^{\bullet} + O_3 \longrightarrow HO_2^{\bullet} + O_2 \qquad \text{(IV.12)}$$

- **The formation of hydrogen peroxide:**

$$HO^{\bullet} + \quad HO^{\bullet} \longrightarrow H_2O_2 \qquad \text{(IV.13)}$$

$$HO_2^{\bullet} + HO_2^{\bullet} \longrightarrow H_2O_2 + O_2 \qquad \text{(IV.14)}$$

III.2. The chemical reactivity of a plasma generated in humid air

Several chemical species exhibit acidic and redox properties in a humid air plasma. The formation of nitrous acid (HNO_2) and nitric acid (HNO_3) leads to an acidification of the reaction medium. At the same time, the formed gaseous species interact in redox systems characterised by high standard potentials, capable of oxidising most organic molecules. **Table IV.1** below lists the standard potentials of various redox couples that may interact in a humid air plasma.

Table IV.1. Standard potentials of some oxidation/reduction couples in a humid air plasma [8,9].

Ox +né ⟷	Red	E°(V/ENH)
$HO^{\bullet} + H^{+} + e$	H_2O	2.85
$O_{(g)} + 2H^{+} + 2e$	H_2O	2.42
$O_3 + 2H^{+} + 2e$	$O_2 + H_2O$	2.07
$HO^{\bullet} + e$	OH^{-}	2.02

$HO_2^{\bullet} + 3H^+ + 3e$	$2\ H_2O$	1.70
$H_2O_2 + 2\ H^+ + 2e$	$2\ H_2O$	1.68
$O_3 + 6\ H^+ + 6e$	$3\ H_2O$	1.51
$HO_2^{\bullet} + H^+ + e$	H_2O_2	1.50
$O_2 + 4H^+ + 4e$	$2\ H_2O_{(aq)}$	1.23
$NO_2 + H^+ + e$	HNO_2	1.09
$NO_2 + 2H^+ + 2e$	$NO + H_2O$	1.05
$NO_3^- + 3H^+ + 2e$	$HNO_2 + H_2O$	0.96
$NO_3^- + 4H^+ + 3e$	$NO + 2\ H_2O$	0.92

The chemical species present in plasma are responsible for its acidic and oxidative properties. Hydroxyl radicals ($HO^{\bullet}$), the most abundant radicals in humid air plasmas, as demonstrated in the study by **Benstaali et al**. [10], are primarily responsible for the oxidative properties due to their high standard potential. On the other hand, the acidic nature is attributed to $NO^{\bullet}$ radicals, which play a key role in the formation of HNO_2 and HNO_3 [11], as illustrated by **Equations IV.7** and **IV.9**.

$$NO + HO^{\bullet} \longrightarrow HNO_2 \qquad \text{(IV.7)}$$

$$NO_2 + HO^{\bullet} \longrightarrow HNO_3 \qquad \text{(IV.9)}$$

IV. CHARACTERISATION OF THE CHEMICAL PROPERTIES OF GLIDARC-TYPE HUMID AIR PLASMA

This section is dedicated to the study of specific properties of humid air plasma, carried out using the experimental setup developed at the LAMES laboratory, previously detailed, for the degradation of the target molecule

IV.1. Evolution of pH

To assess the acidifying effect of the Glidarc plasma, we monitored the pH of 400 ml of a 10^{-4} N NaOH solution treated under the optimal conditions of the Glidarc plasma. The air flow rate was Q = 650 L/h, with a distance of 1.5 cm between the surface of the liquid and the plasma. Measurements were taken over a time interval ranging from 0 to 210 minutes. Samples of the treated solution were collected at various time points to track the pH evolution. The results obtained are presented in **Figure IV.1.**

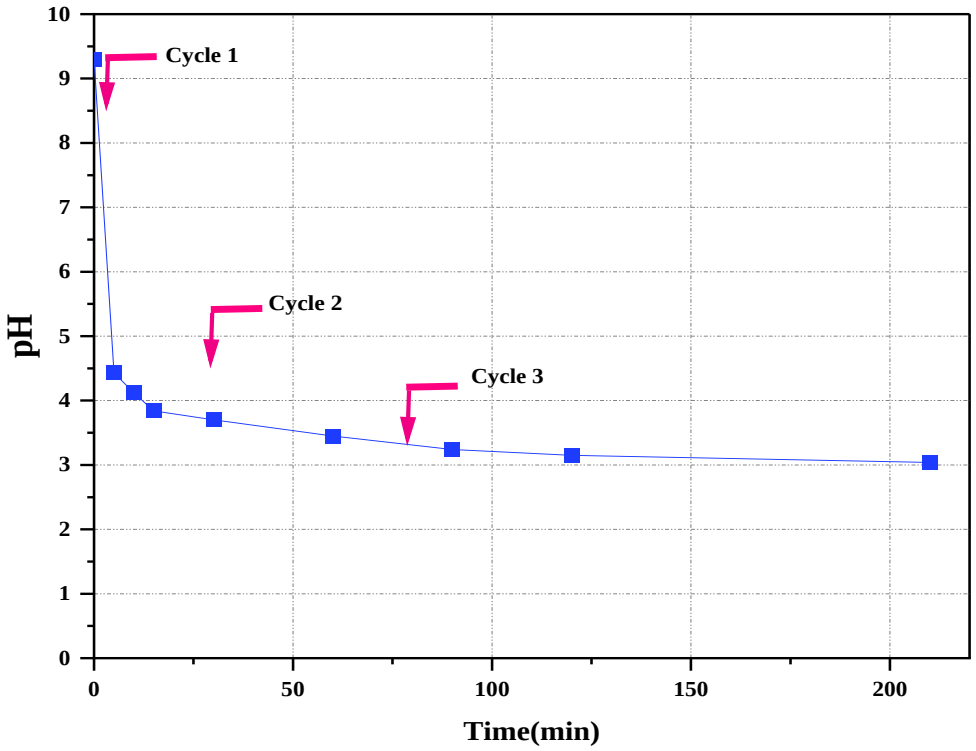

Figure IV.1. Evolution of the pH of the NaOH solution as a function of the treatment time. Exposure times to Glidarc-type plasma: Cycle 1: 0-10 min, Cycle 2: 30-40 min, Cycle 3: 80-90 min.

Figure IV.1 illustrates the decrease in the pH of the NaOH solution during the treatment. This decrease begins after only 5 minutes of exposure to humid air plasma, where the pH drops from 9.303 to 4.43. Then it decreases gradually, reaching approximately 3.04 after 210 minutes

of treatment. This initial pH drop has been attributed to the buffering effect of the HNO_2/NO_2^- system (pKa = 3.3) [6]. Furthermore, **Benstaali et al.** explained the gradual decrease in pH during the treatment by the fact that an increase in treatment time promotes the enhanced production of reactive species that diffuse into the aqueous solution [12]. Among these species, $NO^\bullet$, NO_2, N_2O_4, and N_2O_5 are generated in the gas phase and at the plasma/liquid interface [13]. Additionally, species like NO_2, N_2O_4, and N_2O_5 are hydrated in the aqueous medium, where they convert into nitrous and nitric acids, responsible for the progressive acidification of the medium.

IV.2. Study of the variation in conductivity

The conductivity of the solution affects the oxidative properties of the plasma. To assess this effect, conductivity monitoring was conducted in a 400 ml solution of Orange G at 50 mg/L, subjected to treatment with a Glidarc plasma using humid air and a pulsing system, with each cycle lasting 10 minutes, under the same optimal conditions previously described. Samples were collected at regular intervals, and the conductivity was measured using an Inolab-7310 type conductometer. The results of the conductivity variation over time during treatment are summarised in **Figure IV.2.**

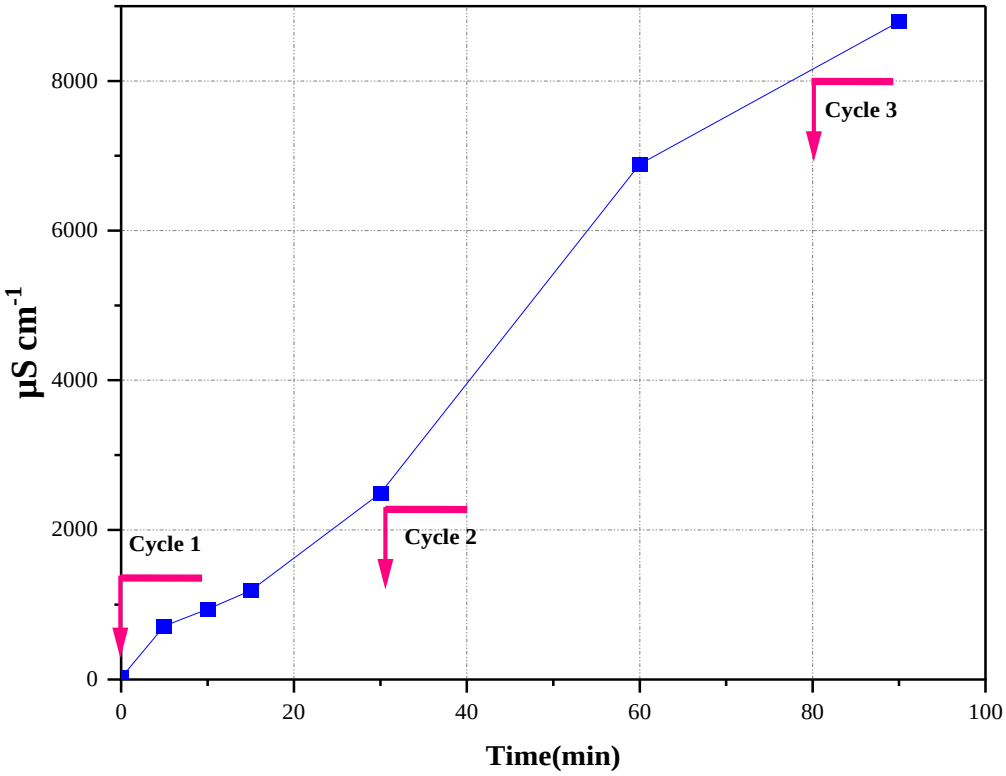

Figure IV.2. Evolution of the conductivity of the OG as a function of the treatment time. Exposure time to Glidarc-type plasma: Cycle 1: 0–10 min, Cycle 2: 30–40 min, Cycle 3: 80-90 min.

This figure illustrates a continuous increase in conductivity as a function of treatment time. After 90 minutes, the conductivity rises from 22 to 8790 µS/cm. This phenomenon was explained by **Du et al.**, who attribute this increase to the formation of H_3O^+ ions induced by electronic and ionic bombardment during the gliding discharge [7]. The primary electrons generated in the discharge collide with water molecules, resulting in an electron impact that leads to the formation of $HO^\bullet$ radicals and H_3O^+ ions (**Equations IV.10** and **IV.11**), both in the liquid and gas phases. These H_3O^+ ions, due to their high mobility in water compared to other similarly sized cations, play a significant role in the increase in conductivity of the medium. Indeed, the rise in conductivity, which measures a solution's ability to conduct electrical current, is primarily attributed to the diffusion of ionic species from the plasma towards the target and depends on the concentration and mobility of ions in solution.

$$H_2O + e \rightarrow H_2O^+ + e \qquad \text{(IV.10)}$$

$$H_2O + H_2O^+ \rightarrow H_3O^+ + HO^\bullet \qquad \text{(IV.11)}$$

V. ELIMINATION OF ORANGE G BY GLIDARC PLASMA

Several studies have been conducted on the degradation of various organic pollutants using high-voltage discharge processes, particularly the Glidarc plasma process in humid air, employed as a plasmagenic gas. These studies have demonstrated that these methods effectively degrade different organic molecules [7,11,14–17]. Further research efforts have focused on improving these processes' efficiency by combining them with advanced oxidation processes, such as the Fenton process, and persulfate activation methods [18–20].

In this work section, we investigate the treatment of organic pollutants (OG) using high-voltage electrical discharge, specifically the Glidarc plasma process in humid air, both as an independent treatment and in combination with other processes.

V.1. Study of OG Degradation Using Plasma alone and Combined with other Processes

The aim of treating OG using gliding arc discharge is to assess the effectiveness and behaviour of the plasma treatment on azo dyes. In this case, a 400 ml solution of OG was subjected to plasma treatment with humid air. Samples were collected at regular time intervals, up to 210 minutes. Each sample was subjected to UV/Visible spectrophotometric scanning across a wavelength range of 200 to 800 nm.

V.1.1. Effect of initial OG solution concentration

The effect of initial OG solution concentration on degradation efficiency by the Glidarc reactor was displayed in **Figure IV.3**.

Figure IV.3 (a, b, c, d) illustrates that the OG presents an absorption band at 260 nm, which is associated with the benzene ring, a notable band at 330 nm that corresponds to the naphthalene ring, and a significant band at 478 nm related to the azo bond. Following plasma discharge treatment, new absorption bands emerge at 200 and 240 nm, which are linked to the formation of multi-substituted benzene derivatives, such as benzene-1,2-dicarboxylic acid, formed through the degradation of the naphthalene ring. The removal of the 330 nm band

indicates the breakdown of the conjugated system containing the –N=N– bond and the degradation of the benzene and naphthalene rings. The gradual reduction of the absorption band at 478 nm over time further demonstrates the destruction of the chromophore [21–23].

On the other hand, the data showed that the OG degradation efficiency at lower initial OG concentrations was higher than at higher initial OG concentrations after 210 minutes of treatment. The main reason was that the amount of plasma-active species formed during the discharge process remained at a specific concentration level for a constant energy input [24]. However, high concentrations of pollutants may lead to the saturation of reactive species, thus decreasing the degradation efficiency.

Furthermore, the results presented in **Figures IV.3.a, b, c**, and **d** have proven that the proposed plasma reactor is effective for the degradation of OG.

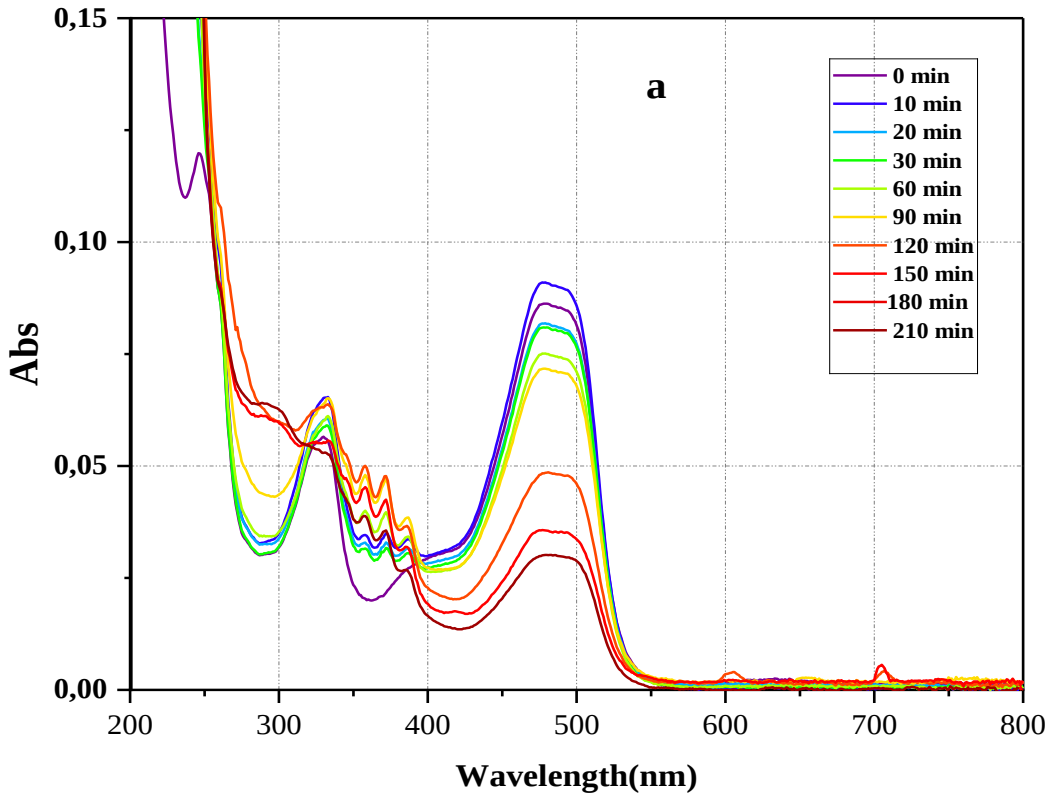

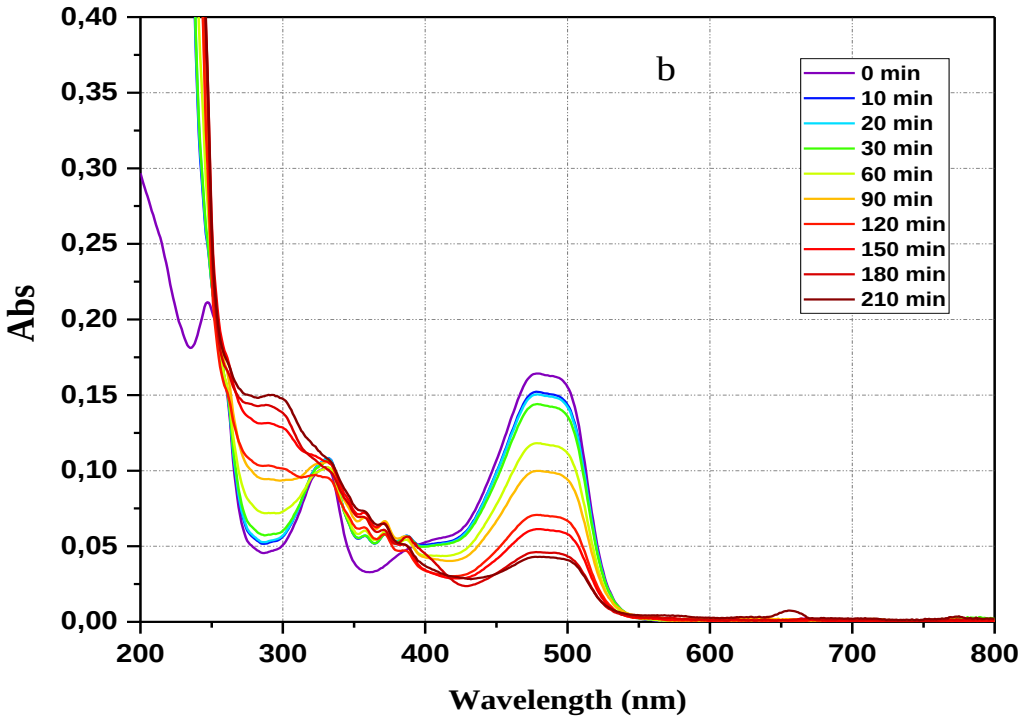
b
0 min
10 min
20 min
30 min
60 min
90 min
120 min
150 min
180 min
210 min
Abs
Wavelength (nm)
0,00
0,05
0,10
0,15
0,20
0,25
0,30
0,35
0,40
200
300
400
500
600
700
800

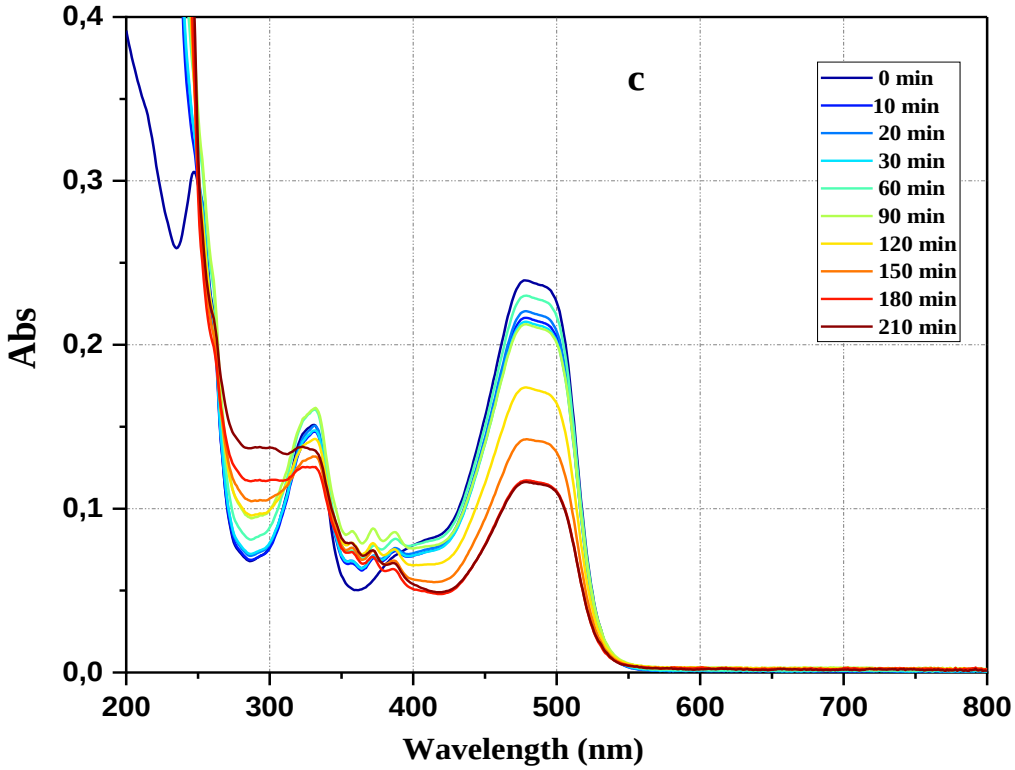
c
0 min
10 min
20 min
30 min
60 min
90 min
120 min
150 min
180 min
210 min
Abs
Wavelength (nm)
0,0
0,1
0,2
0,3
0,4
200
300
400
500
600
700
800

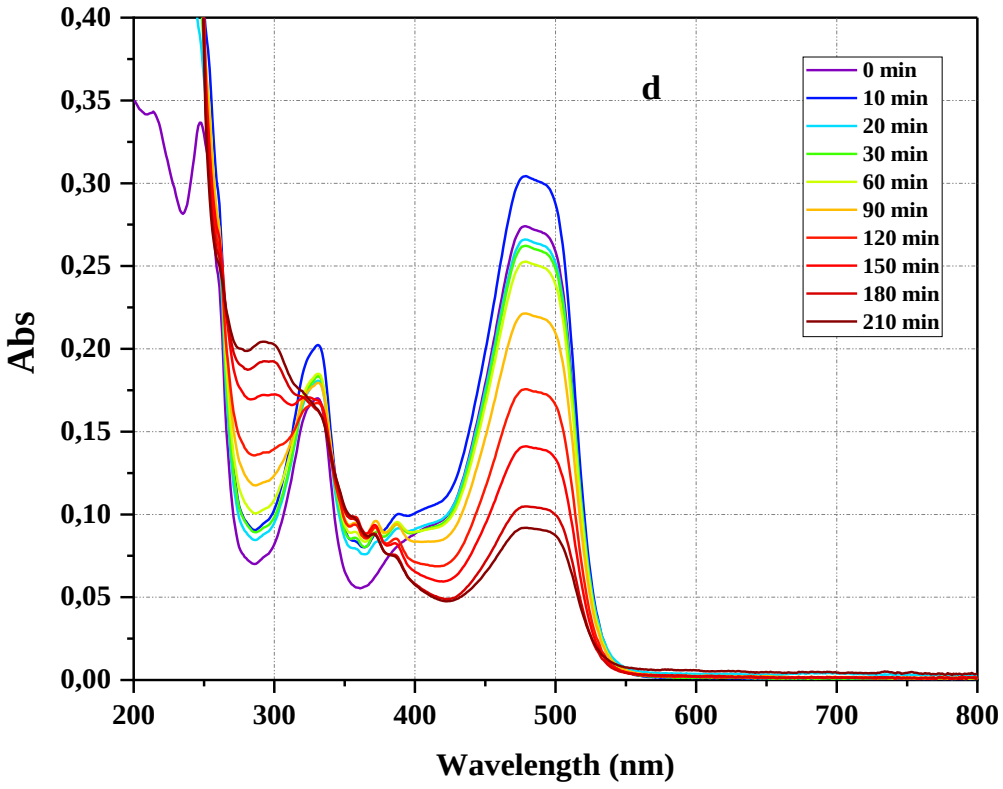

Figure IV.3. UV-Vis spectrum of OG as a function of treatment time**.** Exposure times to Glidarc-type plasma: Cycle 1: 0-10 min, Cycle 2: 30-40 min, Cycle 3: 80-90 min, Cycle 4:130-140 min. pH_0=6 **a** :$[OG]_0$= 3 mg/L, **b** :$[OG]_0$= 5 mg/L, **c** :$[OG]_0$= 7 mg/L, **d** :$[OG]_0$= 10 mg/L.

V.1.2. Effect of the initial pH

The influence of the initial pH variation of the solution on the removal of OG under non-thermal glidarc plasma was studied. The obtained results are presented in Figures a, b, and c of **Figure IV.4**.

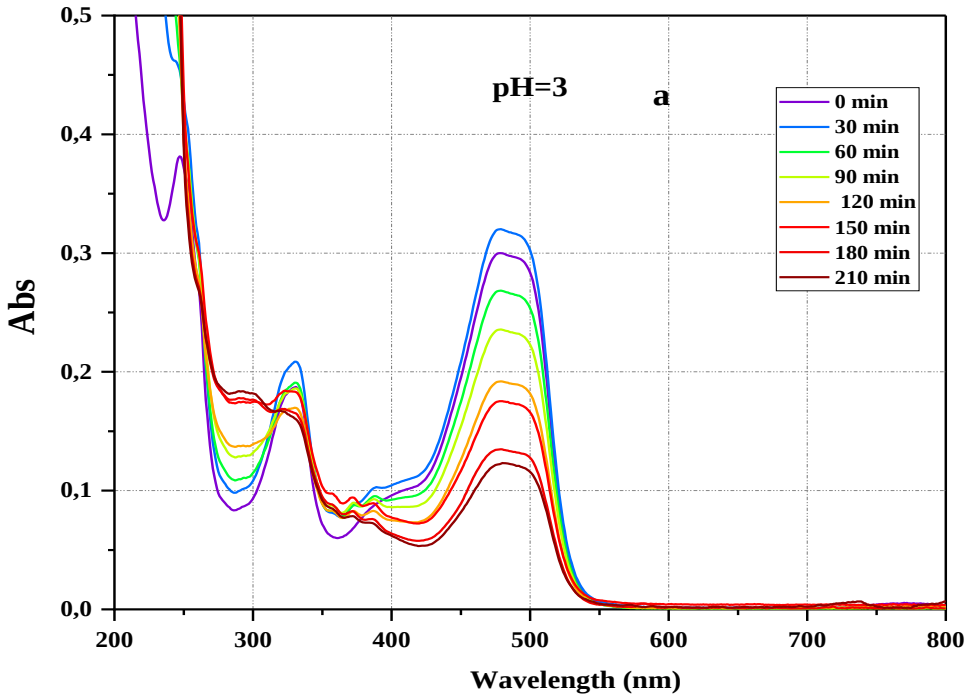
pH=3
a
0 min
30 min
60 min
90 min
120 min
150 min
180 min
210 min
Abs
Wavelength (nm)
0,0
0,1
0,2
0,3
0,4
0,5
200
300
400
500
600
700
800

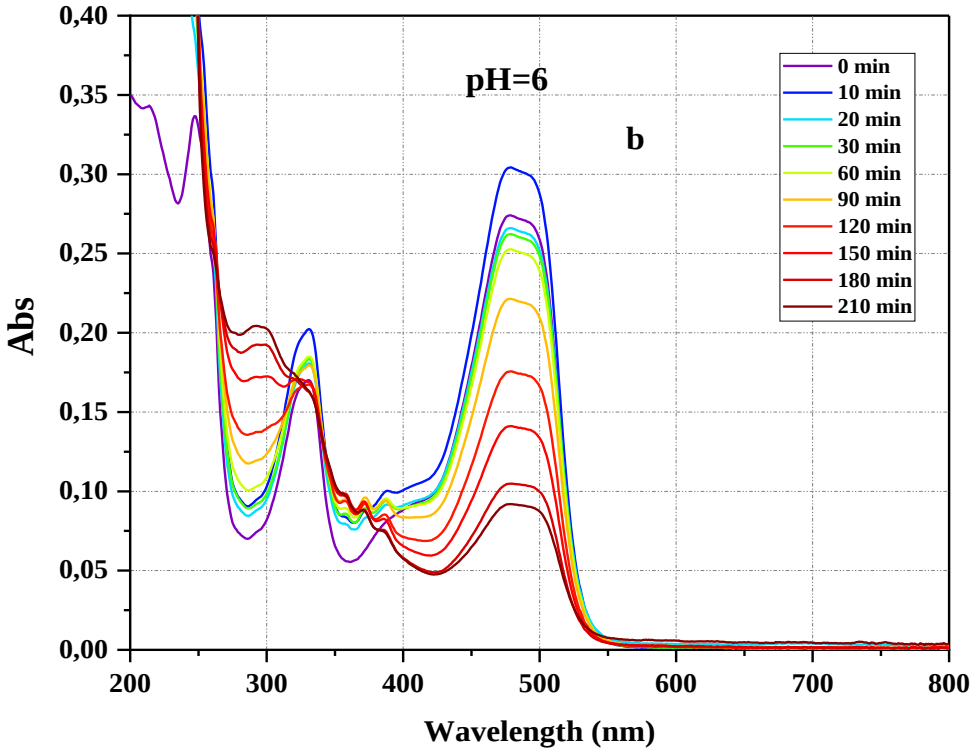
pH=6
b
0 min
10 min
20 min
30 min
60 min
90 min
120 min
150 min
180 min
210 min
Abs
Wavelength (nm)
0,00
0,05
0,10
0,15
0,20
0,25
0,30
0,35
0,40
200
300
400
500
600
700
800

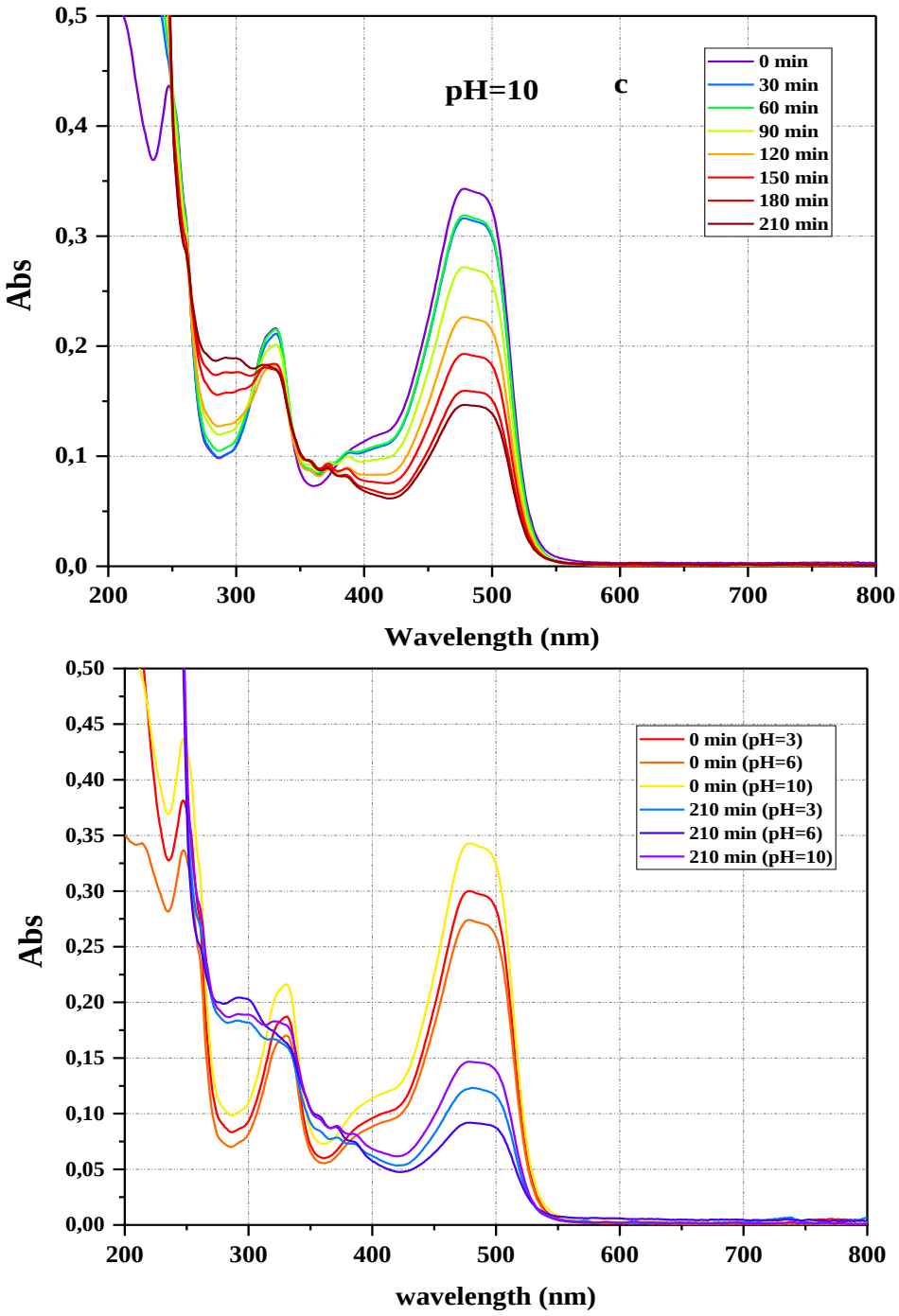

Figure IV.4. UV-Vis spectrum of the effect of pH on the degradation of OG as a function of treatment time**.** Exposure times to Glidarc-type plasma: Cycle 1: 0-10 min, Cycle 2: 30-40 min, Cycle 3: 80-90 min, Cycle 4:130-140 min. **[**OG]$_0$= 10 mg/L **a**: pH$_0$= 3 ,**b:** pH$_0$= 6 ,**c**: pH$_0$= 10.

According to the data above, the dye removal efficiency varies significantly depending on the pH of the solution. A slight difference in the degradation rate of OG by plasma discharge is observed for the tested initial pH values (3, 6, and 10). Indeed, after 210 minutes of treatment, 59.11%, 66.46%, and 57.25% degradation rates were recorded at pH 3, 6, and 10, respectively (**Figure IV.5)**.

These results indicate a more favourable pollutant degradation in neutral environments. The generation of hydroxyl radicals can explain this in solution from hydrogen peroxide produced by the plasma in humid air, which is stable in acidic to neutral environments. In contrast, in basic conditions, hydrogen peroxide is rapidly decomposed.

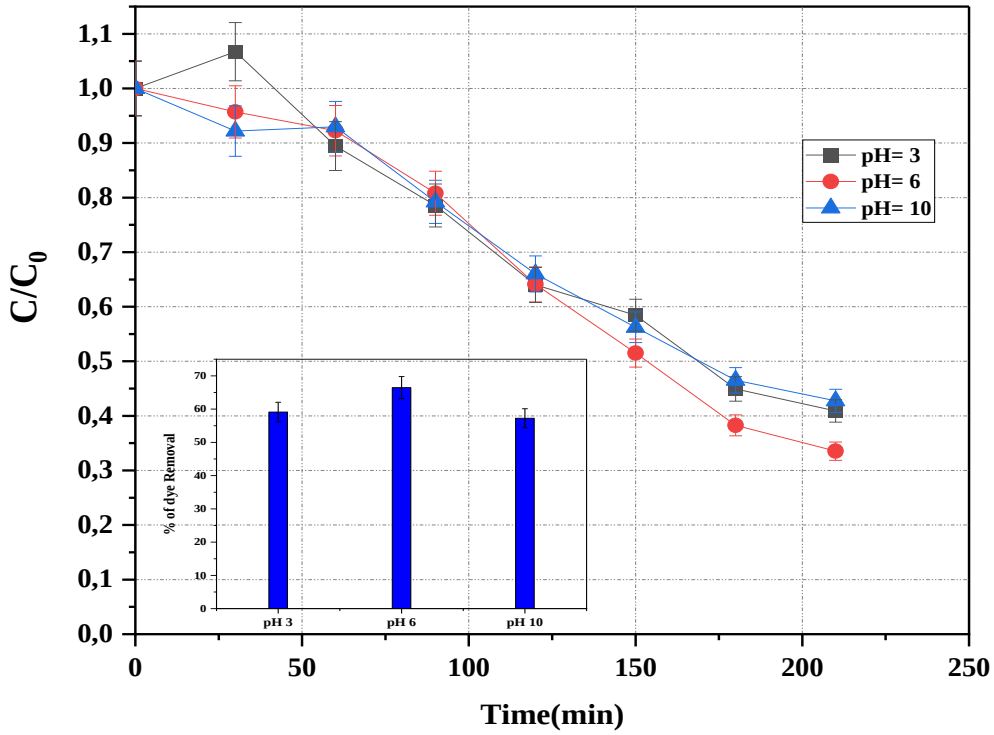

Figure IV.5. Influence of the initial pH on the efficiency of OG degradation (10 mg/L) by non-thermal plasma**.** Exposure times to Glidarc-type plasma: Cycle 1: 0-10 min, Cycle 2: 30-40 min, Cycle 3: 80-90 min, Cycle 4:130-140 min.

V.1.3. Effect of adding H_2O_2

To investigate the impact of hydrogen peroxide (H_2O_2) addition on the degradation of organic pollutants (OG) at 10 mg/L by NTP of the Glydarc type at free pH, several experimental series were conducted by varying the volume of the oxidant (H_2O_2) relative to the volume of the treated solution. The obtained results are presented in **Figure IV.6.**

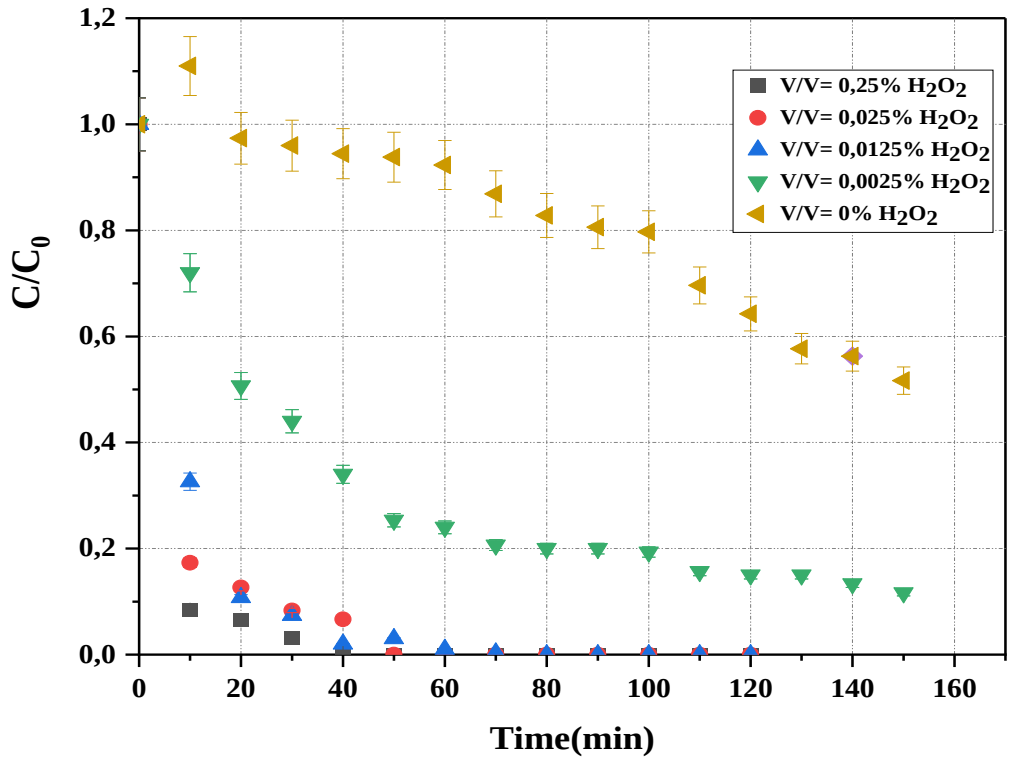

Figure IV.6. Influence of the H_2O_2 on the efficiency of OG degradation (10 mg/L) by non-thermal plasma. Exposure times to Glidarc-type plasma: Cycle 1: 0-10 min, Cycle 2: 30-40 min, Cycle 3: 80-90 min, Cycle 4: 130-140 min.

The experimental data (**Figure IV.6**) show that a complete (100%) degradation of the OG was achieved after 40, 50, and 80 minutes with the respective addition of 0.25%, 0.025%, and 0.0125% of H_2O_2 When 0.0025% of H_2O_2 was added, the degradation rate reached 88.33% after 150 minutes of treatment. In comparison, in the Glydarc system without adding an oxidant (H_2O_2), the degradation rate only reached 48.48% after 150 minutes of treatment.

Furthermore, enhancing process efficiency relies on the initial volume of H_2O_2. This phenomenon can be explained by the fact that H_2O_2 acts as an oxidising agent, facilitating the

generation of hydroxyl radicals ($HO^{\bullet}$) and other reactive species, which play a vital role in the degradation of contaminants. An increased production of these reactive species is therefore correlated with a higher rate of pollutant elimination [25,26].

V.1.4. Effect of periodic acid concentration

In an aqueous medium, periodic acid (H_5IO_6) decomposes into periodate ions (IO_4^-) according to the following reaction [27]:

$$H_5IO_6 \leftrightarrow IO_4^- + H^+ + 2H_2O \qquad \text{(IV.12)}$$

Periodate is a strong oxidant with a redox potential of 1.60 V; however, its ability to independently oxidise and degrade organic pollutants is limited [28]. To overcome this limitation, various activation methods have been proposed, including the use of light, alkali, H_2O_2, ultrasound, and nanocatalysts. These methods facilitate the generation of active species such as $HO^{\bullet}$, $^1O_2$, $IO_3^{\bullet}$, and $O_2^{\bullet -}$, further contributing to the degradation of undesirable pollutants in water.

For instance, **Bendjama et al.** employed a UV/periodate process to degrade emerging organic pollutants. The periodate-assisted UV treatment resulted in a 13,16 fold increase in the degradation efficiency of chlorazol black compared to UV alone [29]. Similarly, **Chadi et al.** demonstrated that periodate can be successfully activated by H_2O_2 to form $HO^{\bullet}$ and periodate species [30]. Furthermore the physical and chemical effects, such as light and H_2O_2, produced by a non-thermal plasma (NTP) system (as cited in Chapter I), can jointly activate periodate, enhancing the energy efficiency of the NTP system and significantly improving the generation of free radicals ($HO^{\bullet}$, $O_2^{\bullet -}$, $^1O_2$, etc.)According to the following mechanism [31–36] :

$$IO_4^- + H_2O_2 \longrightarrow IO_3^{\bullet} + O_2^{\bullet -} + H_2O \qquad \text{(IV.13)}$$

$$IO_4^- \xrightarrow{h\upsilon} IO_3^{\bullet} + O^{\bullet -} \qquad \text{(IV.14)}$$

$$H_2O_2 + O_2^{\bullet -} \longrightarrow HO^{\bullet} + OH^- + {}^1O_2 \qquad \text{(IV.15)}$$

$$IO_4^- + O_2^{\bullet -} + H_2O \longrightarrow {}^1O_2 + H_2O + 2\,OH^- \qquad \text{(IV.16)}$$

$$O_2^{\bullet -} + HO^{\bullet} \longrightarrow {}^1O_2 + OH^- \qquad \text{(IV.17)}$$

$$^1O_2 \longrightarrow {}^3O_2 + h\upsilon\ (\lambda = 643\ nm) \quad \text{(IV.18)}$$

$$^1O_2 \longrightarrow {}^1O_2^* + h\upsilon\ (\lambda = 478\ nm) \quad \text{(IV.19)}$$

$$O^{\bullet -} + H^+ \leftrightarrow HO^\bullet \quad \text{(IV.20)}$$

$$HO^\bullet + IO_4^- \longrightarrow IO_4^\bullet + OH^- \quad \text{k= 4.8 × } 10^8 \text{ M}^{-1}\text{ s}^{-1} \quad \text{(IV.21)}$$

$$IO_4^- + IO_3^\bullet \longrightarrow IO_4^\bullet + IO_3^- \quad \text{k= 2-7 × } 10^8 \text{ M}^{-1}\text{ s}^{-1} \quad \text{(IV.22)}$$

$$2\ IO_3^\bullet \leftrightarrow I_2O_6 \quad \text{k= 7.5 × } 10^8 \text{ M}^{-1}\text{ s}^{-1} \quad \text{(IV.23)}$$

$$2\ IO_4^\bullet \leftrightarrow I_2O_8 \quad \text{(IV.24)}$$

$$2\ HO^\bullet \longrightarrow H_2O_2 \quad \text{k= 5.5 × } 10^9 \text{ M}^{-1}\text{ s}^{-1} \quad \text{(IV.25)}$$

$$I_2O_8 + H_2O \longrightarrow IO_4^- + IO_3^- + 2H^+ + O_2 \quad \text{k= 1.5 × } 10^8 \text{ M}^{-1}\text{ s}^{-1} \quad \text{(IV.26)}$$

$$I_2O_6 + H_2O \longrightarrow IO_4^- + IO_3^- + 2H^+ \quad \text{k= 4.5 × } 10^8 \text{ M}^{-1}\text{ s}^{-1} \quad \text{(IV.27)}$$

Globally, from equations 1–14, it appears that the plasma/periodate reaction system (H_2O_2/UV/ periodate) could serve as a potential source of multiple radicals. These radicals can be classified into two categories:

- Reactive oxygen species (ROS), including $HO^\bullet$, $O_2^{\bullet -}$, and $^1O_2$.
- Reactive iodinated species (RIS), such as $IO_3^\bullet$ and $IO_4^\bullet$.

These species can significantly enhance the degradation of organic substrates (OG) through the plasma glydarc process.

In this context, the degradation of OG (10 mg/L) by periodate ions activated by NTP was monitored at free pH. The concentration of H_5IO_6 used was 50 and 100 mg/L; the results are presented in **Figures IV.7** and **IV.8**.

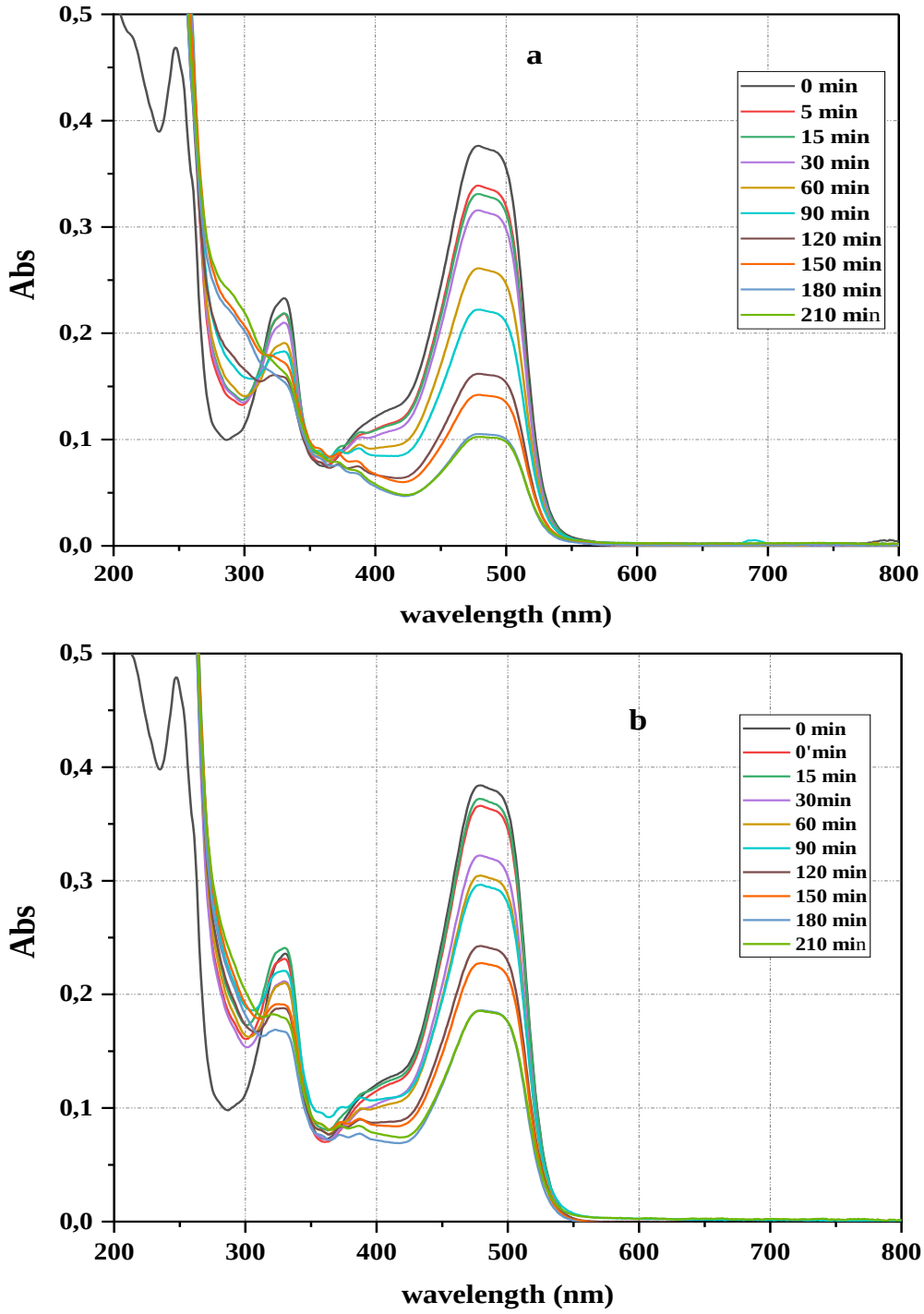

Figure IV.7. UV-Vis spectrum of the effect of periodic acid concentration on OG degradation as a function of treatment time**.** Exposure times to Glidarc-type plasma: Cycle 1: 0-10 min, Cycle 2: 30-40 min, Cycle 3: 80-90 min, Cycle 4:130-140 min. **[**OG]$_0$= 10 mg/L, pH$_0$= 6, **a**: [H_5IO_6]= 50 mg/L ,**b:** [H_5IO_6]= 100 mg/L.

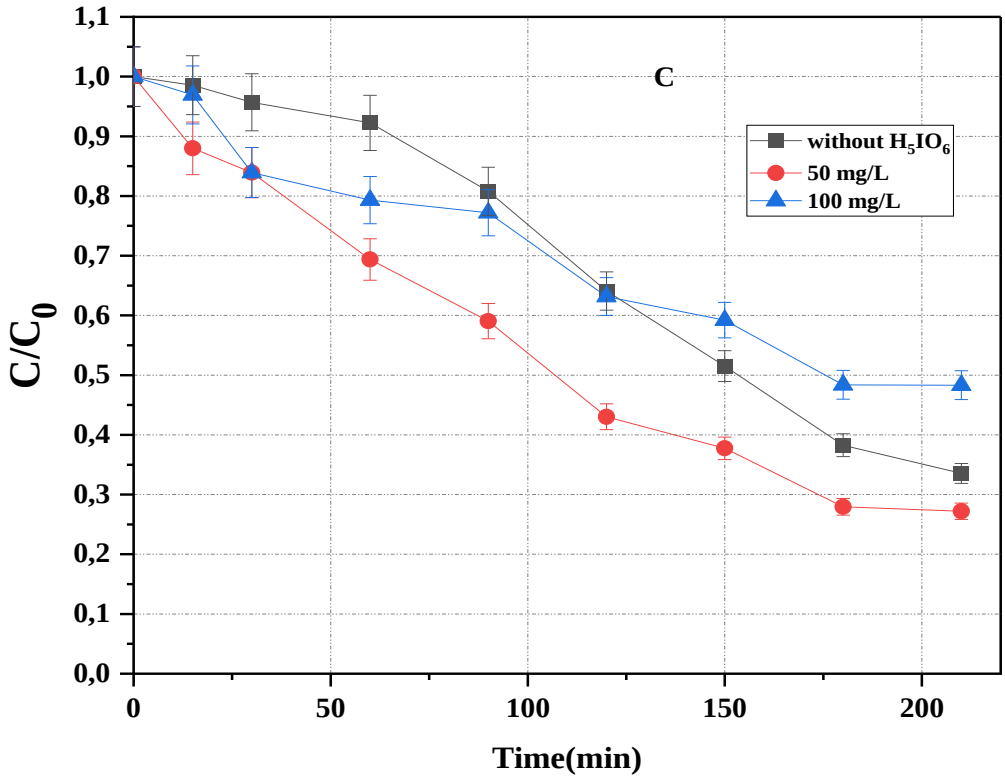

Figure IV.8. Influence of periodic acid on the efficiency of OG degradation (10 mg/L) by non-thermal plasma process. Exposure times to Glidarc-type plasma: Cycle 1: 0-10 min, Cycle 2: 30-40 min, Cycle 3: 80-90 min, Cycle 4: 130-140 min.

The obtained results indicate an enhancement in the degradation of OG in the presence of 50 mg/L of periodic acid, leading to an improvement in the removal efficiency by 6.33% compared to the degradation of the substrate in the absence of H_5IO_6. This behaviour, which shows similarities to the Fenton and electro-Fenton processes [37,38], suggests that the reaction between H_2O_2 and periodate to generate free radicals is extremely rapid, possibly even instantaneous, as a degradation of 72.79% occurred within the 210 minutes of applying 50 mg/L of H_5IO_6. In contrast, at a higher concentration of periodic acid (100 mg/L), inhibition of the process was observed, with a 14.79% reduction in the elimination rate compared to the absence of periodic acid and a 21.12% reduction compared to the presence of 50 mg/L of H_5IO_6.

These results can be attributed to the concentrations of periodic acid in the solution. At moderate concentrations, a sufficient production of free radicals appears to enhance the treatment via non-thermal plasma. However, at very high concentrations, periodate acts as a scavenger for free radicals, reducing the chemical activity of the system and thus decreasing

the effectiveness of the dye removal [39]. Specifically, the IO_4^- ion can trap hydroxyl radicals according to the following **Equations (IV.21)** and **(IV.22):**

$$O^{\bullet} + IO_4^- \longrightarrow IO_4^{\bullet} + OH^- \qquad k= 4.8 \times 10^8\ M^{-1}\ s^{-1} \qquad (IV.21)$$

$$IO_4^- + IO_3^{\bullet} \longrightarrow IO_4^{\bullet} + IO_3^- \qquad k= 2\text{-}7 \times 10^8\ M^{-1}\ s^{-1} \qquad (IV.22)$$

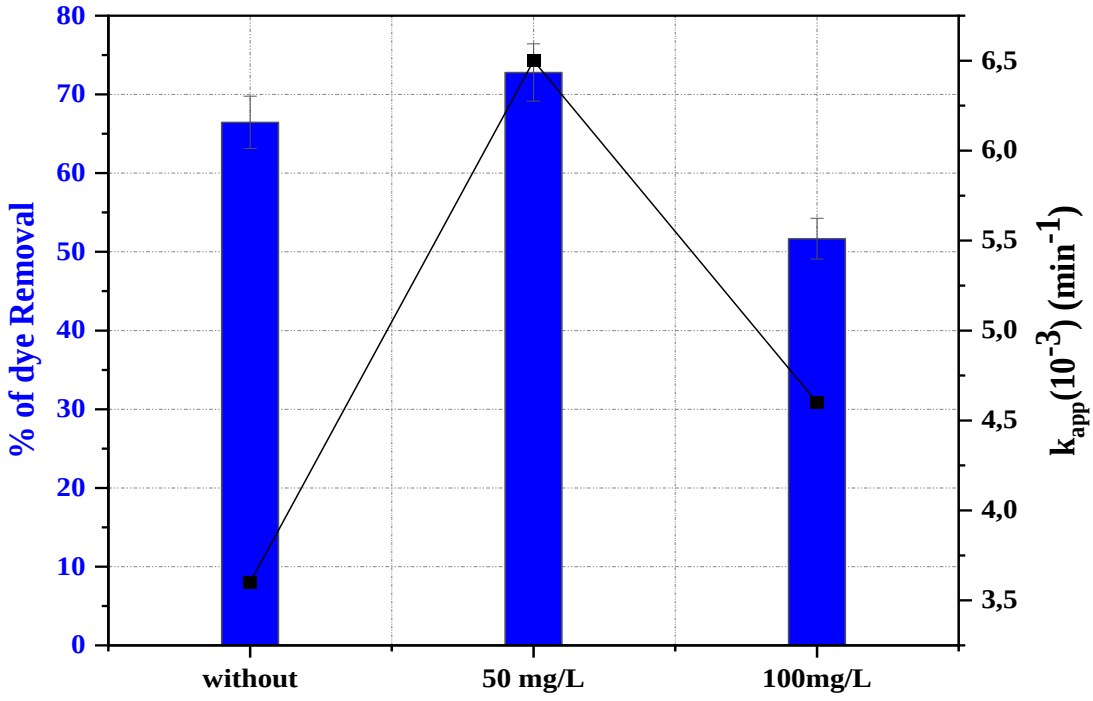

Figure IV.9. Influence of periodic acid on OG removal rate and the variations in pseudo-first-order rate constants by non-thermal plasma process. Exposure times to Glidarc-type plasma: Cycle 1: 0-10 min, Cycle 2: 30-40 min, Cycle 3: 80-90 min, Cycle 4: 130-140 min, $[OG]_0$= 10 mg/L , pH_0=6

Kinetic studies determined the apparent rate constants (kapp) for the studied process (NTP Glydarc / IO_4^-) from the plot of the curve ln $\frac{C_0}{C}$ as a function of time, following the pseudo-first-order equation. The results show that the degradation kinetics of OG changed, with the respective apparent rate constants being 3.6 × $10^{-3}\ min^{-1}$, 4.6 × $10^{-3}\ min^{-1}$, and 6.5 × $10^{-3}\ min^{-1}$ in the presence of 0 g/L, 100 mg/L, and 50 mg/L of periodic acid (**Figure IV.9)**.

V.1.5. Effect of Fe^{3+} concentration

To evaluate the influence of the initial Fe(III) concentration on the efficiency of Orange G degradation via gliding arc discharge, a 10 mg/L OG solution was subjected to four cycles of gliding arc discharge (GAD) in humid air at different time intervals, with varying concentrations of ferric ions (Fe^{3+}), while maintaining an initial solution pH adjusted to 3. The OG concentration was monitored using UV-visible spectrophotometry to assess the degradation efficiency. The results obtained are presented in **Figure IV.10.**

The Glidarc/Fe^{3+} system exhibits characteristics similar to those of the UV/H_2O_2/Fe^{3+} system. As mentioned in the literature review, the plasma-type Gliding arc discharge in humid air leads to hydrogen peroxide (H_2O_2) formation, increasing its concentration during the first few minutes of operation. Various physical phenomena, including UV light emission, accompany this accumulation of H_2O_2. Consequently, adding Fe^{3+}into this system initiates a photo-Fenton-like mechanism.

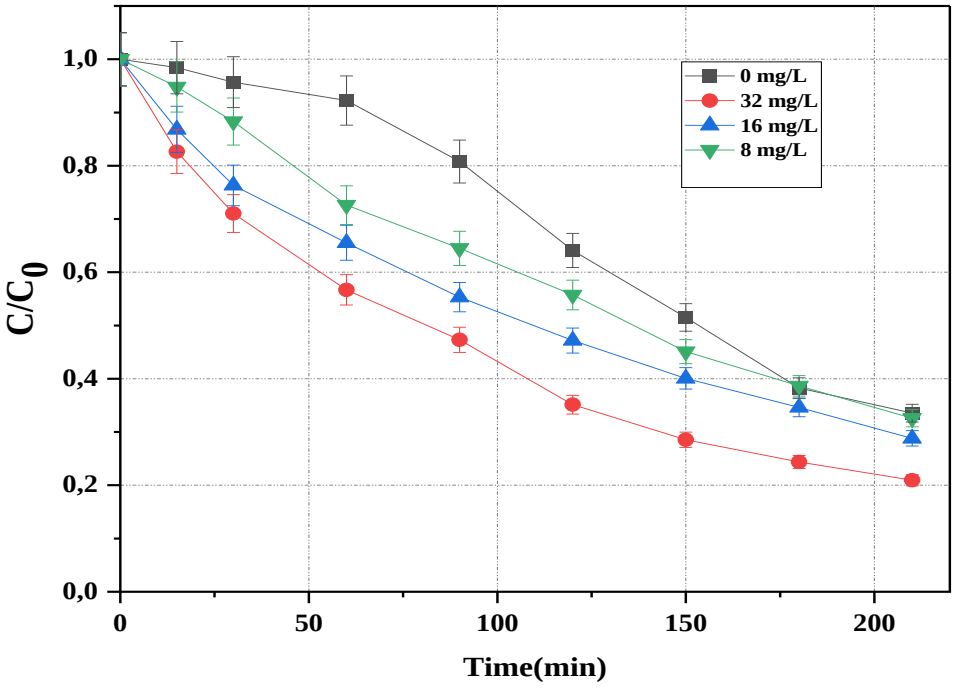

Figure IV.10. Effect of Fe^{3+}concentration on the efficiency of OG degradation**.** Exposure times to Glidarc-type plasma: Cycle 1: 0-10 min, Cycle 2: 30-40 min, Cycle 3: 80-90 min, Cycle 4:130-140 min. **[**OG]$_0$= 10 mg/L , pH$_0$=3, $[Fe_2O_3]$= 0 mg/L-32 mg/L .

As shown by the data in **Figure IV.10**, the presence of Fe^{3+} has enhanced the degradation efficiency of the OG. Specifically, Fe^{3+}concentrations of 8, 16, and 32 mg/L resulted in degradation rates of 67.43%, 71.19%, and 79.06%, respectively. In contrast, in the absence of Fe^{3+}, a degradation rate of 66.46% was observed after a treatment time of 210 minutes under exposure to the Glidarc discharge, which consisted of four cycles of 10 minutes each.

Moreover, the kinetic results of the combination of Glydarc/Fe^{3+} at pH 3 demonstrated an acceleration in the oxidation rate of OG, with k_{app} varying from 3×6 10^{-3} min^{-1}, in the absence of $Fe^{3+}$to 8.8× 10^{-3} min^{-1}, in the presence of 32 mg/L of Fe^{3+}(**Figure IV.11).**

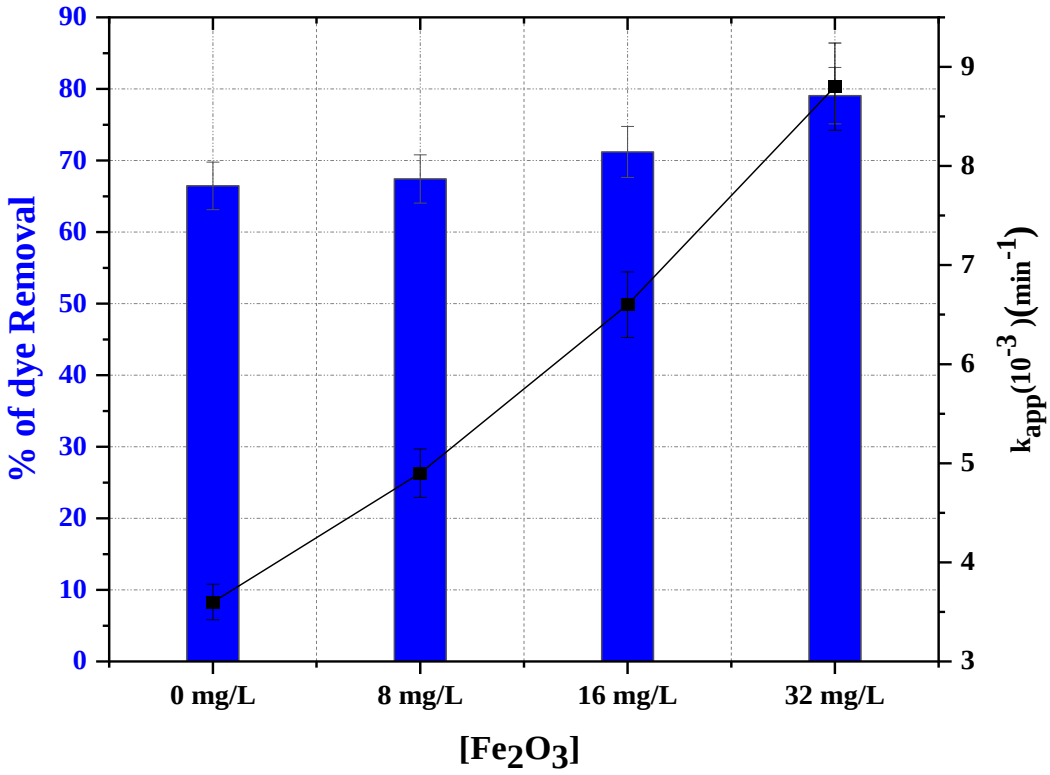

Figure IV.11. Effect of Fe^{3+}concentration on OG removal rate and the variations in pseudo-first-order rate constants by non-thermal plasma process. Exposure times to Glidarc-type plasma: Cycle 1: 0-10 min, Cycle 2: 30-40 min, Cycle 3: 80-90 min, Cycle 4: 130-140 min, $[OG]_0$= 10 mg/L , pH_0=3.

The improvement in degradation rates can be attributed to the presence of Fe^{3+} , which initiates the Fenton-like reaction to generate hydroxyl radicals ($HO^{\bullet}$), regarded as the most

reactive species, through the hydrogen peroxide (H_2O_2) produced during the discharge, according to the reaction mechanism outlined below **(Equations(IV.28)-(IV.33)** [40,41]. Although other radicals, such as $HO_2^{\bullet}$, are also formed, their oxidation potential is lower than that of $HO^{\bullet}$.

$$Fe^{3+} + H_2O_2 \longrightarrow Fe^{2+} + HO_2^{\bullet} + H^+ \quad \text{(IV.28)}$$

$$Fe^{3+} + HO_2^{\bullet} \longrightarrow Fe^{2+} + O_2 + H^+ \quad \text{(IV.29)}$$

$$H_2O_2 + Fe^{2+} \longrightarrow Fe^{3+} + HO^{\bullet} + OH^- \quad \text{(IV.30)}$$

$$HO^{\bullet} + H_2O_2 \longrightarrow H_2O + HO_2^{\bullet} \quad \text{(IV.31)}$$

$$HO^{\bullet} + Fe^{2+} \longrightarrow Fe^{3+} + OH^- \quad \text{(IV.32)}$$

$$HO^{\bullet} + RH \longrightarrow R^{\bullet} + H_2O \quad \text{(IV.33)}$$

Abdelmalek et al. reported similar results in degrading a bisphenol solution using the Glidarc/Fe^{2+} system [42]. However, due to the limited generation of H_2O_2 within the glidarc plasma, we opted to explore the effects of incorporating H_2O_2 into the reaction medium.

V.1.6. Effect of simultaneous addition of H_2O_2 and Fe^{3+}

To evaluate the effect of the simultaneous addition of the two reactants (H_2O_2 and Fe^{3+}) to the Glidarc reactor, we fixed the volume of hydrogen peroxide and varied the concentrations of Fe^{3+} to 8, 16, and 32 mg/L, respectively, while monitoring pH at 3. The results obtained are presented in **Figures IV.12 and IV.13**.

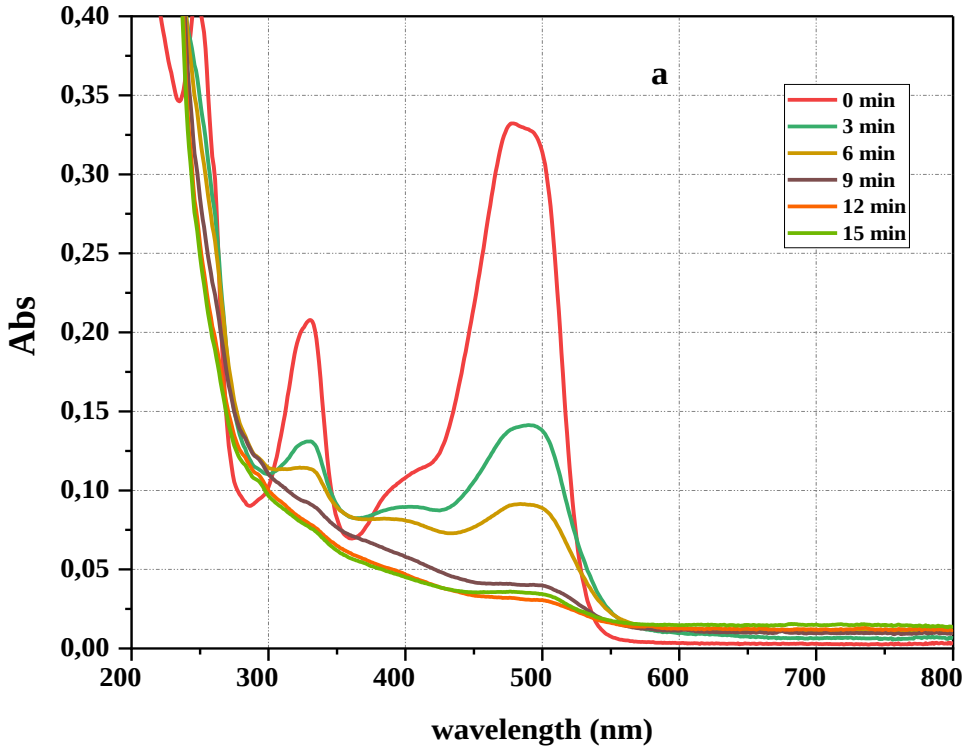
a
0 min
3 min
6 min
9 min
12 min
15 min
Abs
0,40
0,35
0,30
0,25
0,20
0,15
0,10
0,05
0,00
200
300
400
500
600
700
800
wavelength (nm)

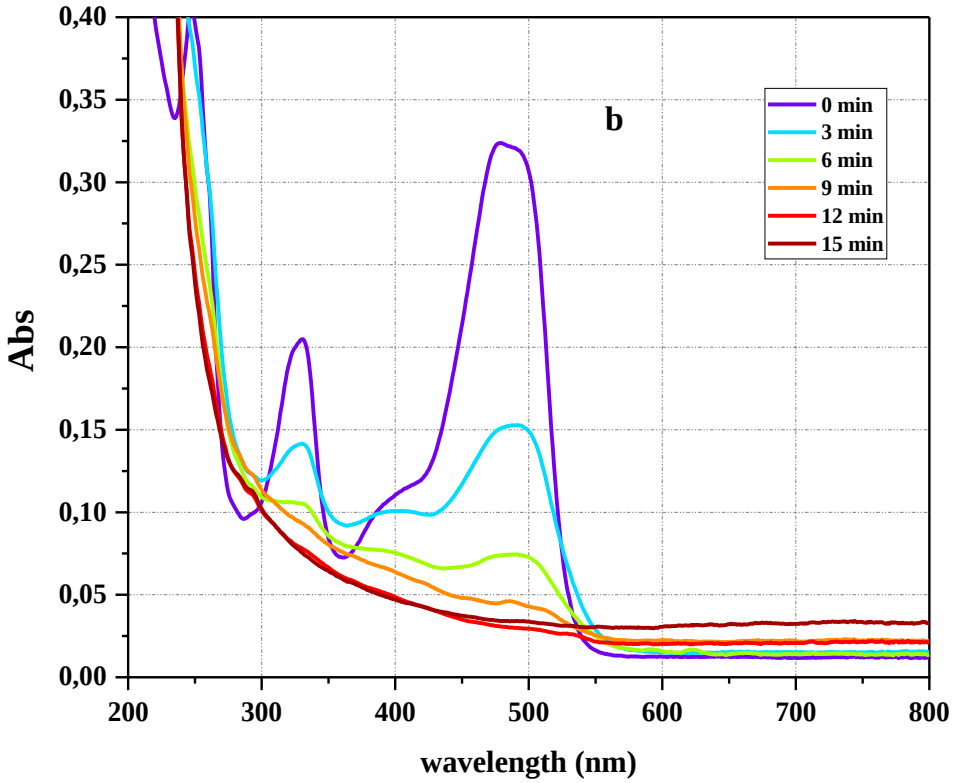
b
0 min
3 min
6 min
9 min
12 min
15 min
Abs
0,40
0,35
0,30
0,25
0,20
0,15
0,10
0,05
0,00
200
300
400
500
600
700
800
wavelength (nm)

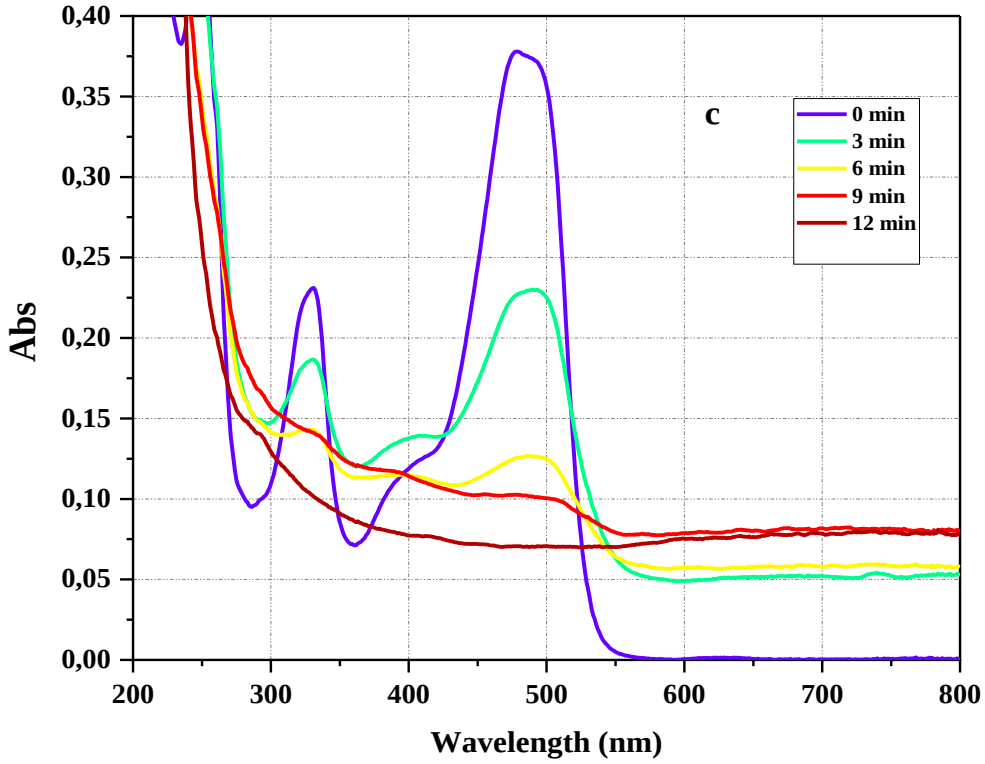

Figure IV.12. UV-Vis spectrum of simultaneous addition of H_2O_2 and Fe^{3+}on OG degradation as a function of treatment time**.** Exposure times to Glidarc-type plasma: 0-10 min, $[OG]_0$= 10 mg/L , pH_0=3, $[H_2O_2]$= 0.025% V/V=3.2 mM , **a**: $[Fe_2O_3] = 8\ mg/L$, **b**: $[Fe_2O_3] = 16 mg/L$, **c**: $[Fe_2O_3] = 32\ mg/L$.

Figure IV.12 (a,b,c) shows that the simultaneous addition of both oxidants, H_2O_2 and Fe^{3+}, accelerates the degradation kinetics of the OG by Glidarc plasma. An increase in the dye degradation efficiency is observed across the entire range of Fe^{3+} concentrations tested (compared to the results obtained in the previous section, **Figure IV.9**).

High degradation rates of 90.48%, 90.42%, and 81.3% after 12 minutes of treatment, with only 10 minutes of plasma exposure, were recorded for Fe^{3+} concentrations of 16 mg/L, 8 mg/L, and 32 mg/L, respectively (**Figure IV.13**). This improvement can be explained by the intensive and efficient production of hydroxyl radicals in the studied reactor, demonstrating the effectiveness of combining electrical discharge processes with Fenton processes in the degradation of organic pollutants [43,44].

However, these results also show that at high Fe^{3+} concentrations, the degradation efficiency decreases. This is due to the scavenging effect of excess Fe^{3+} on the hydroxyl radicals, as illustrated by **Equation IV.34**.

$$Fe^{2+} + HO^{\bullet} \longrightarrow Fe^{3+} + OH^{-} \qquad \text{(IV.34)}$$

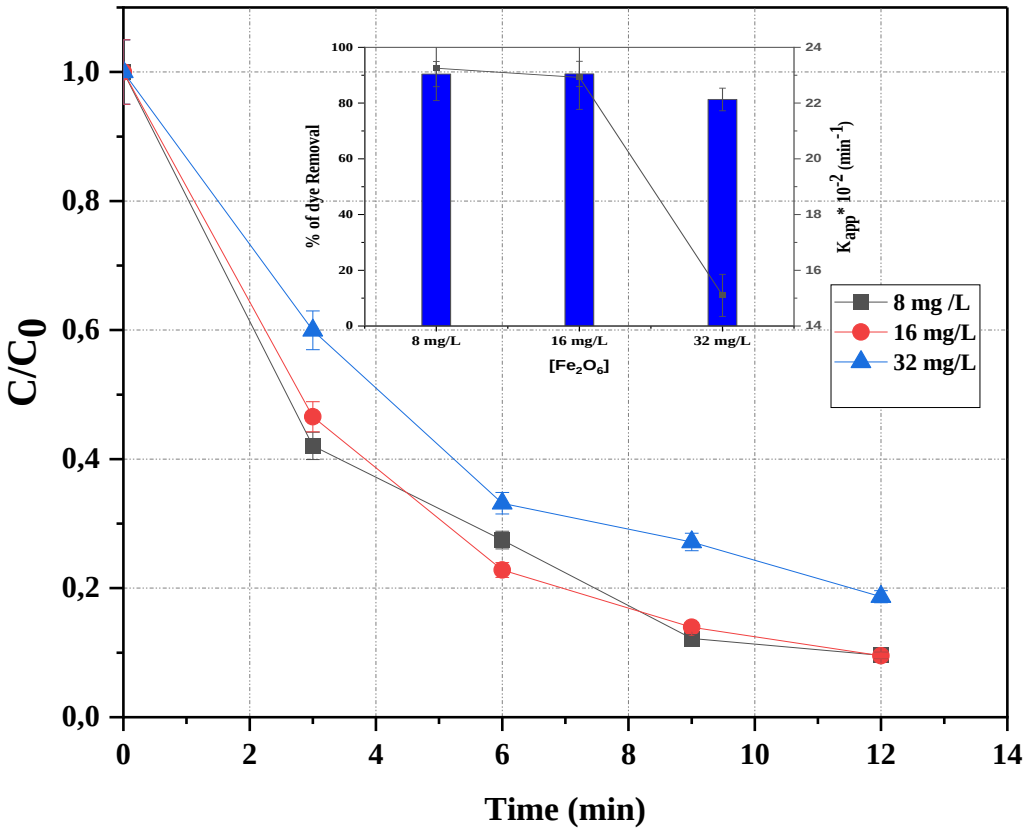

Figures IV.13. Effect of simultaneous addition of H_2O_2 and Fe^{3+} on the efficiency of OG degradation. Exposure times to Glidarc-type plasma: 0-10 min, $[OG]_0$= 10 mg/L , pH_0=3, $[Fe_2O_3]$= 8 mg/L-32 mg/L, $[H_2O_2]$= 0.025% V/V=3.2mM

V.1.7. Effect of potassium persulfate

As part of evaluating the performance of the combination of non-thermal Glidarc plasma with a sulfate radical-based advanced oxidation process for the removal of Orange G from the solution, potassium persulfate was added to the Glidarc reactor. This system treated concentrations of 10 mg/L of OG under free pH conditions. The experimental results are presented in the following figures:

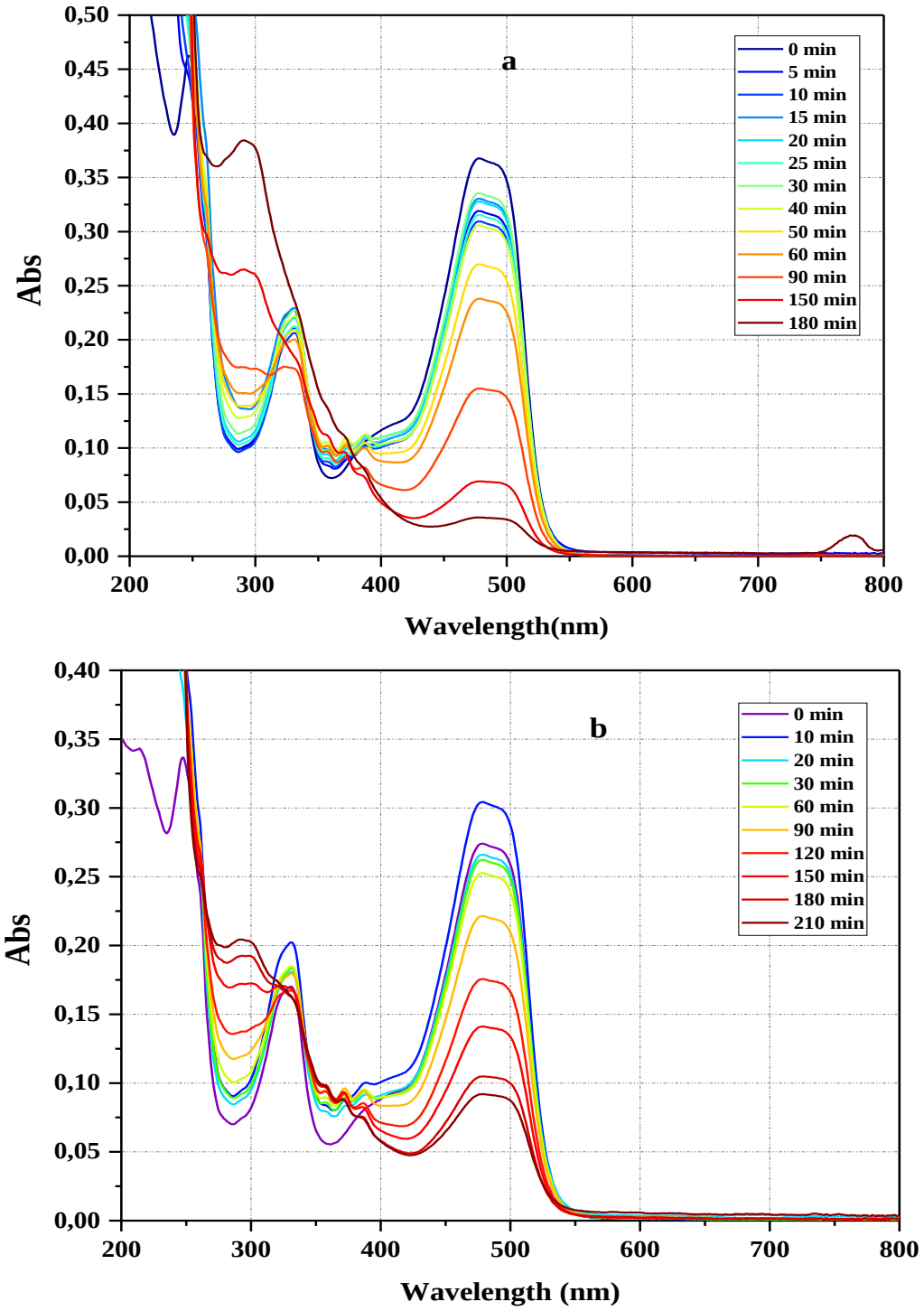

Figure IV.14. UV-Vis spectrum of the presence/ absence of PPS on OG degradation as a function of treatment time**.** Exposure times to Glidarc-type plasma: Cycle 1: 0-10 min, Cycle 2: 30-40 min, Cycle 3: 80-90 min, Cycle 4:130-140 min. **[**$OG]_0$= 10 mg/L , pH_0=6, **a**: [PPS]= 50 mg/L ,**b:** without PPS.

The results obtained showed that the addition of potassium persulfate significantly increased the degradation efficiency of OG. The pollutant removal rate was improved by 28.54% in the presence of 50 mg/L of PPS compared to its absence, as observed in **Figure IV.15**. This enhanced degradation of OG in the plasma system, in the presence of sulfate ions ($S_2O_8{}^{2-}$) in the solution, can be attributed to the activation of persulfate by the discharge plasma. This leads to the formation of more powerful reactive species, such as the sulfate radical ($SO_4^{\bullet-}$).

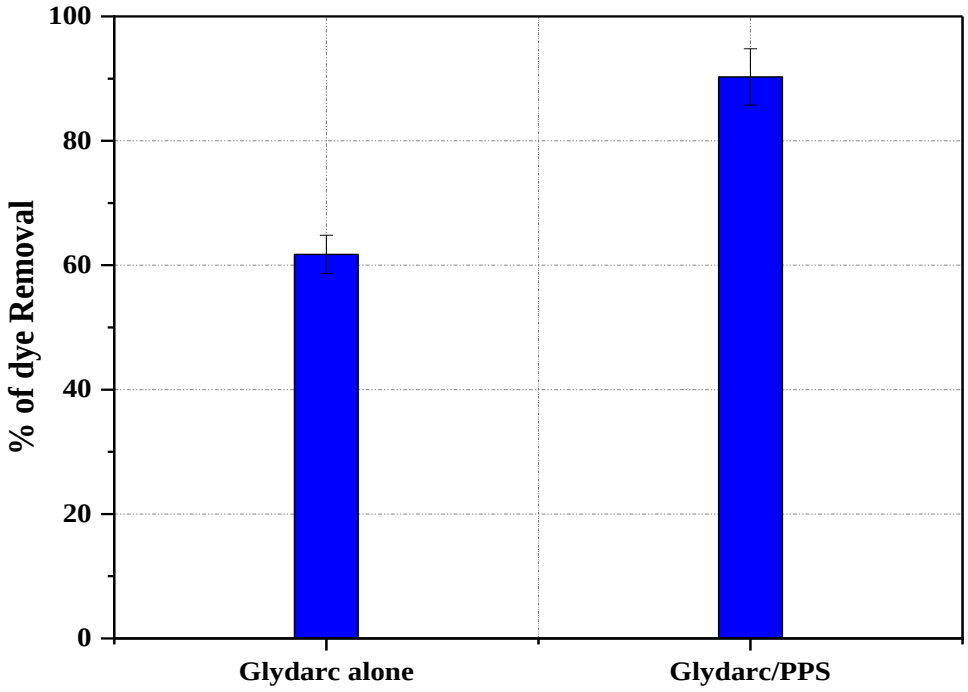

Figure IV.15. The Effect of the presence/ absence of PPS on OG degradation with a gliding arc discharge process under a 180-minute treatment time. Exposure times to Glidarc-type plasma: Cycle 1: 0-10 min, Cycle 2: 30-40 min, Cycle 3: 80-90 min, Cycle 4:130-140 min. **[**OG]$_0$= 10 mg/L , pH$_0$=6, $[PPS]$= 50 mg/L.

As the Glidarc-type plasma generates various physical and chemical effects, including heat, UV irradiation, and the production of reactive species, these effects can activate the persulfate according to the following mechanism [45–47]:

$$S_2O_8^{2-} \longrightarrow 2\,SO_4^{\bullet-} or\ SO_4^{\bullet-} + SO_4^{\bullet-} \qquad \text{(IV.35)}$$

$$SO_4^{\bullet -} + H_2O \rightarrow HO^{\bullet} + H^+ + SO_4^{2-} \quad \text{(IV.36)}$$

$$SO_4^{\bullet -} + OH^- \rightarrow SO_4^{2-} + OH^{\bullet} \quad \text{(IV.37)}$$

VI.2. Energy Efficiency of the OG Degradation

The energy yield (g/kWh) was used to assess the energy efficiency of the Glydarc reactor during the degradation process of 10 mg/L OG, using plasma treatment alone at an applied voltage of 10 kV, as well as in the cases of the combination of Glydarc/Fenton and Glydarc/PS activation processes. The energy consumption for OG degradation was calculated using **Equation (IV.38)** [48]. The energy yield results are shown in **Figure IV.16**.

$$Y(g/kWh) = \frac{C_0(g/L) \times V_0(L) \times \%R \times \frac{1}{100}}{P\ (kW) \times t(h)} \quad \text{(IV.38)}$$

Where:

- C_0 = initial concentration of the pollutant in mg/L
- V_0 = volume of the treated solution in L
- $\%R$ = degradation efficiency at time t (%)
- P = power dissipated in the discharge in kW
- t = time in hours.

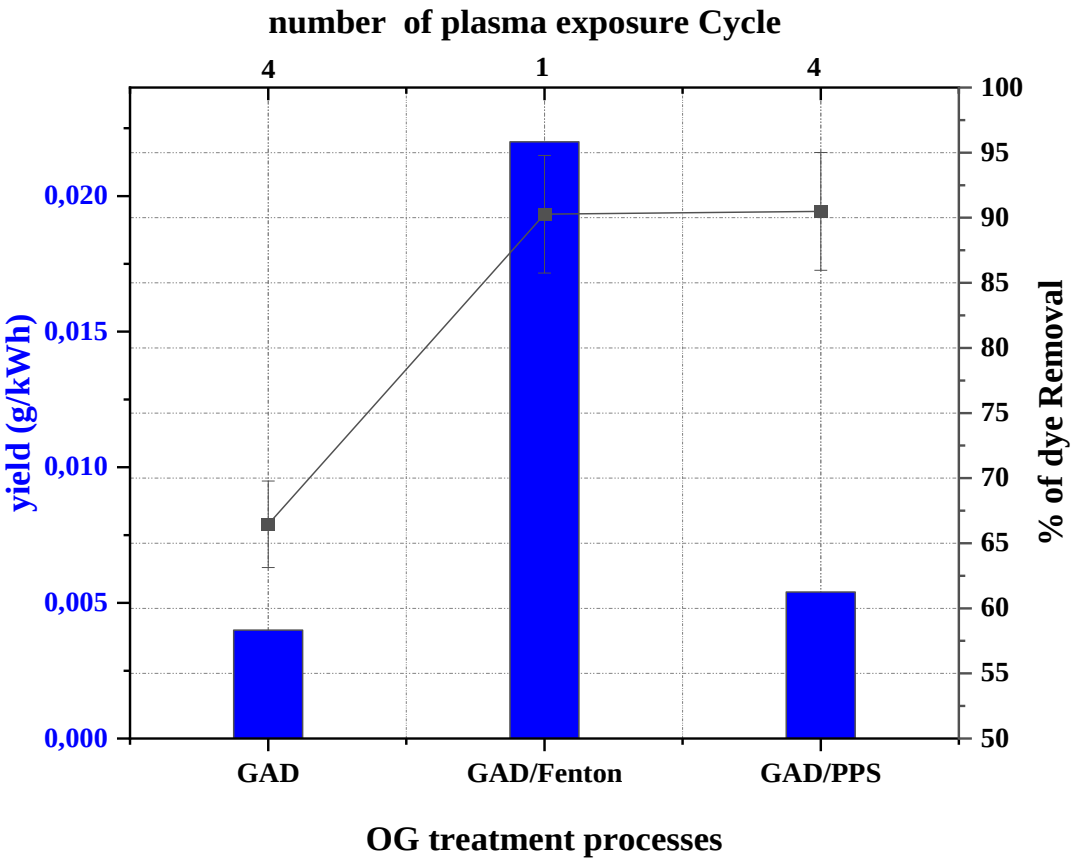

Figure IV.16. Evaluation of Energy Yield during the OG degradation process using the Glidarc reactor. GAD process: **[**OG]$_0$= 10 mg/L, pH$_0$=6, GAD/ Fenton process: [Fe_2O_3]= 16 mg/L, [H_2O_2]= 0.025% V/V,pH$_0$=3, GAD/ PPS process : [PPS]= 50 mg/L, pH$_0$=6

Based on the energy yield calculation, for the degradation of OG at 10 mg/L, the highest energy yield was 0.022 g/kWh during treatment with Gliding arc discharge coupled with the Fenton process, under an exposure time of 10 minutes and an elimination efficiency of 90.48%. However, when the treatment time for OG was increased to 4 exposure cycles, the degradation efficiency of the model substrate decreased to 99.27% and 66.46% in the GAD/PS and GAD alone processes, respectively. Consequently, the energy yield decreased to 0.0054 g/kWh and 0.004 g/kWh, respectively. This shows that the energy yield decreased as degradation efficiency decreased and treatment time increased. This decrease can be attributed to the low collision probability between plasma reactive species and pollutant molecules [49].

Furthermore, the energy yield was proportional to the initial dye concentration, as a higher number of reactant molecules were present in the solution, influenced by the discharge [48].

VII. CONCLUSION

The results presented in this study highlight the following points:

- The analysis of the properties of humid air plasma revealed its acidic and oxidising capabilities.
- The degradation rate of pollutants increases with the decrease in their initial concentration.
- The Glydarc humid air plasma process was effective in a free pH environment.
- The addition of hydrogen peroxide to the Glydarc reactor enhanced degradation, with complete decolourisation achieved at respective volume percentages of 0.25%, 0.025%, and 0.0125% of H_2O_2 after 40, 50, and 80 minutes of treatment.
- The use of periodic acid in the plasma reactor, at a moderate concentration, demonstrated the involvement of other radical entities, beyond the hydroxyl radical, which enhanced the degradation process. However, a high concentration of periodate inhibited the removal of the organic pollutant (OG).
- The presence of Fe^{3+} ions in the Glydarc reactor improved the efficiency of OG degradation across all tested iron concentrations.
- The coupling of the Glydarc system with the Fenton process improved the degradation of OG, achieving degradation rates of 90.48%, 90.42%, and 81.3% for different concentrations of Fe^{3+}, in just 12 minutes of treatment.
- The combination of Glydarc plasma with sulfate radical-based AOP intensified the degradation process of OG by generating sulfate radicals, which are as powerful as hydroxyl radicals.
- The energy yield of OG degradation was calculated at 0.022g/kWh for the GAD/Fenton process, 0.0054g/kWh for the GAD/PPS process, and 0.004g/kWh for the GAD process alone.

The results show that the GAD treatment is ideally suited for dye treatment. This alternative method aligns with green chemistry and sustainable development objectives.

BIBLIOGRAPHICAL REFERENCES

1. Bellakhal, N., Moras, F., Boulay, S, Desanaux, C, Brisset, J. L. The use of gliding arc discharge for pollution abatement of industrial waste waters. Water Waste Environ. Res, 2, 59-68. Water Waste Environ. 2001;2, 59-68.

2. Peyrous R, Pignolet P, Held B. Kinetic simulation of gaseous species created by an electrical discharge in dry or humid oxygen. J Phys Appl Phys. 1989 Nov 14;22(11):1658–67.

3. Samaranayake WJM, Miyahara Y, Namihira T, Katsuki S, Sakugawa T, Hackam R, et al. Pulsed streamer discharge characteristics of ozone production in dry air. IEEE Trans Dielectr Electr Insul. 2000 Apr;7(2):254–60.

4. Lowke JJ, Morrow R. Theoretical analysis of removal of oxides of sulphur and nitrogen in pulsed operation of electrostatic precipitators. IEEE Trans Plasma Sci. 1995 Aug;23(4):661–71.

5. Young Sun Mok, Sung Won Ham, In-Sik Nam. Mathematical analysis of positive pulsed corona discharge process employed for removal of nitrogen oxides. IEEE Trans Plasma Sci. 1998 Oct;26(5):1566–74.

6. Marouf-Khelifa K, Abdelmalek F, Khelifa A, Belhadj M, Addou A, Brisset JL. Reduction of nitrite by sulfamic acid and sodium azide from aqueous solutions treated by gliding arc discharge. Sep Purif Technol. 2006 Jul;50(3):373–9.

7. Du C, Shi T, Sun Y, Zhuang X. Decolorization of Acid Orange 7 solution by gas–liquid gliding arc discharge plasma. J Hazard Mater. 2008 Jun;154(1–3):1192–7.

8. Czernichowski A. Gliding arc: Applications to engineering and environment control. Pure Appl Chem. 1994 Jan 1;66(6):1301–10.

9. Bard, A. J., Parsons, R., Jordan, J. Standard Potentials in Aqueous Solution (Vol. 6). CRC Press. Vol. 6. 1985.

10. Benstaali B, Boubert P, Cheron BG, Addou A, Brisset JL. Density and Rotational Temperature Measurements of the OH° and NO° Radicals Produced by a Gliding Arc in Humid Air. Plasma Chem Plasma Process. 2002;22(4):553–71.

11. Doubla A, Boubabello L, Fotso M, Brisset J. Plasmachemical decolourisation of Bromothymol Blue by gliding electric discharge at atmospheric pressure. Dyes Pigments. 2008;77(1):118–24.

12. Benstaali B, Moussa D, Addou A, Brisset JL. Plasma treatment of aqueous solutes: Some chemical properties of a gliding arc in humid air. Eur Phys J Appl Phys. 1998 Nov;4(2):171–9.

13. Moussa D, Abdelmalek F, Benstaali B, Addou A, Hnatiuc E, Brisset JL. Acidity control of the gliding arc treatments of aqueous solutions: application to pollutant abatement and biodecontamination. Eur Phys J Appl Phys. 2005 Feb;29(2):189–99.

14. Abdelmalek F, Gharbi S, Benstaali B, Addou A, Brisset JL. Plasmachemical degradation of azo dyes by humid air plasma: Yellow Supranol 4 GL, Scarlet Red Nylosan F3 GL and industrial waste. Water Res. 2004 May;38(9):2339–47.

15. Burlica R, Kirkpatrick MJ, Finney WC, Clark RJ, Locke BR. Organic dye removal from aqueous solution by glidarc discharges. J Electrost. 2004 Nov;62(4):309–21.

16. Tsagou-Sobze EB, Moussa D, Doubla A, Hnatiuc E, Brisset JL. Gliding discharge-induced oxidation of a toxic alkaloid. J Hazard Mater. 2008 Mar 21;152(1):446–9.

17. Li J, Sato M, Ohshima T. Degradation of phenol in water using a gas–liquid phase pulsed discharge plasma reactor. Thin Solid Films. 2007 Mar;515(9):4283–8.

18. Wang L, Jiang X, Liu Y. Degradation of bisphenol A and formation of hydrogen peroxide induced by glow discharge plasma in aqueous solutions. J Hazard Mater. 2008 Jun;154(1–3):1106–14.

19. Grymonpré DR, Sharma AK, Finney WC, Locke BR. The role of Fenton's reaction in aqueous phase pulsed streamer corona reactors. Chem Eng J. 2001 Mar;82(1–3):189–207.

20. Liu S, Kang Y. Underwater bubbling plasma assisted with persulfate activation for the synergistic degradation of tetracycline hydrochloride. Environ Res. 2024 Jan;240:117539.

21. Cao J, Wei L, Huang Q, Wang L, Han S. Reducing degradation of azo dye by zero-valent iron in aqueous solution. Chemosphere. 1999 Feb;38(3):565–71.

22. Bandara J, Morrison C, Kiwi J, Pulgarin C, Peringer P. Degradation/decoloration of concentrated solutions of Orange II. Kinetics and quantum yield for sunlight induced reactions via Fenton type reagents. J Photochem Photobiol Chem. 1996 Sep;99(1):57–66.

23. Zhu C, Wang L, Kong L, Yang X, Wang L, Zheng S, et al. Photocatalytic degradation of AZO dyes by supported TiO2 + UV in aqueous solution. Chemosphere. 2000 Aug;41(3):303–9.

24. Wu L, Xie Q, Lv Y, Zhang Z, Wu Z, Liang X, et al. Degradation of methylene blue by dielectric barrier discharge plasma coupled with activated carbon supported on polyurethane foam. RSC Adv. 2019;9(45):25967–75.

25. Sanito RC, You SJ, Wang YF. Degradation of contaminants in plasma technology: An overview. J Hazard Mater. 2022 Feb;424:127390.

26. AlHamad B, Al-Bastaki N. Degradation of Reactive Blue 19 using advanced oxidation methods: gliding-arc plasma discharge. Desalination Water Treat. 2016 Nov;57(51):24352–8.

27. Valkai L, Peintler G, Horváth AK. Clarifying the Equilibrium Speciation of Periodate Ions in Aqueous Medium. Inorg Chem. 2017 Sep 18;56(18):11417–25.

28. Lee C, Yoon J. Application of photoactivated periodate to the decolorization of reactive dye: reaction parameters and mechanism. J Photochem Photobiol Chem. 2004 Jul;165(1–3):35–41.

29. Bendjama H, Merouani S, Hamdaoui O, Bouhelassa M. Efficient degradation method of emerging organic pollutants in marine environment using UV/periodate process: Case of chlorazol black. Mar Pollut Bull. 2018 Jan;126:557–64.

30. Chadi NE, Merouani S, Hamdaoui O, Bouhelassa M, Ashokkumar M. H_2O_2 /periodate (IO_4^-): a novel advanced oxidation technology for the degradation of refractory organic pollutants. Environ Sci Water Res Technol. 2019;5(6):1113–23.

31. Wagner I, Strehlow H. Flash Photolysis in Aqueous Periodate-Solutions. Berichte Bunsenges Für Phys Chem. 1982 Apr;86(4):297–301.

32. Chia LH, Tang X, Weavers LK. Kinetics and Mechanism of Photoactivated Periodate Reaction with 4-Chlorophenol in Acidic Solution. Environ Sci Technol. 2004 Dec 1;38(24):6875–80.

33. Tang X, Weavers LK. Decomposition of hydrolysates of chemical warfare agents using photoactivated periodate. J Photochem Photobiol Chem. 2007 Apr;187(2–3):311–8.

34. Shah SNA, Li H, Lin JM. Enhancement of periodate-hydrogen peroxide chemiluminescence by nitrogen doped carbon dots and its application for the determination of pyrogallol and gallic acid. Talanta. 2016 Jun;153:23–30.

35. Barat F, Gilles L, Hickel B, Lesigne B. Pulsed radiolysis and flash photolysis of iodates in aqueous solution. J Phys Chem. 1972 Feb;76(3):302–7.

36. Barat F, Gilles L, Hickel B, Lesigne B. Transient species in the pulse radiolysis of periodate ion in neutral aqueous solutions. J Chem Soc Chem Commun. 1971;(15):847.

37. Wang S, Wang J. Trimethoprim degradation by Fenton and Fe(II)-activated persulfate processes. Chemosphere. 2018 Jan;191:97–105.

38. Kayan B, Gözmen B, Demirel M, Gizir AM. Degradation of acid red 97 dye in aqueous medium using wet oxidation and electro-Fenton techniques. J Hazard Mater. 2010 May;177(1–3):95–102.

39. Lee C, Yoon J. Application of photoactivated periodate to the decolorization of reactive dye: reaction parameters and mechanism. J Photochem Photobiol Chem. 2004 Jul;165(1–3):35–41.

40. Wang S. A Comparative study of Fenton and Fenton-like reaction kinetics in decolourisation of wastewater. Dyes Pigments. 2008 Jan;76(3):714–20.

41. Walling C. Fenton's reagent revisited. Acc Chem Res. 1975 Apr 1;8(4):125–31.

42. Abdelmalek F, Torres RA, Combet E, Petrier C, Pulgarin C, Addou A. Gliding Arc Discharge (GAD) assisted catalytic degradation of bisphenol A in solution with ferrous ions. Sep Purif Technol. 2008 Oct;63(1):30–7.

43. Tarkwa JB, Acayanka E, Sop BT, Kenyim FB, Nzali S, Laminsi S. Effect of Gliding Arc Plasma-Induced UV Light During the Photo-Fenton Oxidation of 4-Chlorophenol in Aqueous Solution. Plasma Chem Plasma Process. 2021 Jul;41(4):989–1007.

44. Korichi N, Aubry O, Rabat H, Cagnon B, Hong D. Paracetamol Degradation by Catalyst Enhanced Non-Thermal Plasma Process for a Drastic Increase in the Mineralization Rate. Catalysts. 2020 Aug 21;10(9):959.

45. Shang K, Li W, Wang X, Lu N, Jiang N, Li J, et al. Degradation of p-nitrophenol by DBD plasma/Fe2+/persulfate oxidation process. Sep Purif Technol. 2019 Jul;218:106–12.

46. Shang K, Morent R, Wang N, Wang Y, Peng B, Jiang N, et al. Degradation of sulfamethoxazole (SMX) by water falling film DBD Plasma/Persulfate: Reactive species identification and their role in SMX degradation. Chem Eng J. 2022 Mar;431:133916.

47. Guo H, Pan S, Hu Z, Wang Y, Jiang W, Yang Y, et al. Persulfate activated by non-thermal plasma for organic pollutants degradation: A review. Chem Eng J. 2023 Aug;470:144094.

48. Krosuri A, Wu S, Bashir MA, Walquist M. Efficient degradation and mineralization of methylene blue via continuous-flow electrohydraulic plasma discharge. J Water Process Eng. 2021 Apr;40:101926.

49. Manoj Kumar Reddy P, Rama Raju B, Karuppiah J, Linga Reddy E, Subrahmanyam Ch. Degradation and mineralization of methylene blue by dielectric barrier discharge non-thermal plasma reactor. Chem Eng J. 2013 Feb;217:41–7.

GENERAL CONCLUSION

GENERAL CONCLUSION

Advanced oxidation processes (AOPs) have become essential for meeting legislative and regulatory requirements related to environmental protection. Due to the complexity of industrial effluents and the limitations of conventional treatment methods, these processes have proven particularly effective in degrading toxic and non-biodegradable organic pollutants in aqueous environments. In this context, this study aims to investigate the degradation of an azo dye, specifically Orange G (OG), in aqueous media using two advanced oxidation processes: persulfate activation and the electric discharge technique (glydarc plasma).

The first part of the study focuses on the effectiveness of thermal and thermo-metallic activation of persulfate for the treatment of OG, as well as examining the influence of various experimental parameters on the degradation kinetics of the substrate. The experimental results indicate that the degradation of the dye follows first-order kinetics for all the conducted experiments, with the initial degradation rate of the substrate increasing progressively with increasing temperatures (from 40°C to 70°C) and increasing oxidant mass (ranging from 100 to 1000 mg/L). The highest degradation rate was observed under natural pH conditions. Optimal parameters included a natural pH, a potassium persulfate concentration of 300 mg/L, a reaction time of 260 minutes, a temperature of 65°C, and an Orange G concentration of 50 mg/L, resulting in a removal efficiency of 96.9%. However, organic and inorganic substances significantly impacted the removal of Orange G. Additionally, the nature of the water used considerably impacted the degradation process, with the best results obtained in distilled water. The presence of chromium ions (Cr^{6+}) competed with Orange G, inhibiting its degradation. Furthermore, scavenging tests identified sulfate radicals ($SO_4^{\bullet-}$) as the predominant reactive species in the neutral solution. The oxidation kinetics of Orange G were faster in the heat/PS/Fe^{2+} process than in the heat/PS process, with a calculated synergy effect of 68.48% for the heat/PS/$FeSO_4$ process and 88.79% for the heat/PS/Mohr salt process. At the same time, the removal rate of OG was higher in the heat/PS process. Under strongly acidic and strongly basic pH values, the degradation process of the dye by the heat/PS/Fe^{2+} process experienced inhibition. The chemical oxygen demand (COD) reduction was 75.41% after 260 minutes of treatment, and the energy consumption (SEH) was estimated at 1.05×10^{-3} kWh/mg OG.

The second part of this study was dedicated to evaluating the efficiency of the first-generation Glidarc batch reactor in the degradation of an aqueous solution containing the dye Orange G. During this investigation, after optimizing experimental parameters such as the electrode-solution distance and the initial substrate concentration, the acidic and oxidising properties of the Glidarc plasma were confirmed. This confirmation revealed the presence of acidic species such as NO_2^-, NO_3^-, H_3O^+, HNO_3, and HNO_2, as well as particularly reactive and oxidizing species such as $HO^\bullet$, $HO_2^\bullet$, H_2O_2, and $NO^\bullet$. The study also highlighted the effect of different oxidative additives and the catalyst (Fe^{2+}) throughout the treatment process.

Experimental results showed a dye degradation rate of 66.46% after 210 minutes of treatment with Glidarc, with a total exposure time of 40 minutes. The degradation of Orange G (OG) was observed to be more effective in a neutral medium and dependent on the initial dye concentration. The plasma process enabled complete dye degradation, achieving 100% decolorization after 50 minutes of treatment and 20 minutes of discharge exposure in the presence of 3.2 mM hydrogen peroxide. Additionally, adding periodic acid at an optimal concentration enhanced the degradation process. Furthermore, the presence of the Fe^{3+} catalyst facilitated the degradation of OG, with improved results at all tested iron concentrations. The combination of Glidarc plasma with an AOP based on sulfate radicals intensified the degradation of OG. Finally, coupling the plasma process with the Fenton process allowed for efficient pollutant degradation in just 12 minutes of treatment (with 10 minutes of discharge exposure), with an energy yield calculated at 0.022 g/kWh.

The results confirmed the effectiveness of both processes studied and their competitiveness compared to other conventional techniques, particularly advanced oxidation processes (AOPs).

For prospects, we plan to:

- Conduct HPLC-MS analyses of treated samples to identify the intermediate products resulting from pollutant degradation precisely.
- Compare the results of the Glidarc plasma process in a humid air atmosphere with those of other plasma types for treating this pollutant and study the influence of variations in the plasmagenic gas.

APPENDIX

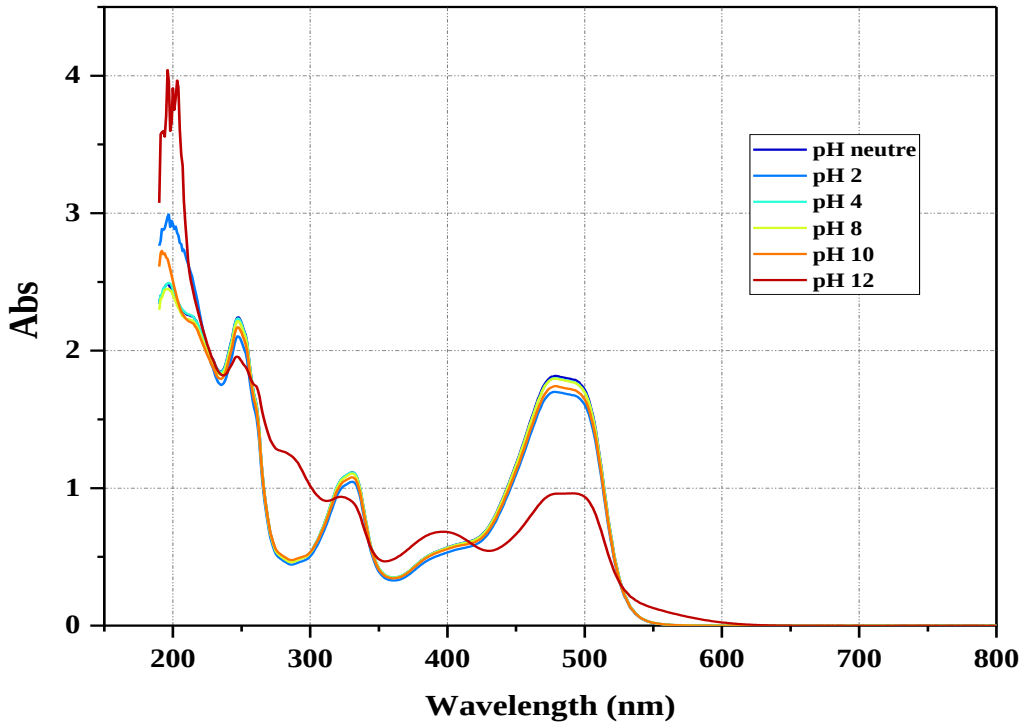

Figure A.1: UV-visible spectrum of OG at different pH levels

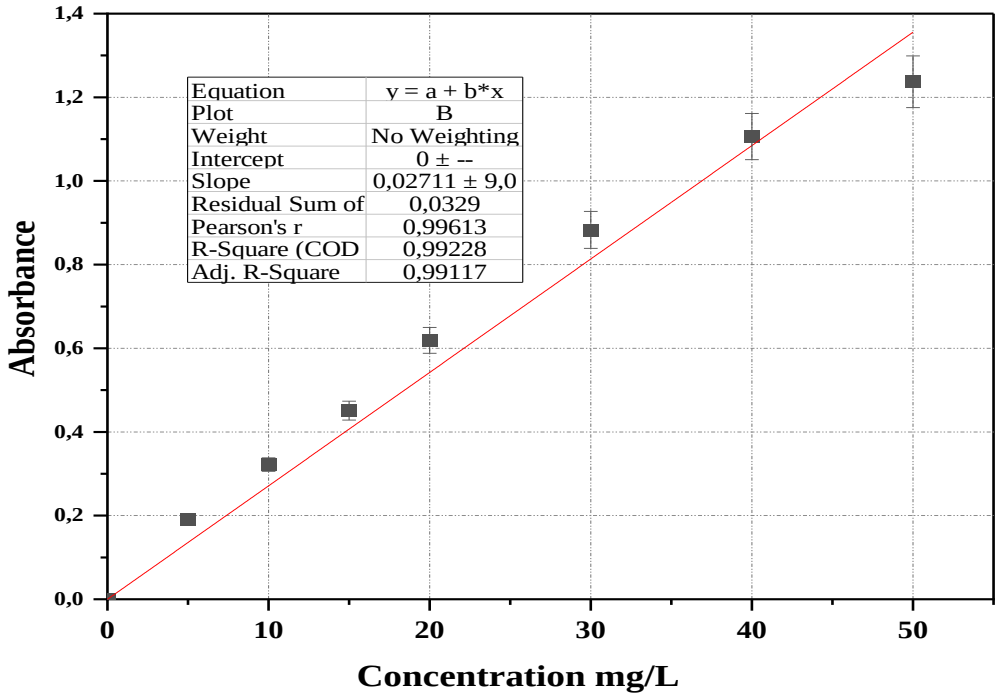

Figure A.2: Calibration Curve of the OG

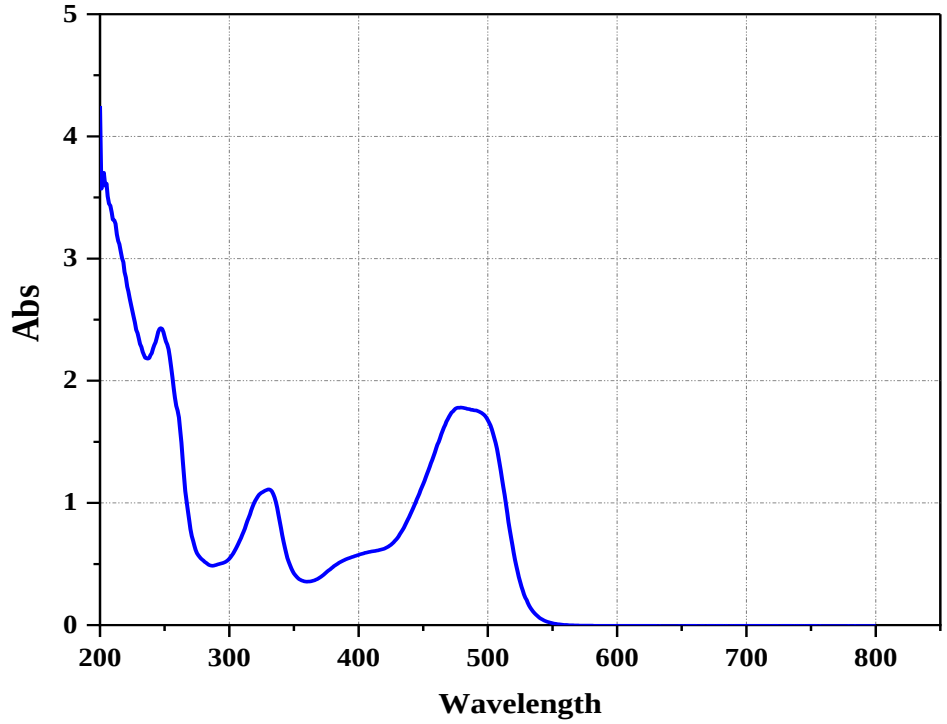

Figure A.3: UV-visible spectrum of H_2O_2

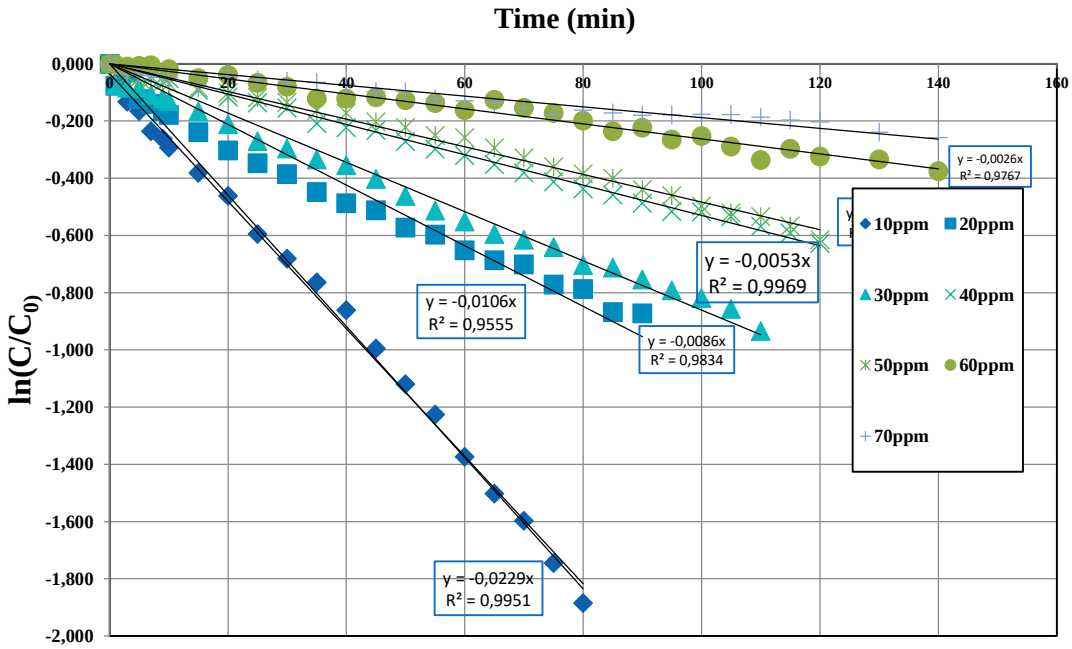

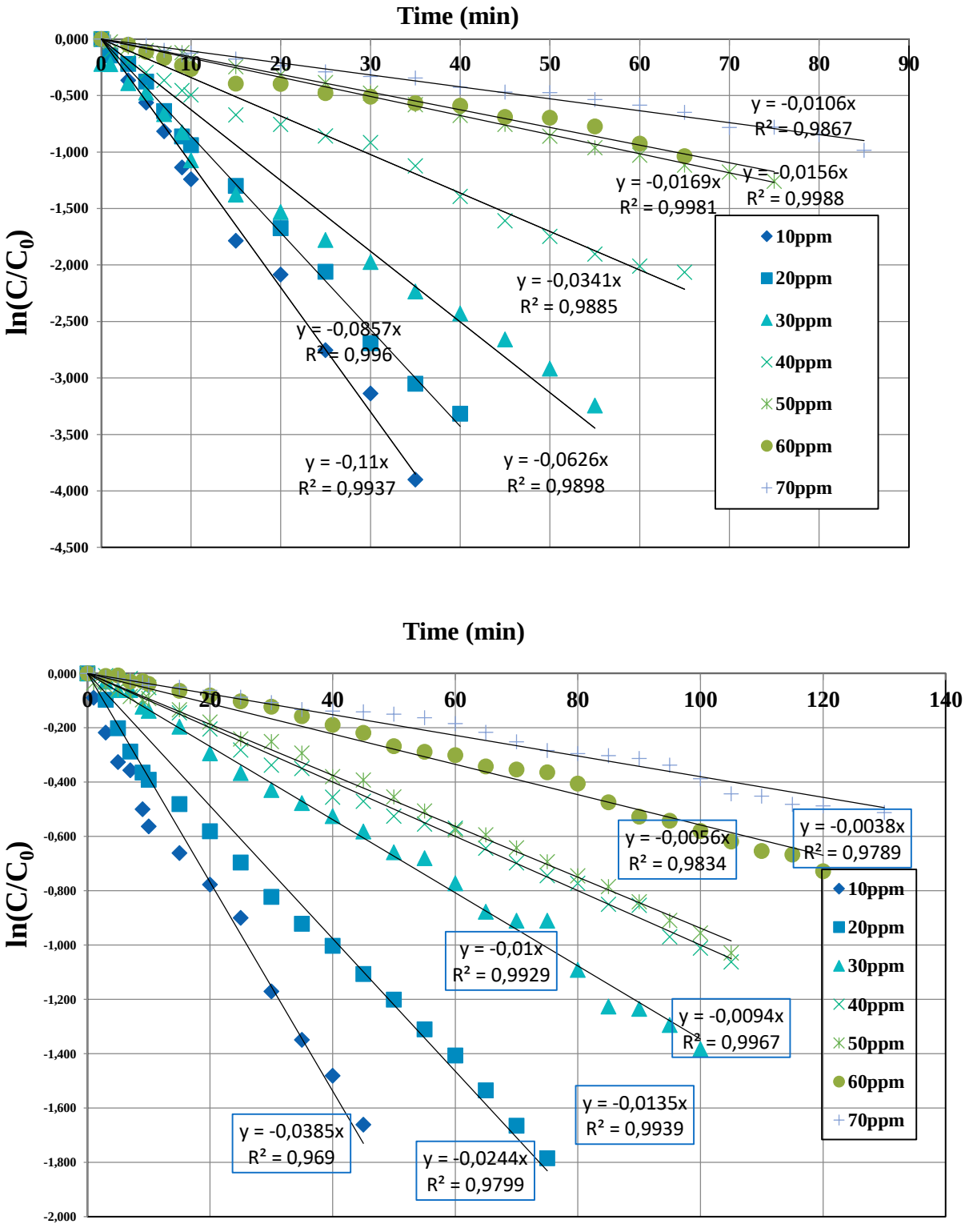

Figure A.4: Representation of the degradation of different concentrations of OG (10 mg/L-70mg/L) by the Heat/PPS process at different concentrations of PPS (100mg/L, 200mg/L, 500mg/L) according to the pseudo-first order kinetic model.